Universidade do Minho
Escola de Engenharia

Francisco de Almeida Garrett Soares da Silva

Bacterial Cellulose Green Composites

Francisco Garrett   Bacterial Cellulose Green Composites

UMinho | 2024

Abril de 2024

Universidade do Minho
Escola de Engenharia

Francisco de Almeida Garrett Soares da Silva

Bacterial Cellulose Green Composites

Dissertation for PhD degree in
Biological Engineering

Work carried out under supervision of
Francisco Miguel Portela da Gama
Maria de Fátima Filipe Poças, PhD

Abril de 2024

ACKNOWLEDGEMENTS

I express profound gratitude to several individuals who played a vital role in facilitating the completion of this thesis through their unconditional support. Their contributions nurtured my personal growth and enhanced my development as a researcher, ultimately leading to the conclusion of this endeavor. First, my heartfelt appreciation goes to my supervisor, Professor Miguel Gama, whose invaluable guidance and the opportunity to be a part of his research group, as a researcher, have been instrumental in shaping my academic journey. I am equally thankful to Professor Fátima Poças, who not only accepted the responsibility of being my co-supervisor but also generously shared her knowledge, guidance, and support during my academic pursuit, particularly crucial in overcoming various obstacles. I extend my gratitude to Professor Paula Teixeira for her guidance on the microbiological experiments and the unwavering support provided during my time in the food microbiology lab. I am also deeply appreciative to Professor Michael Hummel for the warm welcome and untiring support during my time at Aalto University. His guidance and knowledge sharing contributed to the swift development of a proof of concept. I am also grateful to the Centre of Biological Engineering (CEB), Centre for Biotechnology and Fine Chemistry (CBQF), CINATE, Thuringian Institute for Textile and Plastics Research (Rudolstadt, Germany), Bioproducts and Biosystems (Aalto University), and their technical staff for their support throughout this research. Their expertise and assistance played a vital role in carrying out the necessary tasks successfully. Furthermore, I am indebted to all my colleagues from LTEB lab (CEB), CINATE, Food Engineering and Processing lab (CBQF), Food Microbiology lab (CBQF), and the Biopolymer Chemistry and Engineering lab (Aalto), for their aid and companionship. I would also like to express my deepest appreciation to my parents and siblings for their unconditional love and support. Lastly, I would like to extend my thanks to the Portuguese Foundation for Science and Technology (FCT) for providing the PhD grant (SFRH/BD/146375/2019) and all the funding entities that supported this research.

STATEMENT OF INTEGRITY

I hereby declare having conducted this academic work with integrity. I confirm that I have not used plagiarism or any form of undue use of information or falsification of results along the process leading to its elaboration. I further declare that I have fully acknowledged the Code of Ethical Conduct of the University of Minho.

RESUMO

Compósitos verdes de Celulose Bacteriana

Os setores de embalagem alimentar e têxtil utilizam intensivamente materiais à base do petróleo, ressaltando a necessidade urgente de explorar alternativas mais sustentáveis. A celulose bacteriana (CB), produzida por fermentação, oferece vantagens importantes em relação aos materiais mais convencionais, sendo um material biodegradável e com alto desempenho mecânico. No entanto, a CB apresenta algumas limitações para as referidas aplicações: a alta afinidade pela água representa um obstáculo no desenvolvimento de embalagens não hidrofílicas; o elevado grau de polimerização coloca desafios na produção de fibras celulósicas regeneradas, para aplicações têxteis. Neste trabalho foi desenvolvido um compósito laminado, usando CB plasticizada e poli (3-hidroxibutirato-co-3-hidroxivalerato) (PHBV), para aplicação na área das embalagens alimentares. O alto desempenho mecânico da CB e a hidrofobicidade do PHBV permitiram o desenvolvimento de um material com aplicação promissora como embalagem para produtos à base de carne. A CB também foi usada como material de suporte de agentes ativos, onde foi desenvolvido com sucesso um filme de CB funcionalizado, com elevadas concentrações de nanopartículas de ZnO produzidas *in situ*. A atividade antimicrobiana do ZnO (seu mecanismo de ação) e a migração de Zn para o alimento foram caracterizadas. O CB_{ZnO} foi altamente eficaz contra *Campylobacter* spp. em pele de frango (testada como modelo alimentar), tendo-se observado também baixos níveis de migração de Zn à temperatura de armazenamento refrigerado 4 °C. Como alternativa às fibras têxteis, considerou-se o desenvolvimento de fibras celulósicas regeneradas usando CB. As tecnologias Lyocell e Ioncell foram adotadas para avaliar a dissolução da CB e a capacidade de fiação das soluções obtidas. Foram realizados ensaios de fiação bem-sucedidos após a dissolução da CB em N-metilmorfolina-N-óxido e 1,5-diazabiciclo-[4.3.0]-non-5-enium-acetato). Os filamentos desenvolvidos apresentaram bom desempenho mecânico, com elevada rigidez e elasticidade competitiva. Além disso, a mistura da CB com outras fibras (celulósicas) em fim de vida (como por exemplo fibras de viscose) melhora o desempenho mecânico geral, promovendo assim reciclabilidade destas fibras.

Palavras-chave: Celulose bacteriana; Barreira; Antimicrobiano; Lyocell; Ioncell[®]; Reciclabilidade.

ABSTRACT

Bacterial Cellulose Green Composites

Food packaging and textile sectors have long relied on petroleum-based materials, facing nowadays the urgent need to explore more sustainable alternatives. Bacterial cellulose (BC), produced by fermentation, offers key advantages over conventional materials, including high mechanical performance and biodegradability. Yet, certain challenges must be addressed to fully explore its potential. In this work, applications of BC were developed for non-hydrophilic packaging solutions and man-made cellulosic fibre (MMCF) for textile materials.

For food packaging applications, a layered composite based on plasticized BC and poly (3-hydroxybutyrate-co-3-hydroxyvalerate) (PHBV) was developed. The good mechanical performance of BC and hydrophobicity of PHBV allowed to develop a composite with promising application as packaging for meat-based products. BC can also act as a carrier for substances with an active role in food packaging. A functionalized BC film with high concentrations of *in situ* produced ZnO nanoparticles was successfully developed. The antimicrobial activity of ZnO (its mechanism of action) and the pattern of Zn migration onto food were characterised. BC_{ZnO} was highly effective against *Campylobacter* spp. and low Zn migration levels into chicken skin as a food model were obtained at refrigeration temperatures (> 4 °C).

Seeking for an alternative source of textile fibres, the development of MMCF using BC was performed. Lyocell and Ioncell® technologies were used to assess BC dissolution as well as the spinnability of the obtained dopes. Successful spinning trials were achieved after BC dissolution on *N*-methylmorpholine-*N*-oxide and 1,5-diazabicyclo-[4.3.0]-non-5-enium-acetate. The resulting filaments offered competitive mechanical performance, with improved stiffness and competitive elasticity. The Ioncell-BC fibre & yarn properties allowed the development of a fabric. Additionally, the BC blending with end-of-life cellulosic fibres (such viscose fibres) improves the overall mechanical performance, promoting recyclability. Overall, the high potential and great technical performance of BC-based materials is demonstrated.

Keywords: Bacterial cellulose; Barrier; Antimicrobial; Lyocell; Ioncell®; Recyclability

LIST OF CONTENTS

LIST OF FIGURES

Chapter 3

LIST OF TABLES

Chapter 7

LIST OF ABBREVIATIONS AND ACRONYMS

A

ATCC - American Type Culture Collection;

ANOVA - Analysis of variance;

[amim] - allyl-3-methylimidazolium;

AAS – Atomic absorption spectroscopy;

ω – Angular velocity;

B

BC – Bacterial nanocellulose;

BC$_{gly}$ – Bacterial nanocellulose with glycerol

BC$_{PEG}$– Bacterial nanocellulose with polyethylene glycol;

BC$_{gly}$PHBV – Bacterial nanocellulose with glycerol, coated with Poly (3-hydroxybutyrate-co-3-hydroxyvalerate);

BC$_{PEG}$PHBV – Bacterial nanocellulose with polyethylene glycol, coated with Poly (3-hydroxybutyrate-co-3-hydroxyvalerate);

BC$_{neat}$ – non depolymerized bacterial nanocellulose;

BC$_{dep}$ – depolymerized bacterial nanocellulose;

BC$_{blend}$

BC$_{ZnO}$ – Bacterial nanocellulose with zinc oxide;

[bmim] – 1-butyl-3-methyllimidazolium;

C

Cl – Chloride;

3-HV – co-3-hydroxyvalerate

CNC - Cellulose nanocrystals;

CNCH - hydrophobized cellulose nanocrystals;

COD – Chemical oxygen demand;

CFU – Colony forming unit;

CED - cupriethylenediamine aqueous solution;

COP – Cross over point;

CI - Segal crystallinity index;

CIE – Commission Internationale de l'Eclairage;

D

DLS - Dynamic Light Scattering;

DSC - Differential Scanning Calorimetry;

[DBNH] - 1,5-diazabicyclo [4.3.0]non-5-enium;

DP – Degree of polymerization

DR – Draw ratio;

DMAc – Dimethylacetamide;

E

EFSA – European Food Safety Authority

[emim] - 1-ethyl-3-methylimidazolium;

EU – European union;

EVOH - Ethylene vinyl alcohol

ext – exterior;

EDS - Energy-dispersive spectroscopy;

F

FTIR - Fourier-Transform Infrared Spectroscopy;

FCMs – Food contact materials;

G

GRAS - Generally regarded as safe;

Gly – Glycerol;

GPC – Gel permeation chromatography;

H

HPLC - High-Performance Liquide Chromatography;

HS - Hestrin-Schramm

HDPE - High-density polyethylene

HPCS – Hydroxypropyl chitosan;

HRT - Hydraulic retention time;

I

IL – Ionic liquids;

int – interior;

ISO – International organization for standardisation;

L

LDPE - Low-density polyethylene

lcl-PHAs - Long chain length polyhydroxyalkanoates;

LoD – Limit of detection;

LoQ – Limit of quantification;

G'' – Loss modulus;

M

MMCF – Man-made cellulose fibres;

mcl-PHAs - medium chain length polyhydroxyalkanoates;

MWCNTs - Multi-walled carbon nanotubes

MIC - Minimum inhibitory concentration;

MBC - Minimum bactericidal concentration;

MCCD - cefoperazone deoxycholate;

MHA - Müeller-Hinton Agar

MALS – Multi-angle light scattering;

Mw - weight-average molar mass;

Mn - number-average molar mass;

Mw/Mn - polydispersity index;

N

NMMO - N-Methylmorpholine N-oxide;

NPs – Nanoparticles;

NC – Nanocellulose;

NFC - nanofibrilated cellulose;

NFCH - hydrophobized nanobribrilated cellulose;

ns – non-significant;

n – number;

NREL - National renewable energy laboratory;

O

OAc – Acetate;

OTR – Oxygen transmission rate

OLR – Organic loading rate;

OD – Optical density;

P

p - p-value;

PCL - Poly(ε-caprolactone;

PDI - Polydispersity index;

PHAs – Polyhydroxyalkanoates;

PHB – Polyhydroxybutyrate;

PHBV - Poly (3-hydroxybutyrate-co-3-hydroxyvalerate);

PEG - Polyethylene glycol;

PNC - Plant nanocellulose;

PP – Polypropylene;

PET - Polyethylene terephthalate;

PVDC - Polyvinylidene dichloride;

PCL – Polycaprolactone;

PPC – Poly(propylene carbonate);

PS – Polystyrene;

PLA – Polylactic acid;

PVOH - Poly vinyl alcohol;

PdI – Polydispersity;

Gp – Plateau modulus;

PHK - Prehydrolysis kraft pulp;

R

ROS - Reactive oxygen species;

RH – Relative humidity;

RBC – Regenerated bacterial nanocellulose

RT – Room temperature;

Uη - Rheological polydispersity;

λ$_m$ – Relaxation time;

S

SD - Standard deviation;

SEM - Scanning Electron Microscope;

Scl-PHAs - short chain length polyhydroxyalkanoates;

SML – Specific migration limit;

SRT – Sludge retention time;

G' – Storage modulus;

T

TPS – Thermoplastic starch;

Tm – Melting point temperature;

TSA - Tryptic soy Agar

U

UV - Ultraviolet;

UASB - Upflow anaerobic sludge blanket;

X

XRD - X-Ray Diffraction;

W

WHOA - World Organization for Animal Health;

WVP – Water vapour permeability;

WVT – Water vapour transmission rate;

WAXS – Wide angle x-ray scattering;

Z

ZnO – Zinc oxide;

Zn – Zinc;

Zn^{2+} - Ionic zinc;

η$_0$ - zero shear viscosity;

η*# - complex viscosities at the cross over

"Every challenge is an opportunity for growth and a testament to my determination."

CHAPTER 1 – MOTIVATION AND OUTLINE

This chapter introduces an overview of the work developed in this thesis. The motivation and outline of the research work produced is also described, as well as the main scientific outputs.

1.1. Context and Motivation

Most of all petroleum-based materials are used for a short period of time – e.g. as packaging materials and textiles - but then take centuries to degrade. Since 1950, about 6300 million tons of plastic waste have been generated, of which 4977 million accumulated in landfills and waterways [1]. Another emergent problem is the release of microplastics into the air, water and soil, well known to have harmful effects to both terrestrial and marine ecosystems [2]. These plastics are commonly used as both packaging materials and textiles (synthetic fibres) as they provide excellent properties such lightweight, processability, low production cost, mechanical and barrier properties [3]. Concerning food packaging, the demanding requirements (mostly related to barrier and mechanical performance) lead to a high dependence on petroleum-based plastics, despite their negative environmental impacts if not properly disposed [4].

 In the textile industry, the rise of the so called "fast fashion" has exerted significant pressure on textile manufacturers to dramatically escalate global textile production. As a result, there has been a notable dominance of synthetic-based fibres, accounting for over 60% of the market share, followed by cotton at 25% of total global fibre production [5], [6]. Although cotton is biodegradable, its cultivation contributes to excessive water consumption, posing also a significant environmental challenge [7].

Thus, natural and biodegradable materials are much required to replace the synthetic ones, in order to reduce the environmental impact in these industries. While the development of sustainable or renewable polymeric materials is an active research area, the overall performance of most bio-based polymers achieved so far is inferior when compared to traditional petroleum-based polymers. Nanocellulose is regarded as the next generation of renewable reinforcement media for the production of high-performance composites. It has many potential applications addressing a wide range of societal and industrial needs, while meeting the public's perception of more environmentally friendly materials. Plant nanocellulose (PNC) production leads to intensive deforestation and wood (chemical based) processing, an environmental problem if not properly managed. It is a matter of debate if PNC can cover the demand for natural and biodegradable materials, especially considering the large increase of the cellulose-based materials market for plastics replacing in many applications. An alternative to PNC is bacterial nanocellulose (BC), a biomaterial extruded by

bacteria of the genus *Komagataeibacter*, trough (static or agitated) fermentation. The large-scale BC production remains a challenge, due to the low productivities, ineffective fermentation systems, high capital investment and high operating costs. Yet, BC features high porosity, high crystallinity, high degree of polymerization, high mechanical strength in wet state, high water holding capacity, low density and biodegradability. Altogether, it may provide superior results as compared to PNC, through new and environmentally friendly solutions.

This project contributed to the development of sustainable solutions based on the use of BC, as a superior reinforcing and active material for a novel generation of composites with potential application on food packaging and textile applications.

1.2. Thesis outline

This document is divided in 7 chapters. The current chapter (**Chapter 1**) comprises the overview, motivation, research focus and thesis outline. The scientific outputs are also outlined.

Chapter 2 comprises an up-to-date literature review of the main subjects covered in this study. More specifically, this chapter addresses cellulose as biomaterial for food packaging and textile applications. The physico-chemical interaction of nanocellulose with the adjacent polymeric phase, the effect of nanocellulose modification/functionalization on the final properties of the composites, the several production methods for such composites and the effect of nanocellulose on the migration of contaminants into food products, are discussed in the context of food packaging. Concerning textiles, the main technologies for the development of cellulose- based textiles, their surface modification and the recent trends on sustainable cellulose sources, such as BC, are discussed.

Chapter 3 addresses the development of a plasticized BC film with a PHBV coating. Both plasticization and coating were optimized with the main goal of improving both the mechanical and barrier performance, critical parameters for food packaging.

Chapter 4 & 5 addressed the BC functionalization by incorporating zinc oxide (ZnO) nanoparticles through an *in-situ* synthesis method. The synthesis of ZnO was optimized taking in account the effect of concentration and particle size, to ensure higher antimicrobial activity on the composite. Subsequently, the antimicrobial properties of the developed BC_{ZnO} were evaluated by conducting tests against various pathogenic bacteria. Additionally, we extended

our investigation to a real food model (chicken skin) to address the applicability of BC$_{ZnO}$ as an active food packaging. Simultaneously, the migration of zinc ions was assessed, not only into food simulants but also onto chicken skin. Our primary objective was to establish a correlation between the antimicrobial activity of BC$_{ZnO}$ and its migration rate into food products.

In the next two chapters (**Chapter 6 & 7**) we shift our focus towards the application of BC in the textile industry. In **Chapter 6**, both neat and depolymerized BC were evaluated as a potential cellulose source for the development of regenerated cellulose fibres, using the lyocell process. BC samples with varying degrees of polymerization and polydispersity were examined in order to understand the impact of those parameters on the rheology (the flow characteristics of the solution) and the mechanical performance (the strength and durability) of the fibres, demonstrating that by combining celluloses with different degrees of polymerization it is possible to enhance the overall fibre performance.

In **Chapter 7**, the pursuit to develop textiles with BC continues, yet using Ioncell, a technology developed at the bioproduct and biosystems centre (Aalto University, Espoo, Finland). An optimization of the Ioncell process using BC was conducted for the first time, taking into consideration the cellulose concentration and the rheological behaviour of the prepared dopes. Spinning trials were conducted under different conditions (varying extrusion temperatures and draw ratios), with the aim of producing the best-performing fibres. Spinning trials were then scaled up to enable characterization and collection of staple fibres for yarn spinning and knitting purposes. Furthermore, bacterial cellulose was studied as an additive for the recycling of viscose fibres using the [DBNH][OAc] ionic liquid. Multiple dopes were prepared, gradually incorporating increasing amounts of BC, to evaluate the overall performance of the final regenerated cellulose fibre.

Finally, **Chapter 8** provides an overview of the key findings and challenges identified throughout the preceding chapters regarding the utilization of BC in food packaging and textile applications. It offers a comprehensive discussion, highlighting the potential bottlenecks, future prospects and potential opportunities for further research and development of BC-based green composites in food packaging and textile industries.

1.3. Scientific outputs

The elaboration and execution of the experimental work during this PhD thesis originated the following publications in international scientific journals, as well as the participation in several scientific meeting with oral and poster communications.

PUBLICATIONS IN PEER REVIEWED JOURNALS

❖ Soares da Silva, F. A. G., Dourado, F., Gama, M., Poças, F. (2020). Nanocellulose Bio-Based Composites for Food Packaging. *Nanomaterials*, *10*, 2041

❖ Soares da Silva, F. A. G., Matos, M., Dourado, F., AM Reis, M., C Branco, P., Poças, F., Gama, M. (2022). Development of a layered bacterial nanocellulose-PHBV composite for food packaging. *Journal of the Science of Food and Agriculture*, *103* (3), 1077-1087.

❖ Soares da Silva, F. A. G., Bento de Carvalho, T., Dourado, F., Teixeira, P., Gama, M., Poças, F. (2023). Performance of bacterial nanocellulose packaging film functionalised *in situ* with zinc oxide: migration onto chicken skin and antimicrobial activity. *Food Packaging and Shelf Life*, *39*, 101140.

❖ Soares da Silva, F. A. G., Carvalho, M., Bento de Carvalho, T., Gama, M., Poças, F., Teixeira, P. (2023). Antimicrobial activity of in-situ bacterial nanocellulose-zinc oxide composites for food packaging. *Food Packaging and Shelf Life*, 40(19), 101201 .

❖ Soares da Silva, F. A. G., Meister, F., Dourado, F, Gama, M. (2023). Regenerated bacterial celulose fibres. *International Journal of Biological Macromolecules*, 253, 127310.

❖ Soares da Silva, F. A. G., Schlapp-Hackl, I., Nygren, N., Heimala, S., Leinonen, A., Dourado, F., Gama, M., Hummel, M. (2023). Upcycling of cellulosic textile waste with bacterial cellulose. *(submitted)*.

ORAL COMMUNICATIONS IN SCIENTIFIC MEETINGS

❖ Soares da Silva, F. A. G., Dourado, F., Teixeira, P., Gama, M., Poças, F. *In situ* Zinc oxide production on bacterial nanocellulose for active food packaging; The 2022 International conference on nanotechnology for renewable materials. Helsinki (Finland) – 13th - 17th June 2022

❖ Soares da Silva, F. A. G., Dourado, F., Teixeira, P., Gama, M., Poças, F. Development of layered BC composites for Food Packaging; 5th International Symposium on Bacterial Cellulose. Jena (Germany) – 22nd – 23rd September 2022

❖ Soares da Silva, F. A. G., Teixeira, P., Gama, M., Poças, F. Applications of bacterial nanocellulose in active packaging. Advances in Cellulose-based materials in Food Packaging (Seminar). Porto (Portugal) – 22nd – 23rd May 2023

POSTER COMMUNICATIONS IN SCIENTIFIC MEETINGS

❖ Soares da Silva, F. A. G., Matos, M., Dourado, F., AM Reis, M., C Branco, P., Poças, F., Gama, M. Development of bacterial nanocellulose-poly(3-hydroxybutyrate-co-3-hydroxyvalerate) composite for food packaging. First Circul-a-bility conference; Re-thinking Packaging for circular & sustainable food supply chains of the future. Online – 26th - 29th September 2021

❖ Soares da Silva, F. A. G., Meister, F., Dourado, F., Gama, M. Regenerated bacterial celulose fibres. Cellulose fibres conference 2023. Cologne (Germany) – 8th – 9th March 2023

❖ Soares da Silva, F. A. G., Dourado, F., Hummel, M., Poças, F., Gama, M. Development of Bacterial cellulose composites for Food Packaging and Textiles; 14th International Chemical and Biological Engineering Conference, chempor-2023. Bragança (Portugal) – 12nd – 15rd September 2023

1.4.   References

[1]   Souza Machado, A. A., Kloas, W., Zarfl, C., Hempel, S., & Rillig, M. C. (2018). Microplastics as an emerging threat to terrestrial ecosystems. *Global change biology*, *24*(4), 1405-1416.

[2]   Geyer, R., Jambeck, J. R., & Law, K. L. (2017). Production, use, and fate of all plastics ever made. *Science advances*, *3*(7), e1700782.

[3]   Sangroniz, A., Zhu, J. B., Tang, X., Etxeberria, A., Chen, E. Y. X., & Sardon, H. (2019). Packaging materials with desired mechanical and barrier properties and full chemical recyclability. *Nature Communications*, *10*(1), 3559.

[4]   Bharimalla, A. K., Deshmukh, S. P., Vigneshwaran, N., Patil, P. G., & Prasad, V. (2017).

Nanocellulose-polymer composites for applications in food packaging: Current status, future prospects and challenges. *Polymer-Plastics Technology and Engineering*, *56*(8), 805-823.

[5] Textile Exchange (2022). Preferred Fiber & Materials: Market Report 2022, pp. 1–118.

[6] Opperskalski, S., Siew, S., Tan, E., & Truscott, L., (2019). Preferred Fiber & Materials Market Report 2019, pp. 1–87

[7] Shen, L., Worrell, E., & Patel, M. K. (2010). Environmental impact assessment of man-made cellulose fibres. *Resources, Conservation and Recycling*, *55*(2), 260-274.

CHAPTER 2 – LITERATURE REVIEW

This chapter comprises an updated review on the use of cellulose as a biomaterial for food packaging and textile applications. The technical features and requirements of food packaging materials, the use nanocellulose based composites and their processing and the safety of nanocellulose-based materials (considering migration and toxicity) are reviewed. Concerning textiles, the main technologies available for the development of Man-Made Cellulosic Fibres (MMCF) are detailed, highlighting their advantages and limitations. Then, the perspectives for the BC use as a raw material in these industries are discussed.

Adapted from A.G. Soares Silva, F. et al. (2020). Nanomaterials, 10, 2041.

2.1.   Cellulose and nanocelluloses

Cellulose is a remarkable material due to its abundance, renewability and degradability, physical-chemical and morphological properties [1]–[3]. Cellulose can be extracted from plant sources or produced through microbial fermentation [4]. Regardless of the cellulosic source, the chemical formula of the biopolymer is $(C_6H_{10}O_5)_{DP}$ (Figure 2.1). The size of the polymer chain - its degree of polymerization (DP) - depends on the cellulose extraction/production method.
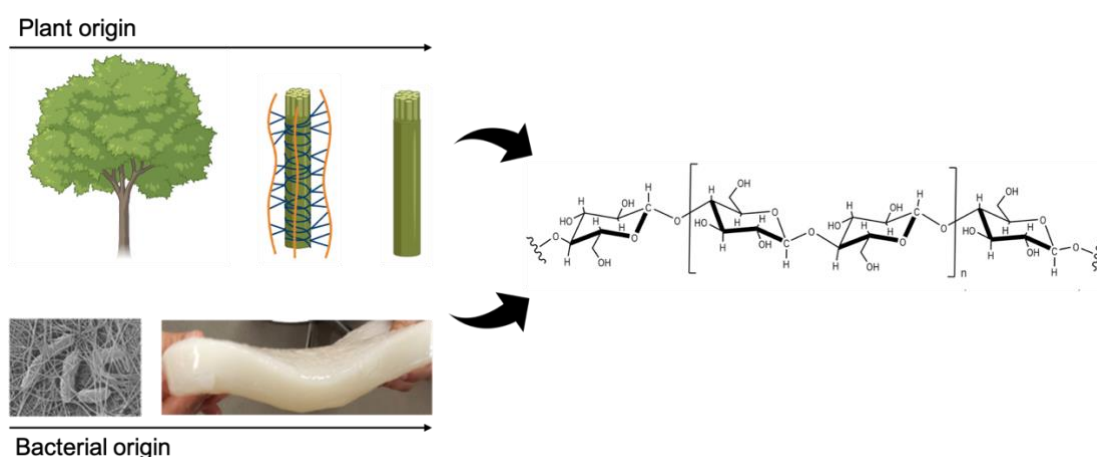
Figure 2.1. Scheme of plant and bacterial-cellulose extraction

Nanocellulose (NC) or nano-structured cellulose is characterised by the nanosize of the fibres (<100 nm) in at least one dimension. The production of these NCs may be categorized into top-down and bottom-up methods. Steam explosion, enzyme-assisted and acid hydrolysis (using sulphuric and hydrochloric acids), followed by mechanical treatments (high pressure homogenization, microfluidization and cryocrushing) are used in top-down methods to deconstruct the vegetable biomass into NC [4], [5]. Depending on the methods used, and on the properties obtained, different NC can be distinguished: nanofibrilated cellulose (NFCs) and cellulose nanocrystals (CNC) [4]–[6]. NFCs are longer and flexible filaments (5-60 nm diameter with 2-10 μm in length), with alternating crystalline and amorphous regions, while CNC has a needle-like shape and is more crystalline (5-70 nm diameter with 100-250 nm in length) (Figure 2.2.). Also, the aspect ratio (ratio between length of the fibre and its diameter), is usually higher on NFCs (up 2000) than CNCs (up to 50). The crystalline domains in NFC have similar dimensions as the CNC. Examples of bottom-up methods are the production of bacterial cellulose (BC), described ahead, and cellulose from tunicates.
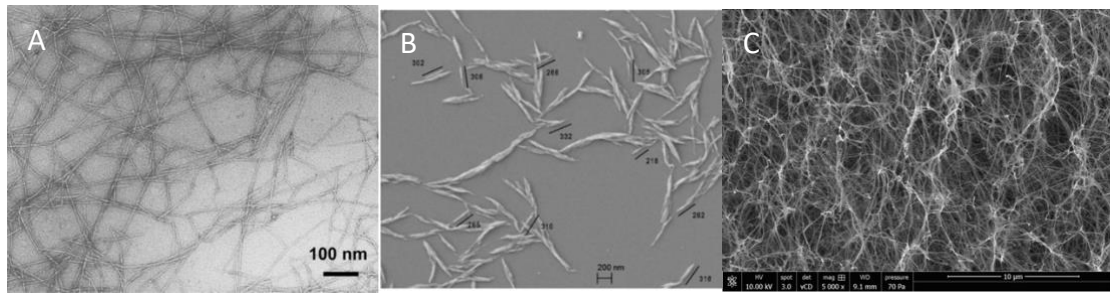
Figure 2.2. (A) nanofibrilated cellulose (NFCs) [7]; (B) cellulose nanocrystals (CNC) [8] and (C) bacterial cellulose (BC)

The plant NC (PNC) has been obtained from a wide variety of sources, namely pine, coconut husk fiber, mengkuang leaves (*Pandanus tectorius*), raw cotton linter, barley wastes, tomato peels, garlic straw residues, forest residues, corncob residue, industrial waste cotton, cassava root bagasse and peels, sugar palm fibres, corn straw and agro-industrial residues [6]. The plant source (fibre dimensions, structure of the cell wall, relative percentage of cellulose, hemicellulose and lignin) and the extraction method will influence the final NC purity and properties.

BC, also a nanocellulose, is a biopolymer extruded by bacteria of the *Komagataeibacter* genus, through (static or agitated) fermentation. BC extrusion starts with the polymerisation of the glucose residues into linear β-1,4 glucan chains, assembled and crystallized for the formation of long and ultra-thin cellulose nanofibres [9]. BC features high porosity, high crystallinity, high degree of polymerization, high mechanical strength in wet state, high water holding capacity, low density, biocompatibility, non-toxicity and biodegradability [10]. Despite these unique properties, there are strong limitations associated with its industrial production due to the high operational costs and low BC yields [10]. Extensive research has been done to promote higher yields by using low-cost raw materials [11]–[15]. BC as sparked interest for several applications (Figure 2.3.): (i) biomedicine, such as tissue regeneration and drug delivery systems; (ii) textile and paper industries, for fibre and coatings production; (iii) food and cosmetic industries, as an emulsifier; (iv) materials, as reinforcing agent for nanocomposite [2], [3], [16]–[24].

In the following sections, the cases of food packaging and textile industries will be analysed regarding the type of raw materials used and their processing.
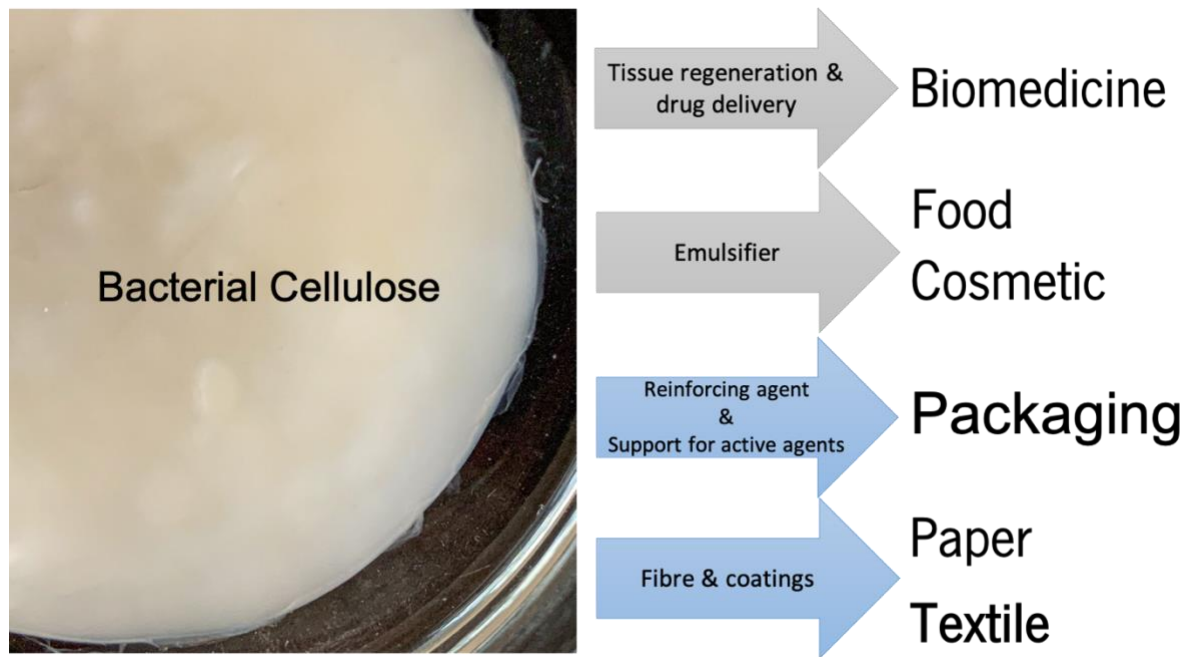
Figure 2.3. BC main applications

2.2. Food Packaging

Packaging plays an essential role in the food supply chain, protecting and containing food from the processing and manufacturing stage, along with distribution, handling and storage, until it reaches the final consumer. Currently, food packaging accounts for the largest share in the total packaging sector (85%) [25]. Globally, plastic materials are the most used (for primary packaging), bearing enticing properties such lightweight, good processability, low production cost and high-performing mechanical and barrier properties [25], [26]. However, there is an increasing concern regarding the massive application of petroleum-based plastics, which are used for a short period of time but then take centuries to degrade. A study by Geyer et al. [27] reported that until 2017, about 6300 million tons of plastic waste were generated, of which 4977 million accumulated in landfills and waterways. Unrecycled plastics leads to an increasing release of microplastics into the air, water and soil, endangering terrestrial and marine ecosystems [28].

In the scope of the European Strategy for Plastics in a Circular Economy, the Directive (EU) 2019/904 was published to prevent and reduce the impact of single use plastic products on the environment (in particular the aquatic), and on human health, as well as to promote the transition to a circular economy [29]. Additionally, the Directive (EU) 2018/852 sets a minimum of 70 % by weight of all packaging waste and a minimum of 55% as recycling targets

for plastic, by the end of 2030 [30]. However, in some countries, the recycling rates are still rather low: in 2020, the European Union recycling rate of packaging plastics is about 40% [31]. Furthermore, mechanical recycling reduces the performance of the materials, making it less attractive [27].

2.2.1. Food packaging: materials and performance requirements

Packaging main goal is to contain food in a cost-effective way, while satisfying the industry and regulatory requirements, as well as the consumer expectations, keeping food products protected from the external environment [26]. For the majority of food products, the protection assured by the package is an essential part of the preservation process. The requirements of a packaging system intended for fresh, frozen, dehydrated, thermal or aseptic processed products, depend on the i) intrinsic properties of the food product, such as water activity and oxidation potential that determine their perishability; ii) extrinsic factors, namely storage temperature, relative humidity and exposure to light, and finally iii) the required shelf-life. All these factors must be taken in account when specifying the required barrier ability to water vapour, oxygen and other gases, including aromas and light (Table 2.1). The physical and mechanical properties are also important [32] during processing, packaging operations and handling through the supply chain. Packaging geometry (e.g. surface area to volume) and the material thickness are variables that largely affect both the barrier and the physical performance of the package. Table 2.1 presents the requirements regarding moisture and oxygen barrier for several foods (information adapted from [33]) together with materials used commonly to pack these foods.

Table 2.1. Barrier properties requirements for specific food products [33] and typical materials used

Product	Water Vapour Transmission Rate (g/m².day) 23 °C	Oxygen permeance (cm³STP/m².day.Pa) 23 °C	Shelf-life (months)	Materials typically used
Low moisture foods, a_w < 0.6				
Nuts, snacks, chips	0.093 - 3.0	$1.6 \times 10^{-6} - 9.6 \times 10^{-5}$	3 – 12	Metallised films, Laminates with Ethylene vinyl alcohol (EVOH), Polypropylene (PP)
Coffee	0.61 - 1.1	$8.7 \times 10^{-6} - 1.3 \times 10^{-5}$	12 – 18	PP or Polyethylene terephthalate (PET) metallised or Aluminium foil laminates
Other dried foods	0.14 - 1.7	$6.8 \times 10^{-7} - 8.2 \times 10^{-6}$	12 – 24	PP or PET metallised, Laminates with EVOH
Oils	< 30	$2.6 \times 10^{-5} - 2.6 \times 10^{-4}$	> 12	PET, Glass
High moisture foods, a_w > 0.9				
Beer	1.4 - 3.0	$4.5 \times 10^{-7} - 2 \times 10^{-6}$	6 - 12	Glass, Polyvinylidene dichloride (PVDC) - coated PET, Metal can
Wine	1.0 1.4	$1 \times 10^{-6} - 9.5 \times 10^{-6}$	> 12	Glass, PET, Bag in box
Fruit juices, soft drinks	0.47 - 12.2	$6.1 \times 10^{-6} - 6.14 \times 10^{-4}$	1 - 18	Glass, PET, Metal cans, bag in box, Aseptic multilayer
UHT milk	2.7 - 5.3	$3.5 \times 10^{-6} - 5.6 \times 10^{-5}$	2.5 - 5	Aseptic multilayer
Hard cheese	50	$8.6 \times 10^{-4} - 3.45 \times 10^{-3}$	2	PP, High-density polyethylene (HDPE)
Fats	5.2 – 9.2	$6.8 \times 10^{-5} - 8.0 \times 10^{-4}$	3	Fat resistant paper, PP
Retorted food	0.40 – 7.6	$5.9 \times 10^{-6} - 5.0 \times 10^{-5}$	3 - 36	Metal can, Glass jar, Laminates: PET or PP with EVOH or polyamide
Fresh foods				
Fruits, vegetables, fresh salads	10 – 4 000	$1 \times 10^{-1} - 2$	0.25	Low-density polyethylene (LDPE), PP
Meat and meat	2 - 100	$2 \times 10^{-4} - 1 \times 10^{-1}$	0.25 – 0.5	Polystyrene (PS) and PET trays

based product				
Dairy products	0.2 - 8	6×10^{-4} - 5×10^{-2}	0.5	HDPE, PP, PS

It is recognised that petroleum-based plastics have great thermomechanical and barrier properties, as well as light weight and low production cost [34], yielding a hard to beat overall performance (Figure 2.4); they are commonly used in food packaging as indicated in Table 2.1.

The environmental impact of non-biodegradable plastics and the increasing need for a more sustainable use of packaging materials in particular, are ever-growing global concerns. Solutions to reduce and in some cases to replace those materials are on top of research efforts. Biopolymers such polylactic acid (PLA), polyhydroxyalkanoates (PHA) and thermoplastic starch (TPS) has been sought as alternative solutions [35].

The most widely exploited due to its biodegradability is PLA [36], which is mainly used in packaging applications. It is presented as films or as thermoformed or injected packages for relative short-term and mild temperature contact conditions, such as fresh salads and beverage drinks, because of the low resistance to temperature. One major limitation commonly referred is the high price and commercial shortage, as compared to conventional plastics. Corn is presently the major raw material used in the production of PLA but second-generation feedstock is under development.

Starch is the second most abundant biopolymer in nature [37]. Thermoplastic starch (TPS) in particular has potential for food packaging application, in spite of its poor mechanical and barrier properties (Figure 2.4). An important commercial application is that of bags for non-packaged fruits and vegetables and as shopping bags, in blends with fossil-based polymers.

Biopolyesters such polyhydroxyalkanoates (PHAs) are obtained through fermentation of bacteria (gram negative, gram positive and archea) [38], [39]. To date, more than 150 different PHAs monomers have been identified, mainly obtained by chemical or physical modification, or through the creation of mutant organisms that produce PHA with functionalized groups [39]. The homopolymer polyhydroxybutyrate (PHB) is the most common. Depending on the number of carbon atoms, PHAs may be classified as short chain length (scl-PHAs), containing 3–5 carbon atoms; medium chain length (mcl-PHAs), comprising

6–14 carbon atoms and long chain length (lcl-PHA), comprising 15 or more carbon atoms [39]. PHA may vary from non-crystalline to highly crystalline, the melting points ranging from 50 °C-177 °C. Usually, mcl-PHAs have lower melting point temperature (between 40-60 °C) if compared with scl-PHAs (Tm up to 180 °C). However, tensile strength, young modulus, and crystallinity of mcl -PHAs are generally poorer than those of scl-PHAs. This material has been drawing attention due to its biodegradability and similarities with conventional plastics, namely polypropylene (PP), yet global production and production cost are not comparable [38].

The above-mentioned biopolymers lack the performance to fulfil the most demanding specific requirements (Table 2.1) for food packaging [33], [40] and apart a few exceptions, commercial applications are yet not volume comparable. Figure 2.4 present the mechanical (tensile strength, elongation at break) and barrier properties (water vapour and oxygen permeability) of conventional plastics and biopolymers. In general, biopolymers have lower elongation values and higher water vapour permeability than conventional plastics (Figure
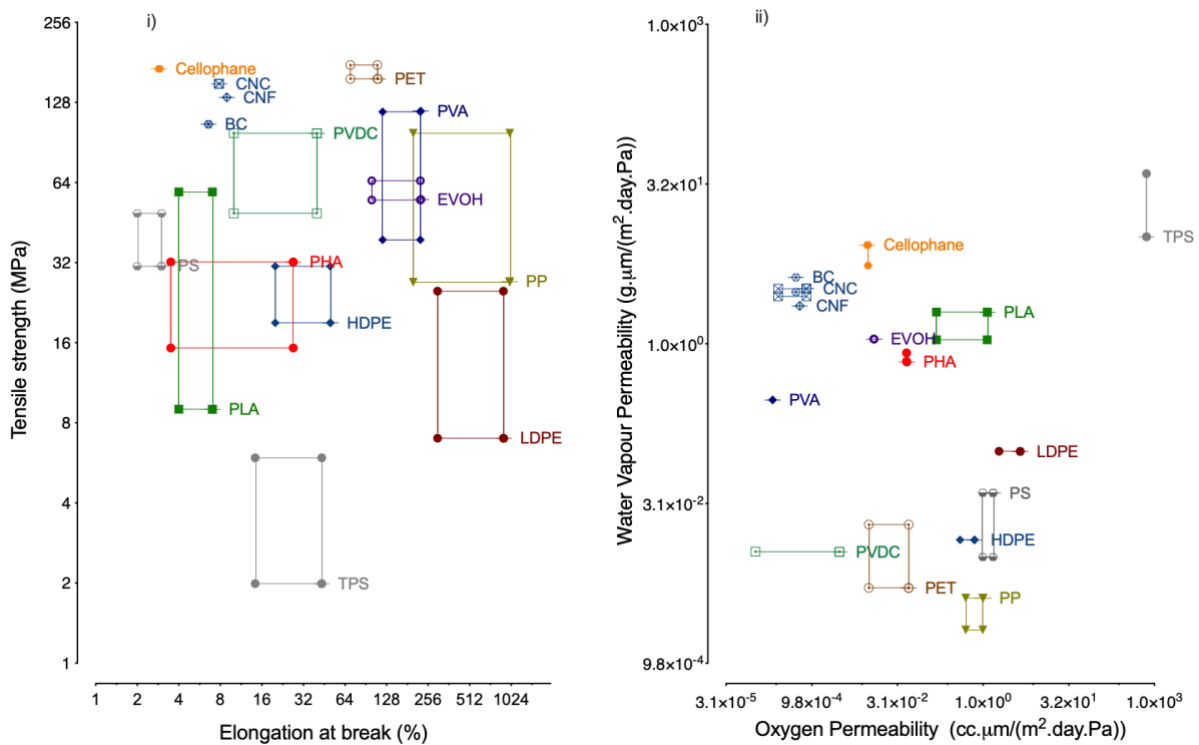
2.4).

Figure 2.4. Properties of synthetic and bio-based polymers: i) Tensile strength (MPa) vs elongation at break (%); ii) Water vapour permeability vs Oxygen permeability; the values, obtained at 23-25 °C and normalized in terms of relative humidity (50% RH), were calculated

from [26], [41], [40], [42]–[55]. PET-Polyethylene Terephthalate; PP-Polypropylene; LDPE- Low density polyethylene; HDPE- High density polyethylene; PS- Polystyrene; PVDC- Polyvinylidene chloride; PVOH- Poly vinyl alcohol; EVOH- Ethylene vinyl alcohol; PLA- Poly lactic acid; PHA- Polyhydroxyalkanoates TPS- Thermoplastic starch;

2.2.2. Nanocellulose based composites processing

Regardless the choice of NC, the conditions to process the components and the composite production method are essential to achieve the dispersion of the fibres in the main matrix, which is critical for the performance of the final material, in particular for packaging applications. Several methods of processing nanocellulosic composites are mentioned in the literature, including solvent casting, impregnation, coating, layer-by-layer assembly, melt processing and all-cellulose composites [56]. In this chapter, only the technologies used in this study (solvent casting, impregnation and coating methods) are described.

The most well-known and simple method is solvent casting, where the nanofibres are added to the polymer suspension. This is stirred at a defined temperature in a reactor, in order to get a homogenous nanoscale suspension before casting onto a suitable surface with controlled thickness [57]. Evaporation at room temperature, vacuum oven drying, hot pressing and compression moulding are examples of different draining and drying procedures referred in literature, which can affect the final properties of the composite [5], [17], [58].

Most of the studies reported with solvent casting involve some degree of modification of the NC for a better dispersion in the hydrophobic matrix [17]. The solvent used is determined by the hydrophobicity/hydrophilicity of the matrix phase. For PHAs and PLA, solvents such as chloroform, acetone, toluene, dichloromethane and dimethylformamide are used [51], [59], [60]. For TPS and PVOH matrices, the solvent is water [53], [58], [61].

Few reports were found concerning solvent casted NC-PHAs composites. In the work of Ten et al. [62] PHBV was dissolved with dimethylformamide at 80 °C and CNC was added at different concentrations (1-5%). The resulting composite showed enhanced young modulus (up to 2.5 GPa) but a low tensile strength (no more than 20 MPa). Patricio et al. [63] used poly (ethylene glycol) (PEG) to increase compatibility between CNC and PHB on the chloroform solvent; the authors claimed that blending without PEG would not result due to CNC

aggregation. The addition of CNC on PHB matrix led to an increment on young modulus (up to 550 MPa) and a decrease on elongation (down to 10 %).

The blend of nanocellulose (either NFC, CNC or BC) with TPS improved the mechanical performance over neat TPS film. However, these NC-TPS composites still showed poor moisture barrier properties [61], [64]–[69].

The thickness and roughness control are crucial to maintain the quality of the film obtained by casting. Pilot scale plants currently use blades and a moving belt to control the thickness of the casted suspension (Figure 2.5). The availability of suitable equipment for good dispersibility of the components and control of the film thickness is still the main limitations for scaling-up [41]. The method is useful when a very small amount of reinforcement is required, although being time and energy-consuming [17].
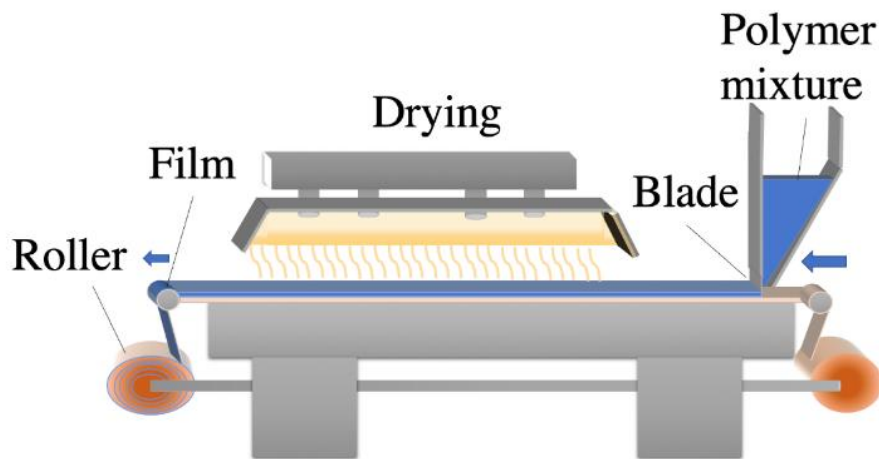
Figure 2.5. Solvent casting scheme

In another example, a 3D nanofibrillar BC network naturally produced by static fermentation, was used (Figure 2.6) [9]. The polymer was added after BC fermentation and washing. Never dried BC membranes were immersed in a polymeric solution, to initiate the migration of the polymer into the bulk of the nanofibrillar network [9]. TPS and PHB are examples of polymers used to form composites with BC by impregnation [66]. Enhanced mechanical performance was reported for BC-TPS composites in comparison to neat TPS films, with higher tensile strength (increased 137.1%) and higher young modulus (increased 132%) [66]. This method, however, presents some drawbacks. It should be noted that the "empty" spaces of wet BC fibrillar network are at micrometric scale, therefore, only nano-sized compounds and polymers may migrate easily (but slowly) into the fibrillar network [21], such as emulsions systems comprising hydrophobic nanoparticles [21]. The scalability is still very

limited due to technical and economic factors. The limited size and (lack of) homogeneity of the BC membrane and the processing in batch mode only, are constrains to increase process capacity [70]. Moreover, upstream, the high cost of the fermentation process and low BC yields [71] are also important limitations. Yet, impregnation method has found interest in the development of functionalized BC for intelligent and active packaging, to produce films [72]–[74] and freshness indicators [75]–[78].
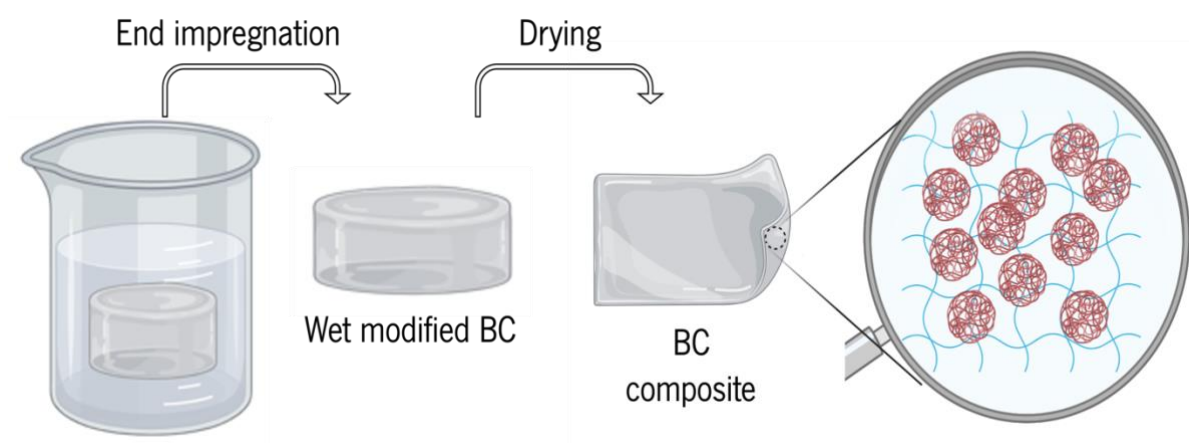
Figure 2.6. Impregnation scheme

The coating process can be defined as the application of a material onto a surface (Figure 2.7), to form a laminated film with good interfacial adhesion [79]. Numerous food packaging applications require good barriers for oxygen and grease, such as fast food, pet food and bakery products [80]. Coating is very common in food packaging and is used for all types of supporting materials, including cellulosic based materials. Most of the paper and board products used for food packaging contains a coating to improve moisture and grease resistance. Several coating techniques are used, such as solvent based coating, extrusion coating, aqueous dispersion, wax, hot melt coating and vacuum coating [81]. Some of the methods are reported to coat a NC layer, others to apply one or more layers where NC is a component of the coating.

In general, the coating of paperboard with NC based layers reduced the oxygen permeability and improved the grease resistance, but high water vapour permeability is still observed [80], [82]–[85]. To reduce the high water vapour permeability of NC, combination with, for example, polypyrrole and PLA were reported [84], [86]. Polypyrrole particles were added to NFC suspensions before coating the paperboard. A decrease in oxygen permeability

and an increase in the mechanical properties were obtained [84]. In another approach, a multilayer coating onto paperboard was produced using PLA as the outer layer, while the CNC was the intermediate one, together yielding low oxygen and water vapour permeability [86]. Transparent multilayer films were produced from NFC thin layers coated on amorphous and semi crystalline PLA substrates. A strong adhesion between the layers was obtained, which led to an improved mechanical performance [87]. Another interesting example is the coating of NFC onto multilayer bio high-density polyethylene (HDPE) film. The NFC layer on the bio-HDPE led to a decrease in oxygen permeability (both at 0%RH and 80% RH) and improved grease resistance. The NFC layer loading did not compromise the already good water vapour barrier of neat bio-HDPE [88].
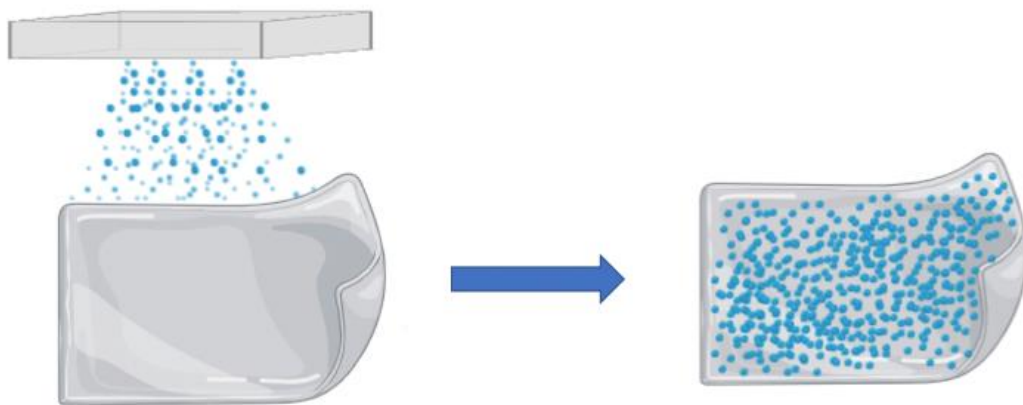
Figure 2.7. Coating scheme

A more recent coating technique is the application of nanofibres produced by electrospinning in the substrate (Figure 2.8.). This methodology is based on high-voltage application in a polymer solution upon extrusion resulting on the formation of nanofibres through the electrostatic repulsion of charges during spinning [89], [90]. This technique is simple and cost effective, easy to set up on a continuous production process (long fibres) [90], [91]. In addition, the large surface area of the produced nanofibres allows to develop layers with high pore volume, different fibre length and fibre diameter, with tunable mass transport properties [91]. However, solvent recovery problems, low productivity and instability are some drawbacks [90]. Different electrospinning set ups for food packaging applications have been reported and a wide variety of polymers have been used: PHBV, PLA, PVA, chitosan, polycaprolactone (PCL), poly(propylene carbonate (PPC), natural cellulose and starch [91]. The electrospinning of BC-PHB mixture was an efficient strategy to obtain high dispersion of BC in

hydrophobic matrices of polyhydroxy butyrate-co-hydroxy valerate (PHBV), where oxygen permeability was improved (in comparison to neat PHBV) [92]. The electrospinning of PHB into both sides of nanopaper (composed of NFC and lignocellulose fibrils), produced a multilayer composite with high water resistance and low oxygen permeability [93].
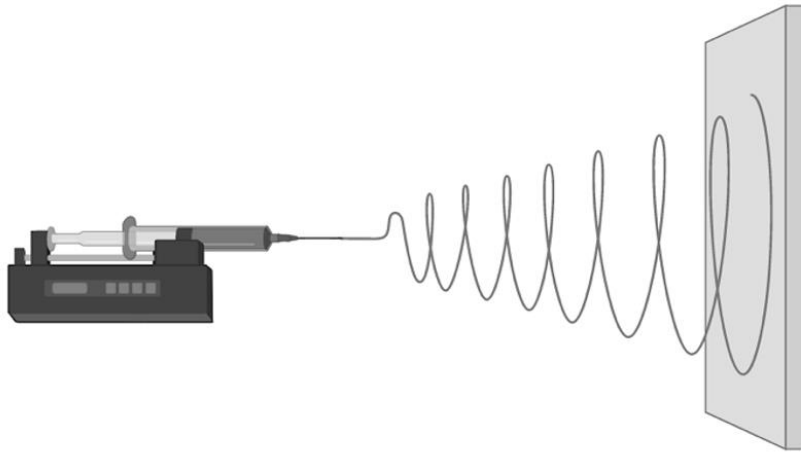
Figure 2.8. Electrospinning scheme

2.2.3. Nanocelulose based composites in food packaging

Nanocellulose (NC) has been used both as a coating and a filler, to produce nanocomposites for food packaging. All the above-mentioned examples of nanocomposite processing were used to produce nanocellulose based composites. Figure 2.9 shows the values of the mechanical and barrier properties of nanocellulosic composites found in the literature. Each column (that refers to a particular material or combination of materials) represents the value range for a specific property (Y axis), regardless of the production method and biopolymer concentration used. The main goal of this figure is to provide an overall comparative view of the mechanical and barrier performance of NC based composites with conventional plastics. NC increases the stiffness of all composites (either with PLA, PHB and TPS), since it led to an increase in young modulus and a substantial decrease on the elongation at break (Figure 2.9).
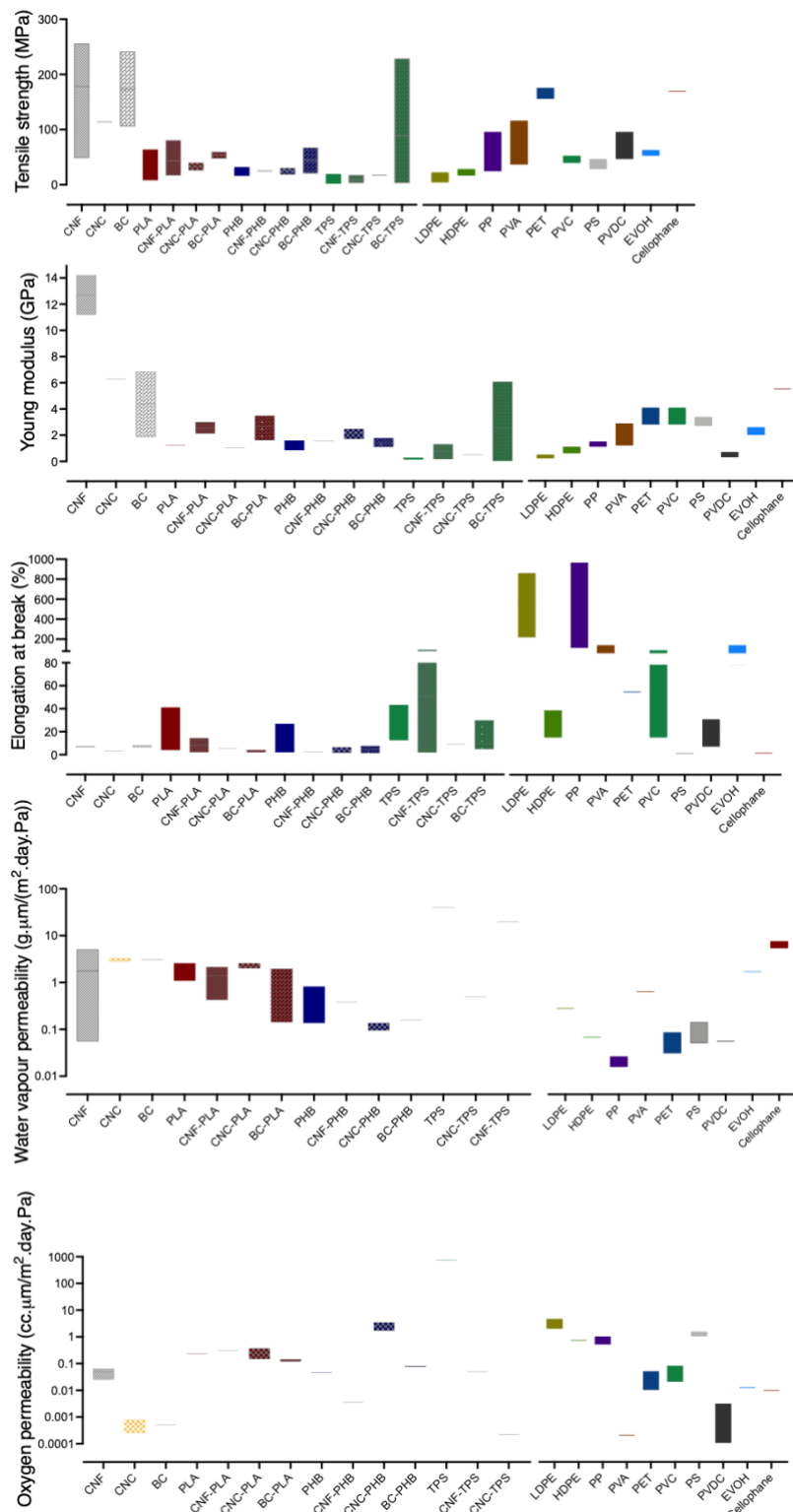
Figure 2.9. Mechanical and barrier properties of nanocellulosic based composites and petroleum based plastics [45], [51], [52], [54], [59], [65]–[69], [88], [92]–[106] PET—Polyethylene Terephthalate; PP-Polypropylene; LDPE—Low density polyethylene; HDPE-High density polyethylene; PS-Polystyrene; PVDC-Polyvinylidene chloride; PVA-Poly vinyl alcohol;

EVOH-Ethylene vinyl alcohol; PLA-Poly lactic acid; PHA-Polyhydroxyalkanoates TPS-Thermoplastic starch; NFC-nanofibrilated cellulose; CNC-cellulose nanocrystals; BC-bacterial nanocellulose; NFCH-hydrophobized nanobribrilated cellulose; CNCH-hydrophobized cellulose nanocrystals; Modified NCs were coloured orange.

The water vapour permeability of PHB, TPS and PLA tends to decrease with the NC incorporation (either NFC, CNC or BC). This is observed for low nanocellulose concentrations (below 5%), which can be well distributed in the relatively hydrophobic matrix, hindering the transmission of water vapour through the composite; however, agglomeration may occur for higher content, leading to null or even reverse effect on water vapour permeability. Concerning the oxygen permeability, there is no significant effect of NC on PLA based composites. NFC and BC decrease the oxygen permeability of PHB and TPS based composites, while CNC substantially reduces it (Figure 2.9). Despite the overall reduction observed, it is important to consider the relative humidity conditions used in the oxygen permeability measurements. Often these are performed in dry conditions and RH values higher than 50% have a strong interaction with the nanofibres network leading to a substantial increase of oxygen permeability (Figure 2.9).

In short, the incorporation of nanocelluloses (BC, CNC and NFC) improves the mechanical properties (increasing stiffness) and decreases the water vapour permeability of PLA, PHB and TPS, due to the enhanced structural properties. This beneficial interaction brings these composites closer to the requirements in food packaging. However, these improvements are still insufficient, since high oxygen and water vapour permeabilities are still observed (higher than that of the petroleum-based plastics) (Figure 2.9).

2.2.4. Active and intelligent Food Packaging

Active and intelligent packaging are concepts that became very attractive for both researchers and industry, as a strategy to delay and prevent contaminations in food. Active packaging is a system that absorbs or releases substances in order to extend food shelf life, providing antimicrobial and antioxidant properties. Intelligent packaging monitors the condition of packaged food or the surrounding environment providing information, for example on the freshness of the food. NCs are inert with respect to these functions but are an excellent support for substances that may play an active or intelligent role in the food packaging system (Figure 2.10).
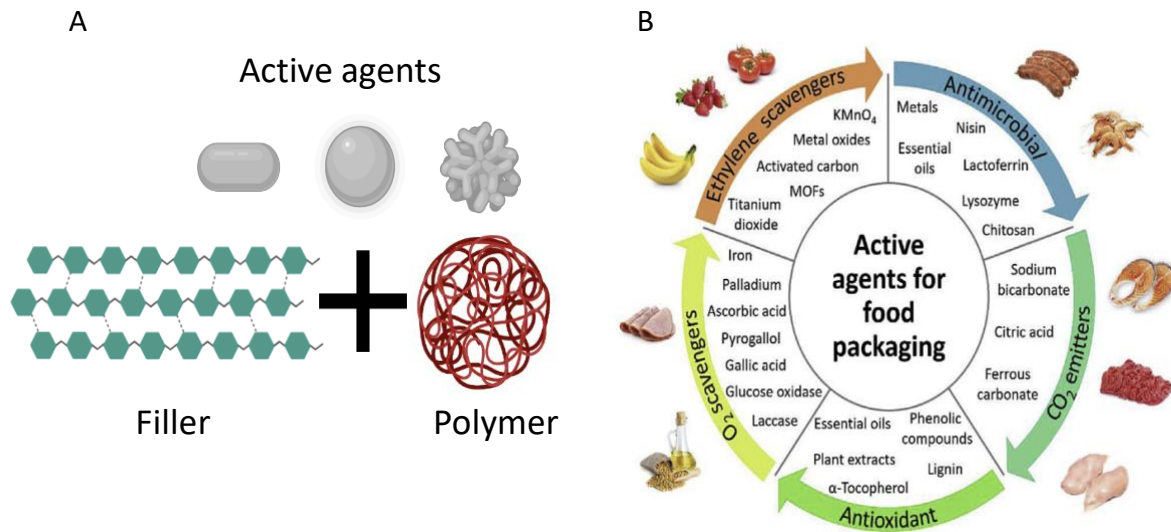
Figure 2.10. (A) Active packaging system and; (B) active agents for food packaging (from[107])

Different active agents to functionalize nanocellulose have been reported, namely zinc oxide [108], flavonoid silymarin [109], ferulic acid and derivatives [110], tannins [111], titanium dioxide [112] and silver [113]. Using BC as support, active substances as zinc oxide (ZnO) nanoparticles (NPs) [108], [114]–[116], zein NPs [117], silver[118], thymol[119], lactoferrin [72] and sorbic acid [120] were applied.

These functionalized BC based composites provide antioxidant and antibacterial activity tested also in real food models [72], [73], [108], [114]–[119]. Among the reported active substances, ZnO stands out for its versatility on multiple applications such cosmetics, ceramics, rubber, paints and food supplements [121].

This material has a 3.37 eV energy band gap and a 60 meV bonding energy, resulting in enhanced insulating properties and robust bonding strength between zinc and oxygen atoms, respectively. These factors are significant for chemical, electrical, and thermal stability of the material. [121]. ZnO has been explored in the food packaging field for their antibacterial activity [122]. The development of ZnO NPs have been extensively studied with the main goal of optimizing antibacterial efficiency, known to be dependent of different parameters such particle size, concentration and morphology [123].

Noteworthy approaches were explored to develop BC_{ZnO} films: (i) never dried BC was immersed into $Zn(NHO_3)_2$ for 24h, then washed with distilled water and subsequently immersed into a NaOH solution (0.2M) to react with $Zn(NHO_3)_2$ and form ZnO NPs within the nanofibre network of BC [74]; (ii) direct impregnation of ZnO nanoparticles into never dried

BC [115]. Although the ZnO increased the water vapour permeability of BC [115], enhanced antimicrobial properties and thermal stability were obtained [74]. The antibacterial activity was tested against gram positive (*S. aureus* and *B. subtilis*) and gram negative (*E.coli* and *P. aeruginosa*), high inhibition zones being achieved.

The antibacterial effect of ZnO NPs mainly relies on the generation of reactive oxygen species (ROS; e.g., $O^{\bullet-}_2$, $HO\bullet$, H_2O_2) and/or the migration of Zn^{2+} [124]. Zn^{2+} migration should be considered for a safety assessment of food products when in contact with a food packaging containing ZnO. The rate of Zn^{2+} migration should be monitored, as the specific migration limit (SML) was established at 5 mg.kg^{-1} by the European Food Safety Authority [125]. Several studies address the study of the Zn^{2+} migration [122], [126]–[129], but only a few are related to NC based composites.

2.2.4.1.   Safety of nanocellulose based composites

In the current European legislation, all materials in contact with food (FCMs) must meet the requirements from the regulation (EC) No 1935/2004 that states the following: "Materials (…), shall be manufactured in compliance with good manufacturing practice and so that, (…) they do not transfer their constituents to food (…) in quantities which could: endanger human health; or bring about an unacceptable change in the composition of the food; or bring about a deterioration in the organoleptic characteristics thereof". These requirements also apply to NC based composites, although this legislation does not address specific provisions for nanomaterials used in food contact materials. The regulation applicable to plastic materials—Regulation (EU) No. 10/201 as well as the Regulation (EC) No. 450/2009 on active and intelligent packaging materials indicate that a specific evaluation is required for substances in nanoform. Nanoparticles mechanisms of mass transfer and interaction with the host materials and with the food may be different from those known at the conventional particle size scale. Therefore, nanoparticles may lead to different exposure and different toxicological properties. Consequently, the pre-market authorisations which are based on the risk assessment of a substance with conventional particle size do not cover the use of the same substance in its nano-dimension which shall only be used if explicitly authorized and mentioned in the positive lists of the above-mentioned regulations [130].

The information relevant for the risk assessment of FCMs containing nanoparticles include three relevant aspects: (i) the characteristics of the nanomaterial used to produce the

material; (ii) the characteristics of the material once it is incorporated into the FCM, as these may differ from the original characteristics, being influenced by the FCM matrix and/or the manufacturing conditions; and, (iii) the characteristics of any nanomaterial that migrates into the food matrix which is influenced by the food environment [131].

Nanoparticles size, shape and aggregation properties, among other factors, may affect the interactions of NC with living cells [132]. The safety of NC in food packaging depends on its transfer into food, which in turn determines the human exposure and on its toxicological profile. Different toxicity testing approaches are recommended to be applicable to nanomaterials depending on their migration behaviour and persistence in the nanoform, namely depending on if it occurs, or not, nanoparticle transformation into the non-nanoform in the food matrix before ingestion, or in the gastrointestinal tract following ingestion [131].

Cellulose and several derivatives are recognized as safe and are already authorized under the European Regulation (EC) No 10/2011 for plastics used in food packaging, for use as polymer additive, production aid and other starting substances. Additionally, for food packaging, cellulose and cellulose acetate butyrate, different alkyl and hydroxyalkyl celluloses are authorised as additives and polymer production aids; and nitrocellulose and lignocellulose are authorised as monomers or other starting substances (Reg 10/2011). However, NC is not specifically listed and therefore it is not currently authorised for food contact applications.

There are few recent studies addressing the toxicity of NC. The endpoints recognised as most important regarding a nanomaterial toxicity are cytotoxicity, (pro-) inflammatory response, potential to generate reactive oxygen species (ROS) and oxidative stress, genotoxicity and integrity of the gastrointestinal barrier [131]. Endes et al. [23] reviewed key studies *in vitro*, *in vivo* and with ecosystem models regarding the biological impact of NC, addressing some of these endpoints. The compiled information revealed some inconsistency in the results achieved, as some studies showed low or no toxicity, while others stress the potential of NC for adverse effects. This was attributed to the variability of the biological systems, test conditions and source of the cellulosic material used, as well as to the lack of thorough characterization of the administered NCs [23]. The physical-chemical characteristics, especially the aggregation level was considered to have a major impact on the results for inflammation. Some of the studies considered in this review, focused the inhalation route [133]–[137] which is of upmost relevance for occupational exposures as nano-sized particles

may be inhaled during composite processing, but not for the use of NC-based composite food packaging.

The effect of NC in the gastrointestinal tract was also addressed. A recent study reported no cytotoxicity on human gut bacteria and gastrointestinal cells after exposure to NFC [138]. In another study, toxicological effects of ingested NC in *in vivo* rat models were considered as non-hazardous when ingested in small quantities [139]. Recently, an *in vivo* tracking (for 21 days) was carried out to assess the potential internalization of BC in the intestine [140]. The authors reported that no intestinal absorption occurred as well as no adverse effects on the gastrointestinal tract. Moreover, the daily BC consumption (for 21 days) had no significant impact in blood biochemistry of Wistar rats [140].

The literature highlights the need for chronic studies to assess long term effects, and the potential detrimental effects of NC on the gut microbiome and absorbance of essential micronutrients. These studies would be of major interest for the application of NC in food packaging systems, where the chronic exposure may arise.

2.2.4.2. Migration

As for the synthetic counterparts, the migration to foods of intentionally added substances from the adjacent polymers and contaminants potentially present on the nanocellulose-based composite, must also be addressed. Besides contaminants and impurities, substances formed during nanocomposite processing, can appear throughout the production chain, when fossil-based, biopolymers and/or active agents are used. The processing of these materials may provide a source of non-intentionally added substances, with potential to migrate to foods upon contact. Potential contaminants from bio-based polymers include: heavy metals, persistent organic chemical contaminants, residues (e.g., pesticides, veterinary medicines), allergens and natural toxins [141]. Chemicals used in the pre-treatment of vegetable NC, by-products and culture media residues of BC are also possible sources for chemical contaminants.

Studies reporting the impact of NC in composites on limiting the migration of components from the polymeric phase have been reported. The effect of incorporating CNC in several plastic films in the overall migration has been studied, particularly for biopolymers, such as PHB, PHBV and PLA. Incorporating CNC on CNC-PHB films significantly reduced the overall migration on both ethanol 10% (v/v) and isooctane simulants [104], [113]. The

incorporation of NFC in PLA (ratio NFC:PLA 1:19) also decreased by 20% the overall migration levels into ethanol 10% [142], [143]. The CNC modification through esterification improved the compatibility with PLA, reducing also the overall migration from the PLA [142]. This effect was observed for low CNC loading. The aforementioned studies showed that the chemical modification of the nanocellulose and the amount incorporated largely influence the migration behaviour. Both factors have an impact on the adhesion between the nanocellulose and the plastic, which may affect the simulant penetration and consequently the migration.

As indicated, these studies focused on overall migration, and as such, characterisation of the migrants was not addressed. The specific migration is an important tool in order to trace potentially toxic substances in the food product, as well as the migration rate of intentionally added substances (for instance, active packaging). The mass transfer of a migrant, from a packaging onto food, occurs mostly through diffusion. The rate of diffusion is highly influenced by food-packaging interactions and external conditions such temperature, migrant concentration (and its solubility) and packaging composition [144]. With the knowledge of food-packaging interactions and environmental conditions along the supply chain, it's possible to foresee the migration rate through modelling. Most migrations models follow the Fick's laws of diffusion, already extensively reviewed [144]–[147].

2.3. Textiles

According to the American Society for Testing and Materials, fibre is defined as any of the various types of matter that form the basic element of a textile, being characterised by having a length of at least one hundred times its diameter [148]. Several naturally occurring fibrous materials are known, as collagen, spider silk and plant cell wall microfibrils [148]. The interest in fibrous materials started with the comprehensive knowledge and utility that textiles provided to our society. Textile is a well-known material, associated to clothing, shelter and basic human physical needs. The high demand of textile products forces the industry to constantly adapt its sources and manufacture [149]. Until the seventeenth century, the most widely used fibres were wool, cotton, silk, hemp and flax. Then, the fibre and yarn production processes were industrialised, with enhanced methods of manufacturing, due to the industrial revolution [148]. During 1900s, the man-made fibres production became an alternative for textiles. Only in the late 1930s synthetic fibres appeared in the textile market [150]. Since mid 1990s they overtook cotton, representing up to 64 % of the global fibre

production in 2021 [151]. The most used synthetic fibre is polyester, with a market share of around 54 % of total global fibre production, followed by Cotton (with 22 % of total global fibre production) [151]. Currently, synthetic fibres have a cost of 1,40-2,00 €/ kg [152].

Both synthetic fibres and cotton production bring about several environmental impacts. Polyester and the raw materials used for its production are non-biodegradable and non- recyclable. In the case of cotton production, huge amounts of land, water, fertilizers and pesticides are required [149]. The lack of resources for cotton production, may reduce its demand and position in the textile market [153]. To fulfil this gap, alternatives for fibre production have been proposed. Figure 2.11 shows the different types of fibres on the textile market.
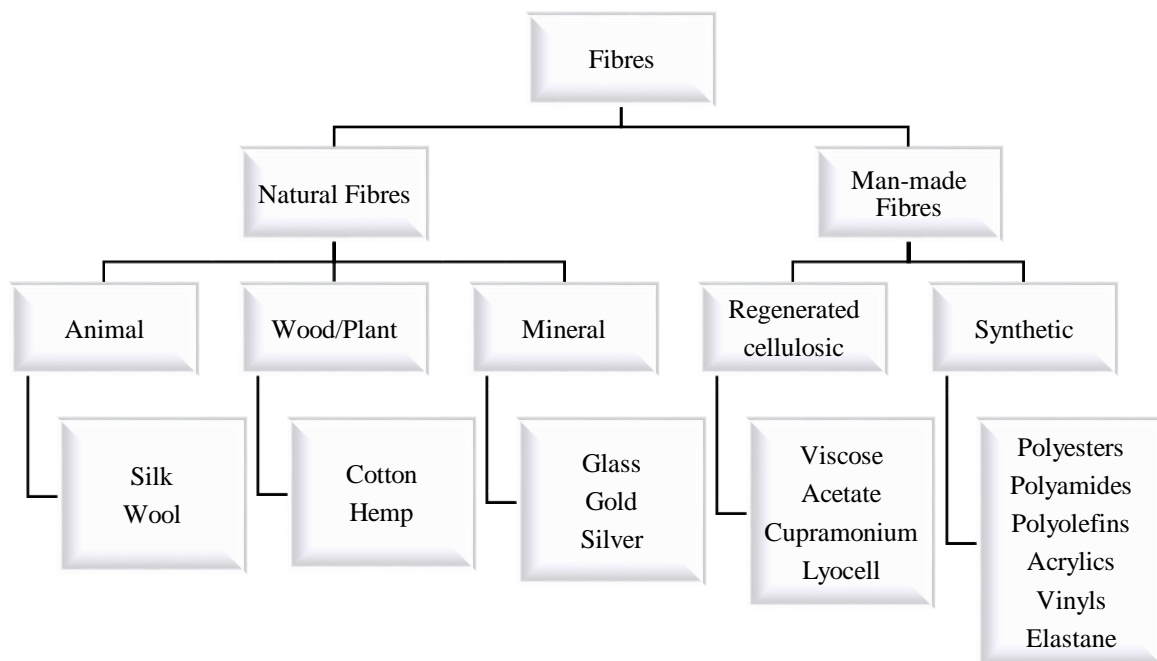
Figure 2.11. Scheme of all types of fibre (adapted from [154])

2.3.1. Regenerated cellulose fibres

For a more sustainable textile production, the demand for natural fibres (cellulosic) have been increasing [155]. However, natural cellulose fibres from vegetable biomass present low mechanical properties due to poor fibre alignment, being not competitive against cotton or synthetic fibres [148]. Cellulose regeneration processes have been developed to overcome these challenges. In short, these processes involve the dissolution of cellulose using organic solvents and spinning of the obtained solution in a regeneration/coagulation bath. This way,

the full molecular alignment of the nanofibres is achieved, which consequently enhance the mechanical properties. Figure 2.12 presents the main regenerated fibres produced for textiles.

Derivatizing processes

Viscose - obtained through the reaction of aged alkali cellulose with carbon disulphide to form cellulose xanthate. Then, cellulose xanthate is regenerated by wet spinning, in a coagulation bath comprising 8-10 % of H_2SO_4, 16-24% $NaSO_4$ and $ZnSO_4$ 1-2%

Modal - fibres produced through viscose process although using beech wood as raw material; developed by Lenzing AG Company

Acetate - produced by acetylating cellulose using acetic anhydride liquid with sulphuric acid as catalyst. The resulting cellulose acetate is dissolved in acetone and spun into fibre through a dry spinning process

Direct dissolution process

Cupro - obtained by dissolving cellulose into cuprammonium solution and then wet spinning to regenerate cellulose.

Lyocell (NMMO) - obtained trough direct dissolution of cellulose with *N*-Methylmorpholine *N*-oxide (NMMO), followed by dry-jet spinning process

Lyocell (ionic solvent) - fibre produced through dry-jet spinning of ionic liquids/cellulose solutions;

LiCL/DMAc - obtained trough dissolution with LiCL/DMAc, followed by wet-sppining; the process uses a low cost solvent but needs a prior activation of the cellulose;

Figure 2.12. Description of the main regenerated fibres on the textile market (adapted from [156])

Among regenerated fibres (Figure 2.12), the processes that involve derivatization of cellulose can be distinguished from those of direct dissolution. Examples of the former include acetate cellulose and viscose, while Cupro, LiCL/DMAc and Lyocell (using NMMO and ionic liquids solvents) are examples of the latter. The main advantage of direct dissolution is that cellulose is dissolved without derivatization of cellulose, thus using less intermediate steps/reagents and contributing for a lower environmental impact on the overall process [156]. Within the scope of this project, Lyocell process will be used, yet the most relevant processes are described briefly below in order to emphasise the main differences.

2.3.1.1.   Acetate cellulose

Acetate cellulose was first produced in commercial scale by Celanese in 1923 [156], with the main aim of producing cigarette filters, for drug delivery use and for textiles. However, cellulose acetate fibres presents certain downsides as poor fibre strength, poor abrasion resistance, and poor thermal retention [157].

2.3.1.2.   Viscose

Viscose is a process (Figure 2.13.) encompassing many steps to convert the solid pulp into a solution [150], [158]. The viscose process begins with an alkalinisation step with NaOH. Afterwards, the shredded alkali cellulose is stored to oxidise (Aging step) [158]. This step allows to reduce the molecular size of cellulose. Then, the alkali cellulose is combined with carbon disulphide (CS_2) to form sodium cellulose xanthate. This step, named xanthation, is the most critical step in viscose process [158]. Thereafter, the sodium cellulose xanthate is dissolved in 5–8% aqueous NaOH to form yellow cellulose xanthate solution, the so-called viscose dope. The solution is ripened for uniform distribution of xanthate groups in cellulose. After the ripening, the viscose dope is filtrated to remove undissolved particles and is de-aerated to remove air bubbles. The viscose fibres are produced using a wet spinning method where the alkaline cellulose solution is extruded through a spinneret into a coagulation bath containing a mixture of acid and salts: sulphuric acid, sodium sulphate and zinc sulphate. In the coagulation bath the cellulose xanthate is converted into cellulose [158]. Currently, carbon disulphide (CS_2) can be reused up to 70% (Figure 2.9), and the remaining 30 % is converted into sulphuric acid (H_2SO_4), to be recycled [159]. However, viscose process is known to cause environmental problems due to the chemicals used. High amounts of sodium hydroxide (NaOH) are used and sodium sulphate is produced as a by-product [160]. The life cycle of the viscose process encompasses other impacts, associated to how reagents are produced and recycled, as well as the consumption of energy and the use of fossil fuel [160].
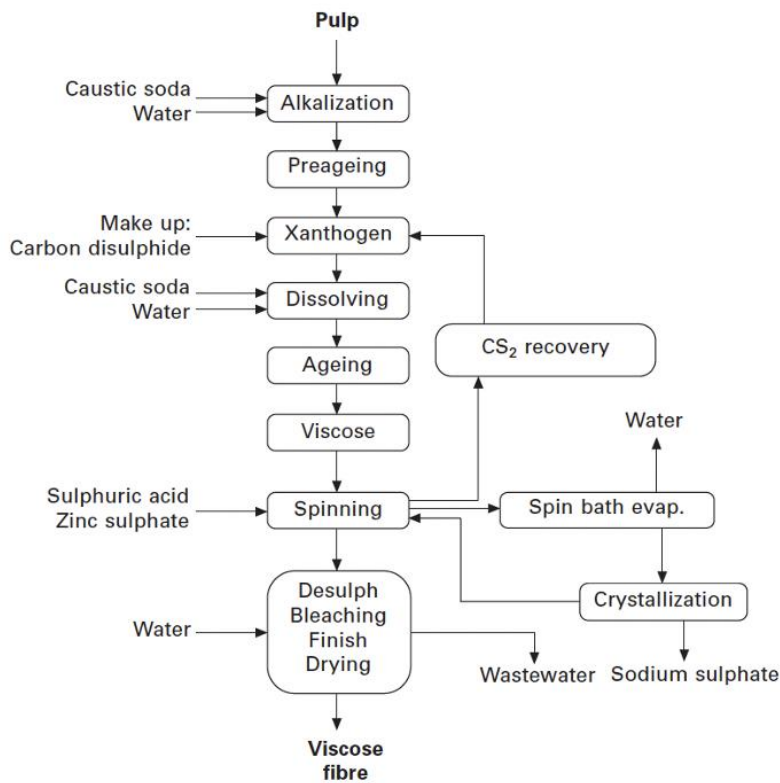
Figure 2.13. Viscose process scheme (from [158])

2.3.1.3. Cupro

Cupro fibre is obtained from the direct dissolution of recycled cotton or wood pulp on cuprammonium solution followed by wet spinning. A combination of copper and ammonium is used as solvent, whereas for fibre regeneration, a caustic soda-based bath is used. This process allows the development of silky smooth like fibres by using linters[161]. However, this processing relies on the use of harmful chemicals (such copper sulphate), which may endanger human health if not disposed properly[161]. Both the solvent and spinning bath may be recycled at some extent. The toxicity of copper salts requires its full recovery, with intensive waste water treatments, which limits the larger scale of cupro[161].

2.3.1.4. LiCL/DMAc

A combination of lithium chloride (LiCL) and dimethylacetamide (DMAc) is used for direct dissolution of cellulose [156]. The common spinning process with LiCL/DMAc cellulose dope is wet-spinning. Before dissolution, the cellulose polymer chains must be activated and

opened into a relaxed conformation in order to facilitate the access of the solvent to the crystalline regions of cellulose molecules. This process can be achieved most effectively by swelling cellulose in a polar medium such as water, followed by adding DMAc at room temperature [156]. As a part of the dissolution mechanism, the Cl^- ion (due to its basicity) interacts with cellulose which is followed by an exchange of DMAc in the lithium coordination sphere by cellulose hydroxyl groups [156]. LiCl/DMAc process exhibits several benefits such the absence of any thermal runaway reactions and high levels of solvent recovery rate during recycling [162]. The need of cellulose activation before dissolution (time consuming and expensive), toxicity, corrosivity and volatility of the solvent are seen as drawbacks of LiCL/DMAc [162], [163].

2.3.1.5.   Lyocell

Lyocell process consists on the direct dissolution of cellulose with N-Methylmorpholine N-oxide (NMMO), and further dry-wet spinning in a coagulation bath (with water) [164], [165]. NMMO is a polar organic solvent that has a great capacity for dissolving cellulose in the monohydrate form (13.3% (m/v) water content) [164], [166]. The excellent dissolving capacity of NMMO is due to its strong N-O dipoles and basicity, making it an excellent hydrogen bond acceptor solvent [164], [166]. Also, NMMO is thermally labile and highly polar [164]. The highly polar N–O bond allows for NMMO to become extremely soluble in water (the high electron density from the oxygen forms hydrogen bonds easily) and the weakness of the bond makes it a strong oxidant [164].

The dissolution process of cellulose includes two stages (Figure 2.14.), swelling and gradual dissolution, where the water originally linked to cellulose is replaced by NMMO [156]. During swelling stage, the NMMO penetrate into amorphous regions of pulp fibre under the osmotic pressure and then enter into the crystalline region of cellulose [167]. In the second stage N-O bonds of the solvent (in monohydrate form) will interact with the hydrogen atom on the hydroxyl group of cellulose and form new hydrogen bonds between NMMO and cellulose, replacing the intermolecular and intramolecular hydrogen bonds in cellulose [156], [164]. The amount of bonded NMMO for each glucose unit is critical in dissolving cellulose, and it was found that on average, nine NMMO molecules for each glucose unit at the cellulose concentration of 7.5 to 10.5% [166].
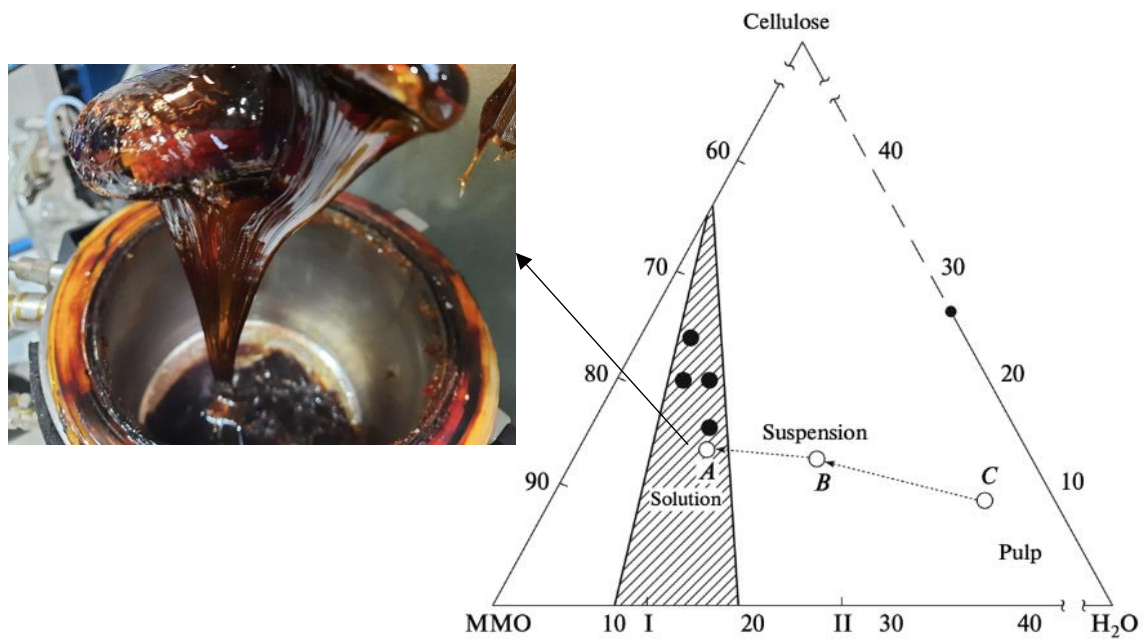
Figure 2.14. Schematic phase diagram of the cellulose–NMMO–H₂O system: (line CBA) variation in the composition of the system during cellulose dissolution via the solid-phase NMMO process (from [168]);

The dissolution of cellulose with NMMO is a complex process, since it depends on several parameters: the amount of cellulose, water and NMMO, the dissolution temperature, the cellulose degree of polymerization and the mechanical agitation during dissolution [165], [169], [170]. High DPs, low temperatures and poor mechanical agitation are known to decrease the dissolution efficiency. Also, too high temperatures (e.g., higher than 120 °C), will cause undesirable loss of NMMO due to degradation [171]. Some stabilizers as isopropyl gallate may be added prior to dissolution to prevent thermal degradation [172]. The chemical structure of NMMO is susceptible to thermal runway reactions due to its cyclic ether as well as N-O constituents hampers the use of redox agents. Despite its complexity, the dissolution zone in the phase diagram (see figure 2.14) is well established at 80 °C for plant-based

celluloses with a DP of 500-600. Lyocell fibres have an average DP of 500-600, higher than viscose (DP of 250 to 350).

Figure 2.15. Lyocell spinning process scheme
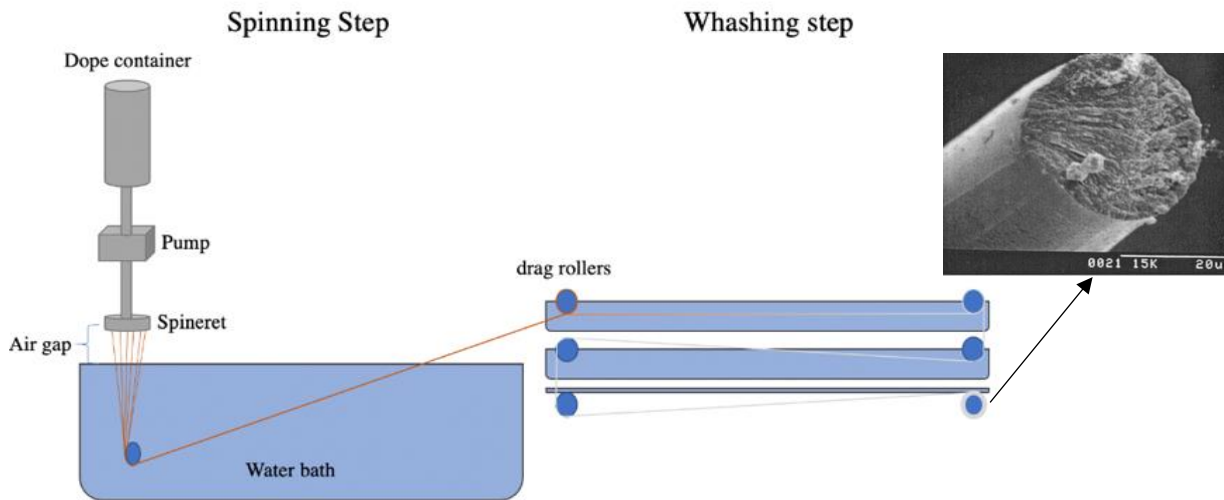
After the cellulose dissolution, the obtained dope is extruded from the spinning nozzle, to an air gap, the formed filament immediately entering into a coagulation bath to regenerate the dissolved cellulose into thin oriented fibres. This process, named dry jet-wet spinning (Figure 2.15), depends highly on the process parameters, particularly the rheological behaviour, air gap, spinning temperature and draw ratio (DR). The elastic behaviour on any dope, allows the spinning using an air gap. This is a critical element of the process as it allows the formation of a highly oriented structure (influences the fibre strength [164]. At optimal air gap and temperature, the increase of take-up speed (rise of DR) leads to superior fibre (at some extent) crystallinity, birefringence, and orientation, thus improving fibre stiffness [164]. It should be pointed out that the high orientation of Lyocell fibres is unique and contributes significantly to the favourable strength of the material. Regardless the orientation achieved, some weaker lateral links between crystallites may lead to fibrillation - fibrous elements exposed at the surface of the fibre under wet abrasion. In the Lyocell process, NMMO solvent may also be recovered (> 99.5% [164], [170]), after treatment with activated carbon, ultrafiltration and evaporation of the water from precipitation bath (Figure 2.15). The recycling process is critical, since NMMO solvent is costly [166]. In order to reduce the cost of mass production of Lyocell, NMMO is usually recovered and reused. Currently, viscose and Lyocell are the most representative processes of regenerated cellulosic fibres, with a 5%

market share in textile fibre production. As viscose, the Lyocell process is already industrialized, and is prone to globally expand in the future.

2.3.1.6.　　　　　Ionic liquids (ILs)

Ionic liquids may be defined as ionised liquids comprising asymmetric and univalent ions (an anion and a cation), whose melting point is below 100°C. Multiple combinations of anions/cations can be used for IL synthesis. These are known to be good solvents of several inorganic and organic materials, which allows the development of composite fibres[153], [173]. The ability of solvation is due to the presence of an anion with high hydrogen bonding basicity (onto hydroxyl groups of the solute) and a cation, which further improves solubility (Figure 2.16) [174].

Cellulose in IL　　　　　Cellulose in IL
(Before Dissolution)　　　　(After Dissolution)
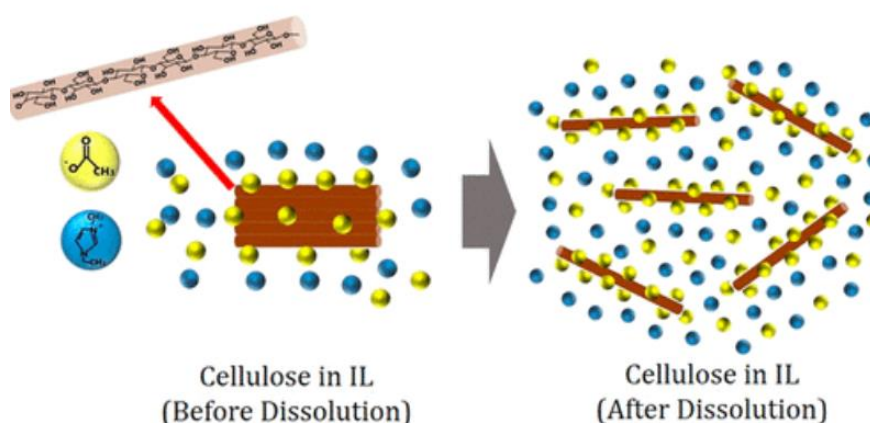
Figure 2.16. Illustration of cellulose dissolution using ILs (from [175])

The wide choice of cations/anions is seen as an advantage, with the possibility to tune its synthesis for specific applications. Additionally, excellent recovery rates are achieved during IL recycling. However, most ILs are too expensive for commercial use, with toxicity and biodegradability issues (depending on the cation/anion used).
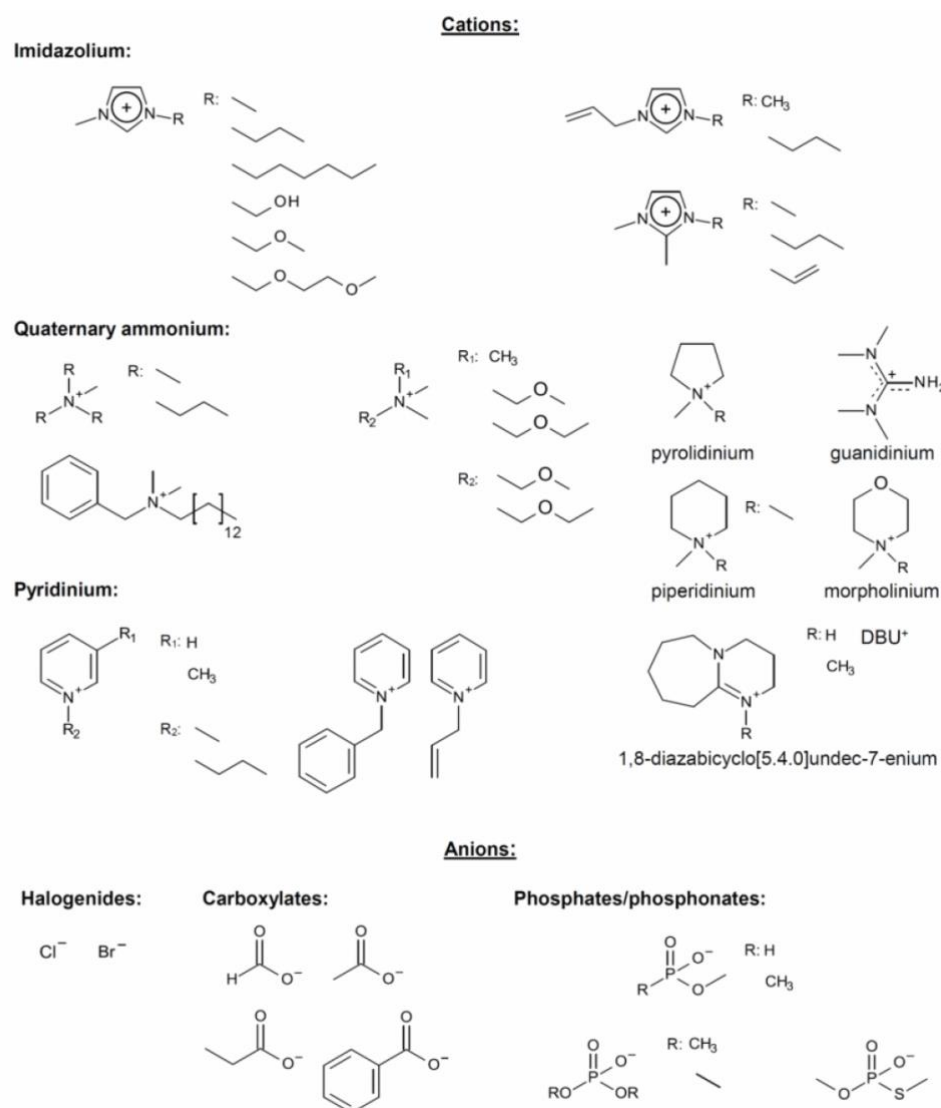
Figure 2.17. Molecular structures of anions and cations of ILs employed as cellulose solvents (from [176])

For cellulose dissolution, a wide combination of cations/anions in ILs were reported (also illustrated in Figure 2.17) [153], [156], [173], [177], [178]. Yet, only a few were used for the development of MMCF. As in Lyocell, dry-wet spinning is used and therefore, the rheological behaviour of the dope is assessed regarding zero-shear viscosity and the viscoelasticity (dynamic moduli). IL based dopes also need a viscoelastic behaviour to withstand the air gap and stretching during spinning. The selection of the IL (as well as cellulose) may influence the rheological and spinning outcome [179]. The resulting ILs based dopes are spun through an air-gap, as in the lyocell process.

The 1-butyl, ethyl or allyl-3-methylimidazolium, such [bmim]Cl, [emim]Cl, [emim]OAc and [amim]Cl were successfully used for fibre spinning [153], [180], [181]. The ones comprising imidazolium and chloride revealed high dissolving capacity and good spinning, although with high melting points [174]. The use of high processing temperatures for dissolution and spinning (higher than 90 °C), led to undesirable cellulose degradation [153]. Furthermore, halides such chloride are known to be corrosive to metal equipment [153], [179]. Non corrosive anion fractions were explored such as acetate. In general, slightly higher viscosities (than NMMO) are obtained with cellulose-ILs solutions, with exception of acetate containing ILs such [emim]OAc and [bmim]OAc. In order to offset the lower viscosity of these acetate containing ILs, high cellulose content was added (up to 20 %m/m) to obtain comparable viscoelastic properties of NMMO and other ILs dopes [180]. As alternative, a non-imidazolium IL such, 1,5-diazabicyclo [4.3.0]non-5-enium acetate ([DBNH][OAc]) was explored for the development of MMCF. The IL [DBNH][OAc] provided a great dissolving capacity (up 17% $m_{cellulose}/m_{dope}$), low melting point (60-80 °C) with low cellulose degradation. Air gap spinning is used for the development of high performing regenerated cellulose fibres. The above-mentioned process is known as Ioncell[®] (Figure 2.18.) and its commercialization is ongoing, with industrialization still to be achieved [182].
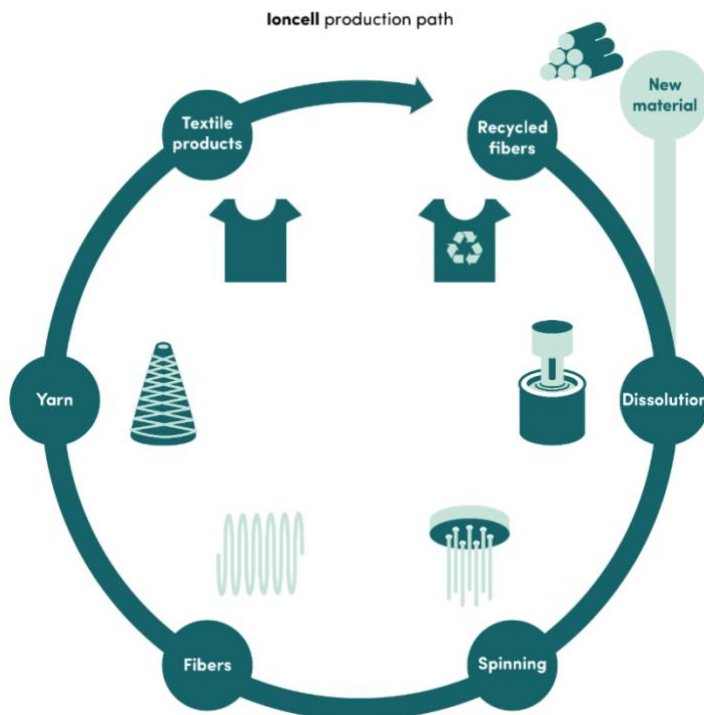
Figure 2.18. Ioncell[®] production path (from [182])

The mechanical performance of synthetic (polyester), natural (cotton) and regenerated cellulose fibres are summarized in the following table.

Table 2.2. Mechanical properties of different textiles fibres

Textile fibres	DP	Linear density (dtex)	Tenacity (cN.tex^{-1})	Elongation (%)	References
Polyester	-	1.15	43-53	44-45	[183]
Cotton	800-1200	0.77-2.56	21-26	7-9	[183]
Viscose	300-450	1.90	18-27	20-25	[183]
Lyocell	550-650	1.3-1.7	42-44	14-16	[183], [184]
Imidazolium ILs	480-1100	0.9-2.2	27-53	8-15	[153]
Ioncell®	1100	1.4-2.0	36-58	9-10	[185]

As observed in Table 2.2, polyester provides outstanding mechanical properties, with high tenacity and elongation, which explains the very high demand for these fibres in the textile industry. Cotton, on the other hand, offers inferior tenacity and elongation despite of the high demand. Regarding MMCF, viscose fibres are the ones with the lowest tenacity yet with the highest elongation (but not comparable to that of synthetic fibres). Lyocell based fibres bears higher stiffness than Viscose and cotton, similar to that of synthetic fibres. The fibres developed from ionic liquids (both imidazolium based and Ioncell®) provided higher variety in the tenacity values yet reaching a maximum of 53 cN.tex^{-1} and 58 cN.tex^{-1} for imidazolium fibres and Ioncell®, respectively. These are the highest values among regenerated cellulose fibres - comparable to synthetic fibres. However, elongation is still rather low if compared to polyester (Table 2.2). In regenerated cellulose fibres, the DP of the resulting fibres, is well correlated to the tenacity of the same fibres. Overall, both Lyocell and Ioncell® are technologies of interest since they provide fibres with great mechanical properties

through sustainable processes (low environmental issues). Lyocell technology is currently an

upscaled process (expanding worldwide) while Ioncell® is near its proof of concept [182].

2.3.2. Textile recycling

The so called fast-fashion is pressuring the textile industry to increase the global fibre production every year. Most of these textiles have a short lifetime, being disposed in landfills, or incinerated. Despite all the environmental impact from the intensive fibre production in the textile industry, the global production of recycled fibre is still rather low (about 9%) [151]. The low recycling rate is explained by the inefficient methods used for textile recycling.

Either synthetic, natural and man-made fibres can be recycled through chemical and mechanical recycling [186]. Mechanical recycling is done by cutting and shredding end-used textile fabrics, to extract fibres to be spun into a yarn or to manufacture non-woven products. During mechanical processing, fibres are shortened, which may hamper their use in yarn open end spinning. Even if the fibres are suitable for yarn spinning, the overall performance should be lower (compared to neat fibres) [186] [187]. For instance, cotton fibres after recycling are blended with virgin cotton fibres, in order to achieve the required performance of a yarn. On the other hand, wool is recycled without any blending. Thermomechanical recycling is used for synthetic fibres, and consists on melting the fibres to be reshaped into other forms. This processing is still not established at industrial level due to high costs related to contaminant removal [186]. Additionally, the resulting recycled fibres have lower quality than the neat synthetic ones and the rate of microplastic release is known to be higher [186].

Another method used in synthetic based textiles fibres is monomer recycling. This chemical-based method lies on the hydrolysis of the polymer into a monomer, to be polymerized again into virgin fibres. An alternative may be polymer recycling, which is widely used on cellulose-based textiles and consists of the cellulose dissolution using the above-mentioned solvents (carbon disulphide, NMMO, IL) (Figure 2.19.).
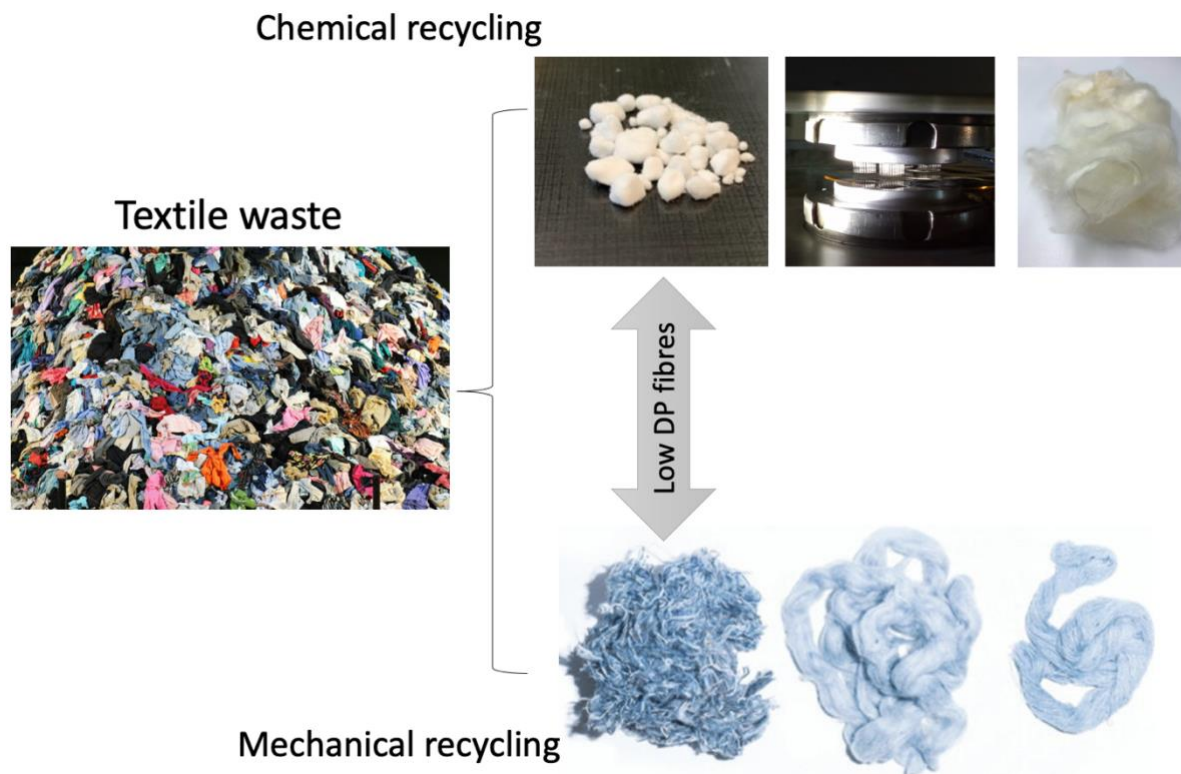
Figure 2.19. Cellulosic waste (textile) scheme

Both Lyocell and Ioncell[®] processes were used to recycle cellulose, with promising results. For instance, cotton waste has been upcycled using lyocell process, already industrialized and commercialized as REFIBRA by Lenzing [188], [189]. The Ioncell[®] process was also effectively used to upcycle hemp waste [187], cotton [190], newspaper [191], paper and cardboard [192] into fibres with the required mechanical performance. The chemical recycling of these post-consumer cellulosic fabrics is complex as significant degradation occurs during their lifetime, due to extensive laundering and usage [193]. As a result, the fibres to be recycled are composed of shortened cellulose chains (low DP), which is unfavourable for lyocell-type spinning technologies. To develop high performing Lyocell based fibres, the cellulose should have an intrinsic viscosity between 400–500 ml.g^{-1} as well as a gaussian like molar mass distribution (well distributed low and high molar mass fractions) [187], [193]. Using cellulose materials with downgraded properties, namely low DP, influences the rheological properties of the spinning solution, thus compromising the fibre structure formation during spinning [193]. To improve the spinning solution behaviour, cellulosic textile

waste may be blended with cellulose containing higher proportions of high molar mass fractions.

2.3.3. BC based nanocomposites for textile industry

As observed on the previous chapters, most studies used plant-based cellulose/nanocellulose for the development of regenerated cellulose fibres. Any of these options succeeded in producing fibres with good mechanical properties, as discussed above. BC has recently been exploited to produce fibre for the textile industry, since this biomaterial comprises long fibres with a high degree of purity. Few studies reported the use of BC fibre in textile making. Chen et al. [194] studied the production of regenerated BC, with or without multi-walled carbon nanotubes (BC/MWCNTs), by dry-wet spinning solutions in LiCL/DMAc and coagulated with ethanol. Well-dispersed and aligned MWCNTs were observed in the cellulose fibres by TEM, showing good adhesion between the BC and MWCNTs in the composite. The mechanical properties were enhanced with the addition of MWCNTs, with a significant increase of the stiffness modulus (up to 38.9 GPa). In another work, BC was dissolved in $NMMO.H_2O$ to produce regenerated fibres. The outcome revealed that whole fibres showed a circular shape with fairly regular size along the fibre axis. The regenerated BC fibres had a cellulose II crystalline structure, lower degree of crystallinity, smaller crystallite sizes, and higher thermal stability than the native BC. Tensile strength and elongation of the regenerated BC fibres was of 5–15 $cN.tex^{-1}$, and 3–8%, respectively [195]. Makarov et al. [196] also produced regenerated BC fibres using NMMO, using a non-conventional process, named solid-phase dissolution. In short, BC is dissolved with NMMO and low contents of water (10% m/m), under higher pressure, high shear rates and at 120°C. The amount of BC dissolved was found to be limited (up to 6% BC), due to high viscosities of the dope. In comparison to plant nanocellulose, low concentrations are used to achieve a good solution with proper viscosity for spinning. Concerning the mechanical performance of the regenerated BC fibre produced, a tensile strength of 47-55 $cN.tex^{-1}$ and elongation at break of 5.5-6.5 % was obtained [196]. More recently, companies like *Nanollose* and HeiQ are exploring BC to develop yarn using Lyocell and Viscose technology [197-198]. Another work studied the regeneration of a composite fibre comprising BC and hydroxypropyl chitosan (HPCS). The solvent for dissolution was also $NMMO.H_2O$ for both BC and HPCS and the resulting solution was extruded by dry-wet spinning. Structure and properties of the composite fibre were characterized in terms of

its morphology, mechanical properties and antibacterial activity. Results revealed that HPCS and BC were homogenously mixed, the fibre composite showed a rough and folded surface morphology and an interior pore structure, as observed analysing the cross-section. Although elongation of the composite fibre was lower than the pure regenerated BC fibre, the tensile strength and modulus was enhanced (an increase up to 50%). In addition, the RBC/HPCS exhibited excellent antibacterial activities against *S. aureus* [199].

Despite the interesting results, the maximum BC concentration (in the dope) did not exceed 8% m/v [196]. In plant celluloses, cellulose concentrations may be as high as 20% m/v. The gap observed is explained by the significant difference between the DP (and molar mass distribution) of BC (up to 2000) and that of plant celluloses used in lyocell and Ioncell® (DP 500-1000). Consequently, BC may require a depolymerization, although it has not yet been demonstrated whether it is indispensable or not. Moreover, BC may play an important role on the chemical recycling of end-of-life fabrics, through the combination of high DP BC with low DP recycled fibres to develop high performing regenerated cellulose fibres.

2.4.   References

[1]   Khalil, H. A., Saurabh, C. K., Syakir, M. I., Fazita, M. N., Bhat, A., Banerjee, A., Fizree, H. M., Rizal, S. & Tahir, P. M. (2019). Barrier properties of biocomposites/hybrid films. In *Mechanical and physical testing of biocomposites, fibre-reinforced composites and hybrid composites* (pp. 241-258). Woodhead Publishing.

[2]   Lee, K. Y., Aitomäki, Y., Berglund, L. A., Oksman, K., & Bismarck, A. (2014). On the use of nanocellulose as reinforcement in polymer matrix composites. *Composites Science and Technology*, *105*, 15-27.

[3]   Fang, Z., Hou, G., Chen, C., & Hu, L. (2019). Nanocellulose-based films and their emerging applications. *Current Opinion in Solid State and Materials Science*, *23*(4), 100764.

[4]   Nunes, T. F. G., Ferreira, P. J., Pujol, P. M., (2014). "Produção, Caracterização e Aplicação de Nanofibras de Celulose." Universidade de Coimbra, Coimbra.

[5]   Bharimalla, A. K., Deshmukh, S. P., Vigneshwaran, N., Patil, P. G., & Prasad, V. (2017). Nanocellulose-polymer composites for applications in food packaging: Current status, future prospects and challenges. *Polymer-Plastics Technology and Engineering*, *56*(8),

805-823.

[6]   de Amorim, J. D. P., de Souza, K. C., Duarte, C. R., da Silva Duarte, I., de Assis Sales Ribeiro, F., Silva, G. S., Farias, P. M., Stingl, A., Costa, A. F. S., Vinhas, G. M. & Sarubbo, L. A. (2020). Plant and bacterial nanocellulose: Production, properties and applications in medicine, food, cosmetics, electronics and engineering. A review. *Environmental Chemistry Letters*, *18*, 851-869.

[7]   Saito, T., Kimura, S., Nishiyama, Y., & Isogai, A. (2007). Cellulose nanofibers prepared by TEMPO-mediated oxidation of native cellulose. *Biomacromolecules*, *8*(8), 2485-2491.

[8]   Anžlovar, A., Kunaver, M., Krajnc, A., & Žagar, E. (2018). Nanocomposites of LLDPE and surface-modified cellulose nanocrystals prepared by melt processing. *Molecules*, *23*(7), 1782.

[9]   Torres, F. G., Arroyo, J. J., & Troncoso, O. P. (2019). Bacterial cellulose nanocomposites: An all-nano type of material. *Materials Science and Engineering: C*, *98*, 1277-1293.

[10]   Jozala, A. F., de Lencastre-Novaes, L. C., Lopes, A. M., de Carvalho Santos-Ebinuma, V., Mazzola, P. G., Pessoa-Jr, A., Grotto, D., Gerenutti, M., & Chaud, M. V. (2016). Bacterial nanocellulose production and application: a 10-year overview. *Applied microbiology and biotechnology*, *100*, 2063-2072.

[11]   Kurosumi, A., Sasaki, C., Yamashita, Y., & Nakamura, Y. (2009). Utilization of various fruit juices as carbon source for production of bacterial cellulose by Acetobacter xylinum NBRC 13693. *Carbohydrate Polymers*, *76*(2), 333-335.

[12]   Lin, D., Lopez-Sanchez, P., Li, R., & Li, Z. (2014). Production of bacterial cellulose by Gluconacetobacter hansenii CGMCC 3917 using only waste beer yeast as nutrient source. *Bioresource Technology*, *151*, 113-119.

[13]   Bilgi, E., Bayir, E., Sendemir-Urkmez, A., & Hames, E. E. (2016). Optimization of bacterial cellulose production by Gluconacetobacter xylinus using carob and haricot bean. *International journal of biological macromolecules*, *90*, 2-10.

[14]   Soares da Silva, F. A., Fernandes, M., Souto, A. P., Ferreira, E. C., Dourado, F., & Gama, M. (2019). Optimization of bacterial nanocellulose fermentation using recycled paper sludge and development of novel composites. *Applied Microbiology and Biotechnology, 103*, 9143-9154.

[15]   Rodrigues, A. C., Fontão, A. I., Coelho, A., Leal, M., da Silva, F. A. S., Wan, Y., Dourado, F., & Gama, M. (2019). Response surface statistical optimization of bacterial

nanocellulose fermentation in static culture using a low-cost medium. *New Biotechnology*, *49*, 19-27.

[16] Ng, H. M., Sin, L. T., Bee, S. T., Tee, T. T., & Rahmat, A. R. (2017). Review of nanocellulose polymer composite characteristics and challenges. *Polymer-Plastics Technology and Engineering*, *56* (7), 687-731.

[17] Oksman, K., Aitomäki, Y., Mathew, A. P., Siqueira, G., Zhou, Q., Butylina, S., Tanpichai, S., Zhou, X., & Hooshmand, S. (2016). Review of the recent developments in cellulose nanocomposite processing. *Composites Part A: Applied Science and Manufacturing*, *83*, 2-18.

[18] Soykeabkaew, N., Tawichai, N., Thanomsilp, C., & Suwantong, O. (2017). Nanocellulose-reinforced "green" composite materials. *Walailak Journal of Science and Technology (WJST)*, *14*(5), 353-368.

[19] George, J., Sreekala, M. S., & Thomas, S. (2001). A review on interface modification and characterization of natural fiber reinforced plastic composites. *Polymer Engineering & Science*, *41*(9), 1471-1485.

[20] Mondal, S. (2018). Review on nanocellulose polymer nanocomposites. *Polymer-Plastics Technology and Engineering*, *57*(13), 1377-1391.

[21] Shah, N., Ul-Islam, M., Khattak, W. A., & Park, J. K. (2013). Overview of bacterial cellulose composites: a multipurpose advanced material. *Carbohydrate polymers*, *98*(2), 1585-1598.

[22] Zhang, Q., Zhang, L., Wu, W., & Xiao, H. (2020). Methods and applications of nanocellulose loaded with inorganic nanomaterials: A review. *Carbohydrate polymers*, *229*, 115454.

[23] Endes, C., Camarero-Espinosa, S., Mueller, S., Foster, E. J., Petri-Fink, A., Rothen-Rutishauser, B., Weder, C., & Clift, M. J. D. (2016). A critical review of the current knowledge regarding the biological impact of nanocellulose. *Journal of nanobiotechnology*, *14* (1), 1-14.

[24] Serpa, A., Velásquez-Cock, J., Gañán, P., Castro, C., Vélez, L., & Zuluaga, R. (2016). Vegetable nanocellulose in food science: A review. *Food Hydrocolloids*, *57*, 178-186.

[25] Huang, J., Dufresne, A., & Lin, N. (Eds.) (2019). Nanocellulose: from fundamentals to advanced materials. John Wiley & Sons.

[26] Sangroniz, A., Zhu, J. B., Tang, X., Etxeberria, A., Chen, E. Y. X., & Sardon, H. (2019).

Packaging materials with desired mechanical and barrier properties and full chemical recyclability. *Nature Communications*, *10* (1), 3559.

[27] Geyer, R., Jambeck, J. R., & Law, K. L. (2017). Production, use, and fate of all plastics ever made. *Science advances*, *3*(7), e1700782.

[28] de Souza Machado, A. A., Kloas, W., Zarfl, C., Hempel, S., & Rillig, M. C. (2018). Microplastics as an emerging threat to terrestrial ecosystems. *Global change biology*, *24*(4), 1405-1416.

[29] European Council, "Directive (Eu) 2019/904 of the European Parliament and of the Council of 5 June 2019 on the reduction of the impact of certain plastic products on the environment," *Www.Plasticseurope.De*, vol. 2019, no. March, pp. 1–19, 2019.

[30] European Parliament and Council, "Directive (EU) 2018/852 of the European Parliament and of the Council of 30 May 2018 amending Directive 94/62/EC on packaging and packaging waste," *Off. J. Eur. Union*, vol. 2018, no. November 2008, pp. 141–154, 2018.

[31] European Statistics-Eurostat, *Energy, transport and environment statistics 2020 edition*. 2020.

[32] Wang, J., Gardner, D. J., Stark, N. M., Bousfield, D. W., Tajvidi, M., & Cai, Z. (2018). Moisture and oxygen barrier properties of cellulose nanomaterial-based films. *ACS Sustainable Chemistry & Engineering*, *6*(1), 49-70.

[33] Langowski, H. C. (2017). Shelf life of packed food and packaging functionality. In *Food Packaging Materials* (pp. 11-66). CRC Press.

[34] Paunonen, S. I. (2013) "Strength and barrier enhancements of cellophane and cellulose derivative films: A review," *BioResources*, 8(2),3098–3121.

[35] Sharma, A., Thakur, M., Bhattacharya, M., Mandal, T., & Goswami, S. (2019). Commercial application of cellulose nano-composites–A review. *Biotechnology Reports*, *21*, e00316.

[36] Vilarinho, F., Sanches Silva, A., Vaz, M. F., & Farinha, J. P. (2018). Nanocellulose in green food packaging. *Critical reviews in food science and nutrition*, *58*(9), 1526-1537.

[37] Tibola, H., Czaikoski, A., Pelissari, F. C., & Menegalli, R. L., (2020) "Starch-based nanocomposites with cellulose nanofibres obtained from chemical and mechanical treatments," *Science Total Environment*, 137683.

[38] Bugnicourt, E., Cinelli, P., Lazzeri, A., & Alvarez, V. A. (2014). Polyhydroxyalkanoate (PHA): Review of synthesis, characteristics, processing and potential applications in

packaging. *Express Polymer Letter*, 8 (11), 791–808.

[39]   Tan, G. Y. A., Chen, C. L., Li, L., Ge, L., Wang, L., Razaad, I. M. N., Li, Y., Zhao, L., Mo, Y., & Wang, J. Y. (2014). Start a research on biopolymer polyhydroxyalkanoate (PHA): a review. *Polymers*, *6*(3), 706-754.

[40]   Mangaraj, S., Goswami, T. K., & Mahajan, P. V. (2009). Applications of plastic films for modified atmosphere packaging of fruits and vegetables: a review. *Food Engineering Reviews*, *1*, 133-158.

[41]   Ferrer, A., Pal, L., & Hubbe, M. (2017). Nanocellulose in packaging: Advances in barrier layer technologies. *Industrial Crops and Products*, *95*, 574-582.

[42]   Fabra, M. J., Lopez-Rubio, A., & Lagaron, J. M. (2014). Nanostructured interlayers of zein to improve the barrier properties of high barrier polyhydroxyalkanoates and other polyesters. *Journal of Food Engineering*, *127*, 1-9.

[43]   Mohsen, A. H., & Ali, N. A. (2018). Mechanical, color and barrier, properties of biodegradable nanocomposites polylactic acid/nanoclay. *J. Bioremediat. Biodegrad*, *9* (6).

[44]   Díez-Pascual, A. M., & Díez-Vicente, A. L. (2014). Poly (3-hydroxybutyrate)/ZnO bionanocomposites with improved mechanical, barrier and antibacterial properties. *International journal of molecular sciences*, *15*(6), 10950-10973.

[45]   Visanko, M., Liimatainen, H., Sirviö, J. A., Mikkonen, K. S., Tenkanen, M., Sliz, R., Hormi, O., & Niinimäki, J. (2015). Butylamino-functionalized cellulose nanocrystal films: Barrier properties and mechanical strength. *RSC Advances*, *5*(20), 15140-15146.

[46]   Maes, C., Luyten, W., Herremans, G., Peeters, R., Carleer, R., & Buntinx, M. (2018). Recent updates on the barrier properties of ethylene vinyl alcohol copolymer (EVOH): A review. *Polymer Reviews*, *58*(2), 209-246.

[47]   Bastarrachea, L., Dhawan, S., & Sablani, S. S. (2011). Engineering properties of polymeric-based antimicrobial films for food packaging: a review. *Food Engineering Reviews*, *3*, 79-93.

[48]   Pelissari, F. M., Ferreira, D. C., Louzada, L. B., dos Santos, F., Corrêa, A. C., Moreira, F. K. V., & Mattoso, L. H. (2019). Starch-based edible films and coatings: An eco-friendly alternative for food packaging. *Starches for food application*, 359-420.

[49]   Plackett, D. (Ed.). (2011). *Biopolymers: new materials for sustainable films and coatings*. John Wiley & Sons.

[50]   P. Shan Teo and W. Shyang Chow, "Water Vapour Permeability of Poly(lactic acid)/Chitosan Binary and Ternary Blends," *KMUTNB Int. J. Appl. Sci. Technol.*, vol. 7, no. 1, pp. 23–27, 2014.

[51]   Espino-Pérez, E., Bras, J., Ducruet, V., Guinault, A., Dufresne, A., & Domenek, S. (2013). Influence of chemical surface modification of cellulose nanowhiskers on thermal, mechanical, and barrier properties of poly (lactide) based bionanocomposites. *European Polymer Journal*, *49* (10), 3144-3154.

[52]   Ruka, D. R., Simon, G. P., & Dean, K. M. (2013). In situ modifications to bacterial cellulose with the water insoluble polymer poly-3-hydroxybutyrate. *Carbohydrate polymers*, *92* (2), 1717-1723.

[53]   Lee, H., You, J., Jin, H. J., & Kwak, H. W. (2020). Chemical and physical reinforcement behavior of dialdehyde nanocellulose in PVA composite film: A comparison of nanofiber and nanocrystal. *Carbohydrate polymers*, *232*, 115771.

[54]   Vartiainen, J., Lahtinen, P., Kaljunen, T., Kunnari, V., Peresin, M. S., & Tammelin, T., (2015) Comparison of properties between cellulose nanofibrils made from Banana, Sugar Beet, Hemp, Softwood and Hardwood Pulps. *O Pap.*, 76(3), 57–60.

[55]   Piringer, O. G., & Baner, A. L. (2000). Permeation of gases, water vapor and volatile organic compounds. *Plastic Packaging Materials for Food: Barrier Function, Mass Transport, Quality Assurance and Legislation*, 239-243.

[56]   Bharimalla, A. K., Patil, P. G., Mukherjee, S., Yadav, V., & Prasad, V. (2019). Nanocellulose-polymer composites: novel materials for food packaging applications. *Polymers for agri-food applications*, 553-599.

[57]   Aulin, C., Salazar-Alvarez, G., & Lindström, T. (2012). High strength, flexible and transparent nanofibrillated cellulose–nanoclay biohybrid films with tunable oxygen and water vapor permeability. *Nanoscale*, *4*(20), 6622-6628.

[58]   Alves, J. S., Dos Reis, K. C., Menezes, E. G. T., Pereira, F. V., & Pereira, J. (2015). Effect of cellulose nanocrystals and gelatin in corn starch plasticized films. *Carbohydrate polymers*, *115*, 215-222.

[59]   Panaitescu, D. M., Frone, A. N., Chiulan, I., Gabor, R. A., Spataru, I. C., & Căşărică, A. (2017). Biocomposites from polylactic acid and bacterial cellulose nanofibers obtained by mechanical treatment. *BioResources*, *12*(1), 662-672.

[60]   Gumel, A. M., & Annuar, M. S. M. (2014). Nanocomposites of polyhydroxyalkanoates

(PHAs). *Polyhydroxyalkanoate (PHA) Based Blends, Composites and Nanocomposites*, 98-118.

[61]   Montero, B., Rico, M., Rodríguez-Llamazares, S., Barral, L., & Bouza, R. (2017). Effect of nanocellulose as a filler on biodegradable thermoplastic starch films from tuber, cereal and legume. *Carbohydrate polymers*, *157*, 1094-1104.

[62]   Ten, E., Turtle, J., Bahr, D., Jiang, L., & Wolcott, M. (2010). Thermal and mechanical properties of poly (3-hydroxybutyrate-co-3-hydroxyvalerate)/cellulose nanowhiskers composites. *Polymer*, *51*(12), 2652-2660.

[63]   S. O. Patrício, P., Pereira, F. V., dos Santos, M. C., de Souza, P. P., Roa, J. P., & Orefice, R. L. (2013). Increasing the elongation at break of polyhydroxybutyrate biopolymer: Effect of cellulose nanowhiskers on mechanical and thermal properties. *Journal of Applied Polymer Science*, *127*(5), 3613-3621.

[64]   Slavutsky, A. M., & Bertuzzi, M. A. (2014). Water barrier properties of starch films reinforced with cellulose nanocrystals obtained from sugarcane bagasse. *Carbohydrate polymers*, *110*, 53-61.

[65]   Martins, I. M., Magina, S. P., Oliveira, L., Freire, C. S., Silvestre, A. J., Neto, C. P., & Gandini, A. (2009). New biocomposites based on thermoplastic starch and bacterial cellulose. *Composites Science and Technology*, *69*(13), 2163-2168.

[66]   Wan, Y. Z., Luo, H., He, F., Liang, H., Huang, Y., & Li, X. L. (2009). Mechanical, moisture absorption, and biodegradation behaviours of bacterial cellulose fibre-reinforced starch biocomposites. *Composites Science and Technology*, *69*(7-8), 1212-1217.

[67]   Savadekar, N. R., & Mhaske, S. T. (2012). Synthesis of nano cellulose fibers and effect on thermoplastics starch based films. *Carbohydrate Polymers*, *89*(1), 146-151.

[68]   Soykeabkaew, N., Laosat, N., Ngaokla, A., Yodsuwan, N., & Tunkasiri, T. (2012). Reinforcing potential of micro-and nano-sized fibers in the starch-based biocomposites. *Composites Science and Technology*, *72*(7), 845-852.

[69]   Hietala, M., Mathew, A. P., & Oksman, K. (2013). Bionanocomposites of thermoplastic starch and cellulose nanofibers manufactured using twin-screw extrusion. *European Polymer Journal*, *49*(4), 950-956.

[70]   Azeredo, H. M., Rosa, M. F., & Mattoso, L. H. C. (2017). Nanocellulose in bio-based food packaging applications. *Industrial Crops and Products*, *97*, 664-671.

[71]   Gama, M., Dourado, F., & Bielecki, S. (Eds.). (2016). *Bacterial nanocellulose: from*

biotechnology to bio-economy. Elsevier.

[72] Padrao, J., Gonçalves, S., Silva, J. P., Sencadas, V., Lanceros-Méndez, S., Pinheiro, A. C., Vicente, A. C., Rodrigues, L. R. & Dourado, F. (2016). Bacterial cellulose-lactoferrin as an antimicrobial edible packaging. *Food Hydrocolloids*, *58*, 126-140.

[73] Jipa, I. M., Stoica-Guzun, A., & Stroescu, M. (2012). Controlled release of sorbic acid from bacterial cellulose based mono and multilayer antimicrobial films. *LWT*, *47*(2), 400-406.

[74] Wahid, F., Duan, Y. X., Hu, X. H., Chu, L. Q., Jia, S. R., Cui, J. D., & Zhong, C. (2019). A facile construction of bacterial cellulose/ZnO nanocomposite films and their photocatalytic and antibacterial properties. *International journal of biological macromolecules*, *132*, 692-700.

[75] Kuswandi, B., Jayus, Oktaviana, R., Abdullah, A., & Heng, L. Y. (2014). A novel on-package sticker sensor based on methyl red for real-time monitoring of broiler chicken cut freshness. *Packaging technology and science*, *27*(1), 69-81.

[76] Pourjavaher, S., Almasi, H., Meshkini, S., Pirsa, S., & Parandi, E. (2017). Development of a colorimetric pH indicator based on bacterial cellulose nanofibers and red cabbage (Brassica oleraceae) extract. *Carbohydrate polymers*, *156*, 193-201.

[77] Moradi, M., Tajik, H., Almasi, H., Forough, M., & Ezati, P. (2019). A novel pH-sensing indicator based on bacterial cellulose nanofibers and black carrot anthocyanins for monitoring fish freshness. *Carbohydrate Polymers*, *222*, 115030.

[78] Liu, H., Shi, C., Sun, X., Zhang, J., & Ji, Z. (2021). Intelligent colorimetric indicator film based on bacterial cellulose and pelargonidin dye to indicate the freshness of tilapia fillets. *Food Packaging and Shelf Life*, *29*, 100712.

[79] Hubbe, M. A., Ferrer, A., Tyagi, P., Yin, Y., Salas, C., Pal, L., & Rojas, O. J. (2017). Nanocellulose in thin films, coatings, and plies for packaging applications: A review. *BioResources*, *12*(1), 2143-2233.

[80] Kumar, V., Elfving, A., Koivula, H., Bousfield, D., & Toivakka, M. (2016). Roll-to-roll processed cellulose nanofiber coatings. *Industrial & Engineering Chemistry Research*, *55*(12), 3603-3613.

[81] Anukiruthika, T., Sethupathy, P., Wilson, A., Kashampur, K., Moses, J. A., & Anandharamakrishnan, C. (2020). Multilayer packaging: Advances in preparation techniques and emerging food applications. *Comprehensive Reviews in Food Science*

and Food Safety, *19*(3), 1156-1186.

[82]   Amini, E., Azadfallah, M., Layeghi, M., & Talaei-Hassanloui, R. (2016). Silver-nanoparticle-impregnated cellulose nanofiber coating for packaging paper. *Cellulose*, *23*, 557-570.

[83]   Mascheroni, E., Rampazzo, R., Ortenzi, M. A., Piva, G., Bonetti, S., & Piergiovanni, L. (2016). Comparison of cellulose nanocrystals obtained by sulfuric acid hydrolysis and ammonium persulfate, to be used as coating on flexible food-packaging materials. *Cellulose*, *23*, 779-793.

[84]   Bideau, B., Loranger, E., & Daneault, C. (2018). Nanocellulose-polypyrrole-coated paperboard for food packaging application. *Progress in Organic Coatings*, *123*, 128-133.

[85]   Tyagi, N., & Suresh, S. (2016). Production of cellulose from sugarcane molasses using Gluconacetobacter intermedius SNT-1: optimization & characterization. *Journal of Cleaner Production*, *112*, 71-80.

[86]   Koppolu, R., Lahti, J., Abitbol, T., Swerin, A., Kuusipalo, J., & Toivakka, M. (2019). Continuous processing of nanocellulose and polylactic acid into multilayer barrier coatings. *ACS applied materials & interfaces*, *11*(12), 11920-11927.

[87]   Meriçer, Ç., Minelli, M., De Angelis, M. G., Baschetti, M. G., Stancampiano, A., Laurita, R., ... & Lindström, T. (2016). Atmospheric plasma assisted PLA/microfibrillated cellulose (MFC) multilayer biocomposite for sustainable barrier application. *Industrial Crops and Products*, *93*, 235-243.

[88]   Vähä-Nissi, M., Koivula, H. M., Räisänen, H. M., Vartiainen, J., Ragni, P., Kenttä, E., ... & Harlin, A. (2017). Cellulose nanofibrils in biobased multilayer films for food packaging. *Journal of Applied Polymer Science*, *134* (19).

[89]   Moreira, J. B., Morais, M. G., Morais, E. G., Silva Vaz, B. & Costa, J. A. V., (2018) Chapter 14 - Electrospun Polymeric Nanofibers in Food Packaging, in *Impact of Nanoscience in the Food Industry*, Grumezescu, A. M., & Holban, A. M., (Eds.) Academic Press, 387–417.

[90]   Kai, D., Liow, S. S., & Loh, X. J. (2014). Biodegradable polymers for electrospinning: Towards biomedical applications. *Materials Science and Engineering: C*, *45*, 659-670.

[91]   Zhao, L., Duan, G., Zhang, G., Yang, H., He, S., & Jiang, S. (2020). Electrospun functional materials toward food packaging applications: A review. *Nanomaterials*, *10*(1), 150.

[92]   Martínez-Sanz, M., Lopez-Rubio, A., Villano, M., Oliveira, C. S., Majone, M., Reis, M., &

Lagaron, J. M. (2016). Production of bacterial nanobiocomposites of polyhydroxyalkanoates derived from waste and bacterial nanocellulose by the electrospinning enabling melt compounding method. *Journal of Applied Polymer Science*, *133*(2).

[93]   Cherpinski, A., Torres-Giner, S., Vartiainen, J., Peresin, M. S., Lahtinen, P., & Lagaron, J. M. (2018). Improving the water resistance of nanocellulose-based films with polyhydroxyalkanoates processed by the electrospinning coating technique. *Cellulose*, *25*, 1291-1307.

[94]   Gitari, B., Chang, B. P., Misra, M., Navabi, A., & Mohanty, A. K. (2019). A comparative study on the mechanical, thermal, and water barrier properties of PLA nanocomposite films prepared with bacterial nanocellulose and cellulose nanofibrils. *BioResources*, *14*(1), 1867-1889.

[95]   Abdulkhani, A., Hosseinzadeh, J., Ashori, A., Dadashi, S., & Takzare, Z. (2014). Preparation and characterization of modified cellulose nanofibers reinforced polylactic acid nanocomposite. *Polymer testing*, *35*, 73-79.

[96]   Arrieta, M. P., Fortunati, E., Dominici, F., López, J., & Kenny, J. M. (2015). Bionanocomposite films based on plasticized PLA–PHB/cellulose nanocrystal blends. *Carbohydrate polymers*, *121*, 265-275.

[97]   Seoane, I. T., Cerrutti, P., Vázquez, A., Manfredi, L. B., & Cyras, V. P. (2017). Polyhydroxybutyrate-based nanocomposites with cellulose nanocrystals and bacterial cellulose. *Journal of Polymers and the Environment*, *25*, 586-598.

[98]   Espino-Pérez, E., Bras, J., Almeida, G., Plessis, C., Belgacem, N., Perré, P., & Domenek, S. (2018). Designed cellulose nanocrystal surface properties for improving barrier properties in polylactide nanocomposites. *Carbohydrate polymers*, *183*, 267-277.

[99]   Osterberg, M., Vartiainen, J., Lucenius, J., Hippi, U., Seppälä, J., Serimaa, R., & Laine, J. (2013). A fast method to produce strong NFC films as a platform for barrier and functional materials. *ACS applied materials & interfaces*, *5*(11), 4640-4647.

[100]   Ramezani, H., Behzad, T., & Bagheri, R. (2020). Synergistic effect of graphene oxide nanoplatelets and cellulose nanofibers on mechanical, thermal, and barrier properties of thermoplastic starch. *Polymers for Advanced Technologies*, *31*(3), 553-565.

[101]   González, K., Retegi, A., González, A., Eceiza, A., & Gabilondo, N. (2015). Starch and cellulose nanocrystals together into thermoplastic starch

bionanocomposites. *Carbohydrate polymers*, *117*, 83-90.

[102] Jung, B. N., Jung, H. W., Kang, D. H., Kim, G. H., Lee, M., Shim, J. K., & Hwang, S. W. (2020). The fabrication of flexible and oxygen barrier cellulose nanofiber/polylactic acid nanocomposites using cosolvent system. *Journal of Applied Polymer Science*, *137*(47), 49536.

[103] Ambrosio-Martín, J., Fabra, M. J., Lopez-Rubio, A., & Lagaron, J. M. (2015). Melt polycondensation to improve the dispersion of bacterial cellulose into polylactide via melt compounding: enhanced barrier and mechanical properties. *Cellulose*, *22*, 1201-1226.

[104] Dhar, P., Bhardwaj, U., Kumar, A., & Katiyar, V. (2015). Poly (3-hydroxybutyrate)/cellulose nanocrystal films for food packaging applications: Barrier and migration studies. *Polymer Engineering & Science*, *55*(10), 2388-2395.

[105] Marais, A., Utsel, S., Gustafsson, E., & Wågberg, L. (2014). Towards a super-strainable paper using the Layer-by-Layer technique. *Carbohydrate polymers*, *100*, 218-224.

[106] Grande, C. J., Torres, F. G., Gomez, C. M., Troncoso, O. P., Canet-Ferrer, J., & Martínez-Pastor, J. (2009). Development of self-assembled bacterial cellulose–starch nanocomposites. *Materials Science and Engineering: C*, *29*(4), 1098-1104.

[107] Vilela, C., Kurek, M., Hayouka, Z., Röcker, B., Yildirim, S., Antunes, M. D. C., Nilsen-Nygaard, J., Pettersen, M. K., & Freire, C. S. (2018). A concise guide to active agents for active food packaging. *Trends in Food Science & Technology*, *80*, 212-222.

[108] Farooq, A., Patoary, M. K., Zhang, M., Mussana, H., Li, M., Naeem, M. A., Mushtaq, M., Farooq, A., & Liu, L. (2020). Cellulose from sources to nanocellulose and an overview of synthesis and properties of nanocellulose/zinc oxide nanocomposite materials. *International journal of biological macromolecules*, *154*, 1050-1073.

[109] Tsai, Y. H., Yang, Y. N., Ho, Y. C., Tsai, M. L., & Mi, F. L. (2018). Drug release and antioxidant/antibacterial activities of silymarin-zein nanoparticle/bacterial cellulose nanofiber composite films. *Carbohydrate Polymers*, *180*, 286-296.

[110] Moreirinha, C., Vilela, C., Silva, N. H., Pinto, R. J., Almeida, A., Rocha, M. A. M., Coelho, E., Coimbra, M. A., Silvestre, A. J. D., & Freire, C. S. (2020). Antioxidant and antimicrobial films based on brewers spent grain arabinoxylans, nanocellulose and feruloylated compounds for active packaging. *Food Hydrocolloids*, *108*, 105836.

[111] Missio, A. L., Mattos, B. D., Ferreira, D. D. F., Magalhães, W. L., Bertuol, D. A., Gatto, D.

A., Petutschnigg, A., & Tondi, G. (2018). Nanocellulose-tannin films: From trees to sustainable active packaging. *Journal of Cleaner Production*, *184*, 143-151.

[112]   El-Wakil, N. A., Hassan, E. A., Abou-Zeid, R. E., & Dufresne, A. (2015). Development of wheat gluten/nanocellulose/titanium dioxide nanocomposites for active food packaging. *Carbohydrate polymers*, *124*, 337-346.

[113]   Zhang, H., Yu, H. Y., Wang, C., & Yao, J. (2017). Effect of silver contents in cellulose nanocrystal/silver nanohybrids on PHBV crystallization and property improvements. *Carbohydrate polymers*, *173*, 7-16.

[114]   Dincă, V., Mocanu, A., Isopencu, G., Busuioc, C., Brajnicov, S., Vlad, A., Icriverzi, I., Roseanu, A., Dinescu M., Stroescu, M., Stoica-Guzun, A., & Suchea, M. (2020). Biocompatible pure ZnO nanoparticles-3D bacterial cellulose biointerfaces with antibacterial properties. *Arabian Journal of Chemistry*, *13*(1), 3521-3533.

[115]   Pirsa, S., Shamusi, T., & Kia, E. M. (2018). Smart films based on bacterial cellulose nanofibers modified by conductive polypyrrole and zinc oxide nanoparticles. *Journal of Applied Polymer Science*, *135*(34), 46617.

[116]   Mocanu, A., Isopencu, G., Busuioc, C., Popa, O. M., Dietrich, P., & Socaciu-Siebert, L. (2019). Bacterial cellulose films with ZnO nanoparticles and propolis extracts: Synergistic antimicrobial effect. *Scientific reports*, *9*(1), 17687.

[117]   Li, Q., Gao, R., Wang, L., Xu, M., Yuan, Y., Ma, L., Wan, Z., & Yang, X. (2020). Nanocomposites of bacterial cellulose nanofibrils and zein nanoparticles for food packaging. *ACS Applied Nano Materials*, *3*(3), 2899-2910.

[118]   Atta, O. M., Manan, S., Ul-Islam, M., Ahmed, A. A. Q., Ullah, M. W., & Yang, G. (2021). Silver decorated bacterial cellulose nanocomposites as antimicrobial food packaging materials. *ES Food & Agroforestry*, *6*, 12-26.

[119]   Wen, Y., Liu, J., Jiang, L., Zhu, Z., He, S., He, S., & Shao, W. (2021). Development of intelligent/active food packaging film based on TEMPO-oxidized bacterial cellulose containing thymol and anthocyanin-rich purple potato extract for shelf life extension of shrimp. *Food Packaging and Shelf Life*, *29*, 100709.

[120]   Jipa, I. M., Stoica-Guzun, A., & Stroescu, M. (2012). Controlled release of sorbic acid from bacterial cellulose based mono and multilayer antimicrobial films. *LWT*, *47*(2), 400-406.

[121]   Sharma, D. K., Shukla, S., Sharma, K. K., & Kumar, V. (2022). A review on ZnO:

Fundamental properties and applications. *Materials Today: Proceedings*, *49*, 3028-3035.

[122] Hakeem, M. J., Feng, J., Nilghaz, A., Ma, L., Seah, H. C., Konkel, M. E., & Lu, X. (2020). Active packaging of immobilized zinc oxide nanoparticles controls Campylobacter jejuni in raw chicken meat. *Applied and environmental microbiology*, *86*(22), e01195-20.

[123] Fatehah, M. O., Aziz, H. A., & Stoll, S. (2014). Stability of ZnO nanoparticles in solution. Influence of pH, dissolution, aggregation and disaggregation effects. *Journal of Colloid Science and Biotechnology*, *3*(1), 75-84.

[124] Kumar, R., Umar, A., Kumar, G., & Nalwa, H. S. (2017). Antimicrobial properties of ZnO nanomaterials: A review. *Ceramics International*, *43*(5), 3940-3961.

[125] EFSA CEF Panel, (2017). "Safety assessment of the substance zinc oxide, nanoparticles, for use in food contact materials,"

[126] Bumbudsanpharoke, N., Choi, J., Jin, H., & Ko, S. (2019). Zinc migration and its e ff ect on the functionality of a low density polyethylene-ZnO nanocomposite film. *Food Packaging and Shelf Life*, 20, 100301.

[127] Vasile, C., Râpă, M., Ştefan, M., Stan, M., Macavei, S., Darie-Niţă, R. N., Tudoran, L. B., Vodnar, D. C., Popa, E. E., Stefan, R., Borodi, G., & Brebu, M. (2017). New PLA/ZnO: Cu/Ag bionanocomposites for food packaging. *Express Polymer Letters*, *11*(7).

[128] Phothisarattana, D., & Harnkarnsujarit, N. (2022). Migration, aggregations and thermal degradation behaviors of TiO2 and ZnO incorporated PBAT/TPS nanocomposite blown films. *Food Packaging and Shelf Life*, *33*, 100901.

[129] Xiao, Y., Liu, Y., Kang, S., Wang, K., & Xu, H. (2020). Development and evaluation of soy protein isolate-based antibacterial nanocomposite films containing cellulose nanocrystals and zinc oxide nanoparticles. *Food Hydrocolloids*, *106*, 105898.

[130] Poças, F., & Franz, R. (2018). Overview on European regulatory issues, legislation, and EFSA evaluations of nanomaterials. In *Nanomaterials for Food Packaging* (pp. 277-300). Elsevier.

[131] EFSA Scientific Committee, Hardy, A., Benford, D., Halldorsson, T., Jeger, M. J., Knutsen, H. K., More, S., Naegeli, H., Noteborn, H., Ockleford, C., Rici, A., Rychen G., Schlatter, J. R., Silano, V., Solecki, R., Turck, D., Younes, M., Chaudhry, Q., Cubadda, F., Gott, D., Oomen, A.,Weigel, S., Karamitrou, M., Schoonjans, R., & Mortensen, A. (2018). Guidance on risk assessment of the application of nanoscience and nanotechnologies

in the food and feed chain: Part 1, human and animal health. *EFSA journal*, *16*(7), e05327.

[132] Serpa, A., Velásquez-Cock, J., Gañán, P., Castro, C., Vélez, L., & Zuluaga, R. (2016). Vegetable nanocellulose in food science: A review. *Food Hydrocolloids*, *57*, 178-186.

[133] Endes, C., Schmid, O., Kinnear, C., Mueller, S., Camarero-Espinosa, S., Vanhecke, D., Foster, E. J., Petri-Fink, A., Rothen-Rutishauser, B., Weder, C., & Clift, M. J. (2014). An in vitro testing strategy towards mimicking the inhalation of high aspect ratio nanoparticles. *Particle and fibre toxicology*, *11*(1), 1-13.

[134] Clift, M. J., Foster, E. J., Vanhecke, D., Studer, D., Wick, P., Gehr, P., Rothen-Rutishauser, B. & Weder, C. (2011). Investigating the interaction of cellulose nanofibers derived from cotton with a sophisticated 3D human lung cell coculture. *Biomacromolecules*, *12*(10), 3666-3673.

[135] Catalán, J., Ilves, M., Järventaus, H., Hannukainen, K. S., Kontturi, E., Vanhala, E., Alenius, H., Savolainen, K. M. & Norppa, H. (2015). Genotoxic and immunotoxic effects of cellulose nanocrystals in vitro. *Environmental and molecular mutagenesis*, *56*(2), 171-182.

[136] Farcas, M. T., Kisin, E. R., Menas, A. L., Gutkin, D. W., Star, A., Reiner, R. S., Yanamala, N., Savolainen, K., & Shvedova, A. A. (2016). Pulmonary exposure to cellulose nanocrystals caused deleterious effects to reproductive system in male mice. *Journal of Toxicology and Environmental Health, Part A*, *79*(21), 984-997.

[137] Silva-Carvalho, R., Silva, J. P., Ferreirinha, P., Leitão, A. F., Andrade, F. K., Da Costa, R. M. G., Cristelo, C., Rosa, M. F., Vilanova, M., & Gama, F. M. (2019). Inhalation of bacterial cellulose nanofibrils triggers an inflammatory response and changes lung tissue morphology of mice. *Toxicological research*, *35*, 45-63.

[138] Lopes, V. R., Strømme, M., & Ferraz, N. (2020). In vitro biological impact of nanocellulose fibers on human gut bacteria and gastrointestinal cells. *Nanomaterials*, *10*(6), 1159.

[139] DeLoid, G. M., Cao, X., Molina, R. M., Silva, D. I., Bhattacharya, K., Ng, K. W., Loo, S. C. J., Brain, J. D. & Demokritou, P. (2019). Toxicological effects of ingested nanocellulose in in vitro intestinal epithelium and in vivo rat models. *Environmental Science: Nano*, *6*(7), 2105-2115.

[140] Rodrigues, A. C., Costa, L., Silva-Carvalho, R., Mota, R., Duarte-Silva, S., Teixeira-Castro,

A., Lamas, N., Oliveira, G. N. P., Wan, Y., Dourado, F., & Gama, M. (2023). Assessment of the gastrointestinal fate of bacterial nanocellulose and its toxicological effects after repeated-dose oral administration. *Environmental Science: Nano*, *10*(3), 781-799.

[141]   Bonwick, G., Bradley, E., Lock, I., & Romero, R. (2019). Bio-based materials for use in food contact applications. *Report to the Food Standards Agency; Fera Science Ltd.: York, UK*.

[142]   Fortunati, E., Peltzer, M., Armentano, I., Torre, L., Jiménez, A., & Kenny, J. M. (2012). Effects of modified cellulose nanocrystals on the barrier and migration properties of PLA nano-biocomposites. *Carbohydrate polymers*, *90* (2), 948-956.

[143]   Yu, H. Y., Yang, X. Y., Lu, F. F., Chen, G. Y., & Yao, J. M. (2016). Fabrication of multifunctional cellulose nanocrystals/poly (lactic acid) nanocomposites with silver nanoparticles by spraying method. *Carbohydrate Polymers*, *140*, 209-219.

[144]   Gavriil, G., Kanavouras, A., & Coutelieris, F. A. (2018). Food-packaging migration models: A critical discussion. *Critical reviews in food science and nutrition*, *58*(13), 2262-2272.

[145]   Poças, M. F., Oliveira, J. C., Pereira, J. R., Brandsch, R., & Hogg, T. (2011). Modelling migration from paper into a food simulant. *Food Control*, *22*(2), 303-312.

[146]   Pocas, M. F., Oliveira, J. C., Brandsch, R., & Hogg, T. (2012). Analysis of mathematical models to describe the migration of additives from packaging plastics to foods. *Journal of Food process engineering*, *35*(4), 657-676.

[147]   Poças, M. F., Oliveira, J. C., Oliveira, F. A., & Hogg, T. (2008). A critical survey of predictive mathematical models for migration from packaging. *Critical reviews in food science and nutrition*, *48*(10), 913-928.

[148]   Texcoms (2019). Textile Technology knowledge series Volume II.

[149]   Muthu, S. S., & Gardetti, M. A. (Eds.). (2020). *Sustainability in the textile and apparel industries* (pp. 163-187). Chem: Springer.

[150]   Woodings, C. (Ed.). (2001). *Regenerated cellulose fibres*. Elsevier.

[151]   Textile Exchange, "Preferred Fiber & Materials: Market Report 2022," no. October, pp. 1–118, 2022.

[152]   Opperskalski, S., Evonne, S., & Truscott, T. (2019). Textile-Exchange_Preferred-Fiber-Material-Market-Report_201. *Text. Exch*, *6*.

[153]   Hummel, M., Michud, A., Tanttu, M., Asaadi, S., Ma, Y., Hauru, L. K., Parviainen, A., King,

A. W. T., Kilpeläinen, I., & Sixta, H. (2016). Ionic liquids for the production of man-made cellulosic fibers: opportunities and challenges. *Cellulose chemistry and properties: Fibers, nanocelluloses and advanced materials*, 133-168.

[154]   *Textile Technology knowledge series Volume II*, vol. II. Texcoms textile solutions, 2019.

[155]   Clemons, C. (2016). Nanocellulose in spun continuous fibers: a review and future outlook. *Journal of Renewable Materials*, *4*(5), 327.

[156]   Sayyed, A. J., Deshmukh, N. A., & Pinjari, D. V. (2019). A critical review of manufacturing processes used in regenerated cellulosic fibres: viscose, cellulose acetate, cuprammonium, LiCl/DMAc, ionic liquids, and NMMO based lyocell. *Cellulose*, *26*, 2913-2940.

[157]   Watabe, Y., Suzuki, Y., Koike, S., Shimamoto, S., & Kobayashi, Y. (2018). Cellulose acetate, a new candidate feed supplement for ruminant animals: In vitro evaluations. *Journal of dairy science*, *101*(12), 10929-10938.

[158]   Kikutani, T. (2009). Handbook of textile fibre structure. *Eichhorn, SJ, Hearle, JWS, Jaffe, M., Kikutani, T., Eds*, 157-177.

[159]   Saxena, S., & Raja, A. S. M. (2014). Natural dyes: sources, chemistry, application and sustainability issues. In *Roadmap to sustainable textiles and clothing: eco-friendly raw materials, technologies, and processing methods* (pp. 37-80). Singapore: Springer Singapore.

[160]   Shen, X., Ji, Y., Wang, D., & Yang, Q. (2010). Solubility of a high molecular-weight bacterial cellulose in lithium chloride/N, N-dimethylacetamide solution. *Journal of Macromolecular Science, Part B*, *49*(5), 1012-1018.

[161]   Matthes, A., Beyer, K., Cebulla, H., Arnold, M. G., & Schumann, A. (2021). *Sustainable Textile and Fashion Value Chains*. Springer International Publishing: Berlin/Heidelberg, Germany.

[162]   Duchemin, B. J. C. (2008). Structure, property and processing relationships of all-cellulose composites.

[163]   Olsson, C., & Westman, G. (2013). Direct dissolution of cellulose: background, means and applications. *Cellulose-fundamental aspects*, *10*, 52144.

[164]   Kim, D. B., Pak, J. J., Jo, S. M., & Lee, W. S. (2005). Dry jet-wet spinning of cellulose/N-methylmorpholine N-oxide hydrate solutions and physical properties of lyocell fibers. *Textile research journal*, *75*(4), 331-341.

[165]   Eckelt, J., Eich, T., Röder, T., Rüf, H., Sixta, H., & Wolf, B. A. (2009). Phase diagram of the ternary system NMMO/water/cellulose. *Cellulose*, *16*, 373-379.

[166]   Fink, H. P., Weigel, P., Purz, H. J., & Ganster, J. (2001). Structure formation of regenerated cellulose materials from NMMO-solutions. *Progress in Polymer Science*, *26*(9), 1473-1524.

[167]   Sayyed, A. J., Mohite, L. V., Deshmukh, N. A., & Pinjari, D. V. (2018). Effect of ultrasound treatment on swelling behavior of cellulose in aqueous N-methyl-morpholine-N-oxide solution. *Ultrasonics Sonochemistry*, *49*, 161-168.

[168]   Golova, L. K., Makarov, I. S., Matukhina, E. V., & Kulichikhin, V. G. (2010). Solutions of cellulose and its blends with synthetic polymers in N-methylmorpholine-N-oxide: Preparation, phase state, structure, and properties. *Polymer Science Series A*, *52*, 1209-1219.

[169]   Singha, K. (2012). Importance of the phase diagram in lyocell fiber spinning. *Int. J. Mater. Eng*, *2*(3), 10-16.

[170]   Perepelkin, K. E. (2007). Lyocell fibres based on direct dissolution of cellulose in N-methylmorpholine N-oxide: development and prospects. *Fibre Chemistry*, *39*(2), 163-172.

[171]   Gunnars, S., Wågberg, L., & Cohen Stuart, M. A. (2002). Model films of cellulose: I. Method development and initial results. *Cellulose*, *9*, 239-249.

[172]   Zhang, S., Chen, C., Duan, C., Hu, H., Li, H., Li, J., Liu, Y., Ma, X., Stavik, J., & Ni, Y. (2018). Regenerated cellulose by the lyocell process, a brief review of the process and properties. *BioResources*, *13*(2), 4577-4592.

[173]   Welton, T. (1999). Room-temperature ionic liquids. Solvents for synthesis and catalysis. *Chemical reviews*, *99*(8), 2071-2084.

[174]   Hauru, L. K., Hummel, M., Nieminen, K., Michud, A., & Sixta, H. (2016). Cellulose regeneration and spinnability from ionic liquids. *Soft matter*, *12*(5), 1487-1495.

[175]   Raghuwanshi, V. S., Cohen, Y., Garnier, G., Garvey, C. J., Russell, R. A., Darwish, T., & Garnier, G. (2018). Cellulose dissolution in ionic liquid: ion binding revealed by neutron scattering. *Macromolecules*, *51*(19), 7649-7655.

[176]   El Seoud, O. A., Kostag, M., Jedvert, K., & Malek, N. I. (2019). Cellulose in ionic liquids and alkaline solutions: Advances in the mechanisms of biopolymer dissolution and regeneration. *Polymers*, *11*(12), 1917.

[177]   Liu, Y. R., Thomsen, K., Nie, Y., Zhang, S. J., & Meyer, A. S. (2016). Predictive screening of ionic liquids for dissolving cellulose and experimental verification. *Green Chemistry*, *18*(23), 6246-6254.

[178]   Mäki-Arvela, P., Anugwom, I., Virtanen, P., Sjöholm, R., & Mikkola, J. P. (2010). Dissolution of lignocellulosic materials and its constituents using ionic liquids—a review. *Industrial Crops and Products*, *32*(3), 175-201.

[179]   El Seoud, O. A., Kostag, M., Jedvert, K., & Malek, N. I. (2020). Cellulose regeneration and chemical recycling: closing the "cellulose gap" using environmentally benign solvents. *Macromolecular Materials and Engineering*, *305*(4), 1900832.

[180]   Kosan, B., Schwikal, K., & Meister, F. (2012). Effects of pre-treatment and dissolution conditions for improved solution and processing properties of cellulose in ionic liquids. *Lenzinger Berichte*, *90*, 76-84.

[181]   Kosan, B., Michels, C., & Meister, F. (2008). Dissolution and forming of cellulose with ionic liquids. *Cellulose*, *15*, 59-66.

[182]   Ioncell®.(April 2023). [Online]. Available: https://ioncell.fi/commercialization/.

[183]   Chen, J. (2015). Synthetic textile fibers: regenerated cellulose fibers. In *Textiles and fashion* (pp. 79-95). Woodhead Publishing.

[184]   Meister, F., & Kosan, B. (2015). A tool box for characterization of pulps and cellulose dopes in Lyocell technology. *Nordic Pulp & Paper Research Journal*, *30*(1), 112-120.

[185]   Sixta, H., Michud, A., Hauru, L., Asaadi, S., Ma, Y., King, A. W., Kilpeläinen, I., & Hummel, M. (2015). Ioncell-F: a high-strength regenerated cellulose fibre. *Nordic pulp & paper research journal*, *30*(1), 43-57.

[186]   Ribul, M., Lanot, A., Pisapia, C. T., Purnell, P., McQueen-Mason, S. J., & Baurley, S. (2021). Mechanical, chemical, biological: Moving towards closed-loop bio-based recycling in a circular economy of sustainable textiles. *Journal of Cleaner Production*, *326*, 129325.

[187]   Rissanen, M., Schlapp-Hackl, I., Sawada, D., Raiskio, S., Ojha, K., Smith, E., & Sixta, H. (2023). Chemical recycling of hemp waste textiles via the ionic liquid based dry-jet-wet spinning technology. *Textile Research Journal*, *93* (11-12), 2545-2557.

[188]   Björquist, S., Aronsson, J., Henriksson, G., & Persson, A. (2018). Textile qualities of regenerated cellulose fibers from cotton waste pulp. *Textile Research Journal*, *88*(21),

2485-2492.

[189]   REFIBRA technology. (Apr 2023) [Online]. Available: https://www.tencel.com/refibra.

[190]   Asaadi, S., Hummel, M., Hellsten, S., Härkäsalmi, T., Ma, Y., Michud, A., & Sixta, H. (2016). Renewable high-performance fibers from the chemical recycling of cotton waste utilizing an ionic liquid. *ChemSusChem*, *9*(22), 3250-3258.

[191]   Ma, Y., Hummel, M., Kontro, I., & Sixta, H. (2018). High performance man-made cellulosic fibres from recycled newsprint. *Green Chemistry*, *20*(1), 160-169.

[192]   Ma, Y., Hummel, M. M. M. S. A., Määttänen, M., Särkilahti, A., Harlin, A., & Sixta, H. (2016). Upcycling of waste paper and cardboard to textiles. *Green Chemistry*, *18*(3), 858-866.

[193]   Wedin, H., Lopes, M., Sixta, H., & Hummel, M. (2019). Evaluation of post-consumer cellulosic textile waste for chemical recycling based on cellulose degree of polymerization and molar mass distribution. *Textile research journal*, *89*(23-24), 5067-5075.

[194]   Chen, P., Kim, H. S., Kwon, S. M., Yun, Y. S., & Jin, H. J. (2009). Regenerated bacterial cellulose/multi-walled carbon nanotubes composite fibers prepared by wet-spinning. *Current Applied Physics*, *9*(2), e96-e99.

[195]   Gao, Q., Shen, X., & Lu, X. (2011). Regenerated bacterial cellulose fibers prepared by the NMMO· H2O process. *Carbohydrate polymers*, *83*(3), 1253-1256.

[196]   Makarov, I. S., Golova, L. K., Vinogradov, M. I., Levin, I. S., Gromovykh, T. I., Arkharova, N. A., & Kulichikhin, V. G. (2019). Cellulose fibers from solutions of bacterial cellulose in N-methylmorpholine N-oxide. *Fibre Chemistry*, *51*, 175-181.

[197]   Jinzarli, M.M., Cass, G.A., Moursounidis, J., Best, W.M. Methods for Producing a Viscose Dope from Microbial Cellulose, Australia, W O 2019/109133 Al, 2019.

[198]   "HeiQ AeoniQ™." [Online]. Available: https://www.heiq-aeoniq.com/our-technology/. [Accessed: 27-March-2024].

[199]   Lu, X., Tang, S., Huang, B., Shen, X., & Hong, F. (2013).Preparation and characterization of bacterial cellulose/hydroxypropyl chitosan blend as-spun fibers.*Fibers and Polymers*,*14*, 935-940.

CHAPTER 3 - DEVELOPMENT OF LAYERED BACTERIAL CELLULOSE-PHBV COMPOSITE FOR FOOD PACKAGING

Most of the current materials used in food packaging are synthetic and non-degradable, raising environmental issues derived from the accumulation of plastics in landfills/waterways. The food industry increasingly needs eco-friendly sustainable materials that meet the food packaging requirements. Bacterial nanocellulose (BC), a biopolymer obtained by fermentation, offers very good mechanical properties as well as the ability to carry and deliver active substances. However, its water vapour permeability is too high for food packaging applications. In this work, a layered biodegradable composite based on BC and polyhydroxyalkanoates (PHBV) was produced, attempting to improve the overall barrier properties. PHBV is a biopolymer with high degree of hydrophobicity and biodegradability, also obtained by fermentation. Wet BC membranes produced by static culture were plasticized by impregnation of solutions of either glycerol (BC_{gly}) or polyethylene glycol (M_W600) (BC_{PEG}). The plasticized BC was then coated with PHBV solution dissolved in formic acid, and oven-dried at 148 °C.

Overall, PHBV coating on plasticized BC reduced significantly the water vapour permeability (from 0.990 to 0.032 g.µm.m^{-2}.day^{-1}.Pa^{-1}) under 50% relative humidity. It increased the hydrophobicity (contact angle from 10-40 ° to 80-90 °), but decreased the stiffness (from 3.1 GPa to 1.3 Gpa) of the composite.

Overall, the mechanical and barrier properties of the obtained layered composite were considered suitable for food packaging applications. The plasticizing (with glycerol or polyethylene glycol) of BC significantly improved the mechanical performance, while PHBV coating reduced the water affinity (vapour and liquid state) on BC.

3.1. Introduction

Petroleum based plastics are the most widely used materials in food packaging, a business still expanding at a growth rate of 20-25% per year [1]. These are very cost-effective materials that comply to the industry and regulatory requirements [2]. Their success relies on the lightweight, relatively easy processability, low production cost and outstanding mechanical and barrier properties [2,3]. However, they have inherent environmental issues since 79% of the produced plastics are still being deposited in landfills and waterways [4], which ultimately may release microplastics (< 5.0 mm) into the air, water and soil [5], providing harmful effects to both terrestrial and marine ecosystems.

Alternatively, biopolymers such as cellulose, polyhydroxyalkanoates, poly lactic acid and thermoplastic starch have been explored for food packaging, although they currently lack the performance to fulfil the most demanding specific requirements in terms of mechanical and barrier properties [6-8]. To improve their performance, nanocomposite technology may be explored [9]. Cellulose is a polymer well-known for its abundance, renewability and degradability, physical-chemical and morphological properties [10-12]. Nanocelluloses from plant biomass have been used in the development of polymeric composites, offering promising performances concerning oxygen permeability at low levels of relative humidity (RH) (comparable to those of ethylene vinyl alcohol - EVOH) and mechanical properties (comparable to those of polyethylene terephthalate - PET) [7]. However, high loadings of nanocellulose are required for the composites to achieve competitive mechanical properties [11] which can compromise other functional properties such as thermosealing. Also, in the production of nanocelluloses, the intensive deforestation and wood processing represent additional environmental problems.

Bacterial nanocellulose (BC), is a biopolymer extruded by bacteria of the genus *Komagataeibacter*, through (static or agitated) fermentation [13]. The large-scale BC production remains a challenge, due to the low productivities, low efficient fermentation systems, high capital investment and high operating costs [14]. Yet, when compared to plant nanocelluloses, BC features higher porosity, higher crystallinity, higher degree of polymerization, higher mechanical strength in wet state and higher water holding capacity [15]. BC has been explored as a filler/reinforcing agent [9,11,16-24], or as main matrix in composites [13,24-27] and as carrier for substances that play an active role in food packaging

[28-34]. When used as filler, in low concentrations (0.5–1.0 %), it enhanced the mechanical performance of bio-based composites [9,11,16-24]. When used as the main matrix, *ex situ* (post-fermentation), polymers, such thermoplastic starch or polyvinyl alcohol was impregnated into the porous nanofibrillar network of BC [7,13], rendering the BC-composites excellent mechanical performance[26] and a functionalized BC for intelligent and active packaging [24,28,29]. However, the water vapour permeability of BC was too high to compete with petroleum-based plastics [7].

To enhance the moisture resistance of BC (or nanocelluloses in general), several hydrophobization strategies have been adopted, including: i) the use of anhydrides (acetic, butyric, hexanoic and alkenyl succinic anhydrides) [35]; ii) hexanoyl chloride suspended in an ionic liquid [36] or iii) the esterification of BC with organic acids [37]. Alternatively, the built-up of a multilayer composite with BC and other known hydrophobic biopolymers such polyhydroxyalkanoates (PHAs) using aqueous media, may efficiently improve the barrier performance towards water vapour and oxygen, while obviating the environmental concerns related to the use of several chemicals/solvents [38].

PHAs are a family of biopolyesters, synthesized by bacteria (gram negative, gram positive and archaea) [39,40], and the most common is the homopolymer polyhydroxybutyrate (PHB) [40]. Despite featuring promising properties for food packaging applications, this class of biopolymers tend to be brittle and have a narrow temperature/time processing window. The addition of co-3-hydroxyvalerate (3-HV) monomers onto PHB (PHB copolymerization to produce Poly (3-hydroxybutyrate-co-3-hydroxyvalerate) (PHBV)) allows the reduction of the melting temperature, improves the brittleness and the temperature/time processing window [41]. The amount of 3-HV influences the elasticity and melting behaviour of the co-polymer [41]. PHBV may also be dissolved in chloroform [42] or formic acid [43], for use in electrospinning.

In this work, never dried BC membranes were first plasticized with glycerol or polyethylene glycol (PEG). Afterwards, the plasticized BCs were coated with PHBV, in order to improve the barrier performance of BC. The mechanical performance of the obtained laminated composites was also evaluated.

3.2. Materials and Methods

3.2.1. BC production and purification

Komagataebacter xylinus ATCC 700178 cells were grown in 1 L conical flasks with 100 mL of Hestrin-Schramm culture medium (HS) [44]: (in g.L^{-1}): 20 glucose (Fluka), 5.0 peptone (Himedia), 5.0 yeast extract (Fisher), 3.39 disodium phosphate di-hydrated (Panreac) and 1.26 citric acid (Panreac). HS was autoclaved at 121 °C for 20 minutes. After inoculation, the culture was incubated for 48 h under static conditions. The formed cellulose pellicle was vigorously shaken to release the bacteria entrapped within the cellulose matrix into the residual medium, which was used for further inoculations (100 mL.L^{-1} of the final fermentation volume). The inoculated fresh culture medium was incubated in cuvettes at 30 °C for 15 days (at a fixed culture medium depth of 1.5 cm). After 15 days of fermentation, BC membranes were washed with NaOH 0.1 M (Panreac), at room temperature, to remove culture medium residues and trapped cells. Afterwards, the membranes were washed with distilled water, also at room temperature, until the pH became that of the distilled water. Then, the membranes were cut into thinner membranes with thickness of 2.0 mm, using a deli slicer (Duegi Affettatrici, type 275-SE).

3.2.2. BC impregnation

BC membranes (with thickness of 2.0 mm and area of 80 cm^2) were immersed in different aqueous solutions (200 mL for each BC membrane) of the plasticizers: glycerol (10 g.L^{-1}) and PEG (10 g.L^{-1}) (Fischer; Mw 600) for 24 h. After impregnation, BC films were rinsed with distilled water to remove residuals on the surface and air-dried at 37 °C for 48 h. Neat BC membranes were also air-dried at 37 °C for 48 h. The relative amount of impregnated material was determined by the following equation:

$$Plasticizer\ (\%) = \left(\frac{m_{plasticizedBNC} - m_{BNC}}{m_{plasticizedBNC}}\right) * 100 \text{ -(1)}$$

3.2.3. Poly (3-hydroxybutyrate-co-3-hydroxyvalerate) (PHBV) production

Poly (3-hydroxybutyrate-*co*-3-hydroxyvalerate) (PHBV) was produced from fruit waste (supplied by the Portuguese fruit juice company SumolCompal, S.A.) using mixed microbial cultures in a three-stage pilot plant. The feedstock was fermented into PHA bioprecursors in a 60 L upflow anaerobic sludge blanket (UASB) reactor as described by Matos M. et al. [45].

This reactor was continuously operated using an organic loading rate (OLR) of 28 ± 2 gCOD.L^{-1}.d^{-1}, pH at 5.4 ± 0.3, an hydraulic retention time (HRT) of 1 day at 30.1 ± 0.2 °C. The fermented end-stream produced was subsequently fed to the following two reactors and it was mainly comprised of lactate (1.0 ± 0.3 gCOD.L^{-1}), acetate (5.4 ± 0.7 gCOD.L^{-1}), propionate (2.1 ± 0.2 gCOD.L^{-1}), ethanol (0.8 ± 0.3 gCOD.L^{-1}), butyrate (9 ± 1 gCOD.L^{-1}) and valerate (2.7 ± 0.3 gCOD.L^{-1}). An aerobic 100 L reactor was assembled to select a mixed microbial culture with a high PHA-storage ability. The reactor was operated as a sequencing batch reactor (SBR) and it was fed with the fermented fruit waste under 12 h feast and famine cycles, as described by Matos M. et al. [45]. The HRT and a sludge retention time (SRT) were set at 1 and 4 days, respectively, and the OLR was maintained at 8.7 gCOD.L^{-1}.d^{-1}. The PHBV was finally produced in a 60 L fed-batch reactor using the mixed culture selected in the second stage of the process as inoculum and the fermented end-stream obtained in the first reactor as feedstock. The culture was pulse-wise fed using the dissolved oxygen response to control the feeding frequency. At the end of the production assays, the cells had an average PHA content of 66 ± 11 % m.m^{-1}. The polymer extraction/purification process was performed using a mixture of non-organic reagents optimized by Biotrend S. A. (Portugal). This process is a confidential patent-pending technology reserved by Biotrend S.A. (Portugal). At the end of the purification procedure the polymer was dried, and a white powder with a 3-hydroxyvalerate content of 21 % m.m^{-1} and a molecular mass of 366 KDa was obtained.

3.2.4. PHBV dissolution and coating

PHBV was dissolved in formic acid at 60 °C and used to coat the plasticized BC with an automatic film applicator (Sheen instruments, UK) at a speed of 100 mm.s^{-1}. After coating and full evaporation of the acid solution, the coated samples were heated at the melting point temperature (148.5 °C for five to ten seconds) in order to melt the PHBV on the surface of BC, improving the adhesion between the two layers. The coating parameters were previously optimized using more readily available kraft paper as substrate, aiming at establishing the operational conditions for the coating process of BC. Four PHBV coating parameters were assessed: the concentration of PHBV in the formic acid (*PHBV (g.L^{-1})*); the gap size of the blade (*Height (mm)*); the volume of the applied PHBV (*Volume/layer (mL)*); and finally, the number of PHBV layers (*# Layers*). For comparison, pure PHBV films were produced through the casting method: PHBV was dissolved in formic acid (at a concentration of 200 g.L^{-1}) at 60 °C and

poured in a metallic container. After solvent evaporation, the casted PHBV was exposed to the melting point temperature as described above. The average thickness and grammage of the casted PHBV films were 64 ± 22 μm and 55.3 ± 12.2 g.m^{-2} respectively.

3.2.5. BC based films and PHBV characterization

Thermal characterization - was performed by differential scanning calorimetry (DSC) (DSC 6000/Jade/Pyris6-PerkinElmer), under nitrogen atmosphere (gas flow of 20 mL.min^{-1}) using about 5-8 mg sample sealed in aluminium pans. The thermal history of PHBV was eliminated by heating from − 25 to 180 °C at a heating rate of 10 °C min^{-1}. Then, the samples were cooled at 10 °C min^{-1} from 180 to − 25 °C and the second temperature scanning was conducted from − 25 to 180 °C, at the same heating rate. The melting point temperature was found to be at 148.5 °C.

Thickness - measurements were performed with a digital thickness gauge (Adamel Lhomargy, France) on all produced films. Six to ten replicates were made for each sample; for each one, five thickness measurements (in different random positions) were made.

Microscopic morphology - neat BC and PHBV, plasticized BC and PHBV coated BC samples were characterized using a desktop scanning electron microscope (SEM) (Phenom-World BV, Netherlands)). All results were acquired using the ProSuite software. The samples were placed in an aluminium pin stub with electrically conductive carbon adhesive tape (PELCO Tabs™). Samples were coated with 2 nm of Au (20 Angstrom) for improved conductivity. The analysis was conducted with intensity image of 5 kV and a varying magnification scale from x3000 to x7000. For the neat PHBV, the analysis was conducted with intensity image of 10 kV and magnification of x2000 with desktop SEM (Jeol JSM-5600).

Mechanical properties - for tensile strength measurements, a texture analyser HD plus C was used. The full width of BC based films (20 mm) was fixed and the initial length was set at 100 mm. A load cell of 30 kg was used and the pre speed test, speed test and post speed test were 30 mm.min^{-1}, 50 mm.min^{-1} and 50 mm.min^{-1}, respectively. For each sample, 6-10 measurements were made.

Surface wettability - was characterized by contact angle using Attension Theta, Biolin Scientific, USA. The dynamic contact angle analysis (video recording) was performed with the embedded software (Biolin Scientific) using the Laplace-young approximation model and the sessile drop method. A drop of 3 μL of distilled water is positioned on the composite's surface

with a microliter syringe and observed over time (up to 60 seconds). Five measurements were made in each sample. The surface wettability was determined as referred on TAPPI T458-14 standard [46].

Barrier properties - the water vapour transmission rate (WVT) was assessed gravimetrically, adapting both the water and desiccant methods from ASTM E96-95 [47]. The test specimen was sealed to the open mouth of a test dish containing distilled water (RH 100%) or calcium chloride (RH 0%), and the assembly was placed in a controlled atmosphere (23 °C; RH 50%). In both cases ΔRH=50%, the former condition being designated as ΔRH$_w$ and the later as ΔRH$_d$. The rate of water vapour transfer driven by the RH difference between the internal (RH 100% or RH 0%) and external (RH 50%) environments was determined by plotting the capsule weight change (g) against the elapsed time (h). The following equations were used to determine WVT (g.m^{-2}.day^{-1}) and water vapour permeability (g.µm.m^{-2}.day^{-1}.Pa^{-1}). For each sample, triplicates were made.

$$(2)\ WVT\ = \frac{G}{A}$$

where WVT-water vapour transmission, G-slope of capsules weight change over elapsed time (g.day^{-1}), A-test sample surface area (m^{-2})

$$(3)\ WVP = \frac{WVTe}{\Delta P}$$

where WVP-water vapour permeability, e-sample thickness (µm), ΔP-vapor pressure difference (Pa)

$$(4)\ \Delta P = S(R1 - R2)$$

where S-saturation vapour pressure (Pa), R1-relative humidity at the source (%), R2-relative humidity at the vapour sink (%).

Oxygen transmission rate (OTR) was measured according to the standardised method (ASTM D3985-17). OTR tests were performed with MOCON Oxtran Model 2/21 at different conditions (RH 0% and RH 50% at 23 °C, and an oxygen concentration of 100% in the coated face and 0% in the uncoated face of the composite). Some samples needed mask foil to reduce the measurement area (from 50 cm^2 to 5 cm^2) and to increase the measuring range of the system. For each sample, triplicates were made.

3.2.6. Statistical analysis

Statistical analysis was supported with Prism version 8.4.3 (GraphPad Software, La Jolla California USA), using one-way (and two-way) ANOVA and Tuckey's post-hoc analysis for pairwise comparison of more than two means. Mean differences were considered statistically non-significant (ns) when p-value was higher than 0.05 (95% of interval of confidence).

3.3. Results and Discussion

3.3.1. Optimization of PHBV coating

The PHBV coating conditions were optimized using kraft paper. Four parameters were optimized with the main goal of minimizing the WVP of the coated papers (Figure 3.1). A film of PHBV obtained by casting, with a grammage of 55.3 $g.m^{-2}$, was prepared as reference. Results for WVP of the optimization trials are presented in Figure 3.1. Significant differences were found only between conditions 5, 6 and 7 and condition 12 ($p<0.05$). No further significant differences were found between the other assays, given the high variability observed for instance under conditions 4 and 8, translating a lack of reproducibility which is not desirable for PHBV coating. Consistent results (decrease in WVP) were observed when: i) a 200 $g.L^{-1}$ PHBV solution was prepared; ii) more than one layer was applied; iii) the lowest gap size of the blade was within 0.20-0.40 mm; iv) the highest volume per layer was applied (2.5 mL) (runs 5-7 in Figure 3.1). Also, a minimum grammage of coated PHBV of 45 $g.m^{-2}$ was required to reduce the WVP (Figure 3.1). No further optimization could be done due to limitations of the coating equipment: the gap size of the blade could not be further lowered, the volume per layer used was already at the maximum capacity of the blade and the solvent used allowed a maximum PHBV dissolution of 200 $g.L^{-1}$. Yet, the WVP values obtained under the conditions 5, 6 and 7 were close to that of casted PHBV (0.025 $g.\mu m.m^{-2}.day^{-1}.Pa^{-1}$) (Figure 3.1), meaning that the coating process produced an homogeneous film, with good substrate coverage, reaching the best possible WVP within the range of tested grammage values. Condition 6 (PHBV 200 $g.L^{-1}$; height: 0.20 mm; volume/layer: 2.5 mL; 2 layers) was thus chosen for further PHBV coating onto BC.

Figure 3.1. Optimization of the PHBV coating conditions leading to lower water vapour permeability; red dotted line represents the water vapor permeability obtained with casted PHBV (grammage 55.3 $g.m^{-2}$); columns represent the mean and error bars represent the standard deviation; "*" $p<0.05$ determined by one way ANOVA; unselected runs with $p>0.05$ determined by one way ANOVA.

3.3.2. BC coating with PHBV

The use of glycerol and PEG as plasticizers of the uncoated (BC$_{gly}$ vs BC$_{PEG}$) and of the PHBV coated BC films (BC$_{gly}$PHBV vs BC$_{PEG}$PHBV) were assessed with regards to the physical, morphological, mechanical and barrier properties.

Table 3.1. Physical characteristics of the PHBV coated BC films (n=6 per sample); data displayed as mean ± standard deviation.

	dry thickness (µm)	Density (g.cm^{-3})	Plasticizer (g.Kg$_{BC}^{-1}$)	PHBV thickness (µm)	Grammage (g.m^{-2})	PHBV (g.Kg^{-1})
BC	33.5 ± 7.3^a	1.08 ± 0.16^a	-	-	15.4 ± 3.8^a	-
PHBV*	64.1 ± 21.9^b	0.89 ± 0.15^{ab}	-	64 ± 22^a	55.3 ± 12.2^b	-
BC$_{gly}$	19.3 ± 5.4^a	1.38 ± 0.12^c	590 ± 7^a	26 ± 8^b	39.6 ± 7.5^b	460 ± 99^a
BC$_{gly}$PHBV	52.8 ± 18.7^b	0.71 ± 0.13^b			57.6 ± 10.4^b	
BC$_{PEG}$	20.0 ± 3.3^a	1.16 ± 0.08^a	580 ± 1^a	31 ± 5^b	65.2 ± 12.0^{bc}	310 ± 79^b
BC$_{PEG}$PHBV	56.0 ± 11.8^b	0.72 ± 0.07^b			85.0 ± 12.6^d	

*Produced by casting method; abcd – t-student test (for plasticizer g.Kg$_{BC}^{-1}$ and PHBV %) and one way ANOVA analysis (p<0.05); BC- Bacterial nanocellulose; PHBV- Poly (3-hydroxybutyrate-co-3-hydroxyvalerate); Gly - glycerol; PEG - polyethylene glycol

Among the uncoated samples, neat BC revealed a higher thickness and a lower density than the plasticized BC films (p<0.05) (Table 3.1). No significant differences were found (p>0.05) between BC$_{gly}$ and BC$_{PEG}$ films, concerning the amount of incorporated plasticizer nor in their dried thickness (Table 3.1). However, BC$_{gly}$ revealed near 20% higher density than BC$_{PEG}$ (p<0.05) (Table 3.1).

After coating the plasticized BC films with PHBV, the overall thickness increased roughly by 30 µm, while the density decreased by 49% for BC$_{gly}$ and 38% for BC$_{PEG}$ (Table 3.1), since PHBV is lighter than BC. Concerning the grammage, PEG impregnation was found to have a greater impact (p<0.05) than glycerol. After PHBV coating, the grammage increased by 23% on BC$_{PEG}$ films and by 31% on BC$_{gly}$ films (Table 3.1). Also from these results, it is worth

mentioning that PHBV represented 46% and 31%, respectively, of the total mass of the BC$_{gly}$PHBV and BC$_{PEG}$PHBV films.

Plasticizing the films with either glycerol or PEG led to higher transparency as compared to neat BC (Figure 3.2). PHBV did not significantly affect the transparency of the plasticized BCs, although the BC$_{gly}$PHBV film was found to be slightly more transparent (Figure 3.2). Concerning the films' morphology, SEM observation showed that BC$_{gly}$ and BC$_{peg}$ were homogeneously coated with PHBV, resulting in a smoother surface, suggesting a good interaction (adhesion) between PHBV and the plasticized BCs (Figure 3.2).
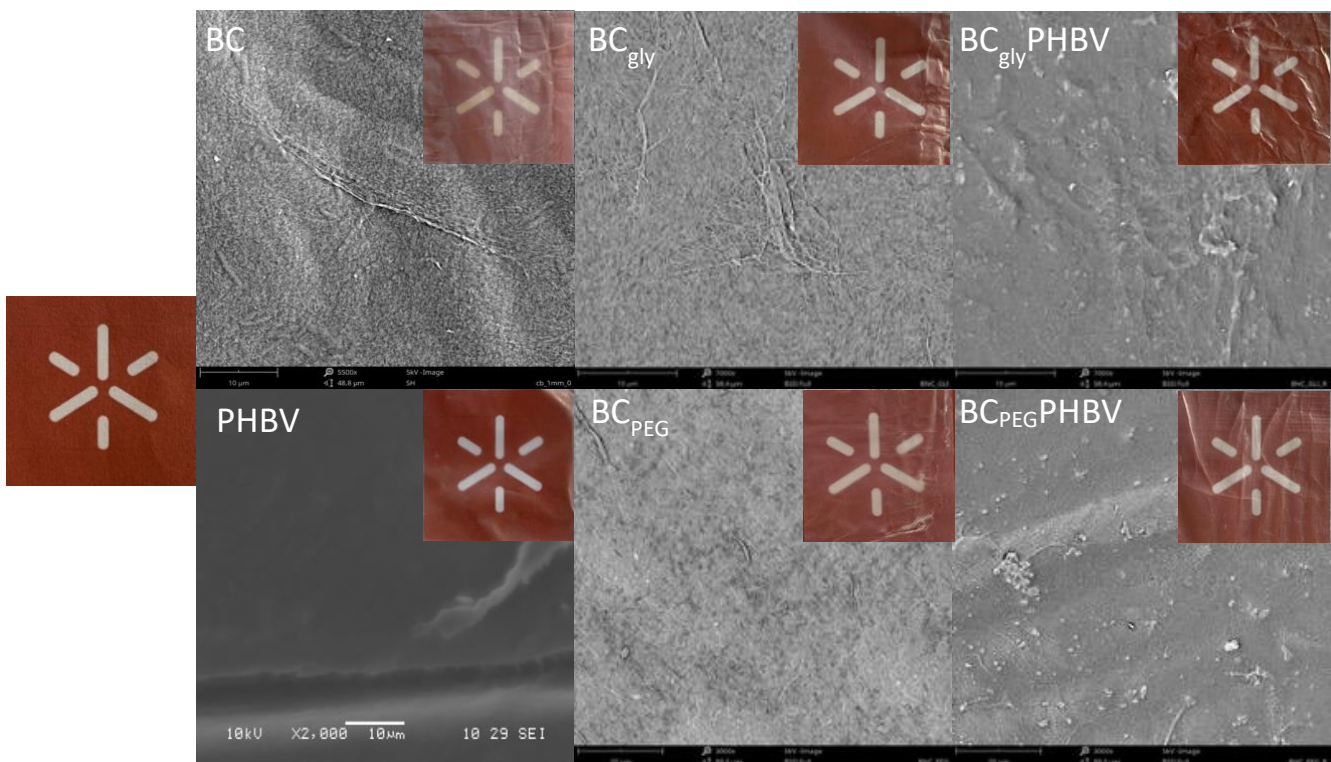
Figure 3.2. Transparency and SEM images of neat PHBV and BC based films. Scale bar: 10 μm for PHBV, BC, BC$_{gly}$, BC$_{gly}$PHBV and 30 μm for BC$_{PEG}$ and BC$_{PEG}$PHBV.

3.3.2.1. Mechanical and barrier properties

Uncoated and PHBV coated BC films (plasticized either with glycerol or PEG) were further characterized regarding their mechanical and barrier properties. Concerning the mechanical properties, all plasticized and PHBV coated BC films presented higher tensile strength, stiffness and elongation values than neat BC ($p < 0.05$) (Figure 3.3). Both PEG and glycerol equally improved the overall mechanical performance of the BC films ($p > 0.05$) (Figure 3.3).

However, a significant decrease in tensile strength and young modulus was observed after PHBV coating ($p<0.05$) (Figure 3.3).

Samples	Thickness (μm)
BC	23.0 ± 3.3
BC$_{gly}$	22.5 ± 3.3
BC$_{gly}$PHBV	63.5 ± 11.7
BC$_{PEG}$	29.7 ± 1.9
BC$_{PEG}$PHBV	45.1 ± 12.4
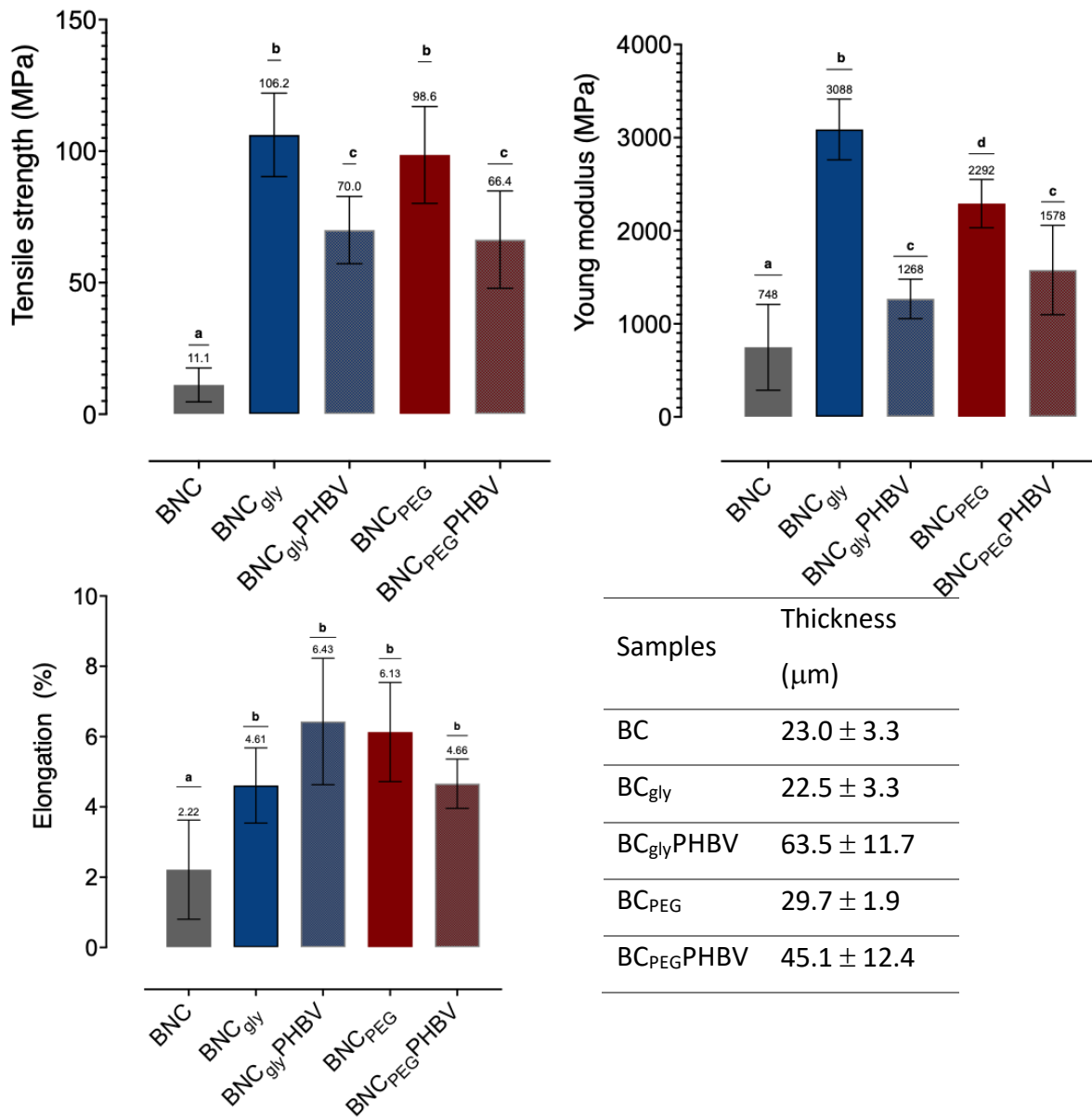
Figure 3.3. Mechanical properties of uncoated and coated BC films (n=6); columns represent the mean and error bars represent the standard deviation; "abc" letters are used to state the non-significantly different groups – ANOVA one way analysis ($p<0.05$).

PHBV coating of BC$_{gly}$ films reduced the WVP by 76% at ΔRH_w 100/50% (% RH inside/outside the capsule,) and 85% at ΔRH_d 0/50%, reaching a minimum value of 0.032 g.μm.m^{-2}.day^{-1}.Pa^{-1} ($p<0.5$) (Figure 3.4). The minimum value of the WVP with BC$_{gly}$PHBV

(obtained for ΔRH_d) is similar to the one obtained with casted PHBV (p>0.5). PHBV coating was not as effective in the case of BC_{PEG} films, since the WVP was reduced by 62% at ΔRH_w 100/50% and 67% at ΔRH_d 0/50%, with a minimum value of 0.122 g.μm.m^{-2}.day^{-1}.Pa^{-1} being obtained, statistically different from that of casted PHBV (p<0.5) (Figure 3.4).

Regarding the performance of the BC based films under different relative humidity conditions, higher WVP values were, as expected, obtained for ΔRH_w, in spite of the water vapor pressure gradient being the same as for ΔRH_d (Figure 3.4). This suggests a higher water absorption capacity in the presence of a saturated atmosphere, which leads to a higher permeability. Results indicate that the moisture effect, i.e. the difference between the WVP determined at higher or lower humidity conditions, is higher for glycerol than for PEG (either on uncoated and PHBV coated BC_{PEG} films) (Figure 3.4). Casted PHBV presented similar WVP values regardless of the humidity conditions (Figure 3.4).
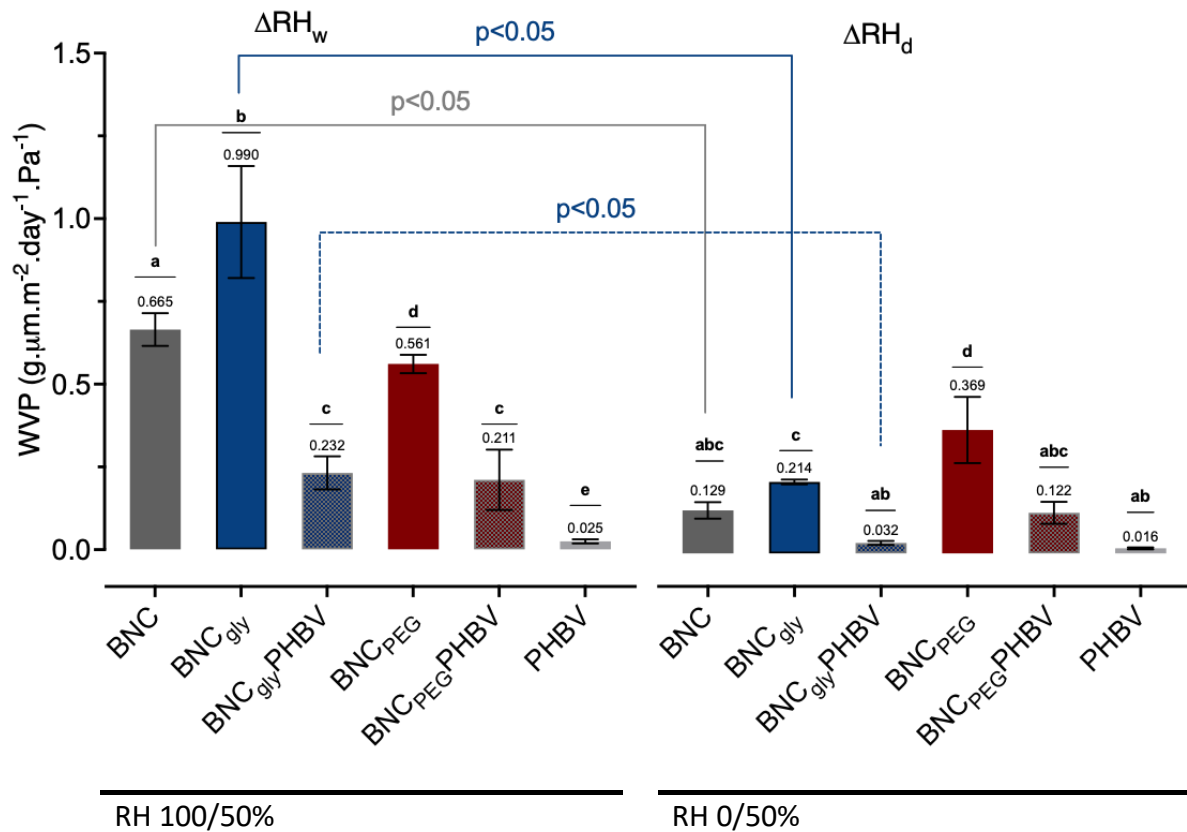
Thickness (μm)		
Samples	ΔRH$_w$	ΔRH$_d$
BC	29.2 ± 2.2	22.7 ± 4.6
PHBV	64.1 ± 21.9	64.1 ± 21.9
BC$_{gly}$	34.7 ± 8.1	16.4 ± 0.8
BC$_{gly}$PHBV	52.8 ± 6.81	39.7 ± 6.23
BC$_{PEG}$	30.6 ± 2.08	37.0 ± 13.4
BC$_{PEG}$PHBV	50.1 ± 6.8	53.2 ± 4.1

Figure 3.4. Water vapour permeability (WVP) of neat BC, casted PHBV, BC$_{gly}$, BC$_{PEG}$, BC$_{gly}$PHBV and BC$_{gly}$PHBV (n = 3) at RH 100/50% (left) and RH 0/50% (right); (RH int/ext% - relative humidity inside/outside the capsule); columns represent the mean and error bars represent the standard deviation; "abc" letters state the non-significantly different groups – ANOVA one way analysis (p<0.05); significant differences obtained within the same

sample at different conditions (RH 100/50% vs RH 0/50%); table shows the average thickness (μm) of each sample (data displayed as mean ± standard deviation).

Concerning oxygen permeability, the results obtained with all the BC based films revealed high variability, thus a quantitative characterization was not possible (Figure 3.5). The arrangement of the BC fibres obtained by fermentation is naturally inhomogeneous. In addition, the equipment used (MOCON Oxtran Model 2/21) is unsuitable for materials with high oxygen transmition rates (detection limit of 2000 cc.m^{-2}.day^{-1} using 100% oxygen flow and measurement area of 50 cm^2). In order to measure the oxygen permeabilities on BC films, an aluminium mask (reducing the measurement area to 5 cm^2) was attached to the sample, reducing the oxygen flow to 21% in some trials. This approach allowed to increase the detection limit of the equipment to 3500 cc.m^{-2}.day^{-1}. However, high variability was still obtained on the measured oxygen permeability values. Therefore, the results are reported as the range of values obtained and plotting the WVP vs oxygen permeability for all BC based films (from oxygen at RH 50% and WVP at ΔRH$_d$ 0/50%), as illustrated in Figure 5. A slight increase on oxygen permeabilities was observed following PHBV coating (Figure 3.5).
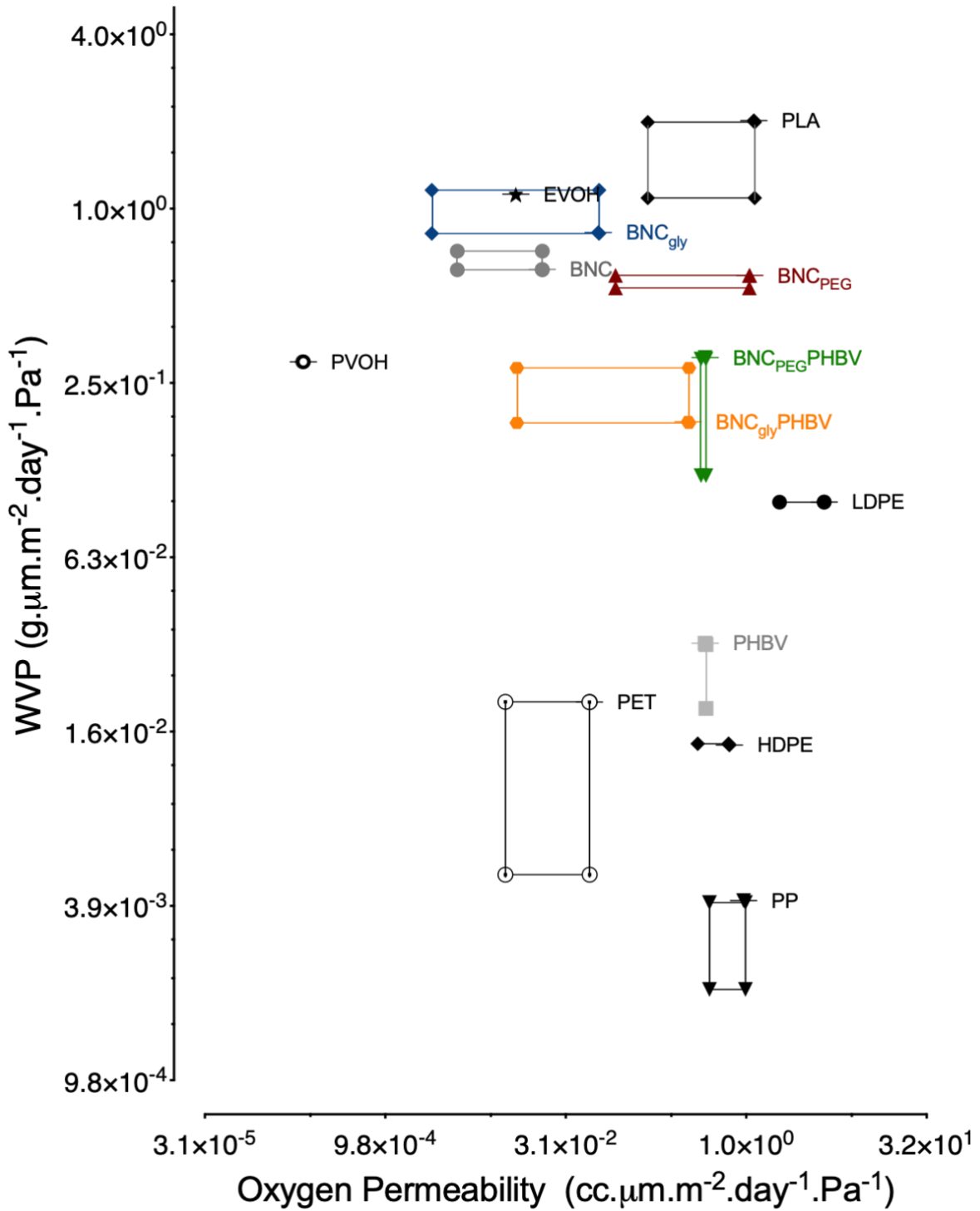
Figure 3.5. Water vapour permeability vs Oxygen permeability of several materials used for packaging and of neat BC, casted PHBV, BC_{gly}, BC_{PEG}, $BC_{gly}PHBV$ and $BC_{gly}PHBV$ films; values obtained at 23-25 °C and RH of (0/50%) for WVP and 50% for oxygen permeability; Values from literature (in black) obtained at 23-25 °C and normalized for RH (50%). PET- Polyethylene Terephthalate; PP-Polypropylene; LDPE- Low density polyethylene; HDPE-

High density polyethylene; EVOH - ethylene vinyl alcohol; PLA – Polylactic acid; PVOH – Polyvinyl alcohol.

In addition to the barrier performance, the contact angles were also measured over a period of 60 s to assess the wettability of the developed films (Figure 3.6). The incorporation of plasticizer influenced the BC wetting. Neat BC contact angles slighty decreased from 50° to 30° throughout the 60 s. When plasticized with glycerol, the contact angles decreased to 20°, being the most hydrophilic material obtained. When BC was incorporated with PEG, high contact angle (above 100°) was observed at very short contact times, although with a rapid decrease to 40°-60° after 60 s. On the other hand, PHBV and PHBV coated BC films had higher contact angles (BC$_{gly}$PHBV- 65°-85°; PHBV- 83°-95°) than uncoated BC films (BC-30°-50°; BC$_{gly}$-10°-40°) ($p<0.05$). When plasticized with PEG, similar contact angle values were obtained in the first 15 s (uncoated BC$_{PEG}$ vs BC$_{PEG}$PHBV) ($p>0.05$). Afterwards, contact angles of BC$_{PEG}$PHBV decreased over the 60 s (ranging from 65°-85° to 56°-82°) at lower rate than uncoated BC$_{PEG}$ (ranging from 55°-78° to 40°-60°) ($p>0.05$). Neat PHBV and PHBV coated BC films display a similar hydrophobicity ($p>0.5$) according to the initial values of contact angle, which decreases slightly overtime in the case of the layered materials (Figure 3.6). Despite BC$_{gly}$ being the most hydrophilic material, it was BC$_{peg}$ that showed the highest wetting capacity when compared to uncoated BC films (BC: 0.177°.s^{-1} vs BC$_{gly}$: 0.105°.s^{-1} vs BC$_{peg}$: 0.734°.s^{-1}). PHBV coating substantially reduced the surface wettability of BC$_{gly}$ and BC$_{peg}$, although BC$_{peg}$PHBV still presented high wettability ($p<0.05$) (Figure 3.6).
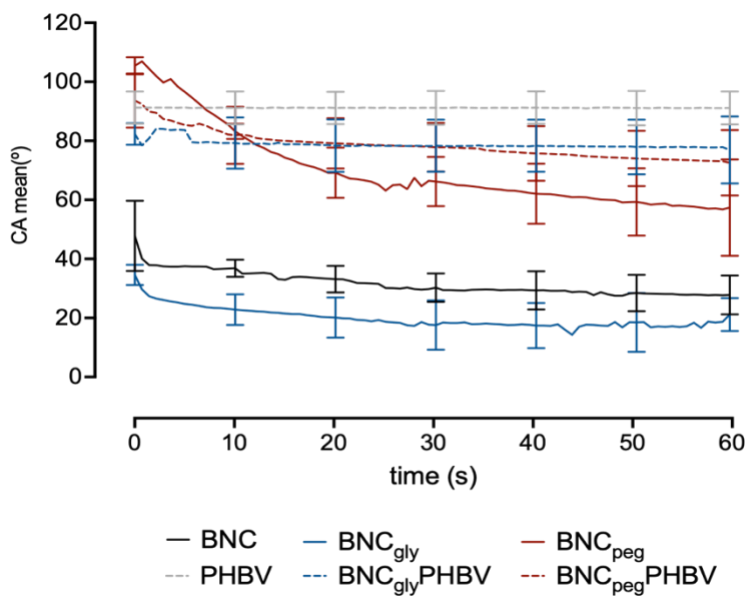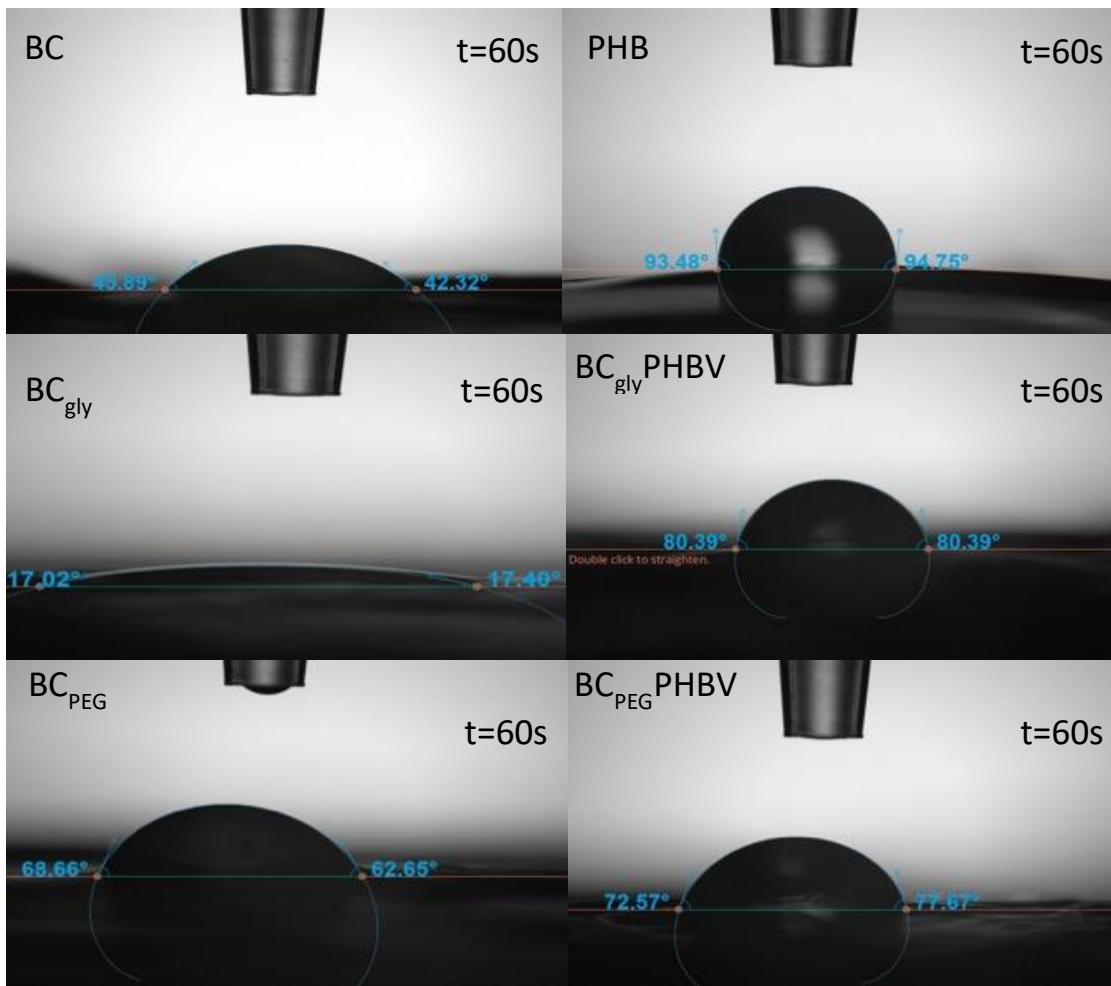
Samples	Surface wettability ($°.s^{-1}$)
BC	0.177 ± 0.080
PHBV	0.0034 ± 0.0086
BC$_{gly}$	0.105 ± 0.058
BC$_{gly}$PHBV	0.033 ± 0.030
BC$_{peg}$	0.734 ± 0.326
BC$_{peg}$PHBV	0.223 ± 0.097

Figure 3.6. Water contact angle of uncoated and PHBV coated BC films (n=5 per condition) after 60 seconds; symbols represent the mean and error bars represent the standard deviation.

3.4. Discussion

Upon drying, BC fibres form a packed network due to the abundant hydroxyl groups which form inter-intramolecular hydrogen bonds [48]. The generated tight network limits the ability of the fibres to move when exposed to tension, making BC brittle (see Figure 3.3), with low elasticity and tensile strength [49]. The incorporation of glycerol and PEG (up to 600 $g.Kg_{BC}^{-1}$) before drying increased the spacing between the fibres and reduced the formation of hydrogen bonds. Plasticization improved the optical properties (higher transparency) (Figure 3.2), tensile strength, stiffness and elasticity (Figure 3.3). In addition, glycerol and PEG interacted well with BC, with no signs of aggregation or phase separation (Table 3.1; Figure 3.2). To the exception of stiffness, the type of used plasticizer did not provide major differences, with glycerol providing a higher young modulus. PEG is referred as a hydrogen bond acceptor whereas glycerol is a hydrogen bond donor and acceptor [50]. PEG has lower density of hydroxyl groups and thus the amount of hydrogen bonds in BC_{PEG} is lower than in BC_{gly}, decreasing the stiffness of the former [50].

As expected, neat BC films presented high water affinity (vapour and liquid) (Figures 3.4 and 3.6). Plasticization affected the barrier performance and wettability. For instance, the incorporation of glycerol further increased the affinity for water (either in liquid and vapour state) (Figures 3.4 and 3.6). Glycerol is a well-known hydrophilic plasticizer with the ability to interact with the surrounding moisture, promoting the rehydration of the plasticized BC. As a result, the cellulose fibres have increased in free volume, facilitating water diffusion through BC_{gly} [48]. On the other hand, the incorporation of PEG led to a lower water diffusion rate (vapour/liquid state) (Figure 3.4 and 3.6). This can be explained by the fact that PEG exhibits an amphiphilic character, being hydrophilic (easily dissolved in water) as well as hydrophobic (when exposed to moisture and contact angles measurements) interactions (Figure 3.4 and 3.6). Similar amphiphilic interactions were observed by Jiang Wu [51] and Pasini [52]. Furthermore, a superior RH environment (ΔRH_w) led to higher water absorption from BC based films, increasing their WVP. Figure 3.4 shows the effect of water under different conditions

(ΔRH_w vs ΔRH_d), although these conditions correspond to the same vapour pressure difference between each sample's face (driving force for water transport). This highlights the need for fully reporting the testing conditions (i.e. the range of RH values used) and not only the differential of vapour pressure applied, which is often overlooked in the literature.

Lower mechanical performance was obtained with PHBV coated BC films (Figure 3.3), as could be expected owing to the brittle nature of PHBV [39,41]. However, the development of a multilayer material (PHBV coated films) may also contribute to the decrease in stiffness since the outer layer (PHBV) may deform easier under tension, compromising the integrity of the composite. The coating process (with high temperature and the use of formic acid) may have also contributed to the decrease of the mechanical performance (Figure 3.3). Despite the lower values of tensile strength and stiffness after PHBV coating, these may be considered satisfactory for food packaging applications. Indeed, the tensile strength and stiffness of PHBV coated BC films are comparable to those of polypropylene (PP), polyvinyl alcohol (PVOH) and ethylene vinyl alcohol (EVOH) [7].

Concerning the barrier properties, $BC_{gly}PHBV$ films showed superior results when subjected to water (vapour or liquid) (Figure 3.4 and 3.6). The coating process in the case of $BC_{gly}PHBV$ films was apparently more successful, since the WVP (ΔRH_d) was similar to that of neat PHBV (Figure 3.4). However, under humid conditions (ΔRH_w), $BC_{gly}PHBV$ films exhibited much higher WVP (as compared to PHBV film under the same conditions), meaning that PHBV was less effective in the layered films (Figure 3.4). PHBV coating on both sides of BC_{gly} may be a solution to diminish the water affinity towards the BC_{gly} layer, hindering the contact of water molecules with the hydroxyl groups of BC. On BC_{PEG} films, a poorer PHBV coating was obtained. PEG is able to interact with the outer PHBV layer (weakening the outer layer against water vapour) due to the good compatibility between PHBV and PEG [52,53]. Indeed, PEG is commonly used as plasticizer for PHBV, thereby compromising the WVP [54].

With regards to the oxygen permeability, only qualitative data was obtained due to the inhomogeneous nature of the BCs films and low detection limit of the equipment. Still, differences in the performance of the BC films were noticeable. BC_{PEG} revealed much higher affinity towards oxygen than BC_{gly} (Figure 3.5). As mentioned above, the fibre network arrangement differs when plasticized with glycerol or PEG, which consequently may alter the diffusion rate of oxygen. Furthermore, the results are in agreement with the literature since

less hydrophilic materials (such as BC_{PEG}) tend to have poorer oxygen barriers [55]. PHBV, being hydrophobic, also increased the oxygen permeability of the layered BC films.

The mechanical and barrier properties of the PHBV film do not match those of reported in the literature [56-59]. This is attributed to the amount of 3-hydroxyvalerate present in different PHBV formulations. The copolymer 3-hydroxyvalerate acts as an internal plasticizer, being responsible for the decrease in crystallinity and increasing in free volume within PHB chains, offering mobility to the polymer chains [59]. Thus, as reported in the literature, higher 3-hydroxyvalerate content, increase the elasticity [59] as well as the water vapor [58,59] and oxygen [56,57] permeabilities. Concerning WVP, the PHBV used in this work (with 21% 3-hydroxyvalerate) compares with that used by Shogren et al. (18% 3-hydroxyvalerate) [58]. On the other hand, our formulation exhibited a higher oxygen permeability (0.426 cc.μm.m^{-2}.day^{-1}.Pa^{-1}) than that of 12% 3-hydroxyvalerate reported by Malmir et al. [57] (0.332 cc.μm.m^{-2}.day^{-1}.Pa^{-1}). Overall, the results confirm the trend between oxygen permeability and 3-hydroxyvalerate content.

In comparison to neat bio-based polymers such polylactic acid (PLA) and petroleum-based plastics such low density polyethylene (LDPE), PHBV coated BC_{gly} films proved to be competitive, showing higher barrier to water vapour than PLA and EVOH, and similar to that of PVOH [2,60-62]. Still, fossil-based plastics such as LDPE, high density polyethylene (HDPE), polyethylene terephthalate (PET) and polypropylene (PP) have lower WVP values [7]. In order to reach lower values of WVP, low molecular weight additives (such as metal oxides) [58] or a different coating material should be chosen, since the minimum possible WVP was achieved with PHBV coating (BC_{gly}PHBV vs PHBV at ΔRH_d vs PHBV at ΔRH_w (Figure 3.4). Coating BC with PHBV on both sides may also help improving the barrier properties. From a food packaging perspective, more data should be gathered (especially on oxygen permeability) in order to fully assess the ability of the PHBV coated BC films application on specific food products. Still, considering only the WVP, the developed PHBV coated BC films (especially BC_{gly}PHBV) may be a good candidate for meat and meat-based products (where WVT should be between 2-100 g.m^{-2}.day^{-1}) or fruits, vegetables and fresh salads (10-4000 g.m^{-2}.day^{-1}) [8]. For a film with a thickness of 40 μm, a WVT of 40 g.m^{-2}.day^{-1} was obtained (Figure 3.4).

3.5. References

[1]   Huang, J., Dufresne, A., & Lin, N. (Eds.). (2019). *Nanocellulose: from fundamentals to advanced materials*. John Wiley & Sons.

[2]   Sangroniz, A., Zhu, J. B., Tang, X., Etxeberria, A., Chen, E. Y. X., & Sardon, H. (2019). Packaging materials with desired mechanical and barrier properties and full chemical recyclability. *Nature Communications*, *10*(1), 3559.

[3]   Bharimalla, A. K., Deshmukh, S. P., Vigneshwaran, N., Patil, P. G., & Prasad, V. (2017). Nanocellulose-polymer composites for applications in food packaging: Current status, future prospects and challenges. *Polymer-Plastics Technology and Engineering*, *56*(8), 805-823.

[4]   Souza Machado, A. A., Kloas, W., Zarfl, C., Hempel, S., & Rillig, M. C. (2018). Microplastics as an emerging threat to terrestrial ecosystems. *Global change biology*, *24*(4), 1405-1416

[5]   Geyer, R., Jambeck, J. R., & Law, K. L. (2017). Production, use, and fate of all plastics ever made. *Science advances*, *3*(7), e1700782.

[6]   Sharma, A., Thakur, M., Bhattacharya, M., Mandal, T., & Goswami, S., (2019). Commercial application of cellulose nano-composites – A review. *Biotechnol Reports* **21**:e00316.

[7]   Silva, F. A. G. S., Dourado, F., Gama, M., & Poças, F., (2020). Nanocellulose bio-based composites for food packaging. *Nanomaterials* **10**(10):1–29.

[8]   Langowski, H. C. (2017). Shelf life of packed food and packaging functionality. In *Food Packaging Materials* (pp. 11-66). CRC Press.

[9]   Oksman, K., Aitomäki, Y., Mathew, A. P., Siqueira, G., Zhou, Q., Butylina, S., ... & Hooshmand, S. (2016). Review of the recent developments in cellulose nanocomposite processing. *Composites Part A: Applied Science and Manufacturing*, *83*, 2-18.

[10]   Khalil, H. A., Saurabh, C. K., Syakir, M. I., Fazita, M. N., Bhat, A., Banerjee, A., ... & Tahir, P. M. (2019). Barrier properties of biocomposites/hybrid films. In *Mechanical and physical testing of biocomposites, fibre-reinforced composites and hybrid composites* (pp. 241-258). Woodhead Publishing.

[11]   Lee, K. Y., Aitomäki, Y., Berglund, L. A., Oksman, K., & Bismarck, A. (2014). On the use of nanocellulose as reinforcement in polymer matrix composites. *Composites Science and Technology*, *105*, 15-27.

[12]   Fang, Z., Hou, G., Chen, C., & Hu, L. (2019). Nanocellulose-based films and their emerging

applications. *Current Opinion in Solid State and Materials Science*, *23*(4), 100764.

[13]   Torres, F. G., Arroyo, J. J., & Troncoso, O. P. (2019). Bacterial cellulose nanocomposites: An all-nano type of material. *Materials Science and Engineering: C*, *98*, 1277-1293.

[14]   Jozala, A. F., de Lencastre-Novaes, L. C., Lopes, A. M., de Carvalho Santos-Ebinuma, V., Mazzola, P. G., Pessoa-Jr, A., ... & Chaud, M. V. (2016). Bacterial nanocellulose production and application: a 10-year overview. *Applied microbiology and biotechnology*, *100*, 2063-2072.

[15]   Gama, M., Dourado, F., & Bielecki, S. (Eds.). (2016). *Bacterial nanocellulose: from biotechnology to bio-economy*. Elsevier.

[16]   Gitari, B., Chang, B. P., Misra, M., Navabi, A., & Mohanty, A. K. (2019). A comparative study on the mechanical, thermal, and water barrier properties of PLA nanocomposite films prepared with bacterial nanocellulose and cellulose nanofibrils. *BioResources*, *14*(1), 1867-1889.

[17]   Panaitescu, D. M., Frone, A. N., Chiulan, I., Gabor, R. A., Spataru, I. C., & Căşărică, A. (2017). Biocomposites from polylactic acid and bacterial cellulose nanofibers obtained by mechanical treatment. *BioResources*, *12*(1), 662-672.

[18]   Wan, Y. Z., Luo, H., He, F., Liang, H., Huang, Y., & Li, X. L. (2009). Mechanical, moisture absorption, and biodegradation behaviours of bacterial cellulose fibre-reinforced starch biocomposites. *Composites Science and Technology*, *69*(7-8), 1212-1217.

[19]   Martins, I. M., Magina, S. P., Oliveira, L., Freire, C. S., Silvestre, A. J., Neto, C. P., & Gandini, A. (2009). New biocomposites based on thermoplastic starch and bacterial cellulose. *Composites Science and Technology*, *69*(13), 2163-2168.

[20]   Ng, H. M., Sin, L. T., Bee, S. T., Tee, T. T., & Rahmat, A. R. (2017). Review of nanocellulose polymer composite characteristics and challenges. *Polymer-Plastics Technology and Engineering*, *56*(7), 687-731.

[21]   Soykeabkaew, N., Tawichai, N., Thanomsilp, C., & Suwantong, O. (2017). Nanocellulose-reinforced "green" composite materials. *Walailak Journal of Science and Technology (WJST)*, *14*(5), 353-368.

[22]   George, J., Sreekala, M. S., & Thomas, S. (2001). A review on interface modification and characterization of natural fiber reinforced plastic composites. *Polymer Engineering & Science*, *41*(9), 1471-1485.

[23]   Mondal, S. (2018). Review on nanocellulose polymer nanocomposites. *Polymer-Plastics*

Technology and Engineering, *57*(13), 1377-1391.

[24]   Shah, N., Ul-Islam, M., Khattak, W. A., & Park, J. K. (2013). Overview of bacterial cellulose composites: a multipurpose advanced material. *Carbohydrate polymers*, *98*(2), 1585-1598.

[25]   Ruka, D. R., Simon, G. P., & Dean, K. M. (2013). In situ modifications to bacterial cellulose with the water insoluble polymer poly-3-hydroxybutyrate. *Carbohydrate polymers*, *92*(2), 1717-1723.

[26]   Savadekar, N. R., & Mhaske, S. T. (2012). Synthesis of nano cellulose fibers and effect on thermoplastics starch based films. *Carbohydrate Polymers*, *89*(1), 146-151.

[27]   Grande, C. J., Torres, F. G., Gomez, C. M., Troncoso, O. P., Canet-Ferrer, J., & Martínez-Pastor, J. (2009). Development of self-assembled bacterial cellulose–starch nanocomposites. *Materials Science and Engineering: C*, *29*(4), 1098-1104.

[28]   Kuswandi, B., Jayus, Oktaviana, R., Abdullah, A., & Heng, L. Y. (2014). A novel on-package sticker sensor based on methyl red for real-time monitoring of broiler chicken cut freshness. *Packaging technology and science*, *27*(1), 69-81.

[29]   Pourjavaher, S., Almasi, H., Meshkini, S., Pirsa, S., & Parandi, E. (2017). Development of a colorimetric pH indicator based on bacterial cellulose nanofibers and red cabbage (Brassica oleraceae) extract. *Carbohydrate polymers*, *156*, 193-201.

[30]   Tsai, Y. H., Yang, Y. N., Ho, Y. C., Tsai, M. L., & Mi, F. L. (2018). Drug release and antioxidant/antibacterial activities of silymarin-zein nanoparticle/bacterial cellulose nanofiber composite films. *Carbohydrate Polymers*, *180*, 286-296.

[31]   Vilela, C., Moreirinha, C., Domingues, E. M., Figueiredo, F. M., Almeida, A., & Freire, C. S. (2019). Antimicrobial and conductive nanocellulose-based films for active and intelligent food packaging. *Nanomaterials*, *9*(7), 980.

[32]   Wang, W., Yu, Z., Alsammarraie, F. K., Kong, F., Lin, M., & Mustapha, A. (2020). Properties and antimicrobial activity of polyvinyl alcohol-modified bacterial nanocellulose packaging films incorporated with silver nanoparticles. *Food Hydrocolloids*, *100*, 105411.

[33]   Padrao, J., Gonçalves, S., Silva, J. P., Sencadas, V., Lanceros-Méndez, S., Pinheiro, A. C., Vicente, A. A., Rodrigues, L. R., & Dourado, F. (2016). Bacterial cellulose-lactoferrin as an antimicrobial edible packaging. *Food Hydrocolloids*, *58*, 126-140.

[34]   Jipa, I. M., Stoica-Guzun, A., & Stroescu, M. (2012). Controlled release of sorbic acid from bacterial cellulose based mono and multilayer antimicrobial films. *LWT*, *47*(2), 400-406.

[35] Tomé, L. C., Brandao, L., Mendes, A. M., Silvestre, A. J., Neto, C. P., Gandini, A., Freire, C. S. R., & Marrucho, I. M., (2010). Preparation and characterization of bacterial cellulose membranes with tailored surface and barrier properties. *Cellulose*, *17*, 1203-1211.

[36] Tomé, L. C., Freire, M. G., Rebelo, L. P. N., Silvestre, A. J., Neto, C. P., Marrucho, I. M., & Freire, C. S. (2011). Surface hydrophobization of bacterial and vegetable cellulose fibers using ionic liquids as solvent media and catalysts. *Green Chemistry*, *13*(9), 2464-2470.

[37] Lee, K. Y., Quero, F., Blaker, J. J., Hill, C. A., Eichhorn, S. J., & Bismarck, A. (2011). Surface only modification of bacterial cellulose nanofibres with organic acids. *Cellulose*, *18*, 595-605.

[38] Cerqueira, M. A., Torres-Giner, S., & Lagaron, J. M., (2018) Nanostructured multilayer films. *In Nanomaterials for Food Packaging: Materials, Processing Technologies, and Safety Issues.* pp. 147–171. Cerqueira, M. A., Lagaron, J. M., Castro, L. M. P., & Vicente, A. A. (Eds.) Elsevier Inc, Amesterdam

[39] Bugnicourt, E., Cinelli, P., Lazzeri, A., & Alvarez, V. A. (2014). Polyhydroxyalkanoate (PHA): Review of synthesis, characteristics, processing and potential applications in packaging.

[40] Tan, G. Y. A., Chen, C. L., Li, L., Ge, L., Wang, L., Razaad, I. M. N., ... & Wang, J. Y. (2014). Start a research on biopolymer polyhydroxyalkanoate (PHA): a review. *Polymers*, *6*(3), 706-754.

[41] Langford, A., Chan, C. M., Pratt, S., Garvey, C. J., & Laycock, B. (2019). The morphology of crystallisation of PHBV/PHBV copolymer blends. *European Polymer Journal*, *112*, 104-119.

[42] Zhang, B., Huang, C., Zhao, H., Wang, J., Yin, C., Zhang, L., & Zhao, Y. (2019). Effects of cellulose nanocrystals and cellulose nanofibers on the structure and properties of polyhydroxybutyrate nanocomposites. *Polymers*, *11*(12), 2063.

[43] Brunetti, L., Degli Esposti, M., Morselli, D., Boccaccini, A. R., Fabbri, P., & Liverani, L. (2020). Poly (hydroxyalkanoate) s meet benign solvents for electrospinning. *Materials Letters*, *278*, 128389.

[44] Hestrin, S., & Schramm, M. J. B. J. (1954). Synthesis of cellulose by Acetobacter xylinum. 2. Preparation of freeze-dried cells capable of polymerizing glucose to cellulose. *Biochemical Journal*, *58*(2), 345.

[45] Matos, M., Cruz, R. A., Cardoso, P., Silva, F., Freitas, E. B., Carvalho, G., & Reis, M. A. (2021). Combined strategies to boost polyhydroxyalkanoate production from fruit waste in a three-stage pilot plant. *ACS Sustainable Chemistry & Engineering*, *9*(24), 8270-8279.

[46]   TAPPI (2014), Surface wettability of paper (angle of contact method). *TAPPI* **T458 cm 04**.

[47]   American Society for Testing and Materials (ASTM) E96 (1995). Standard Test methods for water vapor transmission of materials. *ASTM* **04-06**:1-8.

[48]   Cazón, P., & Vázquez, M. (2021). Improving bacterial cellulose films by ex-situ and in-situ modifications: A review. *Food Hydrocolloids*, *113*, 106514.

[49]   Sun, Y., Meng, C., Zheng, Y., Xie, Y., He, W., Wang, Y., Qiao, K., & Yue, L. (2018). The effects of two biocompatible plasticizers on the performance of dry bacterial cellulose membrane: a comparative study. *Cellulose*, *25*, 5893-5908.

[50]   Domjan, A., Bajdik, J., & Pintye-Hodi, K. (2009). Understanding of the plasticizing effects of glycerol and PEG 400 on chitosan films using solid-state NMR spectroscopy. *Macromolecules*, *42*(13), 4667-4673.

[51]   Wu, J., Zhao, C., Lin, W., Hu, R., Wang, Q., Chen, H., Li, L., Chen, S., & Zheng, J. (2014). Binding characteristics between polyethylene glycol (PEG) and proteins in aqueous solution. *Journal of Materials Chemistry B*, *2*(20), 2983-2992.

[52]   Cabello, S. P., Takara, E. A., Marchese, J., & Ochoa, N. A. (2015). Influence of plasticizers in pectin films: Microstructural changes. *Materials Chemistry and Physics*, *162*, 491-497.

[53]   Catoni, S. E., Trindade, K. N., Gomes, C. A., Schneider, A. L., Pezzin, A., & Soldi, V. (2013). Influence of poly (ethylene grycol)-(PEG) on the properties of influence of poly (3-hydroxybutyrate-co-3-hydroxyvalerate)-PHBV. *Polímeros*, *23*, 320-325.

[54]   Jost, V., & Langowski, H. C. (2015). Effect of different plasticisers on the mechanical and barrier properties of extruded cast PHBV films. *European Polymer Journal*, *68*, 302-312.

[55]   Simon, C., Tuerk, M., & Koch, M. (2014). Oxygen and water vapor permeability and required layer thickness for barrier packaging. *In Shaping the Future by Engineering: Proceedings*, ed. by Ilmenau S. 58th IWK, Ilmenau Scientific Colloquium, Technische Universität Ilmenau, 1-11.

[56]   Jost, V., & Miesbauer, O. (2018). Effect of different biopolymers and polymers on the mechanical and permeation properties of extruded PHBV cast films. *Journal of Applied Polymer Science*, *135*(15), 46153.

[57]   Malmir, S., Montero, B., Rico, M., Barral, L., & Bouza, R. (2017). Morphology, thermal and barrier properties of biodegradable films of poly (3-hydroxybutyrate-co-3-hydroxyvalerate) containing cellulose nanocrystals. *Composites Part A: Applied Science and Manufacturing*, *93*, 41-48.

[58]   Shogren, R. (1997). Water vapor permeability of biodegradable polymers. *Journal of environmental polymer degradation*, *5*, 91-95.

[59]   Modi, S., Koelling, K., & Vodovotz, Y. (2011). Assessment of PHB with varying hydroxyvalerate content for potential packaging applications. *European Polymer Journal*, *47*(2), 179-186.

[60]   Lee, H., You, J., Jin, H. J., & Kwak, H. W. (2020). Chemical and physical reinforcement behavior of dialdehyde nanocellulose in PVA composite film: A comparison of nanofiber and nanocrystal. *Carbohydrate polymers*, *232*, 115771.

[61]   Mangaraj, S., Goswami, T. K., & Mahajan, P. V. (2009). Applications of plastic films for modified atmosphere packaging of fruits and vegetables: a review. *Food Engineering Reviews*, *1*, 133-158.

[62]   Maes, C., Luyten, W., Herremans, G., Peeters, R., Carleer, R., & Buntinx, M. (2018). Recent updates on the barrier properties of ethylene vinyl alcohol copolymer (EVOH): A review. *Polymer Reviews*, *58*(2), 209-246.

CHAPTER 4 – ANTIMICROBIAL ACTIVITY OF *IN SITU BACTERIAL NANOCELLULOSE*-ZINC OXIDE COMPOSITES FOR FOOD PACKAGING

Active substances such as zinc oxide nanoparticles (ZnO) have been extensively explored due to their antimicrobial properties, low cost and scalability. Yet, their effectiveness is highly dependent on their morphology and specific surface area. Bacterial nanocellulose (BC) is a suitable carrier due to its ability to transport and deliver active substances. In the case of nanocellulose-ZnO composites, conclusions drawn from antimicrobial studies are often based on only a few representatives of Gram-positive and Gram-negative bacteria. A more comprehensive study using different species and strains, and different methods to assess antimicrobial activity is required. Therefore, in this work, the antimicrobial activity of ZnO suspensions and BC_{ZnO} films was assessed against a wide range of Gram-negative and Gram-positive bacteria using disc diffusion and viable cell count assays.

Regarding the results of the disc diffusion assay, the increase of ZnO content (21-27% m_{Zn}/m_{BCZnO}) (in both ZnO suspensions and BC_{ZnO} films), increased antimicrobial activity against all Gram-negative bacteria tested and some Gram-positive bacteria. In the viable cell count assay, BC_{ZnO} films were effective against *Escherichia coli* (3 log reduction) and *Listeria monocytogenes* (1-3 log reduction) after 24 h. Low temperatures reduced the antimicrobial activity of BC_{ZnO}.

4.1. Introduction

Active packaging can provide new functionalities very useful for the food industry, with regards for instance to the extension of the shelf life, protecting from foodborne pathogens and preserving the organoleptic properties [1]. Active agents may provide antimicrobial or antioxidant properties. Zinc oxide (ZnO) is a thermally stable metal oxide well-known for its antimicrobial and photocatalytic activities [2]. ZnO has been recognized as safe by the European Food Safety Authority (EFSA), but only as an ultraviolet light absorber in unplasticized polymers up to 2.0% (m/m) [3]. Despite the excellent antimicrobial properties, the effectiveness of ZnO particles is highly dependent on their morphology, size (specific surface area) and applied dosage [4]. Most of the reported studies focus on optimising ZnO characteristics for maximum antimicrobial activity [5], [6].

The incorporation of ZnO into different materials has also been studied to develop active packaging. One example is the incorporation of ZnO into nanocellulose (NC). This is one of the most abundant polymers in nature and, due to its mechanical performance, is highly versatile and can be used in various applications [7]. Among all NCs, bacterial nanocellulose (BC) stands out for its high degree of polymerization, high mechanical performance, long fibres, and water holding capacity. This polymer is produced by *Komagataeibacter* species through fermentation (stirred or static), forming a 3D nanofibrillar gel-like membrane. The water holding capacity of BC is an interesting feature for active food packaging applications, as suspensions comprising active substances (such as ZnO) can be easily incorporated into BC.

Several authors reported the development of NC$_{ZnO}$ and BC$_{ZnO}$ films to be used as alternatives to petroleum-based plastics (such as low-density polyethylene and polypropylene) in active food packaging [8]-[16]. Most of the literature concerns the optimization of ZnO synthesis in combination with nanocellulose to obtain an effective composite with antimicrobial activity [9]-[16]. However, most of the studies have not explored the antimicrobial activity of NC$_{ZnO}$ and BC$_{ZnO}$ against a wide range of bacterial species and strains but have selected one or two representatives of Gram-negative and Gram-positive bacteria. Most studies used *Escherichia coli* and *Staphylococcus aureus,* the bacteria recommended by the International Organisation for Standardisation (ISO 22196:2011) [9], [11], [13], [14], as well as *Klebsiella pneumoniae* [15] and *Bacillus subtilis* [12]. The efficacy of other antimicrobial agents, in particular those derived from plant essential oils (specifically

oregano or thyme) or, chitosan, ethanolic propolis extract, and nisin has been demonstrated considering a wider range of Gram-positive and Gram-negative bacteria [17], [18]. Foodborne pathogenic bacteria such as *Listeria monocytogenes*, *Bacillus cereus*, *Salmonella* spp., *Yersinia enterocolitica* and *Campylobacter* spp.*,* which may be present in several foods (fruits, vegetables, meat and fish derivatives) [19] and have been responsible for several outbreaks of foodborne illness [20], [21], should also be considered when developing active packaging for the food industry. In addition, to understand where nanocellulose-ZnO composites can act, a more comprehensive study using different species is needed. The antimicrobial activity against a pathogen when in contact with NC_{ZnO} and BC_{ZnO}, should also be explored and confirmed using different strains of the same species, as reported by some authors [17], [18], [20].

As protocolled by the World Organization for Animal Health (WOAH), there are several methods for determining bacterial susceptibility to antimicrobials, such as the disc diffusion method and viable cell count assays [22]. The former is a widely used method for a preliminary assessment of the "qualitative" susceptibility (susceptible or resistant) of a bacteria to an antimicrobial agent [23]. The outcome is nominally observed through halos, which represent the inhibition effect. However, through the disc diffusion assay, only verification of bacterial growth inhibition is foreseen, meaning that bactericidal and bacteriostatic effects are not distinguished. Yet, further testing should be made for the minimum inhibitory concentration (MIC) and/or the minimum bactericidal concentration (MBC) determination, using agar or broth serial dilutions. For this purpose, the viable cell count assay may be used, which allows the quantification of the number of active growing cells in a sample (when in contact with an active agent). Hence, this work has the objective of demonstrating the efficiency of BC_{ZnO} in inhibiting bacterial growth and its potential as an active food packaging. This is supported by conducting both disc diffusion and viable cell count assays, revealing the different susceptibility of various strains from a set of bacteria. It is also intended to understand the specific mechanisms of ZnO's impact on bacteria, particularly in relation to ROS and the release of Zn2+. This body of information is important to define the specific application in food packaging.

In this work, a BC_{ZnO} composite was developed, through *in situ* production of wet thin BC membrane discs. The ZnO particles morphology and size (in suspensions and the BC

composite) were characterised. The ZnO concentration in the BC composite was also determined. Antimicrobial studies of ZnO suspensions and BC$_{ZnO}$ (with different ZnO concentrations) were carried out using the disc diffusion assay for screening a wide variety of Gram-negative and Gram-positive bacteria and different strains thereof. The best performing BC$_{ZnO}$ composite was then further tested, using viable cell count assay method, for bactericidal assessment.

4.2. Material and Methods

4.2.1. BC production and purification

Komagataebacter xylinus ATCC 700178 (from the American Type Culture Collection) cells were grown in 1 L conical flasks, containing 100 mL of Hestrin-Schramm culture medium (HS) [24] with the following components (in mg mL^{-1}): 20.0 glucose (Fluka, Charlotte, US), 5.0 peptone (Himedia, Mumbai, India), 5.0 yeast extract (Fisher, Hampton, US), 3.39 disodium phosphate di-hydrated (Panreac, Barcelona, Spain) and 1.26 citric acid (Panreac). Hestrin-Schramm culture medium was autoclaved at 121 ˚C for 20 minutes. The inoculated fresh culture medium was incubated in cuvettes (10 X 20 X 10 cm) at 30 °C for 15 days (at a fixed culture medium depth of 1.5 cm). After 15 days of fermentation, BC membranes were washed with NaOH 0.1 M (Panreac), at room temperature, to remove culture medium residues and trapped cells. Afterwards, the membranes were washed with distilled water, also at room temperature, until the pH became that of the distilled water.

4.2.2. BC$_{ZnO}$ production

The BC membranes were sliced into thinner ones with established thickness of 2.0 mm. Discs with 9.0- and 13.0-mm diameter were prepared. In order to dry BC while preserving its 3D structure, the discs were frozen in liquid nitrogen and lyophilized at -99 °C and 0.0025 bar (Coolsafe 100-9 Pro, Labogene, Allerød, Denmark). The ZnO NPs synthesis was performed as reported elsewhere [25], with slight modifications: a 20 mL solution of NaOH (1 M) was carefully added drop by drop (at a rate of 0.67 mL.min^{-1}) using a syringe pump (New Era Pump systems, New York, US) into a solution containing 100 mL of Zn(CH$_3$COO)$_2$ (Sigma, India) with varying concentrations (0.01 M, 0.03 M, and 0.05 M), along with polyvinyl alcohol (PVOH; Fluka, Germany) at a concentration of 5.0 mg mL^{-1} and the previously prepared BC discs. A

magnetic stirring at 200 rpm and a temperature of 50 °C was employed to the mixture. After complete addition of NaOH, the ZnO suspension was left standing overnight. The BC discs were then washed with ultra-pure water to neutral pH and air dried at 37 °C. The average dry thickness of all films was 20 μm. Different concentrations of $Zn(CH_3COO)_2$ were used to achieve varying $[OH^-]/[Zn^{2+}]$ ratios, aiming to evaluate both the particle size of the resulting ZnO and the quantity of Zn incorporated into the BC during *in situ* production.

For comparison purposes, ZnO NPs suspensions were also prepared, using the same procedure described above, but without BC discs. The ZnO suspension was then washed with ultra-pure water by centrifugation (Eppendorf centrifuge 5430R, Hamburg, Germany) at 4000 rpm until neutral pH, before being freeze-dried at -99 °C and 0.025 mbar (Coolsafe 100-9 Pro). The freeze-dried material was then used to prepare ZnO NPs suspensions (by ultrasonication (Bandelin Sonoplus, Berlin, Germany) with 40% amplitude for 4 min) with different concentrations (10, 20, 30, 50, 75 and 100 mg mL^{-1}), for antimicrobial testing. This wide range of ZnO concentrations (in suspension) allows: i) assessing bacteria susceptibility at different ZnO concentration, and ii) comparing the antimicrobial effectiveness of ZnO when in suspension with the effectiveness when incorporated at similar concentrations into BC.

4.2.3. Physical characterization

BC thickness - a digital thickness gauge (Adamel Lhomargy, France) was used to measure the thickness of all the produced discs. For each sample, five measurements (at random positions) were taken.

Dynamic light scattering analysis - The size of ZnO NPs was estimated using a Zetasizer NanoZS (Malvern Instruments Ltd., Worcestershire, UK). Five measurements of each suspension were performed to obtain the average size (nm) and polydispersity (PdI). Before analysis, ZnO NPs suspensions were subjected to ultrasonication as previously described.

Microscopic morphology - BC and BC_{ZnO} discs were characterized using a desktop scanning electron microscope (SEM) coupled with energy-dispersive spectroscopy (EDS) analysis (Quanta 650). All results were acquired using the ProSuite software. The samples were placed in an aluminium pin stub with electrically conductive carbon adhesive tape (PELCO Tabs™). Samples were coated with 1 nm of Au (10 Angstrom) for improved conductivity. The analysis

was conducted with reduced vacuum and a magnification scale of x5000. The size of ZnO NPs was measured through ImageJ software (version 1.8.0).

Zinc quantification - The concentration of Zn in BC_{ZnO} was determined by atomic absorption spectroscopy (AAS) after digestion by microwave (based on EN 14084). Samples were prepared following the guidelines of EN 13804 [26]: BC_{ZnO} discs (ca 15 mg) were ground into small pieces and evenly weighed into the digestion vessel. Afterwards, 5 mL of nitric acid 65% (HNO_3) (Panreac) and 2 mL of hydrogen peroxide (H_2O_2) (Merck KGaA, Germany) were added, and submitted to microwave digestion (Speedwave MWS-3+, Berghof, Eningen, Germany), as presented in Table 4.1.

Table 4.1. Microwave digestion program

Stage	1	2	3	4	5
T (°C)	130	170	200	100	100
Pressure (bar)	20	20	20	20	20
Time (min)	5	10	15	2	2
Ramp (min)	5	5	1	5	1
Power (watt)	30	40	50	30	20

After microwave digestion, the samples were diluted with ultra-pure water to a final volume of 50 mL and analysed by atomic absorption spectroscopy.

Atomic absorption spectroscopy - An atomic absorption spectrophotometer system (Perkin Elmer Analyst 400, Waltham, US) was used, equipped with a zinc cathode lamp (λ= 213.9 nm). Whenever necessary, samples were diluted with ultra-pure water to reach an absorbance signal within the Zn calibration range (0 - 0.50 mg L^{-1} of Zn). Working solutions of zinc (0 - 0.50 mg L^{-1} of Zn) were prepared using a stock solution of 1000 mg L^{-1}. The solutions were prepared in 10.0 mg mL^{-1} of HNO_3. Five readings were made for all samples and working stock solutions. All samples were found to have concentrations above the limit of detection (LoD – 0.07 mg L^{-1}) and limit of quantification (LoQ - 0.23 mg L^{-1}).

4.2.4. Antimicrobial activity of ZnO and BC$_{ZnO}$

The antimicrobial activity of the developed BC$_{ZnO}$ films was assessed by the disc diffusion method and viable cell counting. All tests were made in duplicate and performed twice for validation. For the disc diffusion assay, cocktails of *Salmonella* and of *Campylobacter* strains were prepared prior to testing. *Salmonella* cocktail comprised a blend of *Salmonella enterica* serovar Typhimurium SLM27C, *S. enterica* serovar Infantis M2016, *S. enterica* serovar Senftenberg 775W, *S. enterica* serovar Enteritidis 545047 and *S.* Enteritidis 517536. *Campylobacter* spp. cocktail comprised a blend of *Campylobacter jejuni* DSM 4688, *C. jejuni* DFVF 1099, *C. jejuni* NCTC 11168, *C. jejuni* CJ305*, C. jejuni* C9*, C. jejuni* C21A, *Campylobacter coli* DSM4689, C. *coli* C3. Stock cultures of the strains were stored at −80 °C. For inocula preparation, *Campylobacte*r strains were streaked onto cefoperazone deoxycholate agar

(MCCD agar; SARSTEDT) at 42 °C, in microaerophilic conditions (5.6% CO_2), for 48 h. *Salmonella* strains were streaked on Tryptic soy Agar (TSA, Biokar Diagnostics, Alonne, France) and incubated at 37 °C for 24 h. Subsequently, colonies were harvested with a sterile loop to prepare a cell suspension for each strain in 1/4 strength Ringer solution (Biokar Diagnostics) adjusting cell density to ca. 10^9 $CFUmL^{-1}$, using a 0.5 MacFarland scale as standard. Bacterial cocktails were prepared by mixing equal volumes of each strain from the same species.

Table 4.2. Bacterial strains and respective source used in the agar diffusion antimicrobial tests

Microorganisms	Species	Sources
	Escherichia coli ATCC 25922	ATCC
	Escherichia coli DSM423 (K12)	DSMZ
	Escherichia coli DSM1576	
	Yersinia enterocolitica NCTC10406	NCTC
	Salmonella Infantis M2016	
	Salmonella Typhimurium	
	Salmonella Enteritidis	
	Salmonella Typhimurium SLM27C	ESB culture collection
	Salmonella Senftenberg 775W	
	Salmonella Enteritidis 545047	
	Salmonella Enteritidis 517536	
Gram-negative	*Campylobacter coli* DSM4689	DSMZ
	Campylobacter jejuni DSM4688	
	Campylobacter jejuni DFVF 1099	DFVF
	Campylobacter jejuni NCTC 11168	NCTC
	Campylobacter jejuni CJ305	
	Campylobacter jejuni C9	
	Campylobacter jejuni C21A	
	Campylobacter coli C3	ESB culture collection
	Acinetobacter calcoaceticus S	
	Acinetobacter calcoaceticus R	
	Acinetobacter baumannii R	
	Acinetobacter baumannii 260	
	Staphylococcus aureus 18MRSA	
	Staphylococcus aureus 6538	
Gram-positive	*Bacillus cereus*	ESB culture collection
	Listeria monocytogenes 2542	
	Listeria monocytogenes FSL J1-117	
	Listeria monocytogenes FSL J031	

Listeria monocytogenes FSL R2499	
Enterococus faecium DSMZ 13590	DSMZ
Enterococus flavescens DSMZ 7370	
Enterococus faecalis ATCC 29212	ATCC

4.2.4.1.   Agar diffusion method

The bacteria selected for antimicrobial tests by the agar diffusion method are presented in Table 4.2. Except for *Campylobacter*, all the other species were grown on Müeller-Hinton Agar (MHA) (Biokar Diagnostics) at 30 °C for 24 h. *Campylobacter* strains were grown on MCCD agar at 42 °C, in microaerophilic conditions (5.6% CO_2) for 48 h. Isolated colonies were suspended in Ringer's solution to obtain a turbidity equivalent to 0.5 McFarland scale (10^9 CFU mL^{-1}). Afterwards, sterile swabs were immersed in each inoculum suspension and spread on previously prepared MHA plates. Then, 20 µL of the ZnO suspensions (from 10 to 100 mg mL^{-1}, as described in 2.2.) were directly inoculated on the contaminated plates. After 24 h of incubation at 30 °C, inhibition zones were measured using Interscience software (Interscience, Cantal, France). Antimicrobial activity (target isolates in Table 4.5) was also evaluated for neat BC and BC$_{ZnO}$ discs with increasing ZnO concentration (obtained using 0.01, 0.03 or 0.05 M of Zn(CH$_3$COO)$_2$). The discs were placed on top of the MHA contaminated plates and inhibition zones were measured using Interscience software after 24 h of incubation at 30 °C. Filter paper discs were used as negative control. The incubation of bacteria (in contact with ZnO suspensions and BC$_{ZnO}$ films) was carried out in an oven, with low light exposure (known to interfere with the ZnO mechanism of action against bacteria).

4.2.4.2.   Viable cell count assay

Isolated colonies of *E. coli* ATCC 25922 and *L. monocytogenes* 2542 grown on TSA for 24 h at 30 °C were suspended in Ringer's solution to obtain an optical density (OD$_{600}$) of 1.0, equivalent to 10^9 CFU mL^{-1}. Then, 10 µL (10^9 CFU.mL^{-1}) of each suspension was inoculated onto BC, BC$_{ZnO}$ and ZnO and incubated for 15 min (also referred as 0h'), 4 h and 24 h at 4 °C (stored in a cold room with low light exposure;) and 22 °C (in an oven with low light exposure). After each incubation period, the contaminated discs were immersed into Ringer's solution (9 mL), vortexed for 1 minute and decimal dilutions were made to 10^{-5}. Further automated dilutions and plating on TSA were performed using the automatic spiral method (easySpiral-Pro, Interscience). Viable cells were counted after 24 h of incubation at 30 °C. The loss of cell viability was determined as follows:

$$R(t) = Log\left(\frac{N}{N0}\right) \qquad (1)$$

where R(t) stands to reduction over time; N corresponds to bacterial population (CFU mL^{-1}) after exposure for a certain time and N0 corresponds the initial bacterial population before exposure (CFU mL^{-1}).

4.2.5. Data handling and statistical analysis

Statistical analysis was supported with Prism version 9.4.1 (GraphPad Software, La Jolla California USA), using one-way (and two-way) ANOVA and Tuckey's post-hoc analysis for pairwise comparison of more than two means. Mean differences were considered statistically non-significant (ns) when p-value was higher than 0.05 (95% of interval of confidence). The default statistical confidence level was considered to be 95% ($p < 0.05$) in all tests.

4.3. Results and Discussion

4.3.1. BC$_{ZnO}$ film characterization

BC$_{ZnO}$ films were characterized concerning the ZnO particle size, polydispersity (PdI) and concentration. It is well known that antimicrobial efficiency of ZnO highly depends on particle size and dosage used [4]. By lowering the particle size of ZnO, specific surface area increases, which improves the activity against bacteria. On the other hand, the amount of ZnO incorporated in the matrix is also important since the minimum effective concentration should be determined for each bacterium. As can be seen in Table 4.3, the method used for ZnO production provided a good range of ZnO particle sizes (between 160 and 230 nm) with a low polydispersity index (0.072 - 0.266) and provided homogeneous ZnO suspensions. The Zn(CH$_3$COO)$_2$ concentration influenced the ZnO particle size obtained, a maximum (230 nm) being observed for the intermediate concentration used (Table 4.3). Concerning polydispersity, all ZnO suspensions may be considered homogeneous, with PdI lower than 0.400 (Table 4.3). The increase of zinc acetate concentration during *in situ* ZnO production, led to higher Zn concentration on BC, from 11.05% m$_{Zn}$/m$_{BCZnO}$ (BC$_{ZnO}$ 0.01M) up to 27.10% m$_{Zn}$/m$_{BCZnO}$ (BC$_{ZnO}$ 0.05M), under the conditions tested (Table 4.3). The ability to control the amount of ZnO incorporated in the BC is of high importance since a minimum amount needs to be ensured, irrespective of the average particle size achieved.

Chapter 4

Antimicrobial activity of *in situ* bacterial nanocellulose zinc oxide composites for food packaging   A.G. Soares Silva, F. | 2024

Table 4.3. Properties of ZnO particles on BC_{ZnO} films; data displayed as mean ± standard deviation.

ZnO suspensions			BC_{ZnO}
$Zn(CH_3COO)_2$	ZnO size (nm)	ZnO PdI	Zn (% m_{Zn}/m_{BCZnO})
0.01M*	158 ± 2	0.266 ± 0.017	11.05 ± 2.87
0.03M	244 ± 9	0.072 ± 0.008	21.12 ± 2.23
0.05M	219 ± 8	0.104 ± 0.037	27.10 ± 2.49

*ZnO suspension used for antimicrobial testing

SEM-EDS observations were carried out to analyse the morphology and distribution of ZnO within the BC fibre network. These are shown in Figure 4.1. ZnO particles were found attached to BC fibres and well distributed.

From SEM images, the ZnO particle size was also determined, and compared with that obtained from DLS measurements presented in Table 4.3. The ZnO particle sizes obtained through SEM are moderately higher than those obtained by DLS for ZnO suspensions (Table 4.3; Figure 4.1). According to SEM observations, the increase in $Zn(CH_3COO)_2$ concentration (0.01 M-0.05 M) led to an increase in ZnO particle size, from an average of 218 nm up to 380 nm. The most frequent ZnO particle size also increased with the Zn concentration used.

Particle size interval	BC$_{ZnO}$ 0.01M	BC$_{ZnO}$ 0.03M	BC$_{ZnO}$ 0.05M
<50 nm	1.3 %	nd	nd
50-150 nm	56.0 %	17.1 %	11.2 %
150-300 nm	38.7 %	47.5 %	50.0 %
300-450 nm	4.0 %	24.1 %	23.5 %
> 450 nm	nd	11.3 %	15.3 %
Average size (nm)	218 ± 85 [a]	358 ± 146 [a]	380 ± 175 [a]
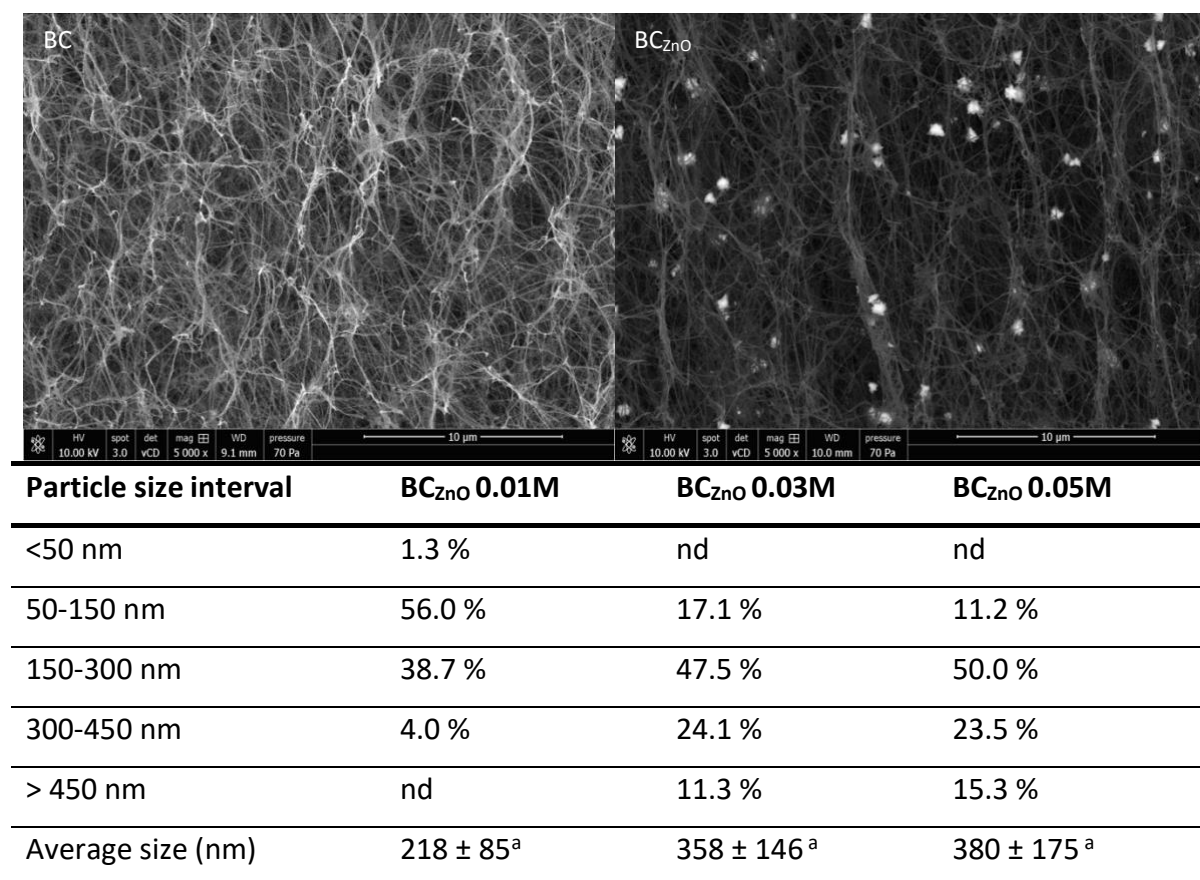
Figure 4.1. SEM observations of BC and BC$_{ZnO}$ and ZnO particle size distribution in BC$_{ZnO}$; last row: data displayed as mean ± standard deviation; the different superscript letters indicate statistically significant differences (p<0.05) ;.

Despite the undesirable effect of increasing Zn(CH$_3$COO)$_2$ concentration in particle size and polydispersity, higher amount of ZnO incorporated may be important to achieve effective antimicrobial activity. The impact of ZnO concentration (and consequently of particle size) on the antimicrobial activity of BC$_{ZnO}$ against different bacteria was then studied.

4.3.2. Antimicrobial activity in the agar diffusion assay

Different concentrations of ZnO NPs (from 10-100 mg L^{-1}) were tested against Gram-negative (*S. Enteritidis, E. coli, Y. enterocolitica, A. baumannii* and *C. coli*) and Gram-positive (*Staph. aureus, B. cereus, L. monocytogenes, En. faecalis*) bacteria, through agar diffusion assay. Results of the tests performed using ZnO suspensions are presented in Table 4.4.

Table 4.4. Antimicrobial activity of ZnO suspensions and BC$_{ZnO}$ discs determined by the agar diffusion method. Results expressed as inhibition halos (mm); data displayed as mean ± standard deviation.

Bacteria strains		ZnO concentration, mg mL^{-1}						ZnO concentration in BC			
		10	20	30	50	75	100	BC (0.0 mL^{-1})	BC$_{ZnO}$ 0.01M mg(27.5 mL^{-1})	BC$_{ZnO}$ 0.03M mg(52.5 mL^{-1})	BC$_{ZnO}$ 0.05M mg(67.5 mg mL^{-1})
Gram-negative	*S.* Enteritidis[1]	0^a	0^a	**10.3±0.8^b**	10.7±0.4^b	12.1±0.9^{bc}	13.7±0.9^c	0^a	0^a	***13.2±1.5^b***	13.3±0.6^b
	E. coli[1] ATCC 25922	0^a	**9.8±0.3^b**	10.2±0.1^b	10.8±0.3^b	11.6±0.1^{bc}	13.9±0.7^c	0^a	0^a	***13.4±3.3^b***	13.4±0.1^b
	Y. enterocolitica[1] NCTC10406	0^a	**9.8±0.7^b**	10.7±0.1^{bc}	11.4±0.5^{bc}	12.4±1.4^c	14.5±1.0^c	0^a	0^a	***12.4±0.6^b***	14.8±1.8^b
	A. baumannii 260 *i*[4]	0^a	0^a	0^a	0^a	0^a	0^a	-	-	-	-
	C. coli[2] DSM4689	**13.4±1.9^a**	*16.1*±1.1^b	19.1±1.5^c	20.0±1.8^c	22.4±2.2^d	24.6±2.1^d	0^a	***13.6±0.8^b***	20.9±4.0^c	27.3±0.9^d
Gram-positive	*Staph. aureus*[1] 6538	0^a	0^a	0^a	**10.8±0.5^b**	12.6±0.5^{bc}	14.1±1.0^c	0^a	0^a	***11.5±0.6^b***	14.5±1.3^b
	B. cereus* [3]	**21.5±0.5^a**	22.6±0.5^a	23.2±0.9^{ab}	25.0±1.5^b	-	27.8±0.5^c	0^a	***21.8±1.3^b***	25.9±0.8^c	28.3±0.3^d
	L. monocytogenes[4] 2542	0^a	0^a	0^a	0^a	0^a	0^a	-	-	-	-

Chapter 4

Antimicrobial activity of *in situ* bacterial nanocellulose zinc oxide composites for food packaging   A.G. Soares Silva, F. | 2024

| *En.   faecalis*[4]   ATCC 29212 | 0[a] | 0[a] | 0[a] | 0[a] | 0[a] | 0[a] | - | - | - | - |

Letters in the same row with different superscripts are significantly different (p<0.05); Numbers in the same column with different superscripts are significantly different

(p<0.05); *Inhibition halos with reduced bacteria growth (not total absence); "-" not measured

Overall, ZnO was effective against Gram-negative bacteria, with *S.* Enteritidis, *E. coli*, and *Y. enterocolitica* showing similar behaviour (p>0.05) when in contact with ZnO (Table 4.4). The increase in ZnO concentration led to higher inhibition of all sensitive bacteria (Table 4.4; p<0.01).

The Gram-positive bacteria *L. monocytogenes* and *En. faecalis* revealed to be resistant to ZnO at all the concentrations tested. *Staph. aureus* and *B. cereus* (both also Gram-positive) proved to be sensitive to ZnO at concentrations of 50 and 10 mg L^{-1}, respectively, or higher (Table 4.4). The Gram-negative bacteria *E. coli* and *Y. enterocolitica* were sensitive to a minimum ZnO concentration of 20 mg L^{-1}, *Salmonella* to 30 mg mL^{-1} and *Campylobacter* spp. to 10 mg mL^{-1} (Table 4.4).
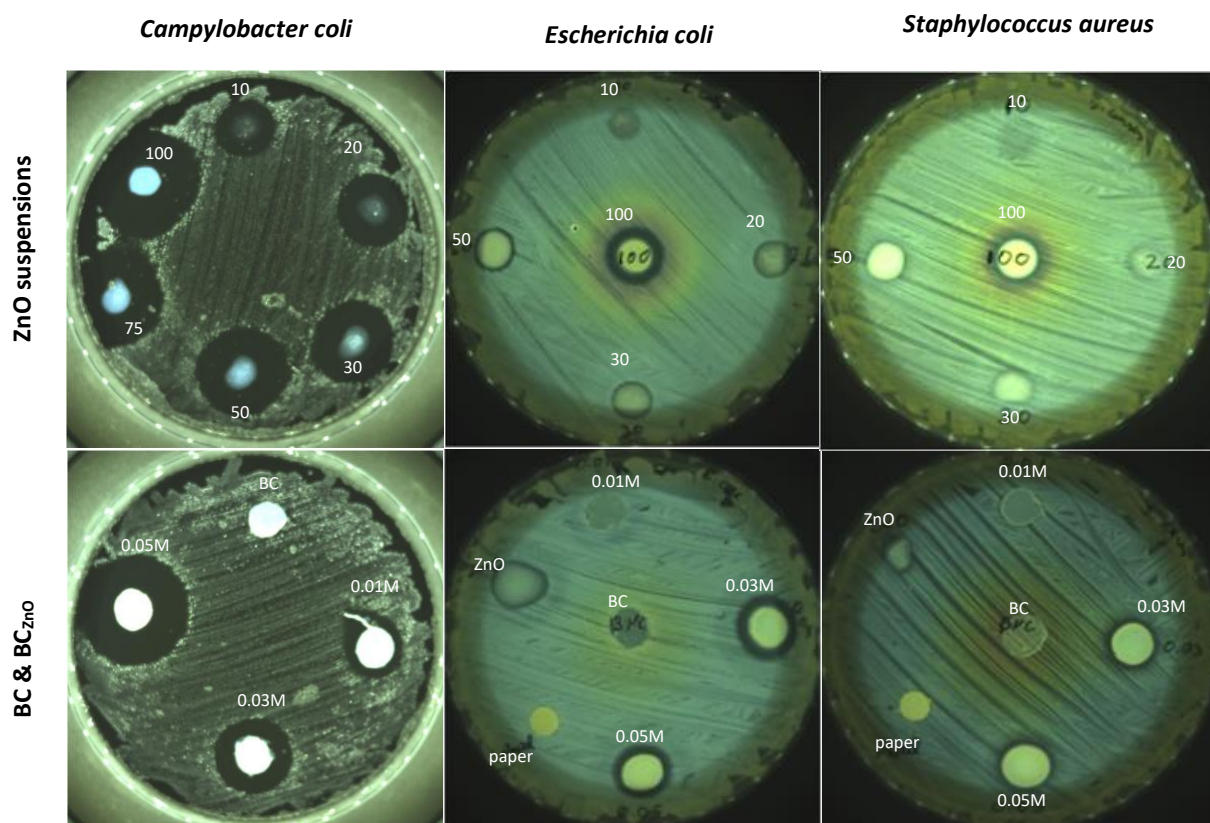
Figure 4.2. Agar diffusion assays with ZnO suspensions (10-100 mg mL^{-1}), neat BC and BC$_{ZnO}$ (0.01M-0.05M)

ZnO was more effective against *C. coli*, when compared to the other tested bacteria (Table 4.4; p<0.01). Only 10 mg mL^{-1} of ZnO was needed to obtain inhibition and the increase

in ZnO concentration led to larger inhibition halos (up to 25 mm; see both Table 4.4 and Figure 4.2). Concerning *B. cereus*, larger inhibition halos were obtained (higher than 20 mm); however, the halo formed corresponds to reduced bacterial growth and not total elimination of growth (Table 4.4). The same assay was carried out with BC_{ZnO} discs, for the bacteria shown to be sensitive to ZnO (Table 4.4).

Only the BC_{ZnO} discs with higher concentrations of ZnO (BC_{ZnO} 0.03M: 21% m_{Zn}/m_{BCZnO} Zn and BC_{ZnO} 0.05M: 27% m_{Zn}/m_{BCZnO}) were effective against all the tested bacteria (Table 4.4). The BC_{ZnO} discs with the lower load of ZnO (BC_{ZnO} 0.01M: 11% of Zn), were only effective against *C. coli* and *B. cereus.* Concerning the dosage effect, higher concentrations (from 21 to 27% m_{Zn}/m_{BCZnO}) led to significantly higher inhibitions of only *C. coli.* and *B. cereus* (Table 4.4; $p<0.01$). Despite the larger ZnO particle size in the more loaded samples (as observed in Figure 4.1), the ZnO dosage proved more important in achieving higher antimicrobial efficiency. Yet, the overall efficiency is lower when ZnO is encapsulated on BC, as compared to the suspensions, as a higher minimum dosage was needed to ensure antimicrobial activity (Table 4.4). The diminished antimicrobial efficiency upon encapsulation may be explained by the higher particle sizes obtained on the BC_{ZnO} (217 – 380 nm *versus* 160 nm for "free" ZnO). Also, the fact that ZnO particles were trapped in the BC fibre matrix, may delay its antimicrobial effect, potentially promoting a prolonged effect over time.

In order to confirm the antimicrobial activity of ZnO (both encapsulated and in suspension) against each specie, additional strains were tested. Qualitative results are provided in Table 4.5. The effects were graded according to the diameters of the inhibition halos. Concerning *E. coli*, no differences were observed between strains, all showing similar inhibition halos. *Salmonella* Infantis and *S.* Typhimurium were slightly more sensitive than *S.* Enteritidis*,* being the minimum ZnO concentration 20 mg mL^{-1}. For the cocktail of *Salmonella* serovars, ZnO suspensions were only effective at a concentration of 30 mg mL^{-1}. Still, superior inhibition zones were observed at these levels of ZnO, as well as on the BC_{ZnO} 0.05 M. For *Acinetobacter* species, only *A. calcoaceticus* (both sensitive and resistant to antibiotics) was inhibited when in contact with ZnO, although BC_{ZnO} 0.05 M was only effective against the sensitive *A. calcoaceticus*. All *L. monocytogenes* and *Enterococcus* spp. strains revealed to be resistant to ZnO NPs*.* Interesting results were obtained with *Campylobacter* isolates, for which greater inhibitions were observed when in contact with ZnO NPs and BC_{ZnO} than for other bacteria. ZnO nanoparticles have been shown to be quite effective against *Campylobacter* spp.

in several studies [27]-[30]. *Campylobacter* spp. are the most common cause of bacterial diarrhoea in developed countries (campylobacteriosis); 70-90% of raw chicken meat (across Europe and North America) was found to be contaminated with *Campylobacter* [27]. Hence, there is extra interest in mitigating the presence of these bacteria in poultry, for example by using pads comprising active agents. The results obtained suggest that BC_{ZnO} films may be used as active pads, to inhibit *Campylobacter* spp. In raw chicken meat. Another study was already conducted with the goal of assessing the antimicrobial activity on chicken skin, where BC_{ZnO} was very effective against *Campylobacter*, indicating BC_{ZnO} potential for active packaging applications in meat-based products [31].

Table 4.5. Screening of the antimicrobial activity of ZnO against different bacterial species and strains.

Bacterial strains*		ZnO (mg mL^{-1})					BC films	
		0	10	20	30	50	BC	$BC_{ZnO\ 0.05M}$
Gram (-)	*E. coli* ATCC 25922	-	-	+	+	+	-	+
	E. coli DSM423(K12)	-	-	+	+	+	-	+
	E. coli DSM1576	-	-	+	+	+	-	+
	S. Infantis M2016	-	-	+	+	+	-	+
	S. Typhimurium	-	-	+	+	+	-	+
	S. Enteritidis	-	-	-	-	+	-	+
	Salmonella (cocktail)	-	-	-	++	++	-	++
	C. coli DSM4689	-	+++	+++	+++	+++	-	+++
	C. jejuni DSM4688	-	+++	+++	+++	+++	-	+++
	Campylobacter (cocktail)	-	+++	+++	+++	+++	-	+++
	A. calcoaceticus S	-	+	+	+	+	-	+
	A. calcoaceticus R	-	+	+	+	+	-	-
	A. baumannii R	-	-	-	-	-	-	-
	A. baumannii 260	-	-	-	-	-	-	-
Gram (+)	*Staph. Aureus* 18MRSA	-	-	++	++	++	-	++
	Staph. Aureus 6538	-	-	-	-	-	-	+
	L. monocytogenes 2542	-	-	-	-	-	-	-
	L. monocytogenes J117	-	-	-	-	-	-	-
	L. monocytogenes J031	-	-	-	-	-	-	-
	L. monocytogenes R2499	-	-	-	-	-	-	-
	En. Faecium DSMZ 13590	-	-	-	-	-	-	-
	En. Faecalis ATCC 29212	-	-	-	-	-	-	-
	En. Flavescens DSMZ 7370	-	-	-	-	-	-	-

Chapter 4
Antimicrobial activity of *in situ* bacterial nanocellulose zinc oxide composites for food packaging   A.G. Soares Silva,

F. | 2024

*Each strain tested twice (duplicates)

The inhibition of bacteria growth is represented as (-;+;++;+++). The symbol "–" represents no inhibition, "+" refers to inhibition halos up to 12mm, "++" refers to inhibition halos between 12-20 mm and "+++" refers to inhibition halos larger than 20 mm.

Compared to previously published data, the current results are consistent when ZnO NPs were tested against *E. coli*, *Salmonella*, *Staph. Aureus, Y. enterocolitica* and *Campylobacter* [27]-[29], [32]-[36]. Despite of the good antimicrobial activity demonstrated by BC_{ZnO}, some discrepancies were found in relation to previous studies reporting antimicrobial activity of ZnO NPs against *L. monocytogenes* [37], [38], *Enterococcus* spp. [39], [40] and *Acinetobacter* spp. [41]-[43]. However, different ZnO NPs sources were used, either commercial [37], [38], [40], [43] or synthesized using precipitation [39] and solvothermal [41], [42] methods. Different ZnO production methods may lead to different characteristics such as particle size and morphology. Most of these studies yielded smaller ZnO particle sizes, in the range of 30-100 nm, which may enhance the antibacterial activity of ZnO [5], [44], [45], while in present work sizes of 160 to 220 nm were obtained (Table 4.3). Additionally, comparison between different studies should be careful and consider all relevant factors. For instance, light conditions during testing are another variable that affects the antibacterial activity of ZnO, since the presence of UV light triggers the synthesis of reactive oxygen species (ROS) [4], [43], [46].

As reviewed by Kumar et al. [6], ZnO affects Gram-positive and Gram-negative bacteria by different mechanisms. The generation of ROS (e.g., $O^{•-}_2$, $HO•$, H_2O_2) is responsible for damage to cells and cellular components through oxidative stress [4], which affects more Gram-positive than Gram-negative bacteria. The latter have an extra outer plasma membrane with a thick lipopolysaccharide, thicker than the peptidoglycan layer of Gram-positive bacteria. These structural differences allow Gram-negative bacteria to resist lipid peroxidation in the presence of ROS [6]. Also, thinner peptidoglycan layers are less negatively charged, therefore less susceptible when in presence of positively charged ZnO NPs. However, according to the results obtained in this study, Gram-negative bacteria were more susceptible to ZnO NPs than Gram-positive bacteria. This difference may be explained by the fact that Gram-negative bacteria are more susceptible to releasing Zn^{2+} from ZnO (another main mechanism of action from ZnO) [6]. The thicker peptidoglycan layer of Gram-negative cells is

more capable of trapping Zn^{2+} from ZnO NPs. However, the ability of a bacteria to resist ZnO NPs, should not rely only on the cell wall structure (Gram-positive vs Gram-negative) but rather on its specific composition. As stated above, Gram-negative bacteria appeared to be more susceptible to BC_{ZnO}, suggesting that the mechanism of action seems to rely more on the Zn^{2+} release rather than ROS generation. This is only increased by exposure to visible and UV light [4]. Our assays were performed under low light exposure; thus ROS generation should not occur significantly (Figures 4.2 and 4.3). Nonetheless, either Gram-positive or Gram-negative bacteria were sensitive/resistant to the developed ZnO NPs (Table 4.4), meaning that other mechanisms should be taken into account. Furthermore, resistance/susceptibility appears to be species and strain dependent (Table 4.5).

4.3.3. Antimicrobial activity – viable cell count assay

In order to study the bacterial inhibition under conditions mimetizing the direct contact of a food pathogen with a packaging material, e.g. the BC_{ZnO} film, the activity against *E. coli* ATCC 25922 and *L. monocytogenes* 2542 was further tested over time (0, 4 and 24 h), at 4 °C and 22 °C by the viable cell count method. The Log(N/N0) was used to express the reduction in cell viability (equation 1).
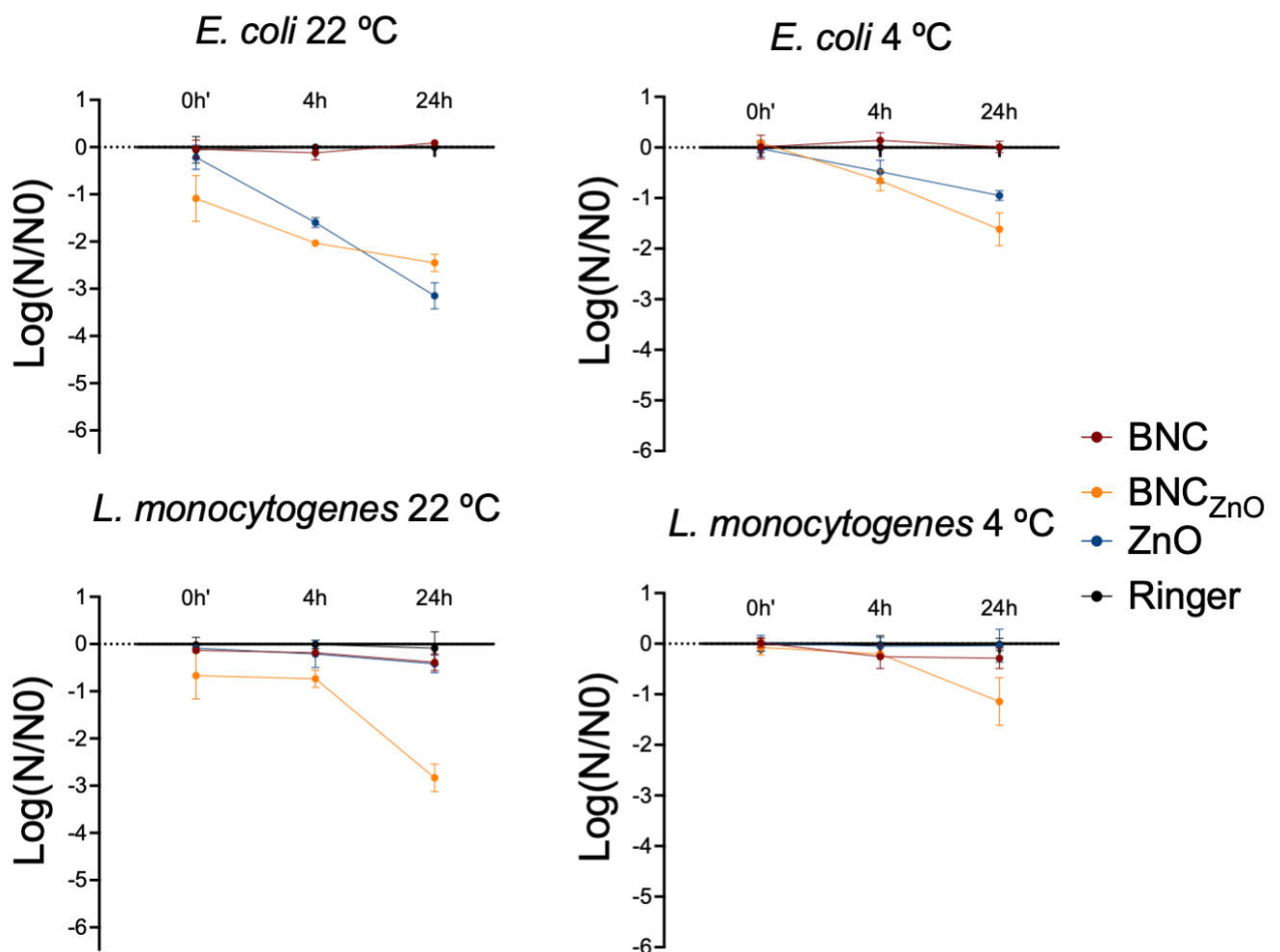
Figure 4.3. Viable cell count assay for *E. coli* and *L. monocytogenes*; see text for statistical differences ($p < 0.05$); symbols represent the mean and error bars represent the standard deviation.

BC$_{ZnO}$ and ZnO suspensions showed antimicrobial activity against *E. coli* after 4 h of contact when stored at 22 °C ($p<0.05$). After 24 h, ZnO was slightly more effective than BC$_{ZnO}$ (3 log reduction for ZnO and 2 log reduction for BC$_{ZnO}$) (Figure 4.3) ($p<0.05$). At 4 °C, the ZnO antimicrobial activity from BC$_{ZnO}$ and suspension was significantly reduced ($p<0.05$), with only a 2 log reduction achieved with BC$_{ZnO}$ and 1 log reduction with ZnO. However, at the lowest temperature, BC$_{ZnO}$ provided higher antimicrobial activity than the ZnO suspension ($p<0.05$).

The cell counts of *L. monocytogenes* were not affected by the ZnO suspension at both temperatures tested ($p<0.05$). However, cell viability decreased after 24 h in contact with BC$_{ZnO}$ (3 log reduction at 22 °C and 1 log reduction at 4 °C) ($p<0.05$). The higher antimicrobial activity of BC$_{ZnO}$ (than ZnO itself) may be explained by the fact that the embedded ZnO (on BC) remains intact, with no signs of aggregation/agglomeration, thus promoting a higher contact area of ZnO with the pathogen.

Overall, the results for *E. coli* are consistent with those obtained using the agar diffusion assay (Figure 4.2 and Tables 4.4 and 4.5). Furthermore, BC$_{ZnO}$ had a bactericidal effect on *E. coli*, as the number of cells decreased over time. On the other hand, the viable cell count method demonstrated that BC$_{ZnO}$ inhibited *L. monocytogenes* (not observed in the agar diffusion tests), also with a bactericidal effect. The latter results (with BC$_{ZnO}$) are consistent with those reporting inhibition of *L. monocytogenes* using ZnO NPs [37], [38].

From a food packaging perspective, the results indicate that BC$_{ZnO}$ may prevent microbial growth under temperature abuse conditions, due to equipment failures and temperature fluctuations along the food chain, from production to consumer stages. Results show that the antimicrobial activity is higher at higher temperatures. ZnO NPs form a strong chemical bond with the hydroxyl groups of cellulose via hydrogen bonding, which hinders ZnO NPs migration into food [47], [48]. Even if ZnO NPs migration occurs, its rate would be relatively low, as ZnO NPs are trapped (due to the high particle size obtained) in the fibre network of BC (Table 4.3) [2]. Hence, the main mechanism of action of BC$_{ZnO}$ material would be through Zn^{2+} migration. Zn^{2+} migration has a significant effect on the inhibition of active transport as well as in the amino acid metabolism and enzyme system disruption [4]. The effect of temperature on Zn transfer from materials to foods and simulants is well known. Higher levels of Zn migration previously observed at higher temperatures [31], [49] were also demonstrated in the present study (Figure 4.3) in parallel with higher antimicrobial activity.

The developed material exhibited high antimicrobial activity against *Campylobacter* species and therefore can be targeted towards meat and poultry-based foods since this bacterium is commonly found in such types of food (applied as pads). Additionally, as mentioned earlier, BC_{ZnO} showed increased antimicrobial activity at higher temperatures, enabling its application in foods subject to significant temperature fluctuations, preventing bacterial growth. However, to explore this application, Zn migration must be monitored, as it is important to prevent excessive migration and mitigate potential risks to consumers. In another study carried out by our research team [31], Zn^{2+} migration was assessed using BC_{ZnO}. Migration onto food simulants was found to be minimal, below the specific migration limit (5.0 mg kg^{-1}). When using chicken skin as a food model, the Zn^{2+} migration was temperature dependent, with migration values surpassing the specific migration limit at temperatures higher than 10 °C [31]. Therefore, it is crucial to assess the antimicrobial activity, migration levels, and the expected abusive temperatures to determine the suitability of employing BC_{ZnO} for food packaging.

4.4. Conclusions

The present study aims to contribute to a better understanding of the antimicrobial activity of ZnO and its mechanism. A cellulosic composite, BC_{ZnO}, was used to assess the effectiveness of ZnO against various bacterial species and strains. Two methods for antimicrobial activity were tested. Results for ZnO NPs and BC_{ZnO} by the disc diffusion method revealed high antimicrobial activity against Gram-negative bacteria, with *S.* Enteritidis, *E. coli*, and *Y. enterocolitica* showing similar behaviour when in contact with ZnO. Inhibition increased with increasing ZnO concentration. The method based on the viable cell counts gave results for *E. coli* in agreement with those of the disc diffusion method, whereas for *L. monocytogenes* a reduction was observed only by viable cell counting. The screening of different bacterial species for the antimicrobial activity of ZnO, as well as the findings from the literature, suggest that the efficiency of ZnO depends on the strain/species tested and that the external factors (light exposure, temperature, ZnO particle size and morphology) impact the ZnO mechanism of action (Zn^{2+} release or ROS generation).

4.5. References

[1]   Yildirim, S., Röcker, B., Pettersen, M. K., Nilsen-Nygaard, J., Ayhan, Z., Rutkaite, R., Radusin T., Suminska P., Marcos, B., Coma, V. (2018). Active Packaging Applications for Food. *Comprehensive Reviews in Food Science and Food Safety*, *17*(1), 165–199. https://doi.org/10.1111/1541-4337.12322

[2]   Kim, I., Viswanathan, K., Kasi, G., Thanakkasaranee, S., Sadeghi, K., & Seo, J. (2022). ZnO Nanostructures in Active Antibacterial Food Packaging: Preparation Methods, Antimicrobial Mechanisms, Safety Issues, Future Prospects, and Challenges. *Food Reviews International*, *38*(4), 537–565. https://doi.org/10.1080/87559129.2020.1737709

[3]   EFSA CEF Panel. (2017). *Safety assessment of the substance zinc oxide, nanoparticles, for use in food contact materials*. *EFSA Journal* (14). https://doi.org/10.2903/j.efsa.2016.4408

[4]   Sirelkhatim, A., Mahmud, S., Seeni, A., Kaus, N. H. M., Ann, L. C., Bakhori, S. K. M., Hasan, H., Mohamad, D. (2015). Review on zinc oxide nanoparticles: Antibacterial activity and toxicity mechanism. *Nano-Micro Letters*, *7*(3), 219–242. https://doi.org/10.1007/s40820-015-0040-x

[5]   Yamamoto, O. (2001). Influence of particle size on the antibacterial activity of zinc oxide. *International Journal of Inorganic Materials*, *3*(7), 643–646. https://doi.org/10.1016/S1466-6049(01)00197-0

[6]   Kumar, R., Umar, A., Kumar, G., & Nalwa, H. S. (2017). Antimicrobial properties of ZnO nanomaterials: A review. *Ceramics International*, *43*(5), 3940–3961. https://doi.org/10.1016/j.ceramint.2016.12.062

[7]   de Amorim, J.D.P., de Souza, K.C., Duarte, C.R., Duarte, I. S., Ribeiro, F. A. S., Silva, G. S., Farias, P. M. A., Stingl A., Costa, A. F. S., Vinhas G. M., Sarubbo, L. A., (2020) Plant and bacterial nanocellulose: production, properties and applications in medicine, food, cosmetics, electronics and engineering. A review. *Environmental Chemistry Letter* 18, 851–869. https://doi.org/10.1007/s10311-020-00989-9

[8]   Bastarrachea, L. J., Wong, D. E., Roman, M. J., Lin, Z., & Goddard, J. M. (2015). Active packaging coatings. *Coatings*, *5*(4), 771–791. https://doi.org/10.3390/coatings5040771

[9]   Lefatshe, K., Muiva, C. M., & Kebaabetswe, L. P. (2017). Extraction of nanocellulose and *in-*

situ casting of ZnO/cellulose nanocomposite with enhanced photocatalytic and antibacterial activity. *Carbohydrate Polymers*, *164*, 301–308. https://doi.org/10.1016/j.carbpol.2017.02.020

[10]   Heidari, H., Teimuri, F., & Ahmadi, A. R. (2022). Nanocellulose-based aerogels decorated with Ag, CuO and ZnO nanoparticles: Synthesis, characterization and the antibacterial activity. *Polyhedron*, *213*, 115629. https://doi.org/10.1016/j.poly.2021.115629

[11]   Wahid, F., Duan, Y. X., Hu, X. H., Chu, L. Q., Jia, S. R., Cui, J. D., & Zhong, C. (2019). A facile construction of bacterial cellulose/ZnO nanocomposite films and their photocatalytic and antibacterial properties. *International Journal of Biological Macromolecules*, *132*, 692–700. https://doi.org/10.1016/j.ijbiomac.2019.03.240

[12]   Mocanu, A., Isopencu, G., Busuioc, C., Popa, O. M., Dietrich, P., & Socaciu-Siebert, L. (2019). Bacterial cellulose films with ZnO nanoparticles and propolis extracts: Synergistic antimicrobial effect. *Scientific Reports*, *9*(1), 1–10. https://doi.org/10.1038/s41598-019-54118-w

[13]   Katepetch, C., Rujiravanit, R., & Tamura, H. (2013). Formation of nanocrystalline ZnO particles into bacterial cellulose pellicle by ultrasonic-assisted in situ synthesis. *Cellulose*, *20*(3), 1275–1292. https://doi.org/10.1007/s10570-013-9892-8

[14]   Shahmohammadi Jebel, F., & Almasi, H. (2016). Morphological, physical, antimicrobial and release properties of ZnO nanoparticles-loaded bacterial cellulose films. *Carbohydrate Polymers*, *149*, 8–19. https://doi.org/10.1016/j.carbpol.2016.04.089

[15]   Janaki, A. C., Sailatha, E., & Gunasekaran, S. (2015). Synthesis, characteristics and antimicrobial activity of ZnO nanoparticles. *Spectrochimica Acta - Part A: Molecular and Biomolecular Spectroscopy*, *144*, 17–22. https://doi.org/10.1016/j.saa.2015.02.041

[16]   Ul-Islam, M., Khattak, W. A., Ullah, M. W., Khan, S., & Park, J. K. (2014). Synthesis of regenerated bacterial cellulose-zinc oxide nanocomposite films for biomedical applications. *Cellulose*, *21*(1), 433–447. https://doi.org/10.1007/s10570-013-0109-y

[17]   Carvalho, M., Albano, H., & Teixeira, P. (2018). In vitro antimicrobial activities of various essential oils against pathogenic and spoilage microorganisms. *Journal of Food Quality and Hazards Control*, *5*(2), 41–48. https://doi.org/10.29252/jfqhc.5.2.3

[18]   Gomes, J., Barbosa, J., & Teixeira, P. (2021). The inhibitory concentration of natural food preservatives may be biased by the determination methods. *Foods*, *10*(5). https://doi.org/10.3390/foods10051009

[19]   Macieira, A., Barbosa, J., & Teixeira, P. (2021). Food safety in local farming of fruits and vegetables. *International Journal of Environmental Research and Public Health*, *18*(18). https://doi.org/10.3390/ijerph18189733

[20]   Oliveira M, Barbosa J, Albano H, Teixeira P (2020) Bacteriocinogenic activity of Leuconostoc lactis RK18 isolated from fermented food. In Fermented Foods: Nutrition and Role in Health and Disease; Kovalyov, O., Ed.; Nova Science Publishers: Hauppauge, NY, USA, 2020; Chapter 3, pp. 159–181.

[21]   Bintsis, T. (2017). Foodborne pathogens. *AIMS Microbiology*, *3*(3), 529.

[22]   World Organisation of Animal Health (2019). Laboratory Methodologies for Bacterial Antimicrobial Susceptibility Testing. *In* OIE Terrestrial Manual 2019, 1-14

[23]   Cotton, G. C., Lagesse, N. R., Parke, L. S., & Meledandri, C. J. (2019). *Antibacterial nanoparticles*. *Comprehensive Nanoscience and Nanotechnology*, 1–5. Elsevier Ltd. https://doi.org/10.1016/B978-0-12-803581-8.10409-6

[24]   Hestrin, S., & Schramm, M. (1954). Synthesis of cellulose by *Acetobacter xylinum*. II. Preparation of freeze-dried cells capable of polymerizing glucose to cellulose. *The Biochemical Journal*, *58*(2), 345–352. https://doi.org/10.1042/bj0580345

[25]   Jaber, B., & Laânab, L. (2014). One step synthesis of ZnO nanoparticles in free organic medium: Structural and optical characterizations. *Materials Science in Semiconductor Processing*, *27*(1), 446–451. https://doi.org/10.1016/j.mssp.2014.07.025

[26]   European Standard (2013). Foodstuffs-determination of elements and their chemical species-general considerations and specific requirements (EN 13804: 2013).

[27]   Hakeem, M. J., Feng, J., Nilqhaz, A., Seah, H. C., Konkel, M. E., & Lua, X. (2020). Active Packaging of Immobilized Zinc Oxide Nanoparticles Controls *Campylobacter jejuni* in Raw Chicken Meat. *Applied and Environmental Microbiology*, *86*(22). https://doi.org/10.1128/AEM.01195-20

[28]   Duffy, L. L., Osmond-McLeod, M. J., Judy, J., & King, T. (2018). Investigation into the antibacterial activity of silver, zinc oxide and copper oxide nanoparticles against poultry-relevant isolates of *Salmonella* and *Campylobacter*. *Food Control*, *92*, 293–300. https://doi.org/10.1016/j.foodcont.2018.05.008

[29]   Windiasti, G., Feng, J., Ma, L., Hu, Y., Hakeem, M. J., Amoako, K., Delaquis, P., Lu, X. (2019). Investigating the synergistic antimicrobial effect of carvacrol and zinc oxide nanoparticles against *Campylobacter jejuni*. *Food Control*, *96*, 39–46.

https://doi.org/10.1016/j.foodcont.2018.08.028

[30] Zhong, X., Wu, Q., Zhang, J., Ma, Z., Wang, J., Nie, X., Ding, Y., Xue, L., Chen, M., Wu, S., Wei, X., Zhang, Y. (2020). *Campylobacter jejuni* Biofilm Formation Under Aerobic Conditions and Inhibition by ZnO Nanoparticles. *Frontiers in Microbiology*, *11*, 1–6. https://doi.org/10.3389/fmicb.2020.00207

[31] Soares da Silva, F. A. G., Bento de Carvalho, T., Dourado, F., Teixeira, P., Gama, M., & Poças, F. (2023). Performance of bacterial nanocellulose packaging film functionalised *in situ* with zinc oxide: migration onto chicken skin and antimicrobial activity. *Food Packaging and Shelf Life*, *39*, 101140.

[32] Xie, Y., He, Y., Irwin, P. L., Jin, T., & Shi, X. (2011). Antibacterial activity and mechanism of action of zinc oxide nanoparticles against *Campylobacter jejuni*. *Applied and Environmental Microbiology*, *77*(7), 2325–2331. https://doi.org/10.1128/AEM.02149-10

[33] Jin, T., Sun, D., Su, J. Y., Zhang, H., & Sue, H. J. (2009). Antimicrobial efficacy of zinc oxide quantum dots against *Listeria monocytogenes*, *Salmonella Enteritidis*, and *Escherichia coli* O157:H7. *Journal of Food Science*, *74*(1). https://doi.org/10.1111/j.1750-3841.2008.01013.x

[34] Jiang, Y., Zhang, L., Wen, D., & Ding, Y. (2016). Role of physical and chemical interactions in the antibacterial behavior of ZnO nanoparticles against *E. coli*. *Materials Science and Engineering C*, *69*, 1361–1366. https://doi.org/10.1016/j.msec.2016.08.044

[35] Li, Y., Xie, S., Xu, D., Shu, G., & Wang, X. (2021). Antibacterial activity of ZnO quantum dots and its protective effects of chicks infected with *Salmonella pullorum*. *Nanotechnology*, *32*(50). https://doi.org/10.1088/1361-6528/ac2846

[36] Bacchu, M. S., Ali, M. R., Setu, M. A. A., Akter, S., & Khan, M. Z. H. (2021). Ceftizoxime loaded ZnO/l-cysteine based an advanced nanocarrier drug for growth inhibition of Salmonella typhimurium. *Scientific Reports*, *11*(1), 1–10. https://doi.org/10.1038/s41598-021-95195-0

[37] Olaimat, A. N., Sawalha, A. G. A., Al-Nabulsi, A. A., Osaili, T., Al-Biss, B. A., Ayyash, M., & Holley, R. A. (2022). Chitosan–ZnO nanocomposite coating for inhibition of *Listeria monocytogenes* on the surface and within white brined cheese. *Journal of Food Science*, *87*(7), 3151–3162. https://doi.org/10.1111/1750-3841.16208

[38] Abdollahzadeh, E., Ojagh, S. M., Hosseini, H., Irajian, G., & Ghaemi, E. A. (2017). Predictive modeling of survival/death of *Listeria monocytogenes* in liquid media: Bacterial responses

Chapter 4

Antimicrobial activity of *in situ* bacterial nanocellulose zinc oxide composites for food packaging   A.G. Soares Silva, F. | 2024

to cinnamon essential oil, ZnO nanoparticles, and strain. *Food Control*, *73*, 954–965. https://doi.org/10.1016/j.foodcont.2016.10.014

[39]   Narayanan, P. M., Wilson, W. S., Abraham, A. T., & Sevanan, M. (2012). Synthesis, Characterization, and Antimicrobial Activity of Zinc Oxide Nanoparticles Against Human Pathogens. *BioNanoScience*, *2*(4), 329–335. https://doi.org/10.1007/s12668-012-0061-6

[40]   Leung, Y. H., Chan, C. M. N., Ng, A. M. C., Chan, H. T., Chiang, M. W. L., Djurišić, A. B., Ng, Y. H., Jim, W. Y., Guo, M. Y., Leung, F. C. C., Chan, W. K., Au, D. T. W. (2012). Antibacterial activity of ZnO nanoparticles with a modified surface under ambient illumination. *Nanotechnology*, *23*(47). https://doi.org/10.1088/0957-4484/23/47/475703

[41]   Shokrollahi, B., Tabatabaee Bafroee, A. S., & Saleh, T. (2021).   Effect of Zinc Oxide Nanoparticles on Loaded Antibiotics Against Multidrug-Resistant *Acinetobacter* spp. . *Avicenna Journal of Clinical Microbiology and Infection*, *8*(2), 51–56. https://doi.org/10.34172/ajcmi.2021.10

[42]   Ghasemi, F., & Jalal, R. (2016). Antimicrobial action of zinc oxide nanoparticles in combination with ciprofloxacin and ceftazidime against multidrug-resistant *Acinetobacter baumannii*. *Journal of Global Antimicrobial Resistance*, *6*, 118–122. https://doi.org/10.1016/j.jgar.2016.04.007

[43]   Yang, M. Y., Chang, K. C., Chen, L. Y., Wang, P. C., Chou, C. C., Wu, Z. Bin, & Hu, A. (2018). Blue light irradiation triggers the antimicrobial potential of ZnO nanoparticles on drug-resistant *Acinetobacter baumannii*. *Journal of Photochemistry and Photobiology B: Biology*, *180*, 235–242. https://doi.org/10.1016/j.jphotobiol.2018.02.003

[44]   Stanković, A., Dimitrijević, S., & Uskoković, D. (2013). Influence of size scale and morphology on antibacterial properties of ZnO powders hydrothemally synthesized using different surface stabilizing agents. *Colloids and Surfaces B: Biointerfaces*, *102*, 21–28. https://doi.org/10.1016/j.colsurfb.2012.07.033

[45]   Babayevska, N., Przysiecka, Ł., Iatsunskyi, I., Nowaczyk, G., Jarek, M., Janiszewska, E., & Jurga, S. (2022). ZnO size and shape effect on antibacterial activity and cytotoxicity profile. *Scientific Reports*, *12*(1), 1–13. https://doi.org/10.1038/s41598-022-12134-3

[46]   Adams, L. K., Lyon, D. Y., & Alvarez, P. J. J. (2006). Comparative eco-toxicity of nanoscale TiO$_2$, SiO$_2$, and ZnO water suspensions. *Water Research*, *40*(19), 3527–3532. https://doi.org/10.1016/j.watres.2006.08.004

[47]   Onyszko, M., Markowska-Szczupak, A., Rakoczy, R., Paszkiewicz, O., Janusz, J., Gorgon-

Kuza, A., Wenelska, K., Mijowska, E. (2022). The cellulose fibers functionalized with star-like zinc oxide nanoparticles with boosted antibacterial performance for hygienic products. *Scientific Reports*, *12*(1), 1–13. https://doi.org/10.1038/s41598-022-05458-7

[48]   Azizan, A., Samsudin, A. A., Shamshul Baharin, M. B., Dzulkiflee, M. H., Rosli, N. R., Abu Bakar, N. F., & Adlim, M. (2023). Cellulosic fiber nanocomposite application review with zinc oxide antimicrobial agent nanoparticle: an opt for COVID-19 purpose. *Environmental Science and Pollution Research*, *30*(7), 16779–16796. https://doi.org/10.1007/s11356-022-18515-5

[49]   Poças, F., & Franz, R. (2018). Overview on european regulatory issues, legislation, and EFSA evaluations of nanomaterials. In *Nanomaterials for Food Packaging: Materials, Processing Technologies, and Safety Issues*, 277–300, Elsevier. https://doi.org/10.1016/B978-0-323-51271-8.00010-3

CHAPTER 5 – PERFORMANCE OF BACTERIAL CELLULOSE PACKAGING FILM FUNCTIONALISED *IN SITU* WITH ZINC OXIDE: MIGRATION ONTO CHICKEN SKIN AND ANTIMICROBIAL ACTIVITY

Zinc oxide nanoparticles (ZnO) are cost-effective antimicrobial agents with great potential for the active packaging industry. Bacterial cellulose (BC) features a porous fibre network, with high absorption capacity, flexible and with good mechanical properties, suitable as a carrier of active agents. In this work, BC_{ZnO} films were developed and optimized regarding the particle size and ZnO concentration. The NaOH dropwise addition to BC membranes immersed in $Zn(CH_3COO)_2$-PVOH enabled the production of ZnO nanoparticles with an z-average of 144 nm and a low polydispersity index. High ZnO incorporation (27 %m_{Zn}/m_{BCZnO}) was obtained, with uniform distribution all over the BC membranes. These composites were then characterized and evaluated for Zn migration using food simulants (10%, 20%, and 50% ethanol) with results lower than the limit. Migration into chicken skin, as a real food model, was low at 4 °C but exceeded the migration limit at 10 and 22 °C. Zn migration was also found to be temperature and pH dependent. When applied to chicken skin, BC_{ZnO} was effective against *E. coli*, *Salmonella* (0.5-1.0 log reduction), and *Campylobacter* spp. (2.0 log reduction), indicating its potential for active packaging applications.

5.1.   Introduction

Active and intelligent packaging has gained significant attention from both industry and research communities, as evidenced by the growing number of publications in the field [1]. Active packaging may be characterized by its ability to absorb or release substances to extend food shelf life, preserve freshness and enhance safety (by inhibiting pathogenic bacteria). In turn, intelligent packaging monitors the condition of the packaged food (and the surrounding environment), offering valuable information for effective food preservation [2]. Both systems have been explored using bio-based polymers such nanocelluloses, chitosan, polylactic acid and polyhydroxyalkanoates as alternatives to petroleum-based plastics [3],[4]. It has been reported that nanocomposite systems often improve the mechanical and barrier properties of neat biobased polymers, which is crucial for producing packaging systems that meet the food protection requirements [5]. However, the high manufacturing costs, difficult scalability and low global production of these bio-based composites still make them uncompetitive when compared to petroleum-based plastics [5],[6]. The functionalization of composites with active agents, through low-cost strategies, may be a step toward increasing their competitiveness.

One of the major bio-based polymers being studied is nanocellulose, which is known for its high crystallinity, degree of polymerization and mechanical strength, low density, biocompatibility, non-toxicity and biodegradability. Nanocellulose is an excellent support or carrier for active substances, such as bacteriocins, metal oxides and organic acids [5]. Nanocellulose may be isolated from plants or produced through bacterial fermentation [5], [7]. Plant-based nanocellulose extraction requires chemicals and intensive wood processing (steam explosion, enzyme-assisted and acid hydrolysis and/or other mechanical methods), which are not free of environmental issues [8]. As an alternative, bacterial cellulose (BC) may be used. BC is a biopolymer produced by bacteria (*Komagataeibacter* genus), using either static or agitated fermentation, and thus through a more sustainable approach [7]. When compared to plant nanocelluloses, BC is naturally produced by static culture as a membrane with high porosity and water holding capacity, mechanically stable in the wet state [9]. For food packaging applications, BC has been studied either as a reinforcing agent [10], as the main matrix [11], [12] as well as a carrier for active agents [13], [14].

Chapter 5

Performance of bacterial nanocellulose packaging film functionalised *in situ* with zinc oxide:
migration onto chicken skin and antimicrobial activity   A.G. Soares Silva, F. | 2024

Zinc oxide (ZnO) is a thermally stable material with photocatalytic and antibacterial activity. In addition, ZnO is well known for its low production cost and for being easily scalable and processable. It is widely used in applications such as drug delivery, cosmetics and medical devices [15]. So far, it is considered safe for food contact materials (FCMs) by the European Food Safety Authority (EFSA), as an ultraviolet light absorber in unplasticized polymers at up to 2.0% (m/m) [16]. More recently, ZnO has been explored in its nano form, since its higher surface area may result in enhanced properties, especially antimicrobial activity [17]. The research community has focused on the relationship between nanoparticle (NP) size and its antimicrobial effect [18], [19]. However, only few studies have focused on ZnO migration into food systems [20] - [22].

In Regulation (EC) No 1935/2004 it is outlined that FCMs must be designed (according to good practices) to prevent migration of their constituents, such that the transferred quantities do not pose a risk to human health, undesirable changes in the food composition, or deterioration of its organoleptic properties. Furthermore, the regulations relating to plastic materials, namely Regulation (EU) No. 10/2011, and active and intelligent packaging materials (Regulation (EC) No. 450/2009), highlight the need for a specific evaluation of substances in nanoform. Thus, it is imperative to understand the potential for mass transfer of nanoparticles (NPs) and the interactions between the composite materials and the food systems [23].

In a scientific study regarding the safety assessment of ZnO nanoparticles in FCMs, EFSA concluded that ZnO NPs do not migrate in nanoform, when incorporated in an unplasticized polymer [16], [24]. Consequently, the safety assessment should focus on the migration of soluble ionic zinc (Zn^{2+}), which must comply with the specific migration limit (SML) of 5 mg.kg^{-1} (Commission, 2007; EFSA CEF Panel, 2017) [16], [24]. The migration of ZnO depends on the matrix where it is incorporated, with several polymers having been tested, such chitosan, gelatin, starch and nanocellulose [5].

The longer fibres, superior water holding capacity and porosity of BC are considered to be appropriate for active food packaging, since it makes relatively easy to incorporate active substances [7],[14]. The literature reports the use of BC as a support for many active agents [25] - [28], and for ZnO in particular [29], [30]. These studies described the optimization of the *in-situ* production or incorporation of ZnO on BC, considering its concentration,

morphology and particle size, to obtain the most effective antimicrobial activity. While reported research has predominantly focused on the antimicrobial efficiency of ZnO functionalized nanocellulose films, studies concerning the migration of Zn (from ZnO) have received limited attention, particularly migration to food models. Hence, in this study, the Zn migration from BC$_{ZnO}$ films is addressed, along with its antimicrobial activity using a real food model, chicken skin.

The production of ZnO in a wet thin BC membrane was studied, using two different in situ production methods. Most of the published work used in situ production of ZnO through direct immersion of the BC membrane. In the present work an alternative *in situ* drop-wise production method was tested. ZnO morphology, particle size, particle distribution within the BC membrane and ZnO concentration were optimized to obtain the best performing composite for active food packaging. The dried composite was then tested for migration using food simulants as well as a real food model, chicken skin. These tests were conducted at different temperatures, and the Weibull model was used to describe the Zn migration from BC. Finally, the antimicrobial activity of BC films with ZnO was tested using the same real food model. This model was selected because BC$_{ZnO}$ is envisaged as an antimicrobial packaging film for fresh/conditioned chicken.

5.2.   Material and Methods

5.2.1.   BC production and purification

The strain *Komagataeibacter xylinus* ATCC 700178 (American Type Culture Collection) was cultured in solid state using Hestrin-Schramm (HS) medium supplemented with 2.0% (w/v) agar (Acros Organics, Geel, Belgium). For pre-inoculum, 100 mL of Hestrin-Schramm culture medium (HS) was prepared in a 1 L conical flasks [31]. HS culture is composed of the following components (in % m/v): 2.0 glucose (Fluka, Buchs, Switzerland), 0.5 peptone (Himedia, Pennsylvania, USA), 0.5 yeast extract (Fisher, Massachusetts, USA), 0.339 disodium phosphate di-hydrated (Panreac, Barcelona, Spain) and 0.126 citric acid (Panreac). HS medium was autoclaved at 121 °C for 20 minutes. The cells from the HS-agar were inoculated onto the previously prepared HS medium using an inoculation loop and incubated under static conditions for 48 hours. The resulting cellulose formed was manually agitated to release the bacteria trapped within the cellulose matrix into the medium. This medium was

subsequently used for further inoculations at a 10% (v/v) ratio to the final fermentation volume of fresh HS medium. The inoculated fresh culture medium was incubated in cuvettes (10x20x10 cm) at 30 °C for 15 days (at a fixed culture medium depth of 1.5 cm). After 15 days of static fermentation, produced BC membranes were washed with 0.1 M NaOH (Panreac) at room temperature to remove any residual culture medium and trapped cells. Subsequently, the membranes were washed with distilled water at room temperature, with multiple water changes, until neutral pH. The membranes were then stored in distilled water at 4 °C until further use.

5.2.2. ZnO NPs and BC$_{ZnO}$ production

The BC membranes were longitudinally sliced into thinner membranes with a thickness of 2.0 mm using a Duegi Affettatrici machine (type 275-SE, Besnate, Italy). Subsequently, discs with diameters of 9.0 mm, 13.0 mm, and 20.0 mm were prepared from these BC membranes. The 13.0 mm discs were used for optimizing the production of BC$_{ZnO}$, while the 9.0 mm discs were employed to assess Zn migration in food simulants. The 20.0 mm discs, were used for Zn migration and antimicrobial testing in chicken skin. The BC discs were frozen in liquid nitrogen and subsequently lyophilised in a freeze drier (Coolsafe 100-9 Pro, Labogene, Allerød, Denmark) at -99 °C and 0.025 mbar until complete dryness.

Prior to ZnO in situ production, two approaches were studied without BC discs: (i) in situ and (ii) drop in situ. The in situ method (i), consisted of the direct addition of 10 mL of NaOH (0.05 M) solution into 2.0 mL solution of Zn(CH$_3$COO)$_2$.2H$_2$O (0.01M) (Sigma; India), at room temperature, to obtain a ZnO suspension. For the drop in situ method (ii), the ZnO NPs synthesis was carried out as follows: a 20 mL NaOH solution (1M) was added dropwise (0.67 mL.min^{-1}; using a syringe pump (New Era Pump systems, Farmingdale, NY) to 100 mL solution of Zn(CH$_3$COO)$_2$.2H$_2$O (0.01M-0.1M), with magnetic stirring at 200 rpm and at 50 °C. After 1 hour, the ZnO suspension was collected for washing. These ZnO NPs were produced, using glycerol (Fisher, Belgium;0.5%m/v) and polyvinyl alcohol (PVOH; FLuka, Germany) (0.5%m/v) as capping agents for ZnO NPs optimization [19]. The obtained ZnO suspension was then washed with ultra-pure water by centrifugation (Eppendorf Centrifuge 5430 R; Germany) at 4000 rpm until neutral pH. Then, ZnO NPs were stored in the fridge for 1 day, before dynamic scattering analysis.

For ZnO in situ production (on BC discs), only the drop in situ was carried out as in situ method had a lower performance regarding particle size and polydispersity (Section 5.3.1. Characterization of the ZnO particles and films). The in situ ZnO synthesis was carried out as follows: a 20 mL NaOH solution (1M) was added dropwise (0.67 mL.min^{-1}; using a syringe pump (New Era Pump systems) to 100 mL solution of $Zn(CH_3COO)_2$ (0.01M-0.05M) with previously immersed (swollen) BC discs (magnetic stirring at 200 rpm and 50 °C was applied). The BC discs were left overnight under stirring and then washed with ultra-pure water until neutral pH, before air drying at 37 °C (in a hot room). All discs (9.0 and 13.0 diameter discs with an average thickness of 20 μm and 20.0 mm diameter discs with an average thickness of 40 μm) were stored in a desiccator until use. The water holding capacity of BC discs, determined by the ratio of the mass of removed water (g) to the mass of dried BC (g), was found to be 85.3 ± 13.8 (g of water removed/g of dried cellulose).

5.2.3. Physical characterization

BC thickness - measurements were performed with a digital thickness gauge (Adamel Lhomargy, France) on all produced BC discs. Three replicates were prepared for each sample and five thickness measurements (at random positions) were taken for each replicate.

Dynamic scattering analysis (DLS) - The size of the ZnO NPs was estimated using a Zetasizer NanoZS (Malvern Instruments Ltd., Worcestershire, UK). Five measurements were taken from each suspension to obtain an average size (nm) and average polydispersity (PdI). Before analysis, ZnO NPs suspensions were subjected to ultrasonication (UW 2070, Bandelin Sonoplus) with 40% amplitude for 4 min.

Morphologic analysis - Neat BC and BC$_{ZnO}$ samples were characterised using a desktop Scanning Electron Microscope (SEM) coupled with energy-dispersive spectroscopy (EDS) analysis (Quanta 650). Prior testing, all samples were frozen in liquid nitrogen, sliced perpendicularly and subsequently lyophilised as previously described. All results were processed with ProSuite software. The samples were placed in an aluminium pin stub with electrically conductive carbon adhesive tape (PELCO Tabs™). Samples were coated with 1 nm of Au (10 Angstrom) for improved conductivity. The analysis was conducted with intensity image of 10 kV, reduced vacuum and a varying magnification scale from x1000 to x5000. The size of ZnO NPs was measured through ImageJ software (version 1.8.0).

Fourier-Transform Infrared Spectroscopy (FTIR) - FTIR analysis of BC, BC$_{ZnO}$ and ZnO (dry-state) was carried out in a Bruker FTIR spectrometer ALPHA II (Bruker Corporation, Billerica, MA, USA) in transmission mode, operating at a resolution of 4 cm^{-1}. The spectra were taken between 4000 and 300 cm^{-1} by averaging 60 scans for each spectrum. All samples were scanned twice for verification purposes.

5.2.4. Migration tests

Food simulants - The specific migration of zinc from BC$_{ZnO}$ films (0.05 M ZnO) into food simulants (ethanol 10%, 20% and 50% (v/v)) as well as into chicken skin was determined. For the food simulants tests, a solid-to-liquid ratio of 2.7 dm^2 L^{-1} was used. The BC$_{ZnO}$ discs were immersed in the food simulant at 60 °C for 15 days, according to Regulation (EU) No. 10/2011 applicable to plastics. During the assay, samples were collected after 1, 3, 5, 7 and 15 days. The simulant samples were analysed for Zn concentration (section 5.2.5).

Chicken skin - The skin from a chicken leg, purchased at a local supermarket, was carefully removed in one piece and stored refrigerated until use. The skin was kept for a maximum of 3 days. The water content of the skin was about 42% (m/m). The skin was cut into discs of similar size to the BC$_{ZnO}$ disc (20 mm). BC$_{ZnO}$ discs (average weight of 15 mg) were brought into contact with the chicken skin discs, resulting in a solid-to-solid ratio of 44.3 dm^2 kg^{-1}. The BC$_{ZnO}$ disc and the skin were left in contact for 7 days at 4 °C, 10 °C and 22 °C. This temperature range was chosen to simulate the different temperature conditions that the food may be exposed to, the first being the recommended one for storage and the two other representing abuse temperatures. Chicken skin samples were collected after 1, 3, 5 and 7 days for determination of Zn concentration. The chicken skin discs were digested as described in section 5.2.5 before zinc determination.

The Zn concentrations obtained (either on food simulants or chicken skin) were normalized to the conventional contact ratio of 6 dm^2 kg^{-1}.

5.2.5. Zinc quantification

The concentration of Zn in BC, BC$_{ZnO}$, in food simulants and chicken skin was quantified by Atomic Absorption Spectrophotometer (AAS) according to standard EN 14084 [32]. The concentration of Zn in the food simulants was determined directly and after microwave

digestion in the case of BC_{ZnO} samples and chicken skin, as described below. As control, the amount of Zn on BC and chicken skin was determined and found to be 0.012 % m/m_{BC} and 0.0008 % $m/m_{chicken}$, respectively.

Samples preparation by microwave digestion - samples were prepared following the guidelines of standard EN 13804 (European standard, 2013): BC_{ZnO} discs (ca 15 mg) and chicken skin (ca 0.2 g) were separately ground into small pieces and evenly weighed into the digestion vessel; then, 5 mL nitric acid 65% (HNO_3) (Panreac, Spain) and 2 mL of hydrogen peroxide (H_2O_2) (Merck KGaA, Germany) were added; finally, the samples were submitted to the microwave digestion program (Speedwave MWS-3+, Berghof, Germany), presented in Table 5.1. After microwave treatment, the digested samples were diluted with ultra-pure water to a final volume of 50 mL and analysed by AAS.

Table 5.1. Microwave digestion program

Stage	1	2	3	4	5
T (°C)	130	170	200	100	100
Pressure (bar)	20	20	20	20	20
Time (min)	5	10	15	2	2
Ramp (min)	5	5	1	5	1
Power (watt)	30	40	50	30	20

Atomic absorption spectroscopy - an atomic absorption spectrophotometer (Perkin Elmer Aanalyst 400, Waltham, MA) was used, equipped with a zinc cathode lamp (λ= 213.9 nm). Whenever necessary, samples were diluted with ultra-pure water to obtain an absorbance signal within the Zn concentration (0–0.50 mg L^{-1} of Zn). Working solutions of zinc (0–0.50 mg L^{-1} of Zn) were previously prepared using a stock solution of 1000 mg L^{-1}, using a 1.0% v/v HNO_3 solution. Five readings were made for all samples and working solutions. The system suitability parameters were determined: limit of detection (LoD – 0.07 mg L^{-1}) and limit of quantification (LoQ - 0.14 mg L^{-1}). All samples had concentrations higher than LoD or LoQ. For the determination of zinc in the migration solutions, working solutions (0–0.50 mg L^{-1} of Zn) were prepared with the food simulants used for the migration tests (ethanol 10%, 20% and 50% v/v) (Honeywell, Germany).

5.2.6. Migration modelling

A kinetic model based on the Weibull distribution function [33] was used to describe Zn migration from BC into chicken skin. The Weibull model was previously applied to describe migration of different substances from plastics and from paper onto simulants [34], [35]. This model is empirical and mathematically simpler than the models describing diffusion according to Fick's law [35] and is represented by the equation (1):

$$C(t) = C\infty * \left(1 - \exp\left(-\left(\frac{t}{\tau}\right)^{\beta}\right)\right) \qquad (1)$$

Where C(t) is the concentration of migrant in food simulant changing with time (t) and C∞ is the concentration at equilibrium. The model has two parameters: τ, the system time

constant, which represents the process rate, and β, the shape parameter, which relates to the initial rate of the process, quantifying the pattern of the curvature observed [35]. This model was fitted to the experimental data obtained in the migration tests for each temperature and the parameters C∞, τ and β were estimated as described in section 5.2.8.

The effect of temperature on the parameters "τ" and "β" was analysed considering the Arrhenius equation (Figure 6), with the general formula:

$$K = A exp(-\frac{Ea}{RT})\tag{2}$$

Equation (2) after natural log becomes

$$\ln(K) = \ln(A) - \frac{Ea}{R}\frac{1}{T}\tag{3}$$

which can be written using the form y = ax + b; where "y" represents "ln(τ)" or "ln(β)"; "x" represents "$1/T$"; and "a" and "b" constants stands for "$-Ea/R$" and "ln(A)", respectively.

5.2.7. Antimicrobial activity of BC$_{ZnO}$ discs

The antimicrobial activity of the BC$_{ZnO}$ discs on chicken skin was explored by the viable cell counting method. Cocktails of different *Salmonella* serotypes and different strains of *C. coli* and *C. jejuni* were prepared for testing. The composition of the cocktails is shown Table 5.2, together with the source of each bacteria strain. All tests were performed in duplicate and validated twice.

Table 5.2. Bacteria used for testing the antimicrobial effect of BC$_{ZnO}$ films in chicken skin

Cocktails	Microorganisms Species	Sources	
-	*Escherichia coli* ATCC 25922	ATCC	
Salmonella	*Salmonella* Infantis M2016	ESB	culture
	Salmonella Typhimurium SLM27C	collection	
	Salmonella enterica serovar Seftenberg 775W		
	Salmonella Enteritidis 545047		
	Salmonella Enteritidis 517536		
Campylobacter	*Campylobacter coli* DSM4689	[a]DSMZ	
	Campylobacter jejuni DSM4688		
	Campylobacter jejuni DFVF 1099	[b]DFVF	
	Campylobacter jejuni NCTC 11168	[c]NCTC	
	Campylobacter jejuni CJ305	ESB	culture
	Campylobacter jejuni C9	collection	
	Campylobacter jejuni C21A		
	Campylobacter coli C3		

[a]German Collection of Microorganisms and Cell Cultures GmbH

[b]Danish Institute for Food and Veterinary Research
[c]National Collection of Type Cultures

5.2.7.1.   Inocula preparation and viable cell count on chicken skin

E. coli ATCC 25922 and *Salmonella* (S. Enteritidis 545047 and cocktail strains) were grown on Tryptic soy Agar (TSA) (BIOKAR, France) at 30 °C for 24 h. For *Campylobacter* (*C. coli* DSM4689 and cocktail strains), cultures were grown in modified charcoal cefoperazone deoxycholate agar (MCCD agar; SARSTEDT) at 42 °C, in microaerophilic conditions (5.6% CO_2) for 48 h. Then, colonies were transferred to Ringer's solution (BIOKAR) to obtain an optical density (OD600) of 1.0, equivalent to 10^9 CFU mL^{-1}. Cocktails (from *Salmonella* and *Campylobacter*) were prepared by mixing equal volumes of each strain from the same genus, in Ringer's solution.

Afterwards, 10 µL (10^9 CFU mL^{-1}) of each culture or cocktail were inoculated on chicken skin samples, of the same diameter as that of BC/BC_{ZnO} discs. The contaminated chicken skin samples were stored for 24 h at 4 °C, to verify that bacteria counts were maintained before applying the BC discs. Then, BC and BC_{ZnO} discs were placed on top of the contaminated samples and stored again for 24 h (48 h since inoculation) at 4 ºC. Contaminated chicken skin samples (at 0 h', 24 and 48 h) were submerged into Ringer's solution (9 mL) and manually diluted (1:10 mL) until 10^5 CFU mL^{-1}. Further dilutions (until 10^1 CFU mL^{-1}) were automatically made with spiral plate (easySpiral-Pro, Interscience). After inoculation, cells on each contaminated sample were counted after 15 min (referred as 0 h'), 24 h and 48 h. In parallel, the number of active growing cells on contaminated chicken skin (without BC/BC_{ZnO} treatment) was monitored throughout the assay. The cell reduction was quantified as follows:

$$Reduction = Log\left(\frac{n}{n0}\right) \qquad\qquad (4)$$

Where "n" corresponds to the CFU mL^{-1} after exposure of the chicken skin to BC/BC_{ZnO} for a certain time (from 24 h to 48 h after inoculation) and "n_0" corresponds the initial concentration (CFU.mL^{-1}), before exposure. Chicken skin inoculated and without any BC disc was also stored for reference. Viable cell counting was also done on uncontaminated chicken skin samples, where no bacteria growth was observed. Figure 5.1 presents the experimental design for the viable cell count on chicken skin.
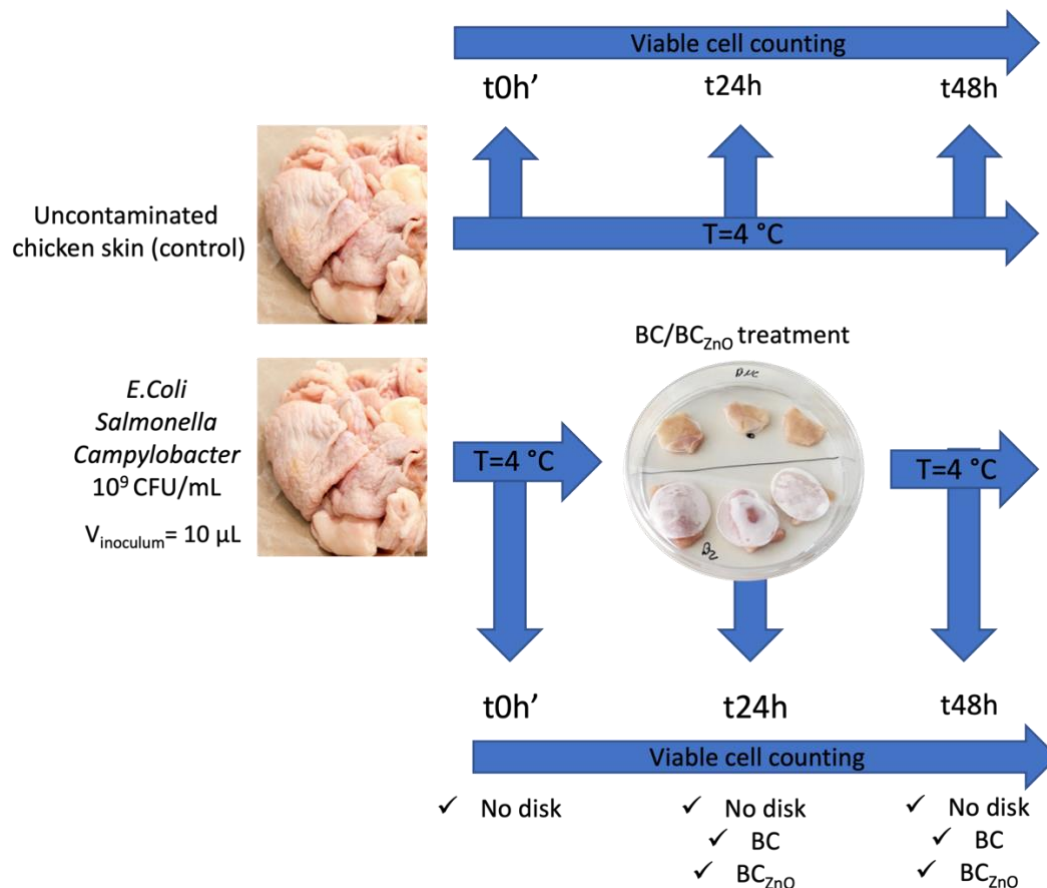
Figure 5.1. Scheme of the experimental design of the antimicrobial assays

5.2.8. Data handling and statistical analysis

Statistical analysis was supported by Prism version 9.4.1 (GraphPad Software, La Jolla California USA), using one-way (and two-way) ANOVA and Tuckey's post-hoc analysis for pairwise comparison of more than two means. Mean differences were considered statistically non-significant (ns) when p-value was higher than 0.05 (95% of interval of confidence). The default statistical confidence level was considered to be 95% ($P < 0.05$) in all tests. Weibull model parameters were estimated with SPSS Statistics software (IBM, Armonk, NY) version 27 by non-linear estimation, using the Levenberg-Marquardt algorithm to minimise the sum of the squares of the differences between the predicted and experimental values. The regression quality was assessed by residuals analysis (normality and randomness), the confidence intervals and the coefficient of correlation R^2.

5.3. Results and Discussion

5.3.1.   Characterization of the ZnO particles and films

5.3.1.1.   Size and polydispersity of ZnO particles synthesized in different conditions

It is well known that the antimicrobial efficiency of ZnO highly depends on particle size, morphology and dosage [16]. Lowering the particle size, thus increasing the specific surface area, improves the reactivity of ZnO against bacteria. In this work, *in situ* and drop *in situ* methods were optimized in what concerns ZnO particle size and its polydispersity, attempting to obtain small particles. The two methods were compared and the use of capping agents (PVOH and glycerol) were used to lower the particle size by preventing ZnO aggregation. Capping agents were compared regarding the performance of producing ZnO with low particle size and without agglomeration. This optimisation was performed in experiments without BC.

As can be seen in Figure 5.2, the methodology Drop *in situ* provided lower ZnO particles sizes (144-211 nm) than the *in situ* approach (278-455 nm). When PVOH was used as the capping agent, the particle size slightly decreased from 208 to 144 nm (Figure 5.2.a). Despite not being statistically different, a downtrend polydispersity index is observed when PVOH was used, providing therefore more homogeneous ZnO suspensions (Figure 5.2.b)). As compared to the control, when glycerol was used as capping agent, particle size increased when using *in situ*. Glycerol had no major effect when using Drop *in situ* (Figure 5.2.a). Hence, the Drop *In situ* method and PVOH capping agent were selected for the following experiments, due to smaller particle size and polydispersity.
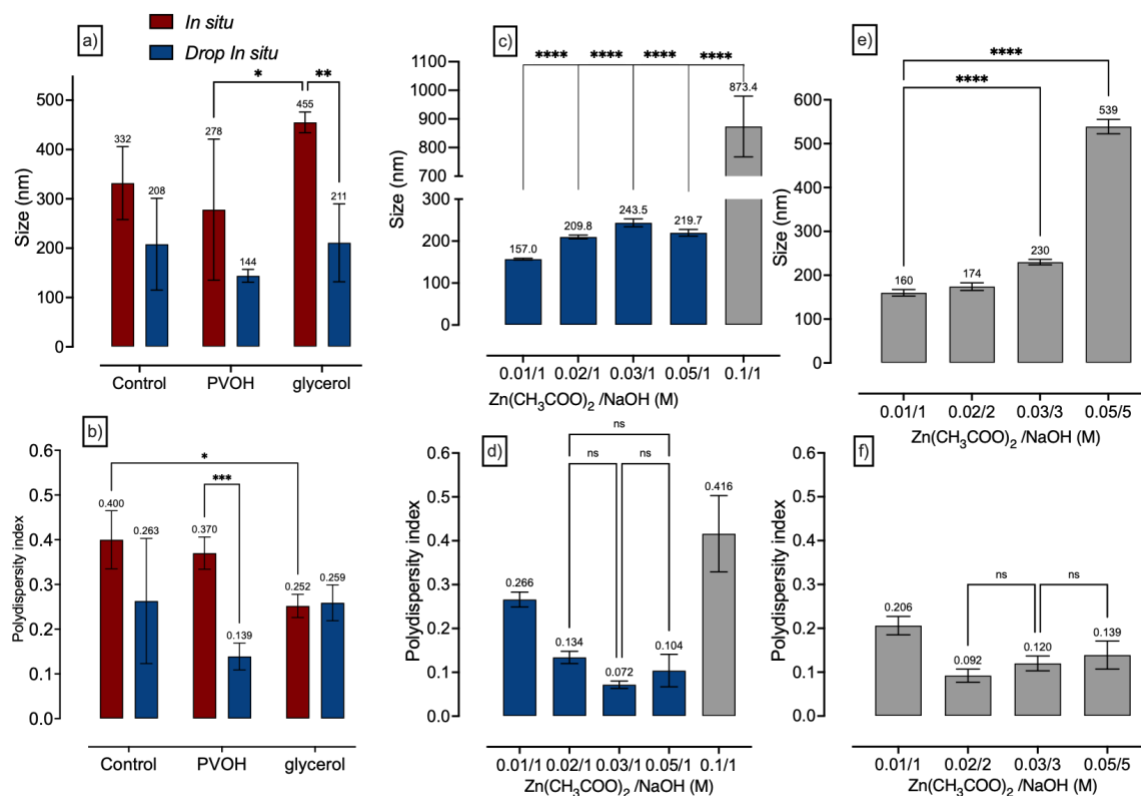
Figure 5.2. ZnO particle size and polydispersity measurements by DLS: a,b) capping optimization with *In situ* and Drop *in situ* methods; c,d) Zn(CH₃COO)₂ concentration optimization for Drop *in situ* method; e,f) Sodium hydroxide concentration optimization for Drop *in situ* method; columns represent the mean and error bars represent the standard deviation; '*' statistical different (p<0.05); 'ns' stands for non-significant (p>0.05).

The effect of zinc acetate concentration on the particle size and polydispersity was assessed for the Drop In situ method. As observed in Figure 5.2.c) and 5.2.d), there is a slight increase in ZnO particle size when zinc acetate increases up to 0.03 M (up to 244 nm). Increasing zinc acetate to 0.05 M, the particle size slightly decreased to 220 nm. When zinc acetate concentration is higher than 0.05 M, a significant (and uncontrolled) increase in particle size and polydispersity was observed. The effect of NaOH concentration was also tested. Results indicated an increase in particle size and polydispersity when higher concentrations of NaOH were used. Since the lowest concentration of NaOH (1 M) is already in excess in relation to Zn(CH₃COO)₂, the lowest concentration was chosen for further experiments. Considering these results, for the following experiments, a concentration of 0.05 M of Zn(CH₃COO)₂ and 1 M of NaOH were used for the synthesis of ZnO with BC. Not only the particle size should be considered for the antimicrobial efficiency, but also the ZnO

amount incorporated in the matrix [36]. Therefore, the highest concentration was considered to maximise the BC$_{ZnO}$ antimicrobial activity. Additionally, higher Zn migration is expected for films with higher Zn concentrations. Therefore, the migration is tested in more aggressive conditions.

5.3.1.2.   ZnO particle size and Zn concentration in BC$_{ZnO}$ films

After BC$_{ZnO}$ production under optimized conditions, ZnO particles were characterized regarding their distribution throughout the fibre network of BC, particle size (measured from SEM-EDS images) and the amount of ZnO on the BC$_{ZnO}$. The distribution of ZnO on the BC$_{ZnO}$ 3D network was observed by SEM in the middle and the edge of the cross-section. Fig. 5.3a shows images of the fibre network of neat BC and with impregnated NPs (identified by EDS). Concerning BC$_{ZnO}$, ZnO particles were found to be well distributed either in the middle and the edge areas, meaning that the dropwise addition of NaOH led to a well distributed formation of ZnO NPs throughout the 3D matrix. Ensuring a well distribution of the ZnO particles is of great importance since it may affect the antimicrobial efficiency of the functionalised material.
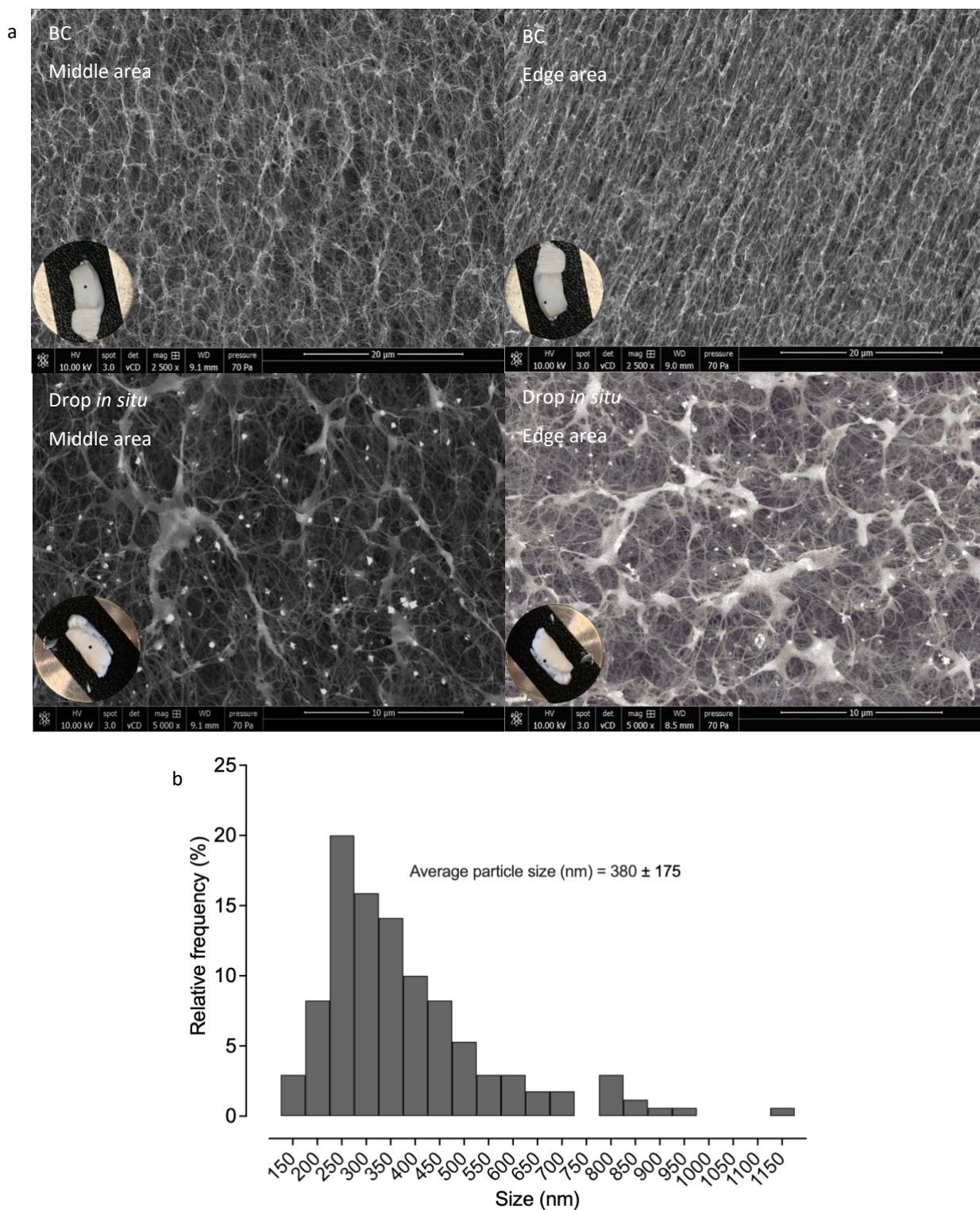
Figure 5.3. a-SEM images of the cross section of neat BC and BC$_{ZnO}$ discs; b-ZnO particle size distribution (measured from SEM images), Zn concentration and estimated mass of ZnO (mg) incorporated in BC$_{ZnO}$ using 0.05 M of Zn(CH$_3$COO)$_2$

Regarding the particle size distribution (see Figure 5.3b), using $Zn(CH_3COO)_2$ at a concentration of 0.05 M led to particle agglomeration, with particles sizes as high as 1150 nm. The most frequent particle size found was 250 nm (with relative frequency of 20%). Additionally, high polydispersity of ZnO particles was found on the BC matrix (150-1050 nm of ZnO). These results showed that BC may have affected the ZnO synthesis, since higher particles sizes and polydispersity were observed when compared to DLS data (Figure 5.2.c) and d) vs Figure 5.3b). Still, the use of 0.05 M $Zn(CH_3COO)_2$ allowed a significant ZnO synthesis in the BC (270 mg.L^{-1} of Zn was found on BC_{ZnO} quantified by AAS; BC_{ZnO} (mg): 6.50 ± 1.10; ZnO (mg): 2.84 ± 0.37).

5.3.1.3.   FTIR spectra

Figure 5.4 displays the FTIR spectra of BC, BC_{ZnO} and ZnO. BC and BC_{ZnO} exhibited similar vibration bands, namely at 1000–1200 and 1300–1400 cm^{-1}, assigned to C-O bonds and to C-H bending, respectively. BC and BC_{ZnO} also displayed bands around 3300–3400 cm^{-1}, related to the O-H groups of water [37]. The BC_{ZnO} spectra features a peak at 350-400 cm^{-1}, which regards Zn-O bond oscillation [38]. The ZnO spectra was also obtained, where it may be observed the same Zn-O peak 400-350 cm^{-1}.
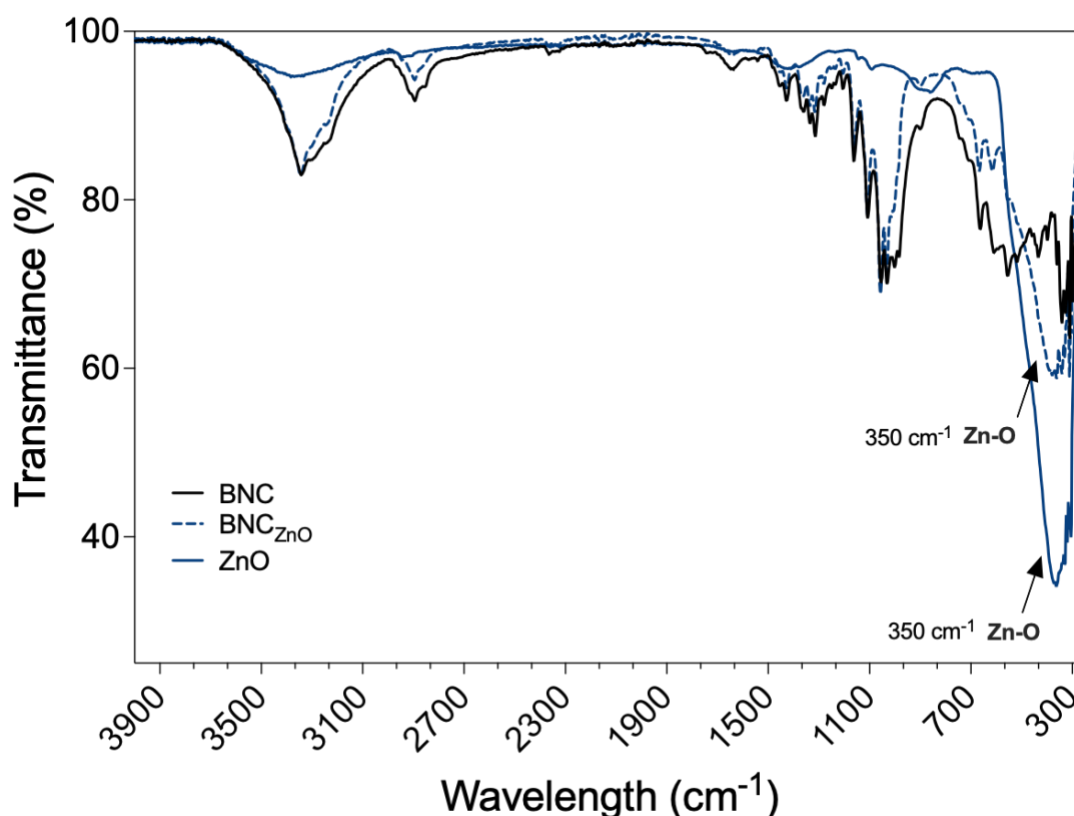
Figure 5.4. FTIR spectrum of BC, BC$_{ZnO}$ and ZnO nanoparticles

5.3.2. Migration tests

5.3.2.1.   Migration into ethanolic solutions

The BC$_{ZnO}$ produced by the Drop *in situ* method was submitted to migration studies, carried out using ethanol solutions as food simulants, at 10, 20 and 50% (v/v). The simulants with 10% and 50% (v/v) ethanol, according to Regulation (EU) No. 10/2011, must be used for materials intended to be in contact with meat-based products. An intermediate concentration of ethanol was additionally included in the study, which is also foreseen in the regulation for processed fish, fruits and vegetables among other products. Migration tests with simulants were conducted at 60 °C for 15 days and the released Zn was quantified. The concentration values in the liquid simulants were converted into mg per kg of food using the solutions density. The observed Zn migration kinetics is presented in Figure 5.5.a).

Higher values of Zn migration into simulants with lower ethanol concentrations were found. This could be expected since Zn has higher solubility in water than in ethanol, as elsewhere reported [39]. Similar results were reported for Zn migration from low density polyethylene-ZnO (LDPE-ZnO) films tested against different simulants (ethanol 10%, acetic acid 4%, distilled water and n-heptane). In those studies, Zn migration was directly correlated with Zn solubility on each food simulant [22].

Concerning the migration kinetics (Figure 5.5.a)), for the lower ethanol concentrations an increase in zinc migration was observed in the initial 8 h, whereas for EtOH50% migration occurred within 2 h; then, an equilibrium seems to have been reached in the next 72 h, no significant differences in concentration being observed ($p > 0.05$). However, after 72 hours of contact, a continuous decrease of Zn in the liquid phase took place in all simulants, down to 0.44 mg L^{-1} after 15 days, suggesting that there was a reabsorption of Zn by the BC$_{ZnO}$ ($p < 0.05$). This is a surprising result, but reabsorption of migrants from cellulose-based materials has previously been reported in the literature [34].

Table 5.3. Zn extraction from BC$_{ZnO}$ on different food simulants (EtOH 10%, 20% and 50%); data displayed as mean ± standard deviation

	Zn extraction %		
	EtOH 10%	**EtOH 20%**	**EtOH 50%**
0	0.0	0.0	0.0
2	0.19±0.01	0.25±0.01	0.10±0.01
4	0.27±0.07	0.28±0.05	0.11±0.01
8	0.35±0.07	0.31±0.03	0.10±0.01
24	0.30±0.05	0.26±0.04	0.10±0.05
72	0.38±0.16	0.34±0.06	0.22±0.02
120	0.22±0.03	0.69±0.49	0.11±0.00
168	0.14±0.05	0.16±0.04	0.15±0.04
360	0.09±0.02	0.06±0.03	0.06±0.02

Zn was detected in all food simulants at levels between 0.39 and 3.6 mg L^{-1} (Figure 5.5.a)), which corresponds to a level of extraction from the BC between 0.1%–0.7%, considering that BC$_{ZnO}$ contains an average of ZnO of 270 mg L^{-1} (Table 5.3). The migration levels obtained with BC$_{ZnO}$ in these food simulants were below the specific migration limit (SML) for soluble ionic zinc (5 mg kg^{-1} food) set out by the European Plastics Regulation (EU) 2016/1416 amending and correcting Regulation (EU) 10/2011 [40].
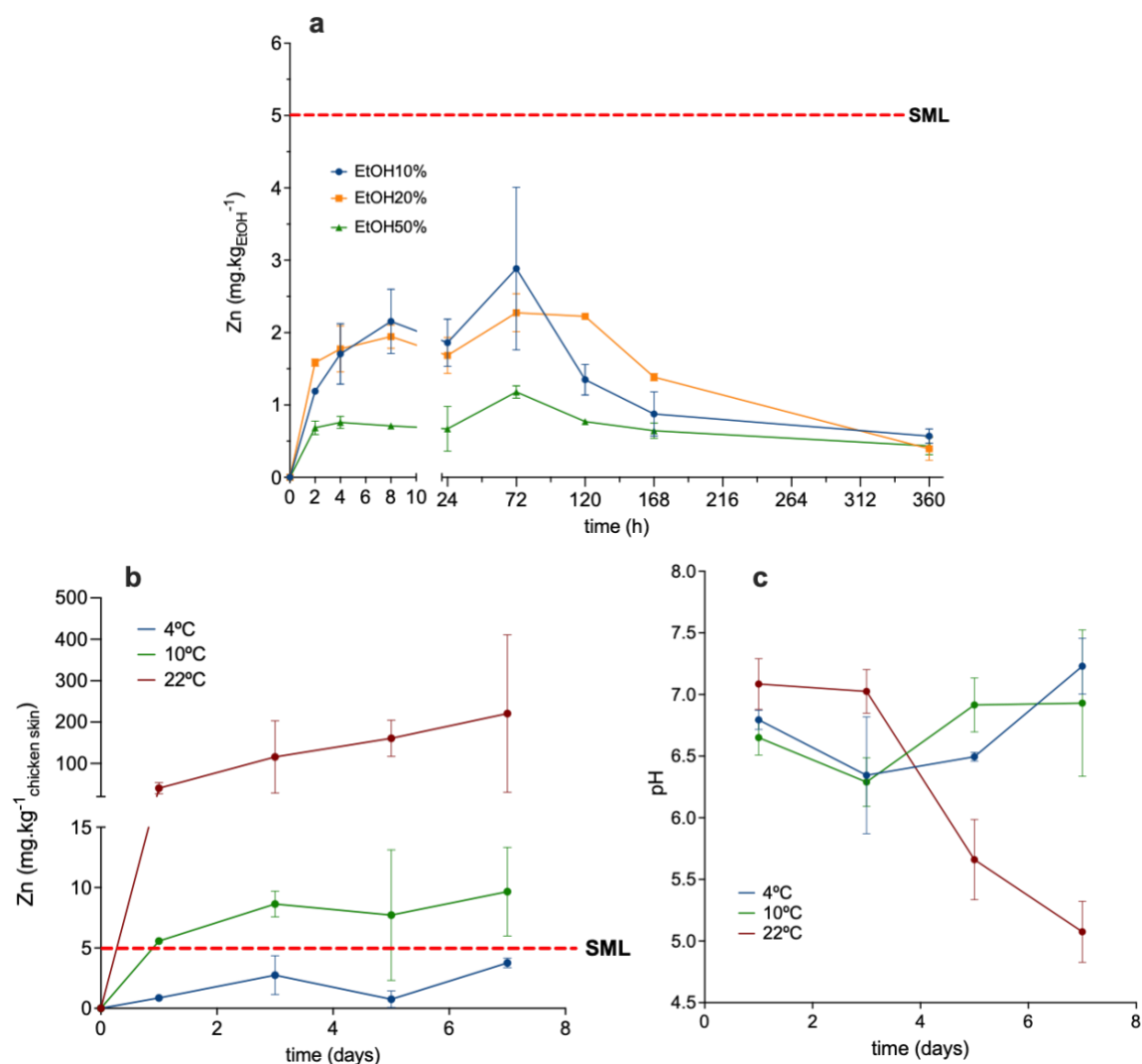
Figure 5.5. Zn migration from BC$_{ZnO}$. a) Migration into food simulants (EtOH 10, 20 and 50%) at 60 °C; b) Migration into chicken at 4, 10 and 22 °C; c) pH of the chicken skin during migration tests; symbols represent the mean and error bars represent the standard deviation.

It is important to mention that only Zn migration was quantified in this assay, and no distinction was made between migration of ZnO NPs or Zn in its ionic form. As previously mentioned, EFSA concluded that ZnO NPs does not migrate in its nanoform, if incorporated in an unplasticized polymer [16], [24]. However, the possible migration of ZnO in nanoform from cellulosic materials should not be ruled out. The migration of ZnO NPs may occur through diffusion and its extent of migration may depend on the particle shape and size of ZnO as well as on the properties of the BC (such porosity and surface area) [17], [41]. Several reasons lead us to consider that most of Zn migration occurs in its ionic form (Zn^{2+}). As perceived in Figure 5.3.b, high particles sizes were produced inside the BC, which may hinder

ZnO migration in its nanoform (low migration rates observed in Figure 5.5.a)). Also, nanocellulose (including BC) can act as adsorbent (of ZnO or Zn^{+2}) due to high surface area, full of surface hydroxyl groups, which facilitates the interaction with ZnO via hydrogen bonding [42] - [44]. This adsorption ability is also seen after 120 h of Zn migration (Figure 5.5. a)). Despite BC having a highly porous structure, which eased the incorporation of $Zn(CH_3COO)_2$ and NaOH for ZnO synthesis, this porous structure was subsequently reduced after BC_{ZnO} drying process, hindering as well the ZnO migration in its nanoform. As described in the experimental section, BC_{ZnO} was air dried. Upon drying, water molecules that maintain the fibre separation are lost, producing hornification, a process that permanently agglomerates and stacks the cellulose fibres [45].

5.3.2.2.   Migration into chicken skin

Following the migration tests with ethanol aqueous solutions, a more realistic model was taken to assess the Zn migration from the BC_{ZnO}. The values of Zn migration into chicken skin are depicted in Figure 5.5.b). The temperature showed to play a very relevant effect on the amount of migrated Zn through time. Most of the release is observed on the first day, slight increasing in the following days. Migration increases with the temperature, specially between 10 to 22 °C. In contrast to the results obtained with ethanol simulants (Figure 5.5. a)), Zn migration to chicken skin was much higher, in particular at higher temperatures. Only at 4 °C, the Zn migration was below the SML (5 mg kg^{-1} food), in agreement with the results obtained using simulants. The Zn level of extraction after 7 days of contact was 0.20% at 4 °C, 0.62% at 10 °C and 14.12% at 22 °C (Table 5.4).

At early stages (until day 3), Zn migration occurs due to the difference in concentration (not in equilibrium) and the migration rate increases with temperature. However, at a later stage (after 3 days) of the migration process, a slight Zn release was observed in the assay at 22 °C, which is explained by the acidification of chicken skin over time (Figure 5.5.b). As reported elsewhere, the release of Zn^{2+} was much higher at an acidic pH than at neutral one [20]. Indeed, ZnO is much more soluble in acidic solutions, such as 4% v/v acetic acid [46], explaining the higher migration to chicken skin at 22 °C (Figure 5.5.b). At lower temperatures (4 °C and 10 °C), pH values were maintained throughout the assay, therefore, the migration occurred to a much lower extent (Figure 5.5.c).

There is plenty of published literature addressing the role of ZnO as antimicrobial and the Zn migration into food simulants, but studies focusing on migration into meat products are scarce. Some of the data available concern the migration to raw chicken [20] and pork [47]. The Zn migration from functionalized absorbing pad into raw chicken meat was determined with levels that did not surpass 5.0 mg kg^{-1}, after 8 days at 4 °C [20]. The Zn migration from a nanocomposite film of soy protein isolate reinforced with cellulose nanocrystals and ZnO NP gave Zn migration into pork up to 20.0 mg kg^{-1} after 6 days at 4 °C on pork [47]. However, those studies do not indicate the pH values of the meat, which is a key parameter, as it is shown in this work. Acidification does have an additional impact on Zn migration rate.

Table 5.4. Zn extraction from BC$_{ZnO}$ on chicken skin at different temperatures (4 °C, 10 °C and 22 °C); data displayed as mean ± standard deviation.

Time (days)	Zn extraction %		
	4 °C	10 °C	22 °C
0	0.0	0.0	0.0
1	0.05±0.02	0.30±0.01	2.16±0.73
3	0.15±0.09	0.46±0.06	3.53±0.42
5	0.04±0.04	0.47±0.36	7.94.±5.18
7	0.20±0.02	0.62±0.24	14.13±12.18

5.3.2.2.1. Simulation of Zn migration using Weibull model

The Weibull kinetic model was fitted to the experimental data obtained for the Zn migration from BC onto chicken skin. The model parameters were estimated for each temperature (Table 5.5). The relevance of C∞, τ and β in the model (model fitting) was assessed statistically, by using the 95% confidence interval (interval is different from 0). The model showed good fitting for 4 °C, with estimated C∞ and τ (statistically different from 0). On the other hand, β was not statistically different from zero, which indicated that this parameter is not relevant in the model. At higher temperatures, the model parameters showed higher error estimations, specially at 22 °C (Table 5.4). At this high temperature, the model does not describe well the experimental data, and a clear distinctive migration pattern

occurs throughout the assay, due to the change of the skin´s pH, that highly increases the Zn migration (Figure 5.5.c and 5.6).

Table 5.5. Weibull model parameters as a function of the temperature; data displayed as mean ± standard deviation.

Temperature	Parameter		95% Confidence Interval	
			Lower Bound	Upper Bound
4 °C	C_∞, mg kg^{-1}	4.08±0.52	2.82	5.34
	τ, days	2.9±0.94	0.550	5.17
	β	1.3±0.63	**-0.228**	**2.84**
10 °C	C_∞, mg kg^{-1}	9.6±3.13	2.14	16.95
	τ, days	1.2±1.15	**-1.55**	**3.88**
	β	0.8±1.28	**-2.22**	**3.83**
22 °C	C_∞, mg kg^{-1}	153.8±17.2	**-235.23**	**542.85**
	τ, days	0.5±1.98	**-3.97**	**4.97**
	β	0.5±3.59	**-7.62**	**8.62**

The shape of the Zn migration curves is well represented by the Weibull model only for Zn migration at 4 °C and 10 °C. The effect of temperature in the model parameters is also represented in Figure 5.6. An exponential effect of temperature in the equilibrium concentration (C_∞) is observed (R2=0.9995), possibly due to the direct effect of temperature combined with the indirect effect on pH, both affecting the zinc solubility and therefore the equilibrium concentration on the simulant. Solubility parameters were used in several migration studies to predict migrant's behaviour onto food [48].

The effect of temperature on the rate of the process (τ parameter) follows an Arrhenius-like pattern (R^2 = 0.9624), and the values of τ ranged from 0.5 to 2.8. Similar observation can be made to β, the behavioural index relating to the initial rate of the process, increased with temperature, following the Arrhenius behaviour (R^2 = 0.903). However, due to the different behaviour of the system observed at 22 °C, the relationship shown in Figure 5.6 is merely indicative as only two valid temperatures (the lower ones) can be considered. It is recognised that to develop a model to simulate the migration of zinc from BC$_{ZnO}$ on chicken

skin and to consider the effect of temperature on the model parameters, data with more temperature levels are required, specially within the range of interest related to the conditions of storage and retailing of the products represented by this simulant.
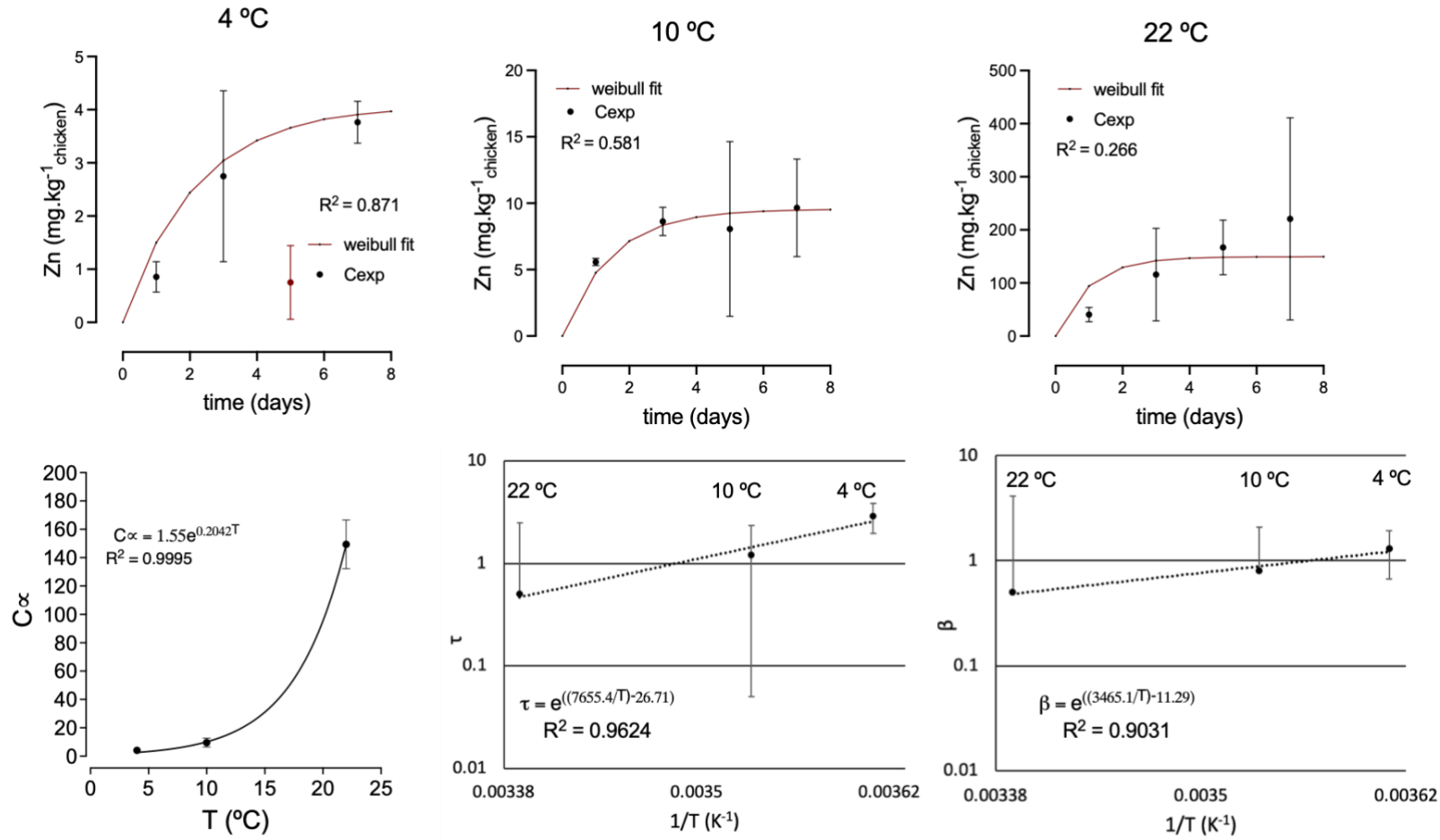
Figure 5.6. Zn migration from BC onto chicken skin at 4 °C, 10 °C and 22 °C, and Weibull parameters estimated for each temperature (Data point at 4 °C, 5 days of contact, coloured in red, not used for modelling); symbols represent the mean and error bars represent the standard deviation.

Chapter 5

Performance of bacterial nanocellulose packaging film functionalised *in situ* with zinc oxide:
migration onto chicken skin and antimicrobial activity   A.G. Soares Silva, F. | 2024

As observed in Figure 5.5.b) and 5.6, Zn migration surpassed the SML (5.0 mg kg-1) at temperatures higher than 10 °C. Although prescribed storage temperatures for meat products are in the range of 4 °C, temperature fluctuations may occur along the food chain supply, triggering higher Zn migration rates. This is a limitation of the developed BC_{ZnO} films, where Zn migration can surpass the SML for higher storage temperatures. To counteract this, strategies should be established to delay Zn migration. Modification of the BC_{ZnO} surface by coating with poly (3-hydroxybutyrate-co-3-hydroxyvalerate) (PHBV), for example, may delay Zn migration. While other authors have reported the difficulty of incorporating ZnO in polymers such PHBV (low adhesion), this may actually favour lower migration rates [49], as the ability of coating BC with PHBV has been demonstrated in previous work [50]. However, a coating may compromise the antibacterial efficiency. Therefore, more research should be done, considering the type of coating used and the grammage applied on the composite, in order to optimize both antibacterial activity and Zn migration.

5.3.3. BC_{ZnO} antimicrobial performance on chicken

The films based on BC_{ZnO} may find an interesting application as an antimicrobial packaging material for meat-based products such as chicken. Therefore, antimicrobial studies with BC_{ZnO} were carried out on chicken skin contaminated with *Salmonella* (S. Enteritidis and cocktail), *E. coli* and *Campylobacter* (*C. coli* and cocktail), common bacteria found in chicken. Only Gram-negative bacteria were assessed because previous work has shown that ZnO was mainly effective against these bacteria. Untreated chicken skin samples (without BC/BC_{ZnO}) were also tested as a control.

Figure 5.7 shows the results of cell counts over time. Overall, in the first 24 h (up to the point where discs were applied), the number of active growing cells remained constant, for all the bacteria tested. After application of the BC_{ZnO} discs, the number of active growing cells was reduced while counts in chicken samples without any disc remained constant. For *E. coli* and *Salmonella* (S. Enteritidis and cocktail), a 0.5 log reduction was obtained after 24 h hour contact. For *Campylobacter* strains, higher inhibition was observed when BC_{ZnO} was in contact with the contaminated chicken skin samples (2.0 to 2.5 log reduction after 24 h). A slight reduction was also observed for the BC film without ZnO for the *Campylobacter* cocktail. These results indicate that the BC_{ZnO} films have antimicrobial effect (especially against

Campylobacter species) on chicken, in agreement with other works that showed antimicrobial effect of ZnO NPs against pathogens on chicken meat samples [20], [29], [51].
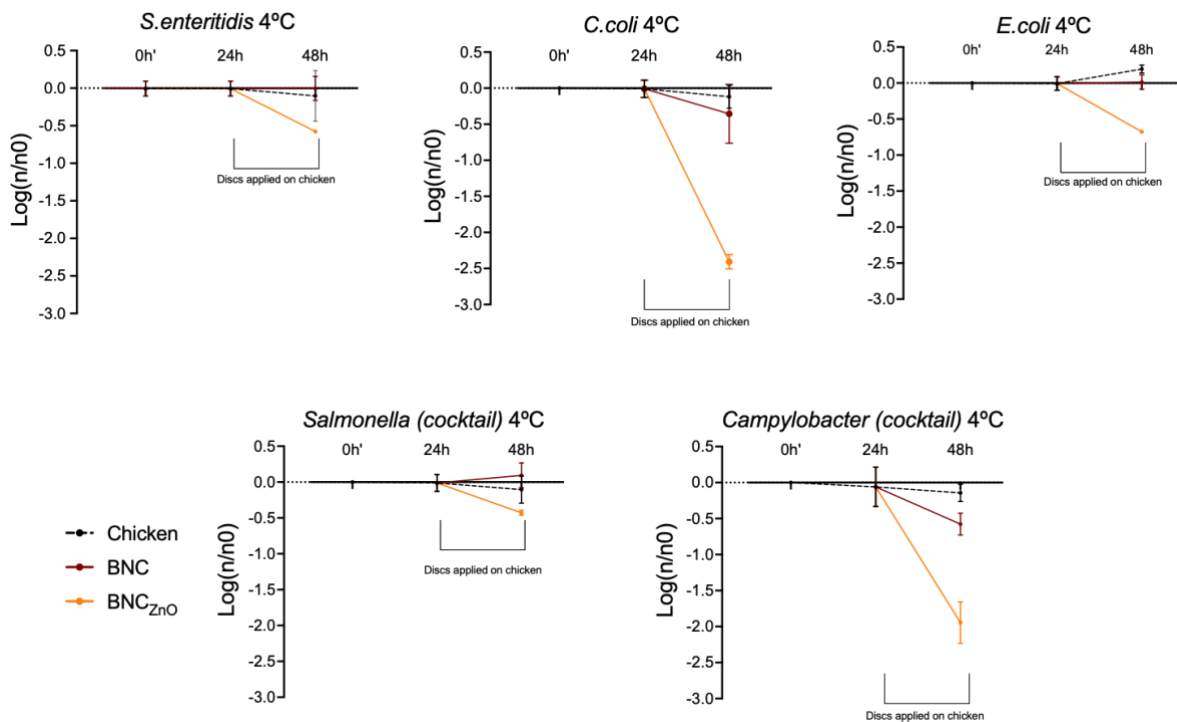
Figure 5.7. Viable cell count for *E. coli*, *Salmonella* and *Campylobacter* on skin chicken, when exposed to BC$_{ZnO}$ and controls (BC and chicken inoculated without any disc); symbols represent the mean and error bars represent the standard deviation.

However, the antimicrobial effect against *E. coli* and *Salmonella* may be considered too low, if considering the Zn migration level on chicken skin at 4 °C, where SML was almost reached (Figure 5.5 and 5.6). Thus, the developed composite still has room for improvement, to increase the antimicrobial effect without increasing the Zn migration levels. This study shows the importance of performing both antimicrobial and migration tests as both mechanisms are important and often correlated when developing an active packaging.

5.4.   Conclusions

Active food packaging has become a very attractive research field. Among the active substances, zinc oxide nanoparticles (ZnO) have been explored due to their antimicrobial properties, whereas bacterial nanocellulose (BC) has been explored as a carrier for active agents. In this study a BC$_{ZnO}$ film was successfully developed, using Drop *in situ* method, which relied on the dropwise addition of NaOH (1 M) to BC pellicles immersed in zinc acetate

solution. Through this method, the ZnO was homogenously distributed within the BC network (confirmed by SEM-EDS), in the form of nanoparticles with sizes ranging 100-300 nm. The increase of $Zn(CH_3COO)_2$ concentration as precursor of ZnO particles promotes the increase of the amount of ZnO retained in the BC matrix, but also leads to larger particle size, with lower specific surface area which can compromise the antimicrobial activity.

The migration tests using food simulants revealed low migration values (lower than SML), with some reabsorption effect after 8 h of contact. In the test of Zn migration into a real food model as chicken skin no reabsorption effect occurred, and Zn migration was temperature and pH dependent. The migration values at 4 °C were lower than the SML, while at higher temperatures (10°C and 22°C) SML was surpassed. The Weibull model was fit to the migration experimental data and the parameters concentrations at equilibrium (C∞), Zn migration rate (τ) and behavioural index relating to the initial rate of the process (β) were estimated at the tested temperatures. The model allows predicting the migration of Zn under different conditions when BC_{ZnO} is in contact with chicken skin, important information before considering the feasibility of using these materials in active food packaging. The antibacterial activity of BC_{ZnO} films was also observed, against *Salmonella* spp., *E. coli* and *Campylobacter* spp., using chicken skin as a food model. In sum, BC_{ZnO} shows a potential for use as an antimicrobial packaging film for fresh/conditioned chicken.

5.5. References

[1]   Vilela, C., Kurek, M., Hayouka, Z., Röcker, B., Yildirim, S., Antunes, M. D. C., Nygaard, J. N., Pettersen, M. K., Freire, C. S. R. (2018). A concise guide to active agents for active food packaging. Trends in Food Science and Technology, 80(August), 212–222. https://doi.org/10.1016/j.tifs.2018.08.006

[2]   Gregor-Svetec, D. (2018). Intelligent Packaging. Nanomaterials for Food Packaging, 203-247. https://doi.org/10.1016/B978-0-323-51271-8.00008-5

[3]   Cerqueira, M. A., Torres-Giner, S., Lagaron, J. M. (2018). Nanostructured multilayer films. Nanomaterials for Food Packaging: Materials, Processing Technologies, and Safety Issues. Elsevier Inc. https://doi.org/10.1016/B978-0-323-51271-8.00006-1

[4]   Kishore, A., Aravind, S. M., & Singh, A. (2023). Bionanocomposites for active and smart food packaging: A review on its application, safety, and health aspects. Journal of Food Process Engineering, 46(5), e14320. https://doi.org/10.1111/jfpe.14320

[5]   Silva, F. A. G. S., Dourado, F., Gama, M., Poças, F. (2020). Nanocellulose bio-based composites for food packaging. Nanomaterials, 10(10), 1–29. https://doi.org/10.3390/nano10102041

[6]   Ibrahim, N. I., Shahar, F. S., Sultan, M. T. H., Shah, A. U. M., Safri, S. N. A., Mat Yazik, M. H. (2021). Overview of bioplastic introduction and its applications in product packaging. Coatings, 11(11), 1423.

[7]   Jedrzejczak-Krzepkowska M., Kubiak K., Ludwicka K., Bielecki S. Chapter 2 - Bacterial NanoCellulose Synthesis, Recent Findings. In: Gama M., Dourado F., Bielecki S. (2016) eds. Bacterial Nanocellulose. Amsterdam: Elsevier

[8]   de Amorim, J.D.P., de Souza, K.C., Duarte, C.R. et al. Plant and bacterial nanocellulose: production, properties and applications in medicine, food, cosmetics, electronics and engineering. A review. Environ Chem Lett 18, 851–869 (2020). https://doi.org/10.1007/s10311-020-00989-9

[9]   Wang, J., Tavakoli, J., & Tang, Y. (2019). Bacterial cellulose production, properties and applications with different culture methods–A review. Carbohydrate polymers, 219, 63-76

[10]   Dileswar Pradhan, Amit K. Jaiswal & Swarna Jaiswal (2022) Nanocellulose Based Green Nanocomposites: Characteristics and Application in Primary Food Packaging, Food Reviews International, DOI: 10.1080/87559129.2022.2143797

[11]   Almasi, H., Mehryar, L., & Ghadertaj, A. (2019). Characterization of CuO-bacterial cellulose nanohybrids fabricated by in-situ and ex-situ impregnation methods. Carbohydrate polymers, 222, 114995.

[12]   Pan, X., Li, J., Ma, N., Ma, X., & Gao, M. (2023). Bacterial cellulose hydrogel for sensors. Chemical Engineering Journal, 461, 142062.

[13]   Cazón, P., Vázquez, M. (2021). Bacterial cellulose as a biodegradable food packaging material: A review. Food Hydrocolloids, 113, 106530.

[14]   Vilela, C., Moreirinha, C., Domingues, E. M., Figueiredo, F. M. L., Almeida, A., Freire, C. S. R. (2019). Antimicrobial and conductive nanocellulose-based films for active and

intelligent food packaging. Nanomaterials, 9(7), 1–16. https://doi.org/10.3390/nano9070980

[15] Wojnarowicz, J., Chudoba, T., Lojkowski, W. (2020). A review of microwave synthesis of zinc oxide nanomaterials: Reactants, process parameters and morphoslogies. Nanomaterials, 10(6). https://doi.org/10.3390/nano10061086

[16] EFSA CEF Panel. (2017). Safety assessment of the substance zinc oxide, nanoparticles, for use in food contact materials. EFSA Journal (Vol. 14). https://doi.org/10.2903/j.efsa.2016.4408

[17] Kim, I., Viswanathan, K., Kasi, G., Thanakkasaranee, S., Sadeghi, K., Seo, J. (2022). ZnO nanostructures in active antibacterial food packaging: preparation methods, antimicrobial mechanisms, safety issues, future prospects, and challenges. Food Reviews International, 38(4), 537-565.

[18] Kumar, R., Umar, A., Kumar, G., Nalwa, H. S. (2017). Antimicrobial properties of ZnO nanomaterials: A review. Ceramics International, 43(5), 3940–3961. https://doi.org/10.1016/j.ceramint.2016.12.062

[19] Sirelkhatim, A., Mahmud, S., Seeni, A., Kaus, N. H. M., Ann, L. C., Bakhori, S. K. M., Hasan, H., Mohamad, D. (2015). Review on zinc oxide nanoparticles: Antibacterial activity and toxicity mechanism. Nano-Micro Letters, 7(3), 219–242. https://doi.org/10.1007/s40820-015-0040-x

[20] Hakeem, M. J., Feng, J., Nilqhaz, A., Seah, H. C., Konkel, M. E., Lua, X. (2020). Active Packaging of Immobilized Zinc Oxide Nanoparticles Controls Campylobacter jejuni in Raw Chicken Meat. Applied and Environmental Microbiology, 86(22). https://doi.org/10.1128/AEM.01195-20

[21] Olaimat, A. N., Sawalha, A. G. A., Al-Nabulsi, A. A., Osaili, T., Al-Biss, B. A., Ayyash, M., Holley, R. A. (2022). Chitosan–ZnO nanocomposite coating for inhibition of Listeria monocytogenes on the surface and within white brined cheese. Journal of Food Science, 87(7), 3151–3162. https://doi.org/10.1111/1750-3841.16208

[22] Polat, S., Fenercioğlu, H., Güçlü, M. (2018). Effects of metal nanoparticles on the physical and migration properties of low density polyethylene films. Journal of Food Engineering, 229, 32–42. https://doi.org/10.1016/j.jfoodeng.2017.12.004

[23]   Poças, F., Franz, R. (2018). Overview on european regulatory issues, legislation, and EFSA evaluations of nanomaterials. In Nanomaterials for Food Packaging: Materials, Processing Technologies, and Safety Issues (pp. 277–300). https://doi.org/10.1016/B978-0-323-51271-8.00010-3

[24]   Commission, T. H. E. E. (2007). Opinion of the Scientific Panel on food additives, flavourings, processing aids and materials in contact with food (AFC) related to a 16th list of substances for food contact materials. EFSA Journal, 5(10), 22–42. https://doi.org/10.2903/j.efsa.2007.555

[25]   Choo, K. W., Dhital, R., Mao, L., Lin, M., & Mustapha, A. (2021). Development of polyvinyl alcohol/chitosan/modified bacterial nanocellulose films incorporated with 4-hexylresorcinol for food packaging applications. Food Packaging and Shelf Life, 30, 100769.

[26]   Missio, A. L., Mattos, B. D., Ferreira, D. de F., Magalhães, W. L. E., Bertuol, D. A., Gatto, D. A.,Pettschnigg A Tondi, G. (2018). Nanocellulose-tannin films: From trees to sustainable active packaging. Journal of Cleaner Production, 184, 143–151. https://doi.org/10.1016/j.jclepro.2018.02.205

[27]   Tsai, Y. H., Yang, Y. N., Ho, Y. C., Tsai, M. L., Mi, F. L. (2018). Drug release and antioxidant/antibacterial activities of silymarin-zein nanoparticle/bacterial cellulose nanofiber composite films. Carbohydrate Polymers, 180(August 2017), 286–296. https://doi.org/10.1016/j.carbpol.2017.09.100

[28]   Zhang, H., Yu, H. Y., Wang, C., Yao, J. (2017). Effect of silver contents in cellulose nanocrystal/silver nanohybrids on PHBV crystallization and property improvements. Carbohydrate Polymers, 173, 7–16. https://doi.org/10.1016/j.carbpol.2017.05.064

[29]   Pirsa, S., Shamusi, T., Kia, E. M. (2018). Smart films based on bacterial cellulose nanofibers modified by conductive polypyrrole and zinc oxide nanoparticles. Journal of Applied Polymer Science, 135(34), 1–10. https://doi.org/10.1002/app.46617

[30]   Wahid, F., Duan, Y. X., Hu, X. H., Chu, L. Q., Jia, S. R., Cui, J. D., Zhong, C. (2019). A facile construction of bacterial cellulose/ZnO nanocomposite films and their photocatalytic and antibacterial properties. International Journal of Biological Macromolecules, 132, 692–700. https://doi.org/10.1016/j.ijbiomac.2019.03.240

[31]   Hestrin, S., Schramm, M. (1954). Synthesis of cellulose by Acetobacter xylinum. II. Preparation of freeze-dried cells capable of polymerizing glucose to cellulose. The Biochemical Journal, 58(2), 345–352. https://doi.org/10.1042/bj0580345

[32]   European Standard (2013). Foodstuffs-determination of elements and their chemical species-general considerations and specific requirements (EN 13804: 2013).

[33]   Hallinan, A. J. (1993). A Review of the Weibull Distribution. Journal of Quality Technology, 25(2), 85–93. https://doi.org/10.1080/00224065.1993.11979431

[34]   Poças, M. de F., Oliveira, J. C., Pereira, J. R., Brandsch, R., Hogg, T. (2011). Modelling migration from paper into a food simulant. Food Control, 22(2), 303–312. https://doi.org/10.1016/j.foodcont.2010.07.028

[35]   Poças, M. F., Oliveira, J. C., Brandsch, R., Hogg, T. (2012). Analysis of mathematical models to describe the migration of additives from packaging plastics to foods. Journal of Food Process Engineering, 35(4), 657–676. https://doi.org/10.1111/j.1745-4530.2010.00612.x

[36]   Gudkov, S. V., Burmistrov, D. E., Serov, D. A., Rebezov, M. B., Semenova, A. A., & Lisitsyn, A. B. (2021). A mini review of antibacterial properties of ZnO nanoparticles. Frontiers in Physics, 9, 641481

[37]   Mota, R., Rodrigues, A. C., Silva-carvalho, R., Costa, L., Martins, D., Sampaio, P., Dourado, F., Gama, M. (2022). Tracking Bacterial Nanocellulose in Animal Tissues by Fluorescence Microscopy, 1–20.

[38]   Gharoy Ahangar, E., Abbaspour-Fard, M. H., Shahtahmassebi, N., Khojastehpour, M., Maddahi, P. (2015). Preparation and Characterization of PVA/ZnO Nanocomposite. Journal of Food Processing and Preservation, 39(6), 1442–1451. https://doi.org/10.1111/jfpp.12363

[39]   Huang, H., Tang, K., Luo, Z., Zhang, H., & Qin, Y. (2017). Migration of Ti and Zn from nanoparticle modified ldpe films into food simulants. Food Science and Technology Research, 23(6), 827-834.

[40]   European Parliament and Council. (2018). Directive (EU) 2018/852 of the European Parliament and of the Council of 30 May 2018 amending Directive 94/62/EC on packaging and packaging waste. Official Journal of the European Union, 2018(November 2008), 141–154. Retrieved from https://eur-lex.europa.eu/legal-content/EN/TXT/PDF/?uri=CELEX:32018L0852

[41]   Zhao, S. W., Guo, C. R., Hu, Y. Z., Guo, Y. R., Pan, Q. J. (2018). The preparation and antibacterial activity of cellulose/ZnO composite: A review. Open Chemistry, 16(1), 9-20.

[42]   Hu, W., Chen, S., Zhou, B., Wang, H. (2010). Facile synthesis of ZnO nanoparticles based on bacterial cellulose. Materials Science and Engineering: B, 170(1-3), 88-92

[43]   Zou, X. H., Zhao, S. W., Zhang, J. G., Sun, H. L., Pan, Q. J., Guo, Y. R. (2019). Preparation of ternary ZnO/Ag/cellulose and its enhanced photocatalytic degradation property on phenol and benzene in VOCs. Open Chemistry, 17(1), 779-787.

[44]   Sayyed, A. J., Pinjari, D. V., Sonawane, S. H., Bhanvase, B. A., Sheikh, J., & Sillanpää, M. (2021). Cellulose-based nanomaterials for water and wastewater treatments: A review. Journal of Environmental Chemical Engineering, 9(6), 106626.

[45]   Martins, D., de Carvalho Ferreira, D., Gama, M., Dourado, F. (2020). Dry Bacterial Cellulose and Carboxymethyl Cellulose formulations with interfacial-active performance: processing conditions and redispersion. Cellulose, 27, 6505-6520.

[46]   Bumbudsanpharoke, N., Choi, J., Jin, H., Ko, S. (2019). Zinc migration and its effect on the functionality of a low density polyethylene-ZnO nanocomposite fi lm, 20(January). https://doi.org/10.1016/j.fpsl.2019.100301

[47]   Xiao, Y., Liu, Y., Kang, S., Wang, K., Xu, H. (2020). Development and evaluation of soy protein isolate-based antibacterial nanocomposite films containing cellulose nanocrystals and zinc oxide nanoparticles. Food Hydrocolloids, 106(April), 105898. https://doi.org/10.1016/j.foodhyd.2020.105898

[48]   Gavriil G., Kanavouras A., Coutelieris F.A. (2018) Food-packaging migration models: A critical discussion, Critical Reviews in Food Science and Nutrition, 58:13, 2262-2272, DOI: 10.1080/10408398.2017.1317630

[49]   Râpă, M., Stefan, M., Popa, P. A., Toloman, D., Leostean, C., Borodi, G., Vodnar, D. C., Wrona, M., Salafranca, J., Nerín, C., Barta, D.G., Suciu, M., Predescu, C., Matei, E. (2021). Electrospun nanosystems based on PHBV and ZnO for ecological food packaging. Polymers, 13(13), 2123.

[50]   Soares da Silva, F A G., Matos, M., Dourado, F., Reis, M A M., Branco, P C., Poças, F., Gama, M. (2022). Development of a layered bacterial nanocellulose-PHBV composite for food packaging. Journal of the Science of Food and Agriculture, (February). https://doi.org/10.1002/jsfa.11839

[51]   Amjadi, S., Emaminia, S., Nazari, M., Davudian, S. H., Roufegarinejad, L., Hamishehkar, H.

(2019). Application of Reinforced ZnO Nanoparticle-Incorporated Gelatin

Bionanocomposite Film with Chitosan Nanofiber for Packaging of Chicken Fillet and

Cheese as Food Models. Food and Bioprocess Technology, 12(7), 1205–1219.

https://doi.org/10.1007/s11947-019-02286-y

The global shortage of cotton for textile production, forces the exploitation of forests´ lignocellulosic biomass to produce man-made cellulosic fibres (MMCF). This has a considerable environmental impact, pressing the textile industry to search for new sustainable materials and to the development of sustainable recycling processes. Bacterial cellulose (BC), an exopolysaccharide produced by fermentation, could represent such an alternative. In particular, we tested the possibility of improving the mechanical properties of cellulose filaments with a low degree of polymerization (DP) by combining them with high DP from BC, so far exploited to little extent in the textile field.

In this work, BC with different degrees of polymerization (DP_{cuaxam}) (BC_{neat}: 927; BC_{dep}:634 and BC_{blend}: 814) were dissolved in *N*-methylmorpholine-*N*-oxide (NMMO) and their spinnability was studied. The rheological behaviour of the dopes was assessed, and all were found to be spinnable, at suitable concentrations (BC_{neat}:9.0%; BC_{dep}:12.2%; BC_{blend}:10.5%). A continuous spinning was obtained and the resulting filaments offered similar mechanical performance to those of Lyocell. Further, the blending of BC pulps with different DPs (BC_{blend}, obtained by combining BC_{neat} and BC_{dep}) allowed the production of fibres with higher stiffness (breaking tenacity 56.4 $CN.tex^{-1}$) and lower elongation (8.29%), as compared to samples with more homogeneous size distribution (neat BC and depolymerized BC).

6.1.   Introduction

The increasing demand for textile products forces the industry to constantly adapt its sources and manufacturing [1]. The most used synthetic fibre is currently polyester, followed by cotton [2]. Although these are interesting materials due to their low production cost, they carry a high environmental impact [2]. Synthetic fibres are used for a short period of time while taking years to degrade. Also, their recycling rate is still low, being often disposed in landfills [3]. Concerning cotton crops, they require high amounts of pesticides and large amounts of water (global water footprint of 5,730 $m^3.ton^{-1}$ in crops production) [2], [4]. An alternative to cotton (natural cellulose fibres) and synthetic based fibres are the Man-Made Cellulose Fibres (MMCF, also known as regenerated cellulose fibres). MMCF are from wood biomass, and have been extensively studied and are commercially available [5]. There are several methods for the development of MMCF, including well established processes such as Acetate, Viscose, Cuprammonium and Lyocell, as well as experimental approaches such as Ioncell® (or other Lyocell type process using ionic liquid as cellulose solvent), carbamate or LiCl/DMAc [2]. These production processes differ primarily in [2], [6], [7]: i) The selection of the solvent—some involving cellulose derivatization (e.g., acetate cellulose [8] and viscose [2]), while others employ direct dissolution (N-Methylmorpholine N-oxide (NMMO) [9], [10], LiCl/DMAc [8] and ionic liquids [11]); ii) The type of fibre spinning—wet spinning versus dry-jet spinning (with an air gap between the spinneret and regeneration bath). The cellulose-based solution is extruded through a spinneret, followed by cellulose regeneration via coagulation in a bath containing an antisolvent. Subsequently, the fibres are subjected to drawing and later gathered as continuous fibres or cut into staple fibres with lengths ranging from 1 to 40 mm.

One of the most promising processes is Lyocell, whereby cellulose is dissolved in *N*-Methylmorpholine *N*-oxide (NMMO), followed by dry-wet spinning in a water-based coagulation bath [9], [12]. In its monohydrate form (water content of 13.3% (m/v)), NMMO is a polar organic solvent that has a great capacity for dissolving cellulose (water content of 13.3% (m/v)) [9], [13]. Cellulose dissolution is a complex process, being dependent on the amount of cellulose, water, NMMO, temperature, degree of polymerization (DP) and mechanical agitation [10], [12], [14]. It includes two stages, swelling and gradual dissolution layer by layer, whereby the water originally linked to cellulose is replaced by NMMO [8].

Celluloses with DPs (higher than 1000), low temperatures (80-90°C) and poor mechanical agitation during dissolution are known to decrease the efficiency of the process. Also, high temperatures (e.g., higher than 120 °C), may cause undesirable and auto-catalytically boosted NMMO degradation [15]. Stabilizers such as isopropyl gallate are used to prevent NMMO's thermal degradation [16]. Despite its complexity, the dissolution zone in the phase diagram is well established at temperatures between 80 and about 100 °C for plant-based celluloses with a DP of 550-650 [12].

Plant-based celluloses are most commonly used as raw material for the development of regenerated cellulose fibres. Despite being recognized as the next generation of renewable biomass for high-performance textiles, environmental issues are a concern, namely due to intensive deforestation and wood (chemically-based) processing. Bacterial Cellulose (BC), synthesized by *Komagataeibacter* sp. via fermentation, may represent a new resource for manufacturing MMCF. Although BC faces challenges regarding a cost-effective scale up, its production offers a lower environmental impact and may provide a valuable option for the production of textiles with special properties or combined with recycled fibres to improve its properties. The development of regenerated BC fibres has so far been explored to very little extent. Gao et al. [17] managed to dissolve neat BC in NMMO monohydrate (NMMO.H_2O), using a cellulose concentration of 7% m/m (DP = 2700). The resulting regenerated fibres had a cellulose II crystalline structure, lower degree of crystallinity (native BC: 74.14% vs Regenerated BC fibres: 60.83%), smaller crystallites (size of the planes (101), (10-1) and (002) was 80, 120 and 81 Å, and 26, 30, 54 Å, respectively for native and regenerated BC), and higher thermal stability than neat BC (decomposition started at 320 °C for RBC and 300 °C for native BC). Yet, these fibres had a lower mechanical performance than commercial Lyocell counterparts (Tenacity: 40 – 44 cN.tex^{-1}, Elongation: 14 – 16 %) [17]. Makarov et al. [18] used an alternative process (developed at the All-Russian Scientific-Research Institute of Polymer Fibres [19], [20] for lyocell fibre production. High-melting hydrate forms of NMMO were used for the dissolution of cellulose, at 105 °C, under compression, shearing and forced plastic flow. Neat BC (DP = 1500) was dissolved at a maximum concentration of 6% m/m, the produced fibres presenting similar mechanical performance to those of Lyocell and Viscose fibres [2], [18]. Considering these studies [17], [18], dissolving BC in NMMO was found to represent a major processing issue, due its high DP (around 1,000-2,000). Although high DPs have a positive effect on the fibre stiffness, it undesirably influences the solubility of BC in different

solvents (including NMMO). Very high DP also increases the viscosity of the dope, potentially hindering its preparation and a proper spinning [21].

The textile industry urgently needs new sources of fibre to meet the needs of a growing world market [11]. The development of technologies for textile fibres recycling may represent a solution, addressing the environmental issues related to the accumulation of huge amounts of used textiles. Therefore, the European Commission unveiled a strategy focused on production of sustainable and circular textiles. One particular goal is the development of "durable, repairable and recyclable textiles. These textiles are intended to predominantly consist of recycled fibres, free of harmful substances, and be manufactured in accordance with social and environmental principles. Currently, the recycling rate of textiles is still low, due to ineffective processes [22]. Mechanical and chemical treatments are used for this purpose, but these are severe and each reutilization cycle further degrades by significantly lowering the DP (often bellow 300), thus deteriorating the fibres' mechanical properties [22]. A crucial objective in achieving sustainable MMCF production involves adapting the processes of regenerated fibres by incorporating recycled cellulose, sourced by end-of-life fibres (such as cotton, hemp, linen, Viscose, or even Lyocell).We hypothesise that BC, with high DP, may play a relevant role in this scenario, by contributing to the improvement of the recycling process through the combination of high DP BC with low DP recycled fibres [23].

To our knowledge this approach has never been studied and therefore the effect of BC's DP on dissolution in NMMO, spinning and mechanical properties of the resulting fibres were analysed. Depolymerisation of BC was optimized by adapting the mercerization and ageing steps from Viscose process. Then, BC samples (with different DPs) were dissolved and spun through dry-jet spinning. The blending of BC with different DPs was carried out in order to see its effect on the rheological behaviour (dope) and mechanical performance (fibre). This way, testing the hypothesis that the combination of celluloses with different DP may improve the properties of the final product. A rheological and mechanical characterization of the prepared dopes and regenerated cellulose fibres was performed.

6.2.   Material and Methods

6.2.1.   BC pulp preparation

Commercial BC membranes from HTK Food Co., Ltd. (Ho Chi Minh City, Vietnam) were washed, by immersing the membranes in a sodium hydroxide solution (0.1M) twice, for 24h,

at room temperature. Then, the BC was washed for several times with distilled water until the pH became that of the distilled water, yielding pure BC. To obtain a BC pulp, the membranes were cut into cubes and wet-ground with a hand-blender. Then, the BC concentration was adjusted to a final value of 0.5% w/v and mechanically processed with a blender (Moulinex TYPE LM935) (6 times for 5 mins each time, allowing cooling between each period), to improve its dissolution in NMMO. Then, the BC pulp was concentrated to c.a. 10% w/v through centrifugation (Multifuge XR3, Thermo Fisher) at 18,000 rpm, at room temperature, followed by filtration (using vacuum pump (Millipore, Model WP6122050)); the dry matter content of each pulp was recorded. A fraction of the pulp was kept until use and another subjected to depolymerisation, as described further.

6.2.2. Optimization of the BC depolymerization

BC depolymerisation was carried out through a mercerization and aging step as described by Jinzarli et al. [24], [25]: never dried BC pulp (10% w/w) was first dispersed in NaOH solution with 5 M to a final BC concentration of 2 %w/w. Each alkaline BC suspension was then subjected to constant magnetic stirring (600 rpm) at 50 °C for 60 min. Then, the mercerized BC was concentrated through centrifugation (18,000 rpm, at room temperature) up to 8-10 % w/v, and poured in a rotary evaporator (Heidolph VV2000) (at 50°C, without vacuum) for the aging step, under constant agitation, for 4h. Afterwards, the BC was washed with distilled water, with several filtrations, until the pH became that of the distilled water. The depolymerised BC was then freeze dried in a freeze drier (Coolsafe 100-9 Pro, Labogene, Allerød, Denmark) at -100°C and 0.025 mbar. The DP of all samples was characterized as described in section 6.2.3.

6.2.3. Estimation of the degree polymerization

The average degree of polymerisation (DP) of the BC pulp was also determined using cuoxam, according to an internal standard specification used at Thüringisches Institut für Textil- und Kunststoff-Forschung (TITK). For this purpose, the intrinsic viscosities in cuoxam $[\eta]_{cuoxam}$ (unit: ml/g) were detected by means of a capillary viscometer and the DP_{cuoxam} was calculated according to the following equation:

$$DP_{cuoxam} = 2 * [\eta]_{Cuoxam} \quad (1)$$

This method is normally used to access Lyocell pulps which typically have DP values in the range of 500 - 650. Due to the high DP of BC, small deviations from the used linear relation between the intrinsic viscosity and the DP_{cuoxam} cannot be ruled out.

6.2.4. Dope preparation of BC NMMO

Three BC dopes were prepared, using pulps with different DPs. BC pulps with a DP_{cuoxam} of 634, 758 and 927 were labelled as, respectively, BC_{dep}, BC_{blend} and BC_{neat}. BC_{neat} refers to neat BC pulp (without any depolymerisation), BC_{dep} refers to the depolymerised BC (see section 6.2.2.) and BC_{blend} refers to a blend of the previous (62% w/w of neat BC and 38% of depolymerised BC). Concerning the BC_{dep}, a mixing step was made before its dissolution in NMMO: the BC was dispersed in deionized water with an ultra-turrax mixer (DIAX 900, Heidolph Germany) and then concentrated with a vacuum filter (with a glass filter).

Before dissolution, the dry matter content of BC_{neat} or BC_{dep} was determined to be 10.3% and 96.0%, respectively. Then, BC pulps (BC_{neat}, BC_{blend} or BC_{dep}) were transferred into a kneader reactor (PML 8, Netzsch, Germany) to be mixed with NMMO (Ravago Chemicals) solvent (60% w/v) and propyl gallate 0.6 % (w/w$_{BC}$). The distillation of water (swelling and dissolution step) from the mixture was made under constant kneading (80-100 rpm), jacket temperature of 95°C and a reduced end-pressure of 20-30 mbar. When the dope reached its monohydrate form (13.3 ± 4% w/w of H_2O), NMMO began to interact with the hydroxyl groups of the cellulose, dissolving it [10]. The process was considered complete when a clear amber coloured dope was obtained (without any gel or fibrous particles) (Figure 6.1-C). Equation 3 was used to determine the final BC concentration:

$$Solid\ content\ (\%) = \frac{mBC}{msolution\ final}\quad (2)$$
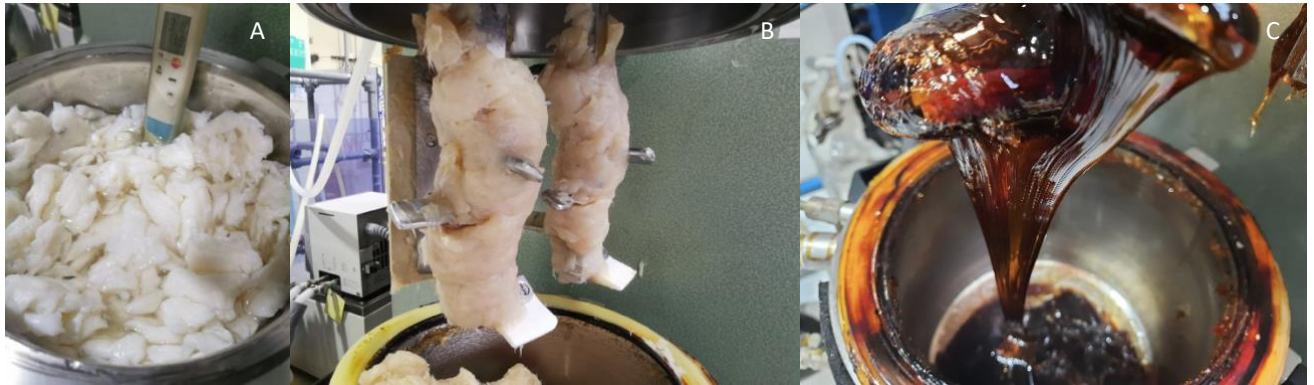
Figure 6.1. A - Mixture of wet BC and NMMO in the vessel; B – aspect of the mixture during dope preparation; C - BC spinning dope

6.2.5. Dry wet spinning

A lab scale dry-wet spinning module (self-construction by TITK) (Figure 6.2) was used for the development of the BC fibres. Each of the produced dopes were transferred into the storage tank of the laboratory spinning line and the dope was left at 85 °C standing overnight to remove air bubbles. Then, each solution was spun at 80 - 95 °C (depending on the dopes solid content) through the spinneret holes (with 7 x 80 holes for staple fibres and 4 x 80 holes for filament, 90 µm spinning hole diameter) with a varying extrusion velocity (9.75-13 m/min) and godet speed of 30 m/min. The generated spinning capillaries passed through an air gap (about 10 mm length) before entering in the coagulation bath (water at room temperature). After filament formation, the multi filament bundle were collected and drawn at the following draw – ratios (DR, ratio between the collecting and extrusion velocity): DR of 2.3; 3.1 and 2.7 for BC_{neat}, BC_{dep} and BC_{blend}, respectively. Concerning BC_{neat} and BC_{dep}, the fibres were cut to a predetermined length of 38 mm (resembling staple fibres of cotton type), washed multiple times with water and air dried at 70 °C until equilibrium moisture content. The BC_{blend} was collected as a multi filament yarn, where additional washing steps and drying godets (rotating) at 90 °C were used, before winding.
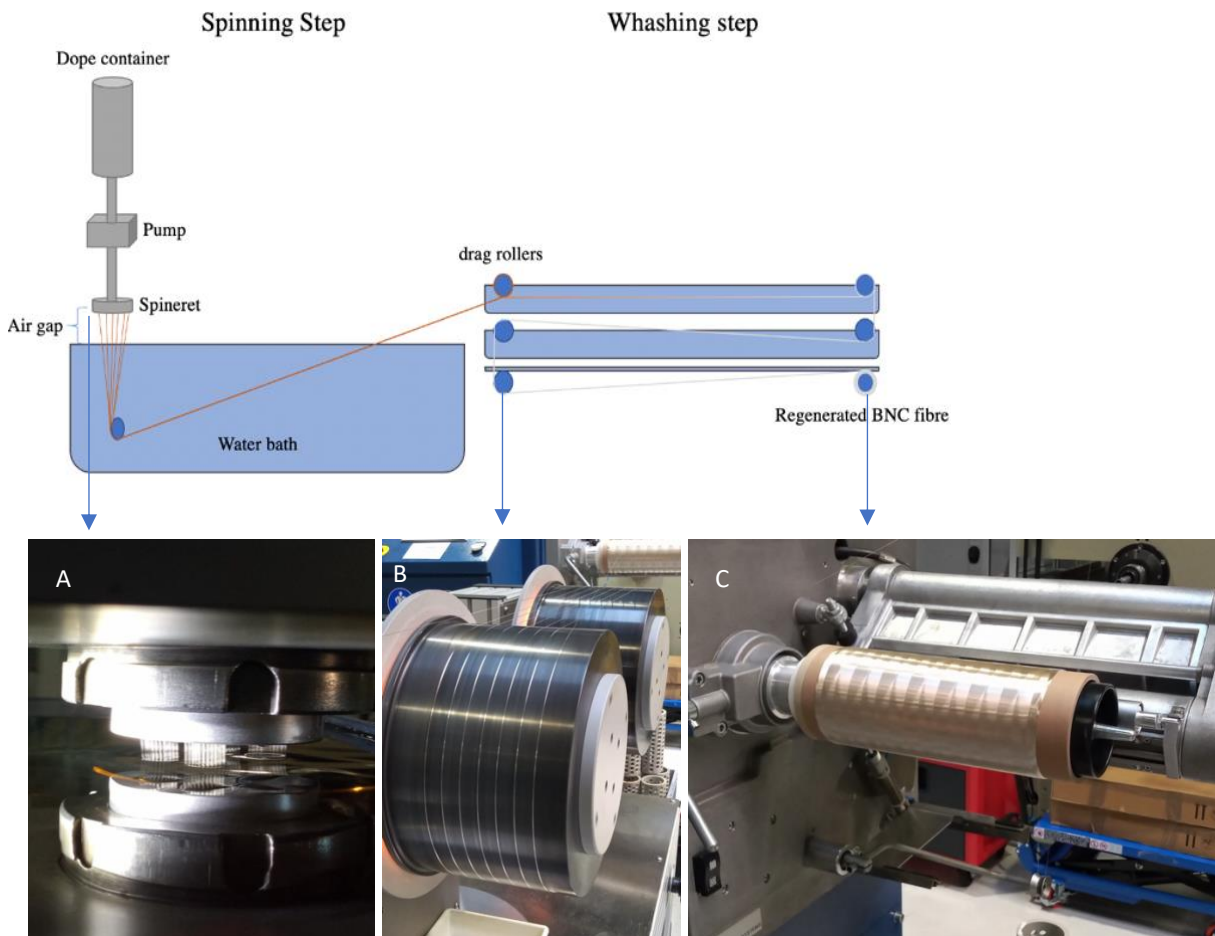
Figure 6.2. Large laboratory spinning line (upper section); Lower section: A- Filament extrusion from the spinning nozzle, through an air gap into a water bath; B- Drawing and drying rollers; C- Fibre collector

6.2.6. Analytical characterization

Determination of the solids content by precipitation, washing and drying

The solids content of the dope was determined by gravimetry after precipitation, washing and drying of the cellulose. About 2 g of dope were accurately weighted, pressed out to a film and washed out the NMMO. Then the cellulose was air dried (105°C) and weighted.

Optical characterisation of the cellulose dopes by polarization microscopy

The optical characterisation of the spinning dopes was carried out using polarization microscopy. A Keyence digital microscope VHX-6000 series and a Zeiss Axiolab light microscope with 10-fold magnification lens were used. A small sample of the dope was placed on a cleaned glass slide and cover slipped and then placed in an oven at 105 °C for 1 h to form a thin uniform film.

Rheological characterisation of the cellulose dopes

The rheological characterisation of the dope was carried out by means of the rotation rheometer HAAKE MARS II, using a cone/plate measuring system (C35/4°). The measurement of the zero shear viscosities occurred by creep tests at shear stress of 90 Pa, applying a measuring temperature of 85 °C. Oscillation mode measurements at 4 different temperatures (60/85/95/110 °C) were carried out for the calculation of the master curves at a reference temperature of 85°C as well as the determination of the values for cross over between storage and loss modulus, plateau modulus and relaxation time spectra determination. Rheological polydispersity was determined from the ratio of zero shear viscosities (η_0) and complex viscosities at the cross over ($\eta*\#$):

$$U\eta = \left(\frac{\eta 0}{\eta *\#}\right) - 1 \ \ (3)$$

Mechanical characterization

BC staple fibres were left for 48h in controlled conditions, humidity of 65% ± 4% and temperature of 20°C ± 2°C. Then, the fibres were subjected to a single-Fibre tester (FAVIMAT+; Textechno Class 1 acc) for breaking force, elongation at break and loop tenacity measurements. For the determination of the linear density, a gravimetric method was used: 10 sets of 50 fibre were tested, using 30 mm bundle length. For the breaking force and elongation at break, 50 single fibres were tested, with 10 mm gauge length, using a pre-load of 0.60 cN/tex and test speed of 10 mm/min (according to standards DIN EN ISO 5079:2021-02 and DIN 53843 T2:1988-03) [26,27]. For the loop tenacity, the similar specifications were used, apart from test speed, which was of 5.0 mm/min (according to standard DIN 53843 T2:1988-03) [27].

6.2.7. Statistical analysis

Statistical analysis was supported with Prism version 9.4.1 (GraphPad Software, La Jolla California USA), using one-way ANOVA and Tuckey's post-hoc analysis for pairwise comparison of more than two means. Mean differences were considered statistically non-significant (ns) when p-value was higher than 0.05 (95% of interval of confidence). The default statistical confidence level was set at 95% (P < 0.05) in all tests.

6.3.   Results and Discussion

6.3.1.   BC depolymerization optimization & dope characterization

BC have a DP of about 1,000, whereas the pulp used in the lyocell process normally have a DP of 550-650. It is known that high DP values increase the dope's viscosity, which in turn limits the concentration of cellulose used on the dope. This may compromise the spinning process, hindering the use of high draw ratios and subsquently the fibre performance (specially mechanical performance). Thus, in this work we analysed in more detail the effect of the DP on the quality of the regenerated (Lyocell) BC fibres. Although not used industrially in the Lyocell process, mercerization was adopted in this study to depolymerize BC in small scale. Mercerization involves an alkaline treatment with sodium hydroxide, to swell the pulp; then, the alkali BC concentrated up to 10% cellulose is allowed to react with oxygen by stirring the dispersion, aging for 4 hours.

As observed in Table 6.1, BC_{neat} was of 978 ± 45, bellow the values reported in the literature [28]. Yet, the difference may be due to the use of different methodologies for measuring the intrinsic viscosity (e.g., solvent used) and the equation for calculating the DP. After mercerization and aging, a significant reduction in DP was observed (BC_{dep} further reduced to 608 ± 47), as expected. As described in the literature, cellulose treatment with NaOH leads to its conversion to soda cellulose (mercerization), reducing the DP as well as the crystallinity [29], the DP reduction being favoured by the presence of oxygen [24]. The study conducted by Strunk et al. [30] and the patent authored by Jinzarli et al. [25] also demonstrated a substantial depolymerization of cellulose (about 2 times in its molecular weight) after aging process. In order to produce a pulp with higher polydispersity, a third pulp (BC_{blend}) was prepared by mixing BC_{neat} with BC_{dep} (as detailed in section 6.2.4).

All BC pulps (BC_{neat}, BC_{blend} or BC_{dep}) were successfully dissolved using NMMO, with no undissolved particles being observed (Figure 6.3). For each case, the final BC concentration of the obtained dope was adjusted according to the estimated DP_{cuoxam}, as well as to previous rheological characterization in smaller scale dopes: 9.0 % for BC_{neat}, 12.2 % for BC_{dep} and 10.5% for BC_{blend} (Table 6.1). The dopes were characterized for their rheological behaviour (Table 6.1). Concerning the zero-shear viscosity (η_0), the lowest value obtained was of 4,951 Pa.s for BC_{dep}, followed by BC_{blend} and BC_{neat} with 20,470 Pa.s and 21,780 Pa.s, respectively (table 6.1).

For spinning, the η_0 is commonly targeted to 5,000 - 10,000 Pa.s, at 85°C. This means that both BC$_{neat}$ and BC$_{blend}$ dopes were out of range, while BC$_{dep}$ dope was in the lower limit. As observed in Table 6.1, BC$_{neat}$ with higher DP highly affected the η_0 of the dope, which consequently limited its concentration for dissolution in NMMO (cellulose concentration in standard pulps is 13%). Considering BC$_{dep}$, higher DP (between 600-650) or higher cellulose concentrations should increase the η_0. Importantly, a direct comparison of the obtained dopes cannot be made, as, along with differences in the DP, they differ in their concentration.

Figure 6.3. Microscopic images (polarized light) of the different BC dopes (scale division 200 μm)

Table 6.1. BC, dope and rheological characterization; data displayed as mean ± standard deviation.

	Sample	BC$_{neat}$	BC$_{dep}$	BC$_{blend}$
Pulp	DP$_{cuoxam}$ BC	978 ± 45	608 ± 47	836 ± 46
Dope	Solid content (wt %)	9.0	12.2	10.5
Rheological	Zero shear viscosity (85°C), η_0 (Pa.s)	21,780	4,951	20,470
	Angular velocity, ω (cross over) (rad/s)	0.60	5.64	0.82
	Storage modulus, G' (cross over) (Pa)	2,352	4,755	2,672
	Plateau modulus, Gp (Pa)	22,300	30,100	26,200
	Rheological polydispersity, $U\eta$	2.9	3.2	3.5
	Relaxation time, λ_m at H*m (s)	11	1.75	13.8

Despite the η_0 values being out of range, other important rheological parameters should be considered, such as the storage modulus (G'), the angular velocity (ω) at cross over point, the plateau modulus (Gp), the rheological polydispersity (Uη) and the relaxation time. As observed in Table 6.1, the combination of using high BC concentrations with lower DP (BC$_{dep}$: DP 608 and 12.2%BC) led to higher ω (5.64 rad/s at cross over), higher G' (4,755 Pa at cross over) and higher Gp (30,100 Pa), as compared to the dope using untreated BC (BC$_{neat}$) (ω: 0.60 rad/s; G': 2,352 Pa; Gp: 22,300 Pa). Concerning the BC$_{dep}$, no special behaviour was observed, when compared to common dissolution pulps [21]. As for the BC$_{neat}$ and BC$_{blend}$ dopes, a lower elastic and viscous behaviour (storage and loss modulus, respectively, at the cross over point, COP) was observed when compared to BC$_{dep}$ (Table 6.1 and Figure 6.4). As mentioned, the higher DP of BC$_{neat}$ limited its concentration used for the dope preparation (Table 6.1). Consequently, when a lower concentration of cellulose (composed mainly of higher cellulose chains) is used, the elastic and viscous behaviour of the dope is decreased. Hence, the cross-over point between G' and G'' is observed at lower ω, G' and G'' (Figure 6.4). Despite these differences in behaviour, a cross over between G' and G'' was still observed, where the dope shows elastic behaviour, important for spinnability (Table 6.1 and Figure 6.4). Moreover, a broader weighted relaxation time spectrum was observed for BC$_{neat}$ and BC$_{blend}$, when compared to BC$_{dep}$ (Table 1; Figure 4).

Relaxation times within 1.00s was obtained for BC$_{dep}$, falling within the typical range for standard pulps (when dissolved in NMMO) [21]. However, pulps with a high DP (BC$_{neat}$ and BC$_{blend}$) exhibited higher relaxation times (Figure 6.4). For BC$_{dep}$, a much lower intensity was observed, with the maximum being shifted to lower relaxation time values. Dopes containing longer cellulose chains (such BC$_{neat}$ and BC$_{blend}$) needed a longer relaxation time. As a result, the dopes' elastic properties (G'>G'') manifest at slower movements (lower angular velocities). Conversely, the depolymerized BC dope exhibited quicker recovery post-deformation (shorter relaxation times), meaning that the exhibiting elastic behaviour (G'>G'') occurs at higher angular velocities (Figure 6.4 and Table 6.1 for ω at crossover).

In short, differences in the rheological characterization between depolymerized BC and neat BC were verified. However, BC$_{blend}$ (containing 62% m/m of BC$_{neat}$ and 38% m/m of BC$_{dep}$), showed similar rheological characteristics to those obtained with BC$_{neat}$. A slight decrease in η_0 as well as an increase in storage modulus and plateau modulus is observed,

mostly related to the decrease in DP (to approximately 800) and the presence of different polymeric chains sizes, resulting from the blending of BC$_{neat}$ and BC$_{dep}$ pulps.
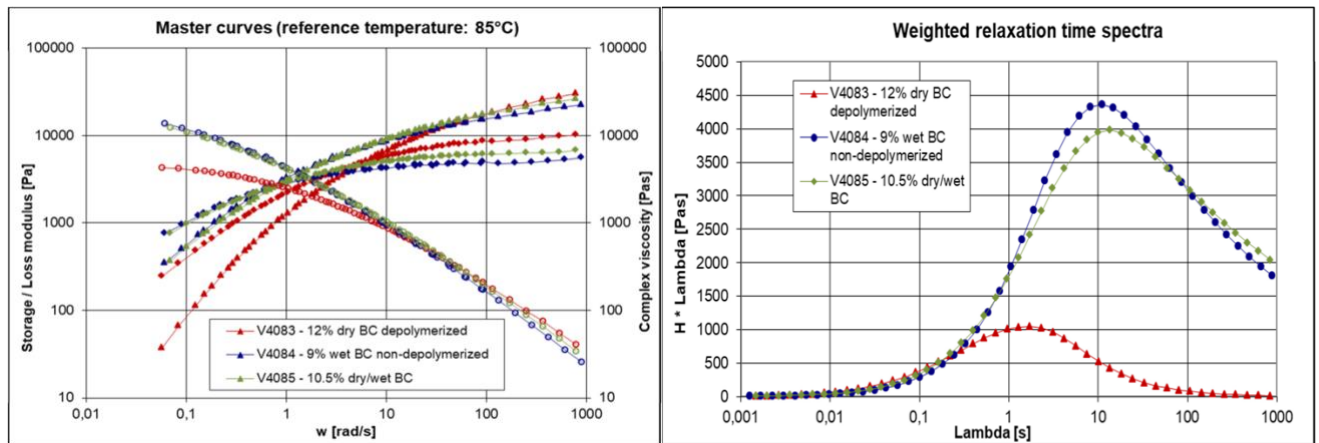
Figure 6.4. On the left, master curves of the spinning dopes from neat and depolymerized BC; triangles - storage modulus; squares - loss modulus; open circles - Complex viscosities; on the right, weighted relaxation time spectra of the spinning dopes.

6.3.2. Spinning

A dope with good spinnability is mainly characterized by the ability to stretch a filament through the air gap for better cellulose alignment along the chain axis. An important feature for aligning the cellulose is the draw ratio (DR) (also known as filament stretching), characterized by the ratio between take-up and extrusion velocity [22], [31]. All BC dopes were considered stable during spinning, being continuously spun for 60, 50 and 360 min, for BC_{neat}, BC_{dep} and BC_{blend}, using a DR of 2.3, 3.1 and 2.7, respectively.

After spinning, 148 g of BC_{neat} and 87g of BC_{dep} staple fibres were collected. For BC_{blend}, a filament yarn (320 single filaments x 1.5 dtex, 2 bobbins of 2,600 and 2,980 m) was collected (Figure 6.2).
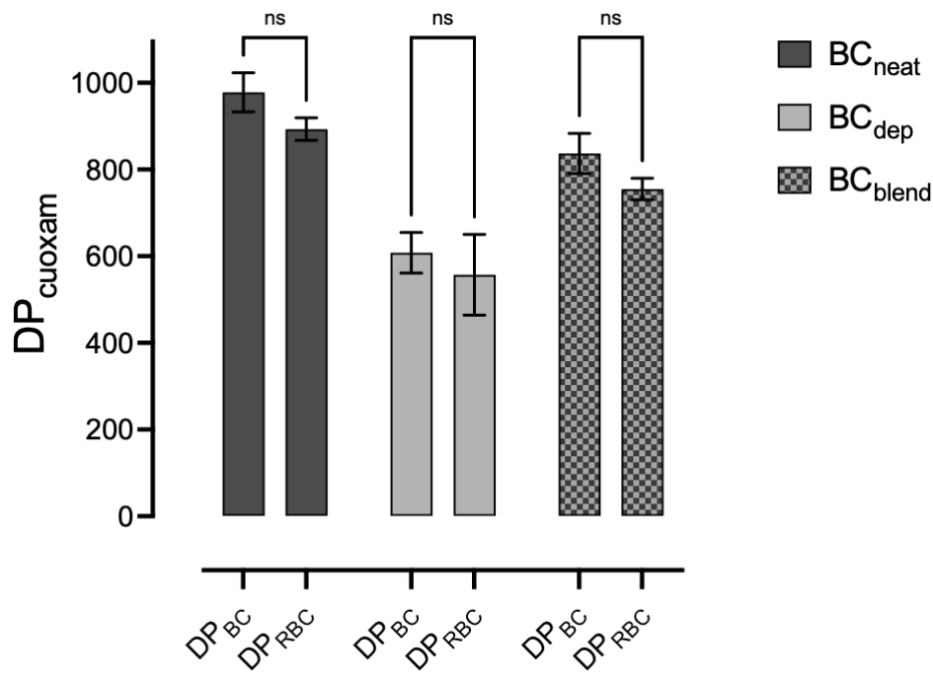
Figure 6.5. DP$_{cuoxam}$ estimation of BC pulps and BC regenerated fibres (RBC); columns represent the mean and error bars represent the standard deviation.

Afterwards, the DP$_{cuoxam}$ was estimated once again, as shown in Figure 6.5. All regenerated BC fibres displayed a similar DP$_{cuoxam}$ to that of the corresponding BC pulp ($p > 0.05$). Although a minor decline in the degree of polymerization of RBC fibres was observed, its non-significance ($p > 0.05$) validates that there was no substantial depolymerization of BC during its dissolution and spinning into highly oriented fibres, proving that all BC pulps were successfully dissolved in NMMO.

6.3.3. Mechanical properties

The collected fibres were analysed with the goal of understanding the effect of DP and of the size distribution on the resulting mechanical properties of the BC fibres. Table 6.2 displays the linear density, breaking force, breaking tenacity, elongation at break, initial modulus and loop tenacity of the RBC fibres, as well as data collected from the literature (Lyocell fibres).

Table 6.2. Mechanical properties of RBC fibres; data displayed as mean ± standard deviation.

Sample	RBC$_{neat}$	RBC$_{dep}$	RBC$_{blend}$	Lyocell [31,32]
Draw-ratio	2.3	3.1	2.7	2.0-10.0
Linear density (dtex)	1.66 ± 0.036[a]	1.70 ± 0.020[b]	1.52 ± 0.020[c]	1.3-1.7
Breaking force (CN)	7.69 ± 1.57[ab]	8.16 ± 1.80[bc]	8.58 ± 1.45[bc]	-
Breaking tenacity (CN.tex^{-1})	46.4 ± 9.46[ab]	48.0 ± 10.6 [ab]	56.4 ± 9.52[c]	40-48
Elongation at break (%)	10.9 ± 1.38[a]	12.1 ± 1.91[b]	8.29 ± 1.14[c]	10-16
Initial modulus (CN.tex^{-1})	978 ± 287[*ab]	1,119 ± 273[*ab]	1,917 ± 334[*c]	2,500-2,700
Loop tenacity (CN.tex^{-1})	14.5 ± 3.54[abc]	15.7 ± 3.76[ab]	12.8 ± 3.55[c]	18-20

* Modulus 0.5%-0.7%, related to bundle linear density; superscript letters indicate statistically significant differences ($p<0.05$); RBC- Bacterial cellulose regenerated fibres;

Significant differences between RBC fibres were obtained, mainly on the linear density and elongation at break ($p<0.05$). RBC$_{blend}$ fibres presented the lowest linear density and elongation at break, followed by RBC$_{neat}$. There were no significant differences ($p > 0.05$) observed between RBC$_{neat}$ and RBC$_{dep}$ in terms of the breaking force, breaking tenacity, initial modulus and loop tenacity. In turn, RBC$_{blend}$ presented higher stiffness (breaking tenacity and initial modulus) ($p<0.05$). From these results, it is perceived that varying the DP and consequently the concentration of BC did not affect the overall mechanical performance of the RBC fibres (Table 6.2). On the other hand, importantly, the blending of pulps with different DPs significantly improved the mechanical performance. This finding is aligned with studies conducted by Michud et al. [32] and Härdelin et al. [33], where the authors noted that the presence of cellulose chains of varying sizes (varying DP) enhances the intermolecular entanglement. This phenomenon influences then the viscoelastic characteristics of the dope, enhancing the drawing during the spinning process, impacting positively in the fibre alignment. All these improvements collectively contribute to an overall superior mechanical performance. Despite the high stiffness of RBC fibres, lower initial modulus (higher deformation under initial stress) and loop tenacity was obtained on RBC fibres. The values

reflect the lower orientation of the cellulose molecules due to the lower DR applied during spinning.

Other parameters to be taken into account are the BC concentration in the spinning solution and the draw ratio applied. The amount of BC used was slightly lower than that used in standard lyocell (13%), in the case of BC_{dep} (12%) but was rather lower in the case of BC_{blend} (10.5%) and BC_{neat} (9.0%), since the amount of BC was adjusted depending on the DP. Consequently, the ability to stretch the fibre during spinning was also limited. The DRs applied were low (between 2-3), yet within the standard values used for commercial lyocell (between 2-10) [34]. To collect fibres with low linear density (1.3-1.5), higher DRs should be applied. However, the stretchability of the spinning solution at higher DRs was limited due to the high DP of BC. For that reason, the selected DR (for each dope), represented the maximum DR without compromising the spinning. Additionally, using lower drawing ratios avoids fibrillation, as reported by Cui et al. [34]. However, the lack of stretching (lower DR) may have influenced the overall mechanical performance. As reported in the literature, the stiffness and elasticity may be tuned by the DR during spinning. Higher DR leads to lower linear densities, which consequently leads to lower elongation at break and higher tenacity [35,36]. The high fibre stretching increases the crystallinity, birefringence and orientation, enhancing the fibre stiffness (initial Young's modulus and tenacity), yet compromising elasticity [9,34]. Even so, as discussed above, very overall good mechanical properties could be achieved using BC_{blend}. Furthermore, the observed differences between the various samples may also be attributed to the different fibre spinning procedures. Both RBC_{neat} and RBC_{dep} were collected as staple fibres, whereas RBC_{blend} was collected continuously into yarn bobbins (section 6.2.5). Differences in the mechanical properties due to lyocell fibre processing (staple fibres vs fibre tow) were elsewhere reported [37]. These differences in the mechanical performance between staple and filaments may be caused by different drying conditions. More specifically, staple fibres could be dried as nearly independent single fibre (without any counterforce), whereas filaments would be dried as a fibre bundle, causing filament-filament-friction and reconditioning of predried bundles wound up on bobbins.

When compared to lyocell fibres, only RBC_{blend} showed significant differences, having higher resistance (higher breaking tenacity), lower elongation at break, lower initial modulus and lower loop tenacity (Table 6.2). The differences encountered between RBC_{blend} and lyocell may be related to the advantage of using a more polydisperse pulp.

Finally, the developed RBC fibres were compared with cotton, polyester and MMCF (such as lyocell, Ioncell® and viscose), regarding its tenacity and elasticity (Figure 6.6).
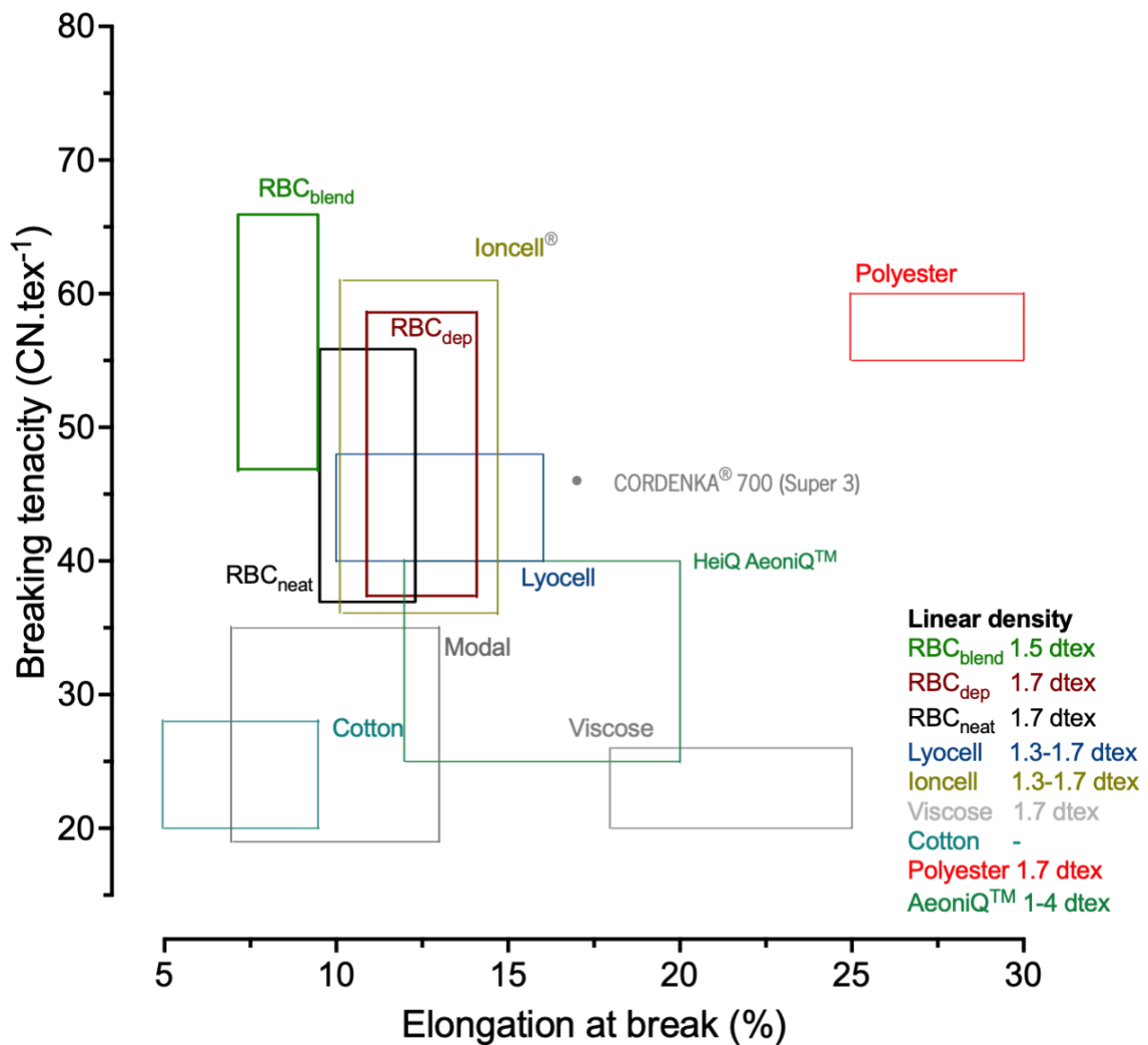
Figure 6.6. Breaking tenacity (CN.tex^{-1}) vs elongation at break (%) of BC fibres, lyocell [2], [24], [38], viscose [24], [39], [40], Modal [39], [41], CORDENKA® 700 (Super 3) [31], Ioncell® [31], [40], [42], cotton [39], [41], polyester [39] and HeiQ AeoniQ^{TM} [43]

The developed RBC fibres stand out for their high tenacity, when compared to all other fibres. RBC$_{blend}$ presented a tenacity comparable to that of polyester. On the other hand, both viscose and polyester have higher elasticity than RBC fibres (Figure 6.6). The production of BC fibres using NMMO is not novel [17], [18], yet the mechanical properties obtained with RBC$_{blend}$ were superior when compared with those reported in the literature.

The findings indicate that BC fibres, which possess higher stiffness, may be useful in the development of strategies for recycling end-of-life fibres through blending. A substantial volume of waste cellulosic textiles (including MMCFs, cotton or linen) degraded by their extensive use and repeated washing is being generated [44, 45]. This waste consists of cellulose with reduced chain length, posing challenges for recycling using viscose or Lyocell-type spinning methods. One approach to circumvent these difficulties involves the incorporation of high DP cellulose (such as BC) to increase the average chain length and widen the molar mass distribution. Spinnable dopes can be developed for Lyocell, facilitating the upcycling of textile waste. Despite its drawbacks in terms of current poor cost-effectiveness and yield at a large scale, BC stands out due to its purity (mainly composed of water and cellulose) and low ecological footprint, as evidenced by the findings in the studies conducted by Forte et al. [46] and Costa et al. [47]. Although technological breakthroughs are still necessary to make BC available at lower cost and at very large scale to match the textile industry needs for new raw materials, it may represent an alternative source of cellulose with high DP. Various fibres were already upcycled, such as hemp waste [48], newspaper [49], paper & cardboard [50], and cotton scraps [51], using Ioncell® and Lyocell technologies. These recycling methods could benefit from small additions of BC to improve both their strength and flexibility.

Indeed, additional research is still needed to validate the benefits of blending BC with other low DP fibres, as this study focused on blending BC with different DPs. Nevertheless, these initial studies have already yielded promising results for upcoming studies into the chemical recycling of end-of-life fibres. Moreover, the application of BC to promote the recyclability of other fibres allows for a more feasible prospect for the large-scale application of BC in the textile industry [52,53].

6.4.   Conclusions

Our findings demonstrated that a high DP – non-depolymerized – BC can be spun through the lyocell process, in contradiction to the common believe that only depolymerized cellulose can be regenerated into high quality fibres. However, the depolymerised BC allowed its dissolution at higher concentrations (up to 13% with DP 500-600). All BC pulps were continuously spun (up to 360 min), with no major losses. The resulting fibres have shown

interesting mechanical performance, particularly RBC$_{blend}$, where higher stiffness was observed. In sum, the blending of BC with different cellulose chains (different DP) improved the mechanical performance of the regenerated cellulose fibres. This demonstrates that BC (a source of long cellulose chains) may be an additive for recycled cellulosic waste materials (with low DP), blending the two materials through dissolution and spinning. Thus, BC may play a relevant role in improving the properties of recycled textile waste and thus it can be considered a promising source of cellulose for textile applications.

6.5. References

[1]   Muthu, S. S., Gardetti, M. A. (Eds.). (2016). *Sustainable fibres for fashion industry* (Vol. 1). Singapore: Springer.

[2]   Felgueiras, C., Azoia, N. G., Gonçalves, C., Gama, M., Dourado, F. (2021). Trends on the cellulose-based textiles: Raw materials and technologies. *Frontiers in Bioengineering and Biotechnology*, *9*, 608826.

[3]   Souza Machado, A. A., Kloas, W., Zarfl, C., Hempel, S., Rillig, M. C. (2018). Microplastics as an emerging threat to terrestrial ecosystems. *Global change biology*, *24*(4), 1405-1416.

[4]   Shen, L., Worrell, E., Patel, M. K. (2010). Environmental impact assessment of man-made cellulose fibres. *Resources, Conservation and Recycling*, *55*(2), 260-274.

[5]   Texcoms. Textile Technology knowledge series Volume II. Vol. II. 2019.

[6]   Deutschmann, O., Knözinger, H., Kochloefl, K., Turek, T. (2000). Heterogeneous catalysis and solid catalysts, 1. Fundamentals. Ullmann's encyclopedia of industrial chemistry

[7]   Woodings, C. (Ed.). (2001). *Regenerated cellulose fibres*. Elsevier.

[8]   Sayyed, A. J., Deshmukh, N. A., Pinjari, D. V. (2019). A critical review of manufacturing processes used in regenerated cellulosic fibres: viscose, cellulose acetate, cuprammonium, LiCl/DMAc, ionic liquids, and NMMO based lyocell. *Cellulose*, *26*(5), 2913-2940.

[9]   Kim, D. B., Pak, J. J., Jo, S. M., Lee, W. S. (2005). Dry jet-wet spinning of cellulose/N-methylmorpholine N-oxide hydrate solutions and physical properties of lyocell fibers. *Textile research journal*, *75*(4), 331-341.

[10]   Perepelkin, K. E. (2007). Lyocell fibres based on direct dissolution of cellulose in N-methylmorpholine N-oxide: development and prospects. *Fibre Chemistry*, *39*(2), 163-172.

[11]   Hummel, M., Michud, A., Tanttu, M., Asaadi, S., Ma, Y., Hauru, L. K., Parviainen, A., King, A.W.T., Kilpeläinen, I. & Sixta, H. (2016). Ionic liquids for the production of man-made cellulosic fibers: opportunities and challenges. *Cellulose chemistry and properties: Fibers, nanocelluloses and advanced materials*, 133-168.

[12]   Eckelt, J., Eich, T., Röder, T., Rüf, H., Sixta, H., Wolf, B. A. (2009). Phase diagram of the ternary system NMMO/water/cellulose. *Cellulose*, *16*(3), 373-379.

[13]   Fink, H. P., Weigel, P., Purz, H. J., Ganster, J. (2001). Structure formation of regenerated cellulose materials from NMMO-solutions. *Progress in Polymer Science*, *26*(9), 1473-1524.

[14]   Singha, K. (2012). Importance of the phase diagram in lyocell fiber spinning. *International Journal of Materials Engineering*, *2*(3), 10-16.

[15]   Gunnars, S., Wågberg, L., Stuart, C. (2002). Model films of cellulose: I. Method development and initial results. *Cellulose*, *9*(3), 239-249.

[16]   Zhang, S., Chen, C., Duan, C., Hu, H., Li, H., Li, J., Liu, Y., Ma, X., Stavik, J., Ni, Y. (2018). Regenerated cellulose by the lyocell process, a brief review of the process and properties. *BioResources*, *13*(2), 4577-4592.

[17]   Gao, Q., Shen, X., Lu, X. (2011). Regenerated bacterial cellulose fibers prepared by the NMMO· H2O process. *Carbohydrate polymers*, *83*(3), 1253-1256.

[18]   Makarov, I. S., Golova, L. K., Vinogradov, M. I., Levin, I. S., Gromovykh, T. I., Arkharova, N. A., Kulichikhin, V. G. (2019). Cellulose Fibers from Solutions of Bacterial Cellulose in N-Methylmorpholine N-Oxide. *Fibre Chemistry*, *51*(3), 175-181.

[19]   Golova, L. K., Borodina, O. E., Kuznetsova, L. K., Lyubova, T. A., Krylova, T. B. (2000). The solid-phase MMO process. *Fibre Chemistry*, *32*(4), 243-251.

[20]   Golova, L. K., Makarov, I. S., Matukhina, E. V., Kulichikhin, V. G. (2010). Solutions of cellulose and its blends with synthetic polymers in N-methylmorpholine-N-oxide: Preparation, phase state, structure, and properties. *Polymer Science Series A*, *52*(11), 1209-1219.

[21]   Meister, F., Kosan, B. (2015). A tool box for characterization of pulps and cellulose dopes in Lyocell technology. *Nordic Pulp Paper Research Journal*, *30*(1), 112-120.

[22]   Haslinger, S., Hummel, M., Anghelescu-Hakala, A., Määttänen, M., Sixta, H. (2019). Upcycling of cotton polyester blended textile waste to new man-made cellulose fibers. Waste Management, 97, 88-96

[23]   Piribauer, B., Bartl, A. (2019). Textile recycling processes, state of the art and current developments: A mini review. *Waste Management & Research*, *37*(2), 112-119.

[24]   Woodings, C. (Ed.). (2001). *Regenerated cellulose fibres*. Elsevier.

[25]   Jinzarli, M. M., Cass, G. A., Moursounidis, J., Best, W. M. (2020). *U.S. Patent Application No. 16/769,721*.

[26]   DIN EN ISO 5079:2021-02 - Textile fibres - Determination of breaking force and

elongation at break of individual fibres (DIN EN ISO 5079)

[27]   DIN 53843 T2:1988-03 - Testing of textiles; Loop tensile testfor Staple Fibres (DIN 53843 T2)

[28]   Choi, S. M., Shin, E. J. (2020). The nanofication and functionalization of bacterial cellulose and its applications. *Nanomaterials*, *10*(3), 406.

[29]   Kunze, J., Fink, H. P. (2005, March). Structural changes and activation of cellulose by caustic soda solution with urea. In *Macromolecular symposia* (Vol. 223, No. 1, pp. 175-188).

[30]   Strunk, P., Lindgren, Å., Eliasson, B., & Agnemo, R. (2012). Chemical changes of cellulose pulps in the processing to viscose dope. *Cellulose Chemistry Technology*, *46*(9-10), 559-569.

[31]   Moriam, K., Sawada, D., Nieminen, K., Hummel, M., Ma, Y., Rissanen, M., Sixta, H. (2021). Towards regenerated cellulose fibers with high toughness. *Cellulose*, *28*(15), 9547-9566.

[32]   Michud, A., Hummel, M., Sixta, H. (2015). Influence of molar mass distribution on the final properties of fibers regenerated from cellulose dissolved in ionic liquid by dry-jet wet spinning. *Polymer*, *75*, 1-9.

[33]   Härdelin L, Perzon E, Hagström B, Walkenström P, Gatenholm P. Influence of molecular weight and rheological behavior on electrospinning cellulose nanofibers from ionic liquids. J Appl Polym Sci. 2013;130(4):2303–10.

[34]   Cui, S., Zhang, Y., Liu, C., Lou, S., Zhang, Y., Zhang, Y., Wang, H. (2022). The influence of the multi-level structure under high drawing on the preparation of high strength Lyocell fiber. *Cellulose*, 1-12.

[35]   Sixta, H., Michud, A., Hauru, L., Asaadi, S., Ma, Y., King, A. W., Kilpelainen, I., Hummel, M. (2015). Ioncell-F: a high-strength regenerated cellulose fibre. *Nordic pulp   paper research journal*, *30*(1), 43-57.

[36]   Kim, T., Kim, D., Park, Y. (2022). Recent progress in regenerated fibers for "green" textile products. *Journal of Cleaner Production*, 134226.

[37]   Adusumalli, R. B., Keckes, J., Martinschitz, K. J., Boesecke, P., Weber, H., Roeder, T., Sixta, H., Gindl, W. (2009). Comparison of molecular orientation and mechanical properties of lyocell fibre tow and staple fibres. *Cellulose*, *16*(5), 765-772.

[38]   Röder, T., Moosbauer, J., Wöss, K., Schlader, S., Kraft, G. (2013). Man-made cellulose

fibres—a comparison based on morphology and mechanical properties. *Lenzinger Berichte*, *91*, 7-12.

[39] Rana, S., Pichandi, S., Parveen, S., Fangueiro, R. (2014). Biosynthetic fibers: production, processing, properties and their sustainability parameters. In *Roadmap to Sustainable Textiles and Clothing*, 109-138

[40]   Michud, A., Tanttu, M., Asaadi, S., Ma, Y., Netti, E., Kääriainen, P., Persson, A., Berntsson, A., Hummel, M., Sixta, H. (2016). Ioncell-F: ionic liquid-based cellulosic textile fibers as an alternative to viscose and Lyocell. *Textile Research Journal*, *86*(5), 543-552.

[41] Latif, W., Basit, A., Rehman, A., Ashraf, M., Iqbal, K., Jabbar, A., Baig, S.A., & Maqsood, S. (2019). Study of mechanical and comfort properties of modal with cotton and regenerated fibers blended woven fabrics. *Journal of Natural Fibers*, *16*(6), 836-845.

[42] Ma, Y., You, X., Nieminen, K., Sawada, D., & Sixta, H. (2023). Influence of DP and MMD of the pulps used in the Ioncell® process on processability and fiber properties. *RSC Sustainability*.

[43] "HeiQ AeoniQ™." [Online]. Available: https://www.heiq-aeoniq.com/our-technology/. [Accessed: 27-March-2024].

[44] Palme A, Idström A, Nordstierna L, Brelid H. Chemical and ultrastructural changes in cotton cellulose induced by laundering and textile use. Cellulose. 2014;21(6):4681–91.

[45] Jasińska I. Industrial washing conditions as factor that influence the cellulose structure and mechanical strength of bed linens. Sci Rep. 2023;13(1):12214. Available from: https://doi.org/10.1038/s41598-023-38969-y

[46] Forte, A., Dlourado, F., Mota, A., Neto, B., Gama, M., & Ferreira, E.C. (2021). Life cycle assessment of bacterial cellulose production. The International Journal of Life Cycle Asssessment, 26 (5), 864-878.

[47] Aragão, J. V., Costa, A. F., Silva, G. L., Silva, S. M., Macêdo, J. S., Galdino Jr, C. J., Milanez, V.F.A. & Sarubbo, L. A. (2020). Analysis of the environmental life cycle of bacterial cellulose production. *Chemical Engineering*, *79*.

[48] Rissanen, M., Schlapp-Hackl, I., Sawada, D., Raiskio, S., Ojha, K., Smith, E., & Sixta, H. (2022). Chemical recycling of hemp waste textiles via the ionic liquid based dry-jet-wet spinning technology. *Textile Research Journal*, 93(11-12), 2545-2557

[49] Ma, Y., Hummel, M., Kontro, I., & Sixta, H. (2018). High performance man-made

cellulosic fibres from recycled newsprint. *Green Chemistry*, *20*(1), 160-169.

[50]   Ma, Y., Hummel, M. M. M. S. A., Määttänen, M., Särkilahti, A., Harlin, A., & Sixta, H. (2016). Upcycling of waste paper and cardboard to textiles. *Green Chemistry*, *18*(3), 858-866.

[51]   "REFIBRA technology." [Online]. Available: https://www.tencel.com/refibra. [Accessed: 30-May-2023].

[52]   Textile Exchange. Preferred Fiber & Materials: Market Report 2022. 2022;(October):1–118.

[53]   Dourado F, Fontão A, Leal M, Rodrigues AC. Evaluation of an Industrial Bacterial NanoCellulose Fermentation Process. Bacterial Nanocellulose. Elsevier B.V.; 2016. 199–214 p. Available from: http://dx.doi.org/10.1016/B978-0-444-63458-0/00012-3

Currently the textile industry relies strongly on synthetic fibres and cotton, which contribute to many environmental problems. Man-made cellulosic fibres (MMCF) can offer sustainable alternatives. Herein, the development of Lyocell-type MMCF using bacterial cellulose (BC) as alternative raw material in the Ioncell® spinning process was investigated. Bacterial cellulose is well known for its high degree of polymerization (DP), crystallinity and strength. In this work, BC was successfully dissolved in the ionic liquid (IL) 1,5-diazabicyclo[4.3.0]non-5-enium acetate [DBNH][OAc] to produce solutions with excellent spinnability. BC staple fibres displayed enhanced mechanical properties and crystallinity (CI) in comparison to fibres produced from standard prehydrolysis kraft wood pulp (PHK): breaking tenacity BC: >52 cN.tex^{-1} vs PHK fibres :<49 cN.tex^{-1}; crystallinity Index BC: <60 % vs PHK fibres: <35 %. The staple fibres were spun into a yarn which was knitted into garments, demonstrating the potential of BC as suitable cellulose source for textile production. BC is also a valuable additive when recycling waste cellulose textiles with a low DP such as viscose fibres. The high molecular weight and crystallinity of BC enhanced the spinnability in a viscose/BC blend and improved the mechanical performance of the resulting fibres as compared to fibres spun solely from viscose fibres.

7.1.   Introduction

The high demand of textiles and apparel has led to a continuous increase in the production of textile fibres and filaments, which reached 118.6 million metric tons in 2022 [1]. Amidst the stagnant production of cotton (24% market share), the global market is dominated by unsustainable synthetic fibres (up to 60%) [2]–[5]. The majority of synthetic fibres are made of non-renewable sources, are not biodegradable and have a low recycling rate, while the cultivation of cotton requires substantial amounts of arable land, water, fertilizers and pesticides [6]. To reduce the environmental impact associated with the production of textile fibres, man-made cellulosic fibres (MMCF) are attracting increasing attention as alternative sources for textiles [7].

Globally, only 6% of textiles are produced by MMCF, its production involving either derivatization of cellulose or direct dissolution [5]. The most common MMCF are viscose-types (5.8 million tonnes in 2022 [5]), despite the environmental concerns (high amount of chemical usage) associated with their production [8]. The viscose process comprises multiple steps in which the cellulose is degraded intentionally to arrive at solutions suitable for wet spinning. Lyocell is one promising alternative process in which a direct solvent such as *N*-methylmorpholine *N*-oxide (NMMO) monohydrate is used for direct dissolution without prior chemical derivatization of the cellulose. Highly oriented fibres (with good mechanical performance) are obtained using this process and more than 99% of the solvent is recovered [9], [10]. The global Lyocell capacity is continuously increasing (from ca. 300 kt in 2019 to ca. 400 kt in 2022), which reflects the increasing demand for more sustainable regenerated cellulose fibres [11], [12]. Despite of being a promising technology, NMMO is known to be sensitive to high temperatures (higher than 120 °C) in the presence of transition metal ions. Stabilizers such as propyl gallate are used to prevent thermal runaway reactions of NMMO during cellulose dissolution [13].

More recently, the direct dissolution of cellulose in ionic liquids (ILs) has been explored. These are defined as salts (*i.e.* consisting of a cation and an anion) with a melting point below 100 °C [14]. The appropriate selection of anions and cations allows to tuning the IL properties and the ability to dissolve biopolymers in a selective way [14]. During dissolution, the anions of the IL compete with the cellulose intermolecular hydrogen bonds whereas the cations stabilize the

negatively charged units, enhancing solubility [6], [15]. Several studies demonstrated that imidazolium-based ILs are effective for cellulose spinning, yet induce some cellulose degradation at higher temperatures (>90 °C) [14], [16]. Additionally, anions like halides were found to be highly corrosive [17], [18]. More recently, non-imidazolium-based ILs such as 1,5-diazabicyclo[4.3.0]non-5-enium acetate ([DBNH][OAc]) were proposed as solvent in Lyocell-type spinning [17]. These superbase-based ILs show a high cellulose dissolution capacity (17%$m_{cellulose}$/m_{dope}), with great spin stability using dry jet-wet spinning [17], [19]–[21]. The resulting fibres, also known as Ioncell fibres, have shown competitive mechanical and structural properties when compared to other commercial MMCF [14], [17], [19].

Another concern related to the increasing use of MMCF is associated to the concomitant consumption of plant-based cellulose. While proving to be a good source for the production of high-performance textiles fibres, such as Tencel and Ioncell, environmental issues arose, such as the increasing need for intensive deforestation and wood (chemically based) processing. To guarantee a sustainable supply of cellulose for MMCF, alternative sources have to be explored. Bacterial cellulose (BC) could be one alternative, produced via bacterial fermentation, e.g. by the genus *Komagataeibacter*, through agitated or static fermentation [22]. While BC is well known for its high-purity, crystallinity, degree of polymerization (DP) and mechanical performance, its production still needs to be improved due to low yields and high processing cost with the current fermentation systems [23],[24].

BC has been applied mostly in the biomedical, food and cosmetic sectors [25]–[27]. However, interest in using BC in the textile industry is growing. The research community has been exploring ways to create high quality textiles, using BC. For instance, Kaminski et al. [28] and Fernandes et al. [29] demonstrated ways of developing modified BC to manufacture "ready-to-use" fabrics and leather, respectively. Another promising approach concerns the development of regenerated BC fibres [30],[31]. In the literature, the high DP of BC (around 1,500-2,500) is addressed as a setback for obtaining a high quality and spinnable dope. While a high DP is often related to a superior mechanical performance, its processing (mainly dissolution) was proven to be challenging as only low concentrations of BC were successfully dissolved [32], [33]. Conversely,

this limitation may be diminished if [DBNH][OAc] IL is used, since several studies reported effective dissolutions (and spinning) of high DP cellulose (as high as 1200) [19], [34].

Only small amounts (10% of the total global fibre production) of textiles are recycled. Most of the garments are incinerated or end up in landfills [20], [35], [36]. Responding to this alarming situation, the European Commission presented a strategy for the development of sustainable and circular textiles. Among different goals to be achieved, one addresses the effort to achieve "durable, repairable and recyclable textiles, to a great extent made of recycled fibres, free of hazardous substances, produced in respect of social rights and the environment". Hence, there is an urgent need for sustainable solutions that enable the recycling of end-of-life fibres. Recycling cellulosic fibres may be challenging as end-of-life cotton, viscose or Lyocell can show a wide range of DP. Laundering, UV-irradiation, or other environmental impacts can cause a significant DP reduction during the lifetime of the textile. Mechanical and/or chemical treatment of the textile waste leads to further cellulose depolymerization (as low as DP 300), which limits their applicability for the production of recycled MMCF. One way to compensate for these low DP fibres is to blend them with high DP cellulose, such as BC, to improve the viscoelastic properties of the resulting solution and further its spinnability by broadening the molar mass distribution [32], [35].

In this work, the dissolution of BC using [DBNH][OAc] was first optimized, considering the BC concentration and the rheological behaviour of the prepared dopes. Spinning trials were done under different conditions to achieve the best performing fibre. Then, the process was scaled to collect larger amounts of staple fibres for yarn spinning and knitting into garments, as a demonstration that BC is a suitable candidate for textile production via the Ioncell® technology.

Finally, we show that BC can be used to enable chemical recycling of textile waste with a very low DP. Viscose fibres, representing cellulosic textile fibres with the lowest DP, were re-spun into virgin fibres using BC as additive. Several solutions in [DBNH][OAc] were prepared with different amounts of BC to assess the overall performance of the final regenerated cellulose fibre comprising viscose and BC.

7.2.   Material and Methods

7.2.1.   BC pulp preparation

Commercial BC membranes from HTK Food Co., Ltd. (Ho Chi Minh City, Vietnam) were washed with NaOH (0.1M; Fisher) followed by distilled water until the pH of the filtrate became neutral. To obtain a BC pulp, the membranes were cut into cubes and wet-ground with a hand-blender. Then, the concentration was adjusted to 0.5% m/v and mechanically processed with a blender (Moulinex TYPE LM935) (6 times for 5 mins each time, allowing cooling between each period). Then, the BC pulp was air dried at 50 °C and milled using a high-speed grinding machine 600G. Prehydrolysis kraft (PHK) pulp (Stora Enso, Enocell) was milled to a powder with Fritsch pulp with 0.5 mm mesh. Viscose fibres, obtained from Kelheim Fibres GmbH, were milled using a Wiley Mini Mill 475-A.

Before processing, the dry matter content of each pulp was determined as described by the ISO 638:2008 standard. Three samples (from each pulp) of 0.1 g were weighed and dried at 105 °C for 24 h. Afterwards, dried samples were cooled down in a desiccator and weighed, and the dry matter content was determined.

7.2.2.   Estimation of the degree of polymerization

The DPs of all cellulose pulps, which is correlated with the intrinsic viscosity, were characterized according to SCAN-CM 15:88. BC (96% m/m, dry basis), PHK (92% m/m, dry basis) and viscose fibres (95% m/m, dry basis) were each dissolved using cupriethylenediamine aqueous solution (CED, CAS:14552-35-3, M:, $CuC_4H_{20}N_4O_2$; Oy FF-Chemicals Ab). For this, about 250 mg of each sample was weighed into plastic bottles with five copper rods and further filled with 25 mL deionized water. The plastic bottles were shaken for 30 min in a Kauko Lehtinen shaking device, at room temperature (RT). Then, 25 mL of CED was added (yielding a final concentration of around 0.005 g/mL) and again shaken for 30 min, for cellulose dissolution at RT. All samples were then placed in a 25 °C water bath (Mistral Multi-stirrer) before measurement. The intrinsic viscosity of all solutions was measured using a capillary viscometer. Then, the determined intrinsic viscosity was used to estimate the DP using formula (1) (described in SCAN-CM 15:88):

$$DP = \left(\frac{\eta}{Q}\right)^{1/a} \quad (1)$$

Where Q and a parameters, are defined as follows:

When DP < 950, Q = 0.42 and a = 1;

When DP > 950, Q = 2.28 and a = 0.76;

7.2.3. [DBNH][OAc] IL preparation

1,5-Diazabicyclo[4.3.0]non-5-ene (99%, CAS: 3001-72-7, M: 124.18, $C_7H_{12}N_2$, Fluorochem, UK) and acetic acid (glacial, 100%, CAS: 64-19-7, M: 60.05, $C_2H_4O_2$, Merck, Germany) were used as received. [DBNH][OAc] was prepared (in a customized 6L reactor) by slowly adding equimolar amounts of acetic acid to DBN at 70 °C under constant stirring [17].

7.2.4. Preparation of spinning dopes

Before dissolution, [DBNH][OAc] was first melted at 70 °C in a water bath. Then, the melted [DBNH][OAc] was transferred to a customized kneader system, pre-heated to 75-85 °C. Then, the air-dried BC pulp (dry matter content of 96 %m/m) was slowly added, with manual stirring to a final concentration (dry $m_{cellulose}/m_{dope}$) of 10%, 12% and 13%. For the recycling of viscose fibres, blends of viscose and BC were prepared, maintaining the total cellulose concentration at 16% (dry $m_{cellulose}/m_{dope}$). Blends with (%viscose/%BC) 16%/0%, 14%/2%, 13%/3% and 12%/4% (labelled as Vis16, Vis14BC2, Vis13BC3, and Vis12BC4 respectively) were prepared for spinning trials. The mixtures were stirred (30 rpm) at 75-85 °C under reduced pressure (50-60 mbar) until complete dissolution was observed (> 180 min). Each produced dope was then filtered by means of a hydraulic press filtration device (200 bar, metal filter fleece, 5–6 µm absolute fineness, Gebr. Kufferath AG, Germany) to remove residual undissolved particles and impurities. The filtered solutions were shaped to the dimensions of the spinning cylinder and kept in a cold room (4 °C) until use [17].

7.2.5. Spinning trials

PHK pulp, BC and blended BC/viscose fibres were spun using a small-scale customized dry-jet wet spinning unit (Fourné Polymertechnik, Germany) [21]. The solid, shaped [DBNH][OAc]-

cellulose dopes were loaded into the cylinder and the samples were heated to 70 °C for melting. Dopes were then extruded at 55–85 °C (depending on the rheology data of each dope, as described later) through a single hole spinneret (100 μm diameter, length-to-diameter ratio of 0.2). The produced filaments passed a 0.5-1.0 cm airgap, were immersed into a water coagulation bath and collected at godets utilised for stretching the filaments via the variation of the take-up speed. The air gap distance, immersion depth inside the water bath, deflection angle, the retention distance of the filament bundle and the temperature of the coagulation bath (5 °C) were kept constant throughout all spinning trials. The extrusion rate was fixed at 1.3 m/min, while the take-up velocity of the godet was varied from 6–23 m.min^{-1}, resulting in draw ratios (DR = $v_{take-up}/v_{extrusion}$) of 5.0 to 18.

Additionally, for BC spinning at larger-scale, another dry-jet wet spinning unit (Fourné Polymertechnik, Germany) was used. The shaped [DBNH][OAc]-BC dope was extruded at 65–80 °C through a multi hole spinneret (200 & 400 holes; 100 μm diameter, length-to-diameter ratio of 0.2), using the same conditions as above. The extrusion rate was fixed at 3.5 m.min^{-1}, while the take-up velocity of the godet was varied from 7–63 m.min^{-1}, resulting in draw ratios (DR) of 2.0 to 18. The collected filaments (small and large unit) were cut into 4 cm segments for yarn production and 10 cm pieces for analysis. All the fibres were washed with hot water (60 °C) and air dried at ambient temperature.

7.2.6. Yarn spinning

Yarn spinning was performed as described by Michud et al. [37]. Firstly, the staple fibres were treated with target amount of 0.25% m/m$_{fibre}$ of lubricant; 80/20% of Afilan CVS (ARCHROMA, Switzerland) and Leomin PN (ARCHROMA, Switzerland), respectively. The fibres were submerged into a solution (liquor ratio of 1:20) comprising Afilan CVS (0.677 g.L^{-1}) and Leomin PN (0.233 g.L^{-1}) and heated at 45 °C for 5 min (manually stirred). Then, the fibres were pressed to reach 300% pick-up and air dried. Next the fibres were opened using a Mesdan Lab Trash Analyzer 281C (Mesdan SpA, Italy) and left overnight in a conditioned room (65% RH; 20 °C). The opened fibres were fed into batches of 25 g for carding (carding machine 337A, Mesdan SpA, Italy) and rolled into slivers using Stiro lab 3371 (Mesdan SpA, Italy) for roving, stretching

and doubling. Slivers were drafted twice, in the second one two slivers were combined and drafted together. Finally, two doubled slivers were combined into roving. The roving was then ring spun (Ring Lab 82BA; SER.MA.TES srl, Italy) into a 20 tex yarn (Nm 50, Ne 30). The yarn had Z torsion and the number of twists per meter (TPM) was 700. The calculated twist multiplier expressed in Ne was 3.26. The linear density of the spun yarn was determined from 10-m skeins (n=6; expressed in tex).

7.2.7. Knitting and bleaching

The knitting of the yarn was done in a Stoll ADF 32W E7.2 (14gg), where 4 samples were developed, two samples with an "interlock" pattern (stitch size: NP5 and NP6 =9.5; sample size: 150 stitches, 400 rows) and two samples with a "racking & single knit" pattern (stitch size: NP5 and NP6 = 10.0 (mock rib + racking), NP22 = 11.0 (single knit); sample size: 120 stitches, 200 rows) [38]. Additional samples were knitted using a Knotyong machine Labknitter 297E (Mesdan SpA, Italy), for bleaching assays. The bleaching was carried out under the following conditions: the samples were submerged in a container with a solution comprising 2.0 g.L^{-1} H$_2$O$_2$ (29.7%; CAS: 7722-84-1 M: VWR), 7.0 g.L^{-1} Na$_2$SiO$_3$ (Na$_2$O: 7.5-8.5 %; SiO$_2$: 25.5-28.5 %, CAS: 1344-09-8, VWR), 0.5 g.L^{-1} NaOH (99.1%, CAS: 1310-73-2; M: VWR) and 1.8 g.L^{-1} Na$_2$CO$_3$ (99.8%, CAS: 144-55-8 M: VWR). Then, these containers were placed in a Testex Infrared lab dyeing machine TD130 and subjected to a temperature of 90 °C for 2 h.

7.2.8. Dope and fibre characterization

Molecular weight distribution

As previously described by Pitkänen et al. [39], the molecular weight distribution was measured with gel permeation chromatography (GPC) using a Dionex Ultimate 3000 HPLC system equipped with a Shodex DRI (RI-101), and a Viscotek/Malvern SEC/MALS 20 multi-angle light scattering (MALS) detector. About 0.05 g of each pulp/sample was subjected through a solvent exchange process, consecutively using water, acetone, and DMAc (4 mL of each reagent). The contact between pulp/sample and each solvent was maintained overnight for effective activation. After solvent exchange, cellulose samples were dissolved in LiCl/DMAc (90 g.L^{-1}) and stirred overnight, to ensure full dissolution. The samples were then diluted (from 90 g.L^{-1} to 9.0 g.L^{-1}). The diluted samples were filtered using 0.2 µm filters onto plastic vials before measurements. 100 µl of each sample solution was placed into the four columns system (PLgel MIXED-A) operating at a flowrate of 0.75 ml.min^{-1}. A narrow polystyrene standard (Mw = 96 000 g.mol^{-1}, Đ = 1.04, refractive index increment, ∂n/∂c, 0.146 mL.g^{-1}) was used to obtain the detector constants for MALS and DRI, whereas a broad polystyrene sample (Mw = 248 000 g.mol^{-1}; Đ=1,73) was applied to test the calibration of the detectors. A ∂n/∂c value of 0.136 mL. g^{-1} was used for celluloses in 0.9% LiCl in DMAc. After GPC analysis, the parameters weight-average molar mass (Mw), number-average molar mass (Mn), polydispersity index (Mw/Mn) and the proportion of long cellulose chains (DP>2000) and short cellulose chains (DP<100) were obtained.

Optical characterisation of the cellulose dopes by polarization microscopy

The optical characterisation of the spinning dopes was carried out using polarization microscopy. A Zeiss Axio with heating stage microscope (10X magnification lens) was used. A small sample of the dope was placed on a cleaned glass slide (with cover), and heated to 80 °C for 15 min before optical observations.

Rheological characterisation of the cellulose dopes

The rheological characterisation was carried out as described by Michud et al. [32], with slight modifications. An Anton Paar Physica MCR 302 rheometer with a plate-plate geometry of 25 mm diameter and 1 mm gap size was used. The rheological behaviour was determined by dynamic frequency sweep tests from 100 to 0.01 s^{-1}, at varying temperatures (50-90 °C). Zero shear viscosity (η_0^*) and crossover points (G' = G'') were determined by using the Cross model assuming the validity of the Cox-Merz rule [40].

Mechanical characterization

Fibre testing was carried out in accordance with EN ISO 5079 and EN ISO 139 standard procedures. The fibres were conditioned overnight at a relative air humidity of 65% and 20 °C. Next, the fibres were subjected to a single-fibre tester (Textechno Herbert Stein Favigraph) for the measurement of linear density (titer), tenacity and elongation at break in conditioned (RH 65% & T 20 °C) and wet state (fibres soaked for 10 seconds before measurements). Tensile testing was done under the following settings: 20 fibres per sample; gauge length of 20 mm; 20 cN maximum capacity of load cell; test speed of 20 mm.min^{-1}. The mechanical properties of the yarn were determined (following ISO 2062) using MTS400 tensile tester set with a 50N load cell. The testing speed was 250 mm.min^{-1}, and the gauge length was 250 mm.

Birefringence

Three fibres (from each sample) with similar linear density to its average (± 0.1 dtex) were attached to a microscope slide and observed with a Zeiss Axio Scope.A1 microscope with a Zeiss Tilting Compensator B. The thickness of the fibre was determined from the linear density and the assumption of a density of 1.5 g/cm^3. The total orientation factor f_t was determined by dividing the birefringence with 0.062, the maximum birefringence of cellulose [41].

Scanning electron microscopy

The morphology of PHK and BC fibres were analysed using scanning electron microscope (Zeiss; Sigma VP), with a variable pressure and a 5kV operating voltage. For cross-section imaging, the samples were prepared as follows: a bundle of fibres was immersed in water and

subsequently frozen with liquid nitrogen. The ice was then shattered, to collect the cryo-fractured fibres [37]. After drying, the fibres were vertically attached to SEM sample holders and sputter-coated with 80 Au/20 Pd (5nm thickness) in a Quorum 150R S plus sputtering device.

Carbohydrate & Elemental analysis

The national renewable energy laboratory (NREL) protocol was followed for the determination of structural carbohydrates and lignin in the samples [42]. About 0.30 g of each sample (duplicates) was submitted to acid hydrolysis, using H_2SO_4 72% (v/v). Firstly, 3 ml of H_2SO_4 72% (v/v) was added to the sample and heated to 30 °C for 60 minutes (stirred every 5 minutes). Then, the resulting suspension was diluted to 4% of H_2SO_4. Simultaneously, a sugar recovery standard was prepared (composed of glucose (1000 mg), mannose (50 mg), galactose (50 mg), and xylose (50 mg)) to be used as reference. The samples and sugars were hydrolysed in a Systec DE-23 autoclave at 121 °C for 60 min, after which the samples were filtered through VitraPOR Borosilicate 3.3 crucibles. The remaining residue was dried and weighed for the determination of the acid insoluble non-saccharides, whereas the filtrate was diluted with milli-Q water by a factor of 100 and measured in a Dionex ICS-3000 HPAEC-PAD. For solubilized lignin quantification, samples were measured by UV-spectrometry (Shimadzu UV-2550) at a wavelength of 205 nm.

Brightness

The brightness and colour were measured with a SpectroScan (16130-818) and Spectrolino by GretagMacbeth, following the methods of the ISO 2470-1:2009 standard. Five scans were performed on each sample (bundle of fibres or knit), with the sample positioned above a white surface. The scans were taken at various locations on the bundle/knit. The measurements were conducted using a polarized filter, D65 illumination and an observer angle of 10°.

XRD measurements

The crystalline properties of the fibres were measured by XRD with a Xenocs Xeuss 3.0 X-ray diffractometer in transmission mode. Bundles of fibres were placed on sample plate and scanned for WAXS analysis, using a CuKα radiation (λ=1.5406 Å operated at 50 KV/0.6 mA combined with a Dectris Eiger2 R 1M detector (detector – sample distance: 56 mm)). After data collection, scattering profiles were corrected by subtracting a blank measurement (air scattering) [21]. The Segal crystallinity index (CI; %) was determined by the following equation:

$$CI \, [\%] = \frac{It - Ia}{It} * 100 \quad (1)$$

where "I_t" is the total intensity of the (0 2 0) peak at 21.7° 2θ, and "I_a" is the amorphous intensity at 16° 2θ for cellulose II.

Statistical analysis

Statistical analysis was supported with Prism version 9.4.1 (GraphPad Software, La Jolla California USA), using t-student analysis for unpaired comparison of two means. Mean differences were considered statistically non-significant (ns) when the p-value was higher than 0.05 (95% of interval of confidence). The default statistical confidence level was 95% (P < 0.05) in all tests.

7.3. Results and Discussion

7.3.1. BC – Ioncell$^{®}$ fibre production

7.3.1.1. Degree of polymerization & GPC

The quality of the regenerated fibres (in particular their mechanical performance) is connected to the macromolecular properties of the cellulosic constituents such as the intrinsic viscosity and molar mass distribution (weight fraction of short and long-chain molecules). The viscosity and key-parameters derived from the molar mass distribution for BC, viscose and standard PHK pulp (Enocell) as reference are summarized in Table 7.1.

Table 7.1. Viscosity, degree of polymerization and molar mass distribution of BC and PHK; data displayed as mean ± standard deviation.

Sample	$[\eta]$ mL.g^{-1}	DP_v*	M_w kDa	M_n kDa	PDI M_w/M_n	DP<100 %	DP>2000 %
BC pulp	646 ± 18	1686 ± 15	585.0	527.3	1.1	1.9	28.5
PHK pulp	414 ± 1	939 ± 1	147.5	78.5	1.9	1.5	8.1
Viscose fibre	175 ± 5	417 ± 3	48.0	21.4	2.3	19.0	3.9×10^{-2}

*degree of polymerization calculated from the intrinsic viscosity

The BC displayed a slightly lower intrinsic viscosity and a lower weight-average molar mass as compared to values found in literature (BC: 919 ml.g^{-1}, 564 - 752 kDa (Table 7.1) [43,44]. However, the BC samples have been obtained from different sources - different strains and different cultivation conditions, hence the differences observed were not unexpected. However, the cellulose chains in BC pulp were longer ($[\eta]$: 646 mg.L^{-1}; DP: 1686) than those in PHK pulp ($[\eta]$: 414.2 mg.L^{-1}; DP: 939). This is also seen in the molar mass distribution (Figure 7.7), with M_n and M_w of BC being higher, yet the molar mass distribution was narrower, resulting in a lower polydispersity index. As expected, the substrates also differed in their share of long cellulose chains. BC pulp is comprised of approximately 29% of cellulose chains with a DP>2000, whereas PHK only accounted for 8%. Only low amounts of short cellulose chains, often attributed to small cellulose chains or hemicellulose (only on plant cellulose) were found in both pulps (about 1-2%). Despite the longer cellulose chains, BC appears to be suitable for dissolution in [DBNH][OAc] and subsequent spinning, since the intrinsic viscosity is close to the values of 400-500 mg/L, considered optimal for the Ioncell$^®$ technology [19,32].

As expected, the viscose fibres intended for recycling (in section 7.3.3.) had much shorter cellulose chains ($[\eta]$: 175 mg.L^{-1}; DP: 417) compared to BC and PHK (Table 7.1). In addition to the lower molecular weight (both Mw and Mn; 19% of DP<100), the cellulose in viscose fibres also exhibited a wider molar mass distribution (Mw/Mn of 2.3) than BC and PHK (Table 7.1).

7.3.1.2.   Dope characterization

All BC dopes (with concentrations of 10-13%) dissolved readily in [DBNH][OAc], with no undissolved particles remaining in the dope after filtration (Figure 7.1). Undissolved cellulosic particles were found on the filter, which, although being in trace amounts only, might have contributed to a slight decrease in the final cellulose concentration.

Before filtration
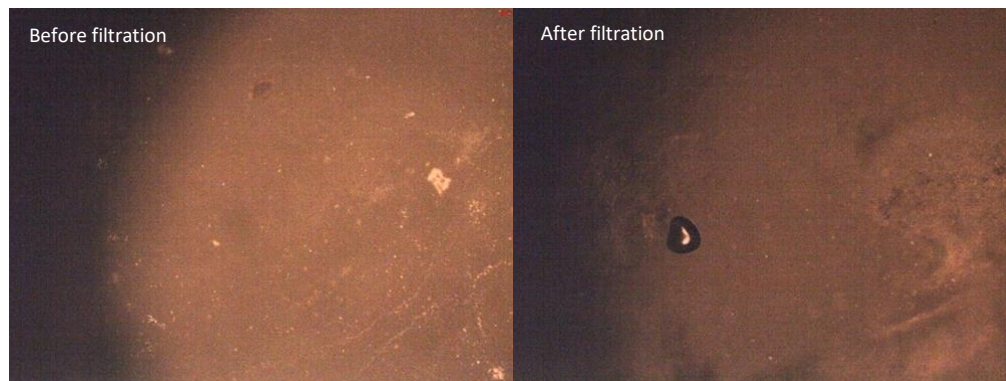
After filtration

Figure 7.1. Microscopic images (polarized light) of [DBNH][OAc]-BC 13%; image on left is the dope before filtration and image on the right is the dope after filtration; the pictures were taken at 10x magnification

The concentrations reported in Tables 7.2 and 7.3 refer to the theoretical values without considering any variations caused by the filtration of undissolved particles. The dopes were characterized by rheological measurements, in order to compare them with the reference material (PHK) and values from literature (Figure 7.2 & 7.3), and to determine the appropriate spinning conditions. The rheological properties of the PHK pulp solution was found to be in line with the literature [17], in spite of the slight differences of the average molecular weight: η_0 decreased from 30 000 Pa.s to 15 000 Pa.s with increasing temperature (70 °C - 90 °C); the dynamic moduli at the cross over point (COP – cross over between the storage and loss modulus) was around 4 000 Pa (70 °C – 90 °C) and ω increased from 0.7 to 2.5 s^{-1}, respectively.
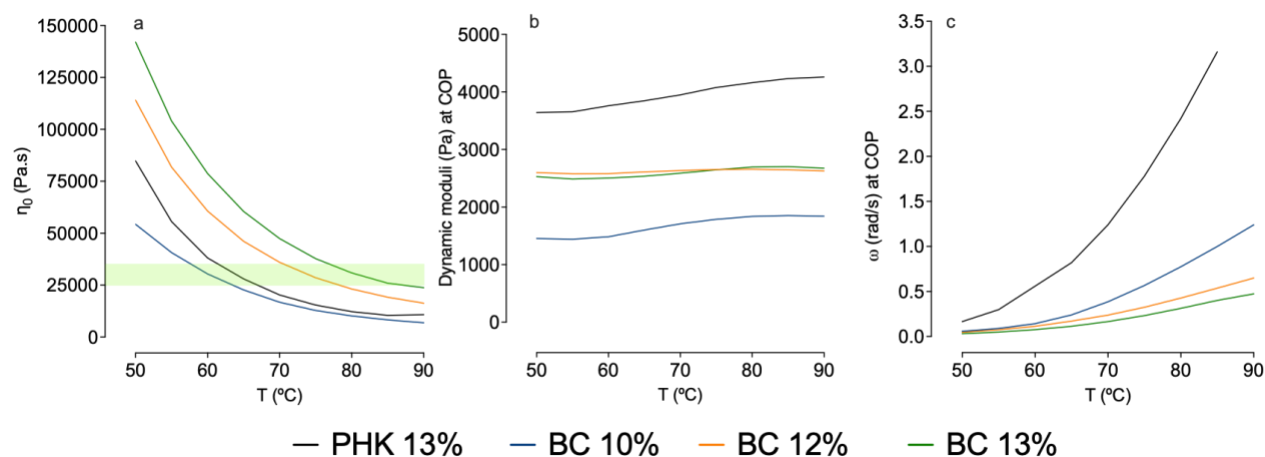
Figure 7.2. Rheological properties of PHK/BC-[DBNH][OAc] dopes: a) Zero shear viscosity (η_0) vs temperature, estimated from PHK/BC [DBNH][OAc] dopes (optimal η_0 highlighted in green); b) Dynamic moduli (at COP) at different temperatures; c) Angular frequency (at COP) at different temperatures; c) Angular frequency (at COP) at different temperatures.

The zero-shear viscosity (η_0) increases with the polymer concentration in the dope and decreases with the processing temperature. When compared to PHK (13 %), only the dope with 10 % BC had a lower η_0, yet similar at higher temperatures (T>70 °C) (Figure 7.2a). In general, as reported by Sixta et al. [17], the targeted η_0 for cellulose-[DBNH][OAc] dopes is between 25,000 - 35,000 Pa.s (Figure 7.2a - highlighted in green). For the dope with BC 10 %, the optimal η_0 was reached at 60 °C, whereas for the standard dope (PHK) this is observed between 65 and 70 °C. When the BC concentration was increased up to 12 % and 13 %, the optimal temperatures for spinning increased to 70-75 °C and 75-85 °C, respectively (Figure 7.2a).

All dopes showed a visco-elastic behaviour, displaying a cross over between storage and loss moduli (COP), although at different angular frequencies and dynamic moduli (Figure 7.2b and 7.2c). The viscoelastic properties are influenced by the molar mass distributions of the polymeric solute. The BC based dopes displayed lower dynamic moduli (PHK 13 % - 3500-4300 Pa vs BC 13 % - 2500-3000 Pa) and lower angular frequencies (PHK 13 % - 0.60-3.16 s^{-1} vs BC 13% - 0.032-0.47 s^{-1}) across all temperatures tested. Increasing the concentration from 10% to 12% led to higher dynamic moduli (from $\cong$ 1500 to $\cong$ 2500 Pa) and lower angular frequencies (more

noticeable at higher temperatures) (Figure 7.2b and c). Dopes with BC 12 and 13 % presented similar dynamic moduli, yet ω was slightly higher for BC 12 % (Figure 7.2b and c).

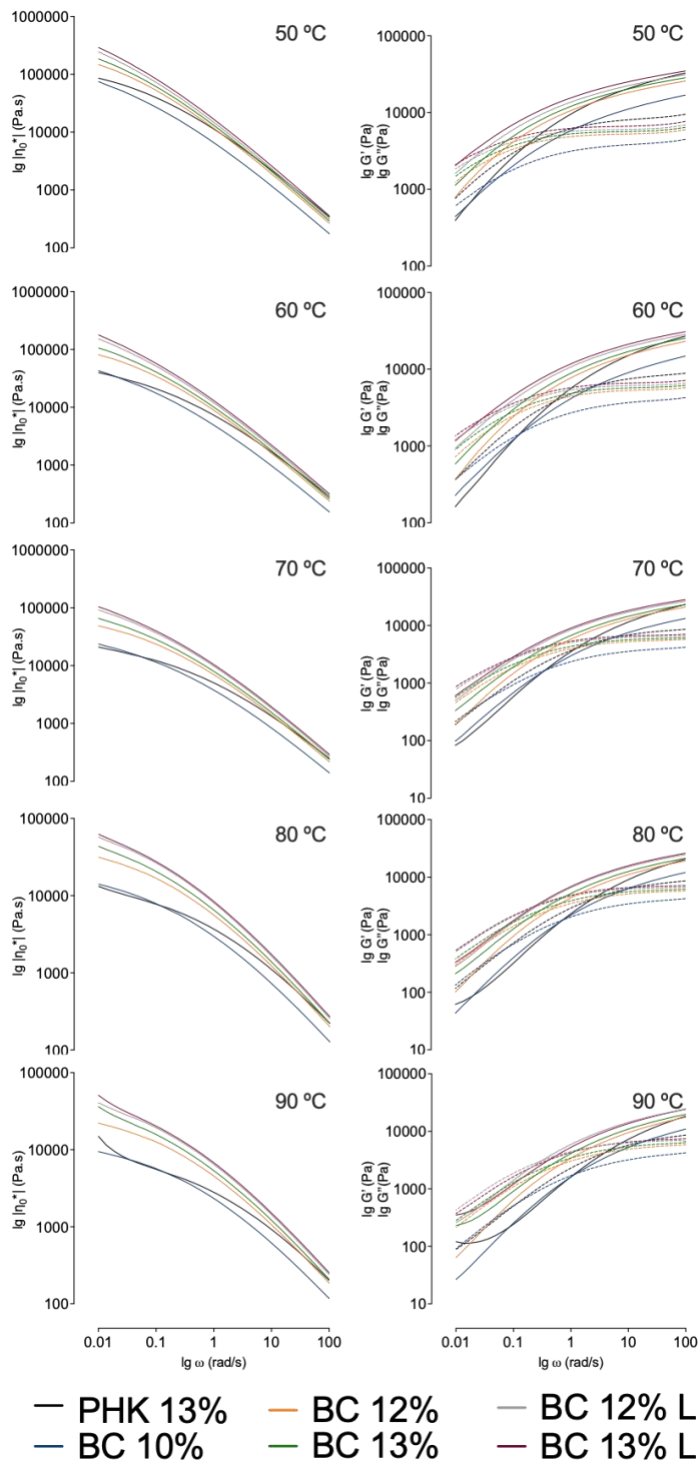**Figure 7.3.** Logarithmic of Zero shear viscosity & logarithmic of storage and loss modulus (G' & G'') vs logarithmic angular frequency of [DBNH][OAc] of all dopes, from 50-90°C

In short, PHK and BC dopes have distinct rheological properties. Having higher DP and longer cellulose chains, BC shows an increased η_0 (and higher optimal spinning temperatures, up to 80-85°C), but a lower overall elasticity, when compared to the dope prepared with PHK. These rheological features provide information about the optimal spinning conditions, mainly extrusion temperature and ability to stretch the filaments in the air gap [17].

7.3.1.3.   Fibre spinning

Spinning trials, using a monofilament spinning device, were performed in order to pre-evaluate the spinnability performance of each material produced. The spinnability of any dope may be defined, according to the draw ratio (DR) achievable, as: DR<2 non-spinnable, 2–8 poor, 8–14 good, >14 excellent [35]. Targeting a high DR, the spinning of each material was optimized by: i) varying the temperature of extrusion, taking in account the rheology data; ii) by varying the godet speed while collecting the regenerated cellulose fibres, in order to assess the maximum DR as well as the time stable spinning until filament rupture. The main results regarding the spinning trials are illustrated in Table 7.2. As observed in the rheology data, the predicted optimal temperature for spinning BC was higher compared to PHK and increased with the BC concentrations. Optimal spinning conditions were found at slightly lower temperature than estimated from the rheology data (Figures 7.2 & 7.3 and Table 7.2). The maximum DR of the PHK pulp reference material was 12, yet stable spinning for longer period of times was only possible at DR10 and DR8. These DR values are lower than those reported by Sixta et al. [17], where a maximum DR of 18 using 13 % PHK was possible. The discrepancy in results is due to different spinning set-ups. Herein, a monofilament device was used, in which the single fibre is more susceptible to external disturbances. Despite these limitations, excellent spinnability was achieved with BC-based dopes, particularly for the higher concentrations tested, a maximum DR of 18 being reached for 13 % BC.

Table 7.2. Dry jet-wet spinning of PHK/BC-[DBNH][OAc] dopes, using a small unit with monofilament

Cellulose concentration (%)	Optimal T [°C]	Maximum DR	Continuous Spinning*
PHK 13 %	68	12	DR 8
BC 10 %	58	8	DR 6
BC 12 %	70	14	DR 13
BC 13 %	77	18	DR 18

*Fibre collected for more than 4 min;

After the optimization of the BC concentration on a monofilament spinning device, fibres were spun from a 13 % BC-[DBNH][OAc] solution on a larger multifilament unit to validate the spinnability on a larger scale and to characterize the fibres comprehensively. The respective dope had a higher η_0 than the same dope produced at a smaller scale (Table 7.3 and Figure 7.4). This difference in η_0 is attributed to more efficient dissolution provided by the larger equipment, slightly increasing the total amount of dissolved cellulose on the dope, and consequently increasing the η_0. To compensate for this increase in viscosity, the total cellulose content was reduced (12 %), which provided the target viscosity of 25000 - 35000 Pa.s [17]. This dope showed excellent spinnability (DR8 until DR16) [35], with higher fibre breakage being noticed only at DR18. Dopes with a BC concentration of 13 % could only withstand a maximum DR of 14, yet a stable continuous spinning was possible at lower DR (8, 10 and 12) (Table 7.3). Fibres for further testing and yarn spinning were spun at DR 8 (to obtain fibres with a linear density between 1.0-2.0 dtex).

Table 7.3. Large scale spinning of BC-[DBNH][OAc]; optimal temperature; maximum DR; (continuously) at specific DR

Parameters	Cellulose on dope (%)	BC 13 % Small scale		BC 13 % Large scale		BC 12 % Large scale	
Rheological	Temperature [°C]	80	85	80	85	80	85
	Zero shear viscosity, η_0 (KPa.s)	30.9	26.0	44.0	35.9	41.0	33.4
	Angular velocity, ω (COP) (rad/s)	0.31	0.40	0.24	0.33	0.25	0.34
	Dynamic moduli, (COP) (Pa)	2700	2700	3100	3200	3100	3100
Spinning	Optimal T [°C]	77		80		82	
	Maximum DR	18		14		18	
	Spinning	Continuous (DR 14)		Continuous (DR12)		Continuous (DR16)	
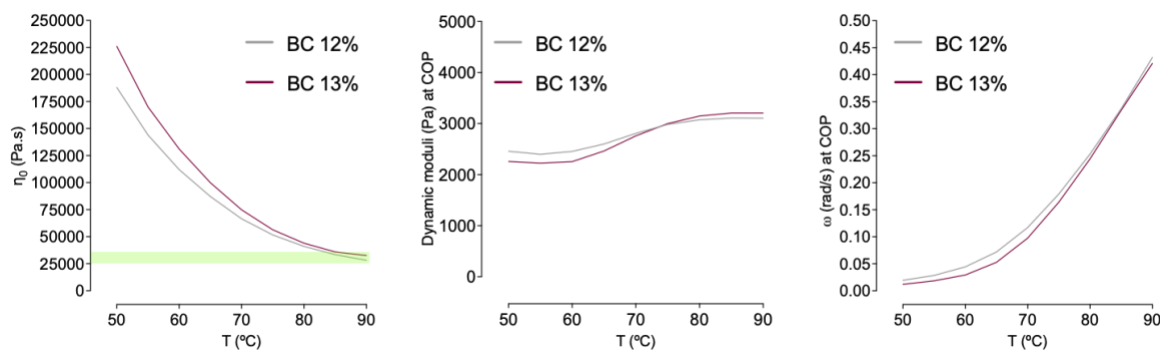
Figure 7.4. Rheological properties of BC-[DBNH][OAc] dopes (produced on a large kneader): a) Zero shear viscosity vs temperatures, estimated from BC [DBNH][OAc] dopes (optimal η_0 coloured as green); b) Dynamic moduli (at COP) at different temperatures, estimated from BC-[DBNH][OAc] dopes; c) Angular frequency (at COP) at different temperatures, estimated from BC-[DBNH][OAc] dopes

7.3.1.4.   Fibre characterization

The collected fibres were analysed in terms of their mechanical performance, birefringence, crystallinity and chemical composition. The mechanical properties of the collected fibres from all produced dopes (mono- and multi-filament spinning) are presented in Figure 7.5.

These properties include linear density, breaking tenacity, and elongation at break, under both standard and wet conditions.

The tenacity of the PHK fibres under standard conditions was similar to values reported for Ioncell fibres earlier [17,35]) but generally slightly lower than for BC fibres collected at each maximum DR (BC 10 % - DR 7; BC 12 % - DR 13 and BC 13 % - DR 18) ($p < 0.05$). Although not statistically significant among all BC fibres, there is an upward trend in tenacity values (ranging from 52 to 57 cN tex^{-1}) with increasing cellulose content and DR (Figure 7.5). The incorporation of higher concentrations improves the elasticity in the filaments prior to coagulation, which helps to withstand higher DRs [17,19,45,46]. As expected, an increasing DR resulted in a lower elongation, as well as lower linear densities (as low as 0.79 dtex at DR 18). Most BC fibres exhibited lower elasticity compared to PHK fibres ($p < 0.05$), except for BC 12 % DR 10 and BC 13 % DR 14 fibres ($p > 0.05$). The intrinsic properties of the given pulps also affected the overall mechanical performance of the resulting fibres. The presence of longer cellulose chains in BC (Table 1) contributed to the development of stiffer fibres. Other relevant studies reported the same outcome when using cellulosic materials with higher [η] and Mw [17,19,47]. Concerning the used spinning setup, fibres produced in a multi-filament spinning device showed better performance, with significantly improved elongation (multi-filament: 10.46 - 12.08 % vs. mono-filament: 7.98 - 9.51 %), while maintaining similar tenacity levels (ranging between 52 and 57 cN tex^{-1}). These fibres outperformed the ones reported for Ioncell process (using standard PHK), especially considering tenacity (PHK: 40 - 47 cN tex^{-1} vs BC: 52 - 57 cN tex^{-1}) [17,19,21,32].

The measurements in wet state showed the same trends for the tenacity, elongation and linear density dependence on the DR and dope concentration. The fibres spun with the monofilament unit had a lower tenacity and higher elongation under wet conditions (Figure 7.5). These differences between wet and dry conditions are typical for MMCFs and can be attributed to the fibre's ability to absorb water upon exposure. The less oriented amorphous regions within the fibre are more prone to moisture absorption, as the hydrogen bonds become more accessible for water. Consequently, after water exposure, the fibre's capacity to withstand axial external forces diminishes, leading to reduced tenacity and increased elongation at break (48). This difference was less pronounced for the fibres produced through multi-filament spinning (dope BC 12 %).

Tenacity and elongation were similar under both dry and wet conditions, indicating a higher crystallinity and less accessible hydrogen bonds to absorb water in the BC fibres.
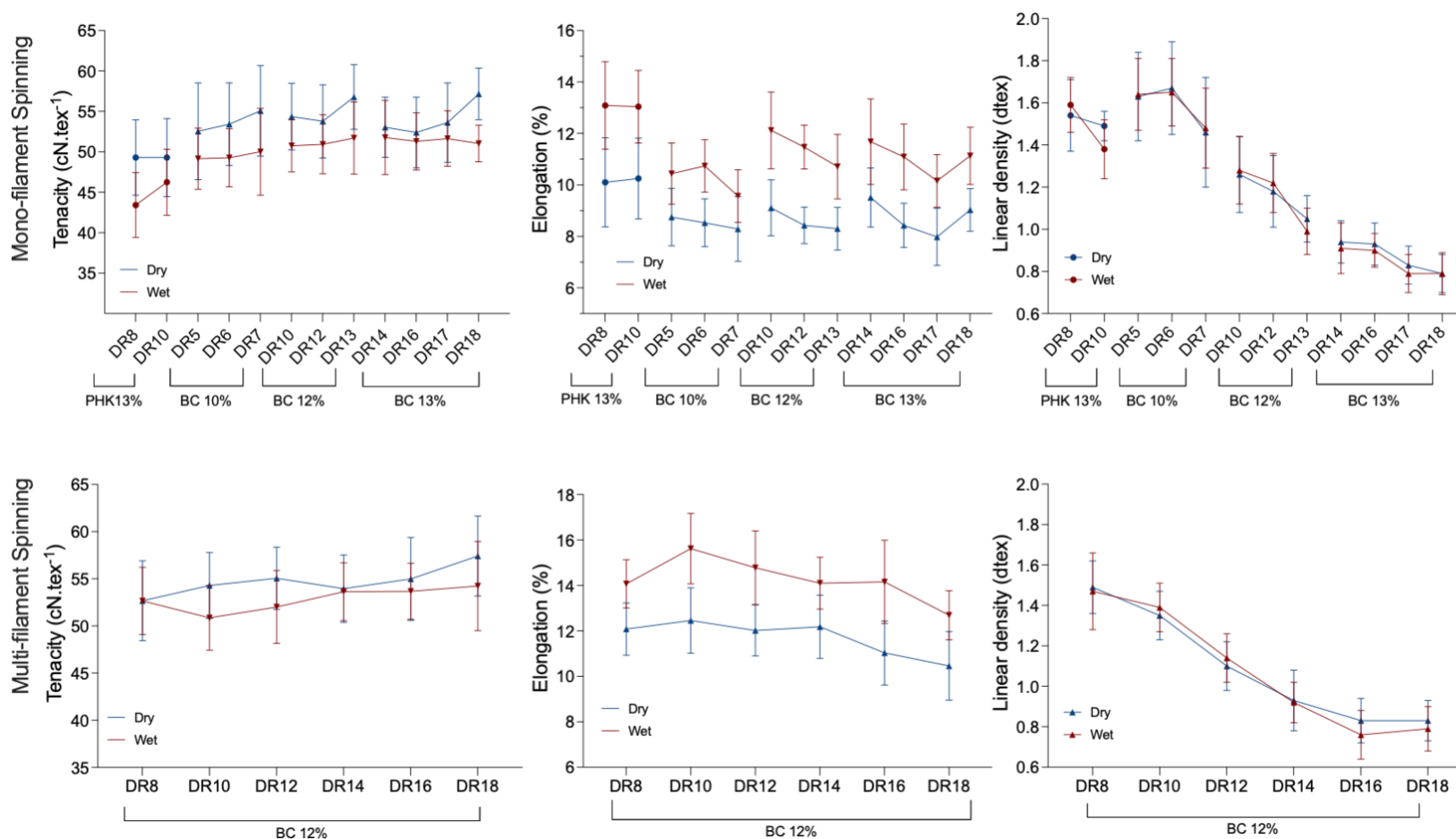
Figure 7.5. Tenacity (cN.tex^{-1}), elongation at break (%) and linear density (dtex) of all collected fibres, from different dopes produced at different DR, using mono- or multifilament spinning; "Dry"- conditioned fibres at 65% RH, 20 °C; "Wet" – fibres submerged in water for 10 s prior testing; symbols represent the mean and error bars represent the standard deviation.

In order to understand the improved mechanical performance achieved with BC fibres, the structure was further studied with regards to total orientation (determined via the fibres' birefringence), crystallinity index and morphology (by SEM) (Figure 7.6). Concerning total orientation, no significant differences were found between PHK and BC fibres, or between samples obtained with different DR (Figure 7.6; p>0.05). Although, generally, high DRs lead to better fibre alignment, the total orientation reaches a plateau value already at moderate DRs [17]. Herein, all fibres showed a similar total orientation which was comparable with those reported for other Ioncell and Lyocell fibres, and higher than those of viscose and modal [32,49].

The degree of crystallinity differed more significantly between BC and PHK fibres (BC: 54-66% vs PHK: 41%). The Segal crystallinity index found for the PHK fibres was slightly higher than in other PHK fibres reported in the literature (32-37%) [11,17,19,35]. The BC fibres are more crystalline than PHK fibres, reflected in the toughness, with increased tenacity and lower elongation (Figures 7.5 & 7.6). Also, a fibre structure with more ordered crystalline regions impacts on the total orientation of the fibre (Figure 7.6), apart from the DR used for spinning [50]. The crystallinity of BC decreased slightly with increasing DR in the small spinning unit, although changes were largely within the magnitude of the standard deviation of each value (Figure 7.6). From this data, it is perceived that BC fibres presented a highly oriented and cohesive structure, without any impurities, confirmed also by SEM (Figure 7.6).
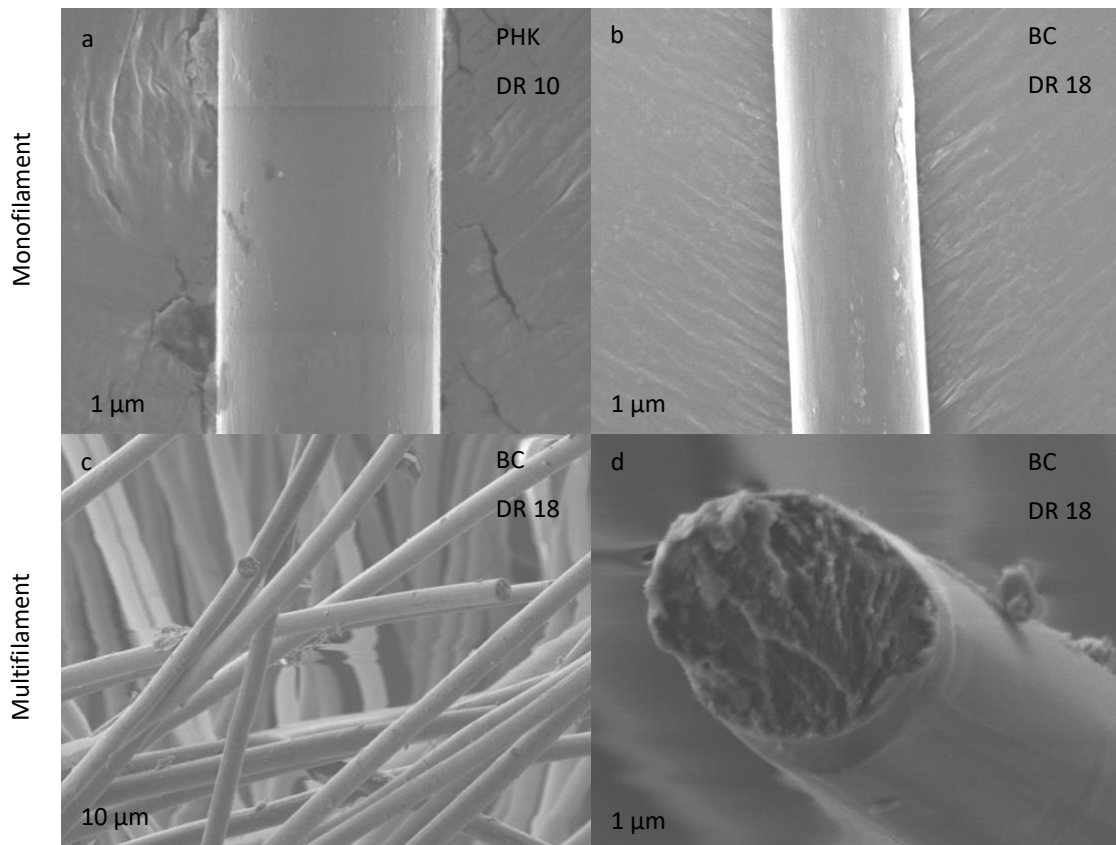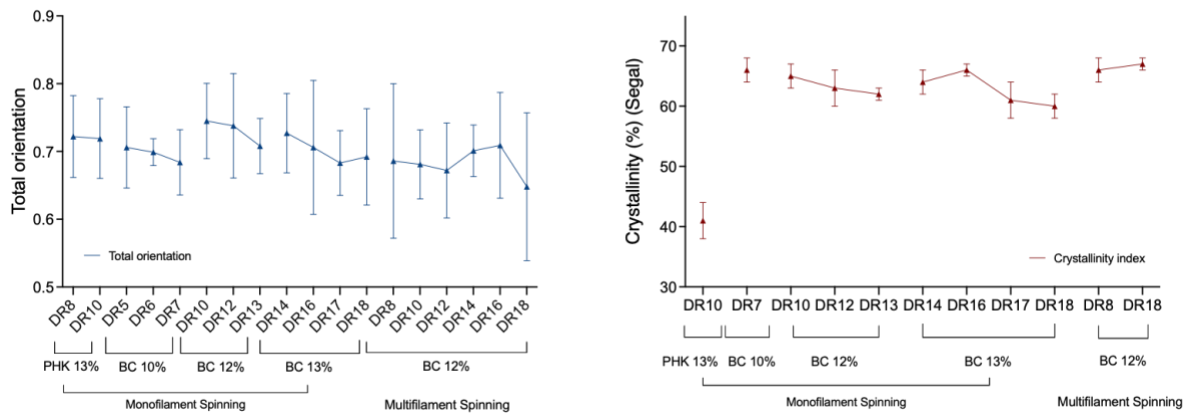
Figure 7.6. Total orientation and crystallinity of all collected fibres; SEM images of PHK and BC fibres: a) surface of PHK fibres produced from [DBNH][OAc]-PHK 13 % using a monofilament setup; symbols represent the mean and error bars represent the standard deviation; b) surface of BC fibres produced from [DBNH][OAc]-BC 13 % using a monofilament setup; c) surface of BC fibres produced from [DBNH][OAc]-BC 12 % using a multifilament setup; d) Cross – section of BC fibres produced from [DBNH][OAc]-BC 12 % using multifilament setup.

The spun fibres (multifilament) were further characterized in terms of their chemical composition, namely elemental analysis, carbohydrate analysis, DP and molar mass distribution, to track any potential polymer degradation during the dissolution and spinning

processes (Table 7.4). The amounts of carbon and hydrogen remained the same in the BC pulp and fibre, being also in line with values reported by Tomé et al. [51] and Volova et al. [52] (Table 7.4). Compared to PHK [53], BC is composed only of cellulose (no hemicellulose or lignin), which may also affect the overall performance of the fibre. Only very low amounts of nitrogen were found in the fibres, showing that [DBNH][OAc] was removed efficiently from the fibres after spinning (Table 7.4). Carbohydrate analysis revealed similar amount of cellulose in both BC pulp and fibre (around 90 %). The total amount of residue (non-saccharides) found in the BC pulp was around 5 %, attributed to components from the fermentation and washing processes. In the fibre, the amount of non-identified residues slightly increased to 6.84 %, associated to the dissolution and spinning process. Regarding depolymerisation during dissolution and spinning of BC, the DP was found to be similar between pulp and BC regenerated fibres, yet some depolymerisation was seen in both the intrinsic viscosity (DP) ($p<0.05$) and GPC data (Table 7.4 and Figure 7.7). Both M_w and M_n decreased after dissolution and spinning of BC, leading to an increase in the fraction of short chains (DP<100: from 1.92 % to 11.71 %) and, consequently a decrease in the fraction of long chains (DP>2000: from 28.45 % to 21.37 %) (Table 7.4). Indeed, some depolymerisation occurred on BC during dissolution with [DBNH][OAc] and spinning [54], yet not being significant to decrease the average DP.

Table 7.4. Elemental analysis (% nitrogen, carbon, hydrogen; sulphur); carbohydrate analysis (% Cellulose; acid insoluble) and DP estimation of BC pulp and BC fibres (collected at DR 8 from large spinning); data displayed as mean ± standard deviation.

Analysis		BC pulp	BC fibres
Elemental analysis	**Nitrogen (%)**	0.081 ± 0.004	0.098 ± 0.006
	Carbon (%)	43.26 ± 0.02	42.01 ± 0.74
	Hydrogen (%)	6.23 ± 0.04	6.17 ± 0.04
Carbohydrate analysis	**Cellulose (%)**	94.89	93.16
	Non-saccharides	5.11	6.84
Depolymerization	**DP**	1686 ± 15[a]	1660 ± 8[b]
	Mw (KDa)	585	446
	Mn (KDa)	527	407
	PDI (Mw/Mn)	1.11	1.10
	DP<100 (%)	1.92	11.71

DP>2000 (%)		28.45	21.37

"a" "b" – t-student statistical difference
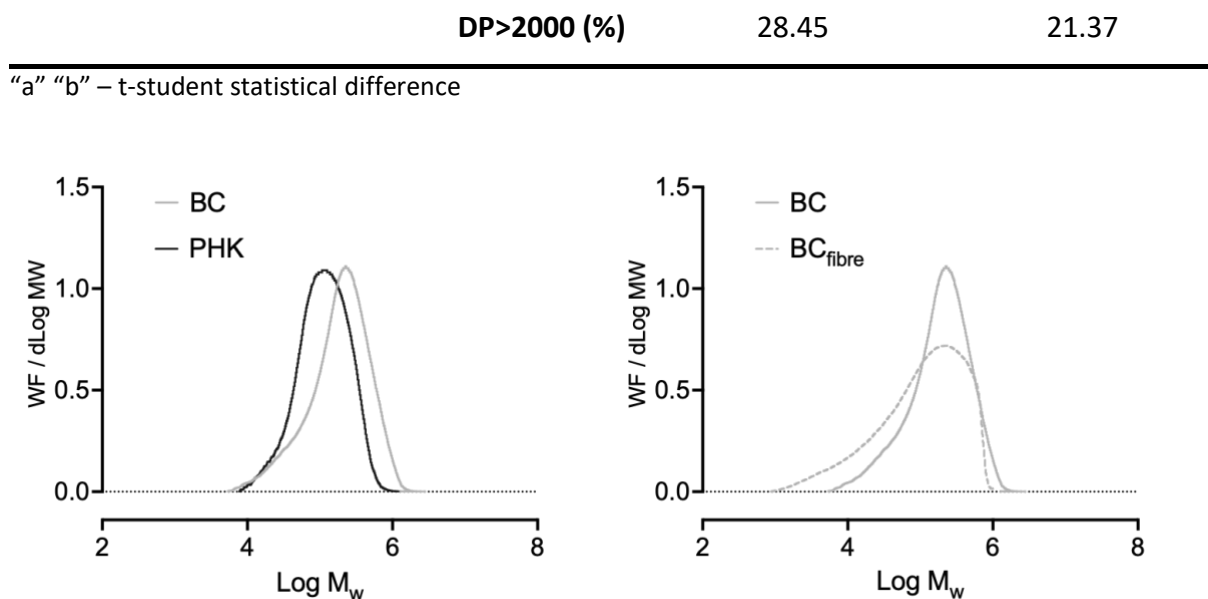
Figure 7.7. Logarithmic illustration of the molar mass distribution of BC, PHK and BC fibre

7.3.2. Yarn and knitting of BC

The staple fibres spun with the multifilament spinning unit (collected at DR 8) exhibited good mechanical performance (tenacity of 53 cN.tex^{-1}; elongation of 12%, and titre of 1.5 dtex), a high orientation and a low amount of impurities (Figures 7.5 and 7.6), and were converted into a yarn using a laboratory ring-spinning unit. It is difficult to compare yarns spun on a laboratory scale with commercially produced products using industrial yarn spinning devices. Therefore, a couple of benchmark staple fibres (both experimental and commercial) were selected to produce reference yarns: Ioncell® fibres spin from PHK pulp, viscose, and Tencel.

The BC-fibre yarn had a tenacity, elongation, and yarn count of 25.3 cN.tex^{-1}, 7.8% and 19.8 tex, respectively. The tenacity was slightly lower than in the case of yarn spun from PHK-pulp Ioncell® fibres are reported by Michud et al. [37]: tenacity of 34.4 cN.tex^{-1} and 7.4% of elongation at a yarn count of 27 tex. However, BC yarn outperformed both Tencel (tenacity, elongation and yarn count of 26 cN.tex^{-1}, 9% and 20 tex, respectively) and viscose yarns (tenacity, elongation and yarn count of 17 cN.tex^{-1}, 18% and 31.5 tex, respectively) [37], [55]. The yarn was then knitted into small fabrics (Figure 7.8). Recently, the company *Nanollose*

also produce fabrics from BC using Lyocell and Viscose processes [56], and by depolymerization through mercerization to achieve suitable spinnable solutions [57].

Figure 7.8. On the left: picture of fibres, yarn and knitted BC; on the right: unbleached vs bleached knitted BC samples

MMCFs are usually off-white due to chromophore formation during the spinning process and undergo subsequent bleaching stages to arrive at white fibres. Colour measurements (using CIE Lab system) were done to monitor the colour of the fibres and knitted fabrics. Comparing fibres spun at DR8 and DR18, the brightness seemed to increased slightly at higher DR (Table 7.5). However, this might be an effect of the reduced fibre diameter which alters light scattering and reflectance. The original BC fabric (unbleached) presented a yellowish hue with reduced lightness. Dissolution, filtration, and spinning at temperatures of 80-85 °C may have led to aforementioned chromophore formation. The same discolouration was noticed by Parviainen et al. [58] after treating cellulosic substrates in [DBNH][OAc]. A standard bleaching procedure allowed to remove most of the yellowish colour (b* decreased from 14.8 to 9.1; L* increased from 79.7 to 81.7) (Table 7.5).

Table 7.5. Colour measurement (CIELAB color space) of BC fibres and the resulting Knit: where $\Delta\mathrm{E} = ((\Delta\mathrm{L})^2 + (\Delta\mathrm{a})^2 + (\Delta\mathrm{b})^2)^{0.5}$, L* represents the lightness value from black to white, a* the green to magenta opponent colors and b* the blue to yellow opponent colours; data displayed as mean ± standard deviation.

Sample	L*	a*	b*	ΔE[1]
BC fibres (DR8)	82.4 ± 1.7	2.8 ± 0.5	7.3 ± 0.3	4.27 (>2.0)
BC fibres (DR18)	84.6 ± 1.5	-0.9 ± 0.3	7.0 ± 1.2	
BC fabric (unbleached)	79.7 ± 0.9	2.4 ± 0.2	14.8 ± 0.2	6.10 (>2.0)
BC fabric (Bleached)	81.7 ± 0.6	1.4 ± 0.1	9.1 ± 0.3	

1 Δ**E** <1.0: Not perceptible by the human eye; Δ**E** = 1-2: Perceptible through close observation; Δ**E** = 2-10: Perceptible at a glance

7.3.3. BC to enable recycling of low-DP textile waste

At present, industrial BC cultivation and isolation is still limited by high operational costs and low BC yields [46], [59], [60]. These challenges must be overcome before fully BC-based textiles and garments can be produced at large scale and competitive costs. However, already now BC could be a viable and valuable additive in the recycling of cellulosic textile waste with low DP. The depolymerization of cellulose in textiles made from cotton, MMCFs, hemp, linen, etc. is inevitable and largely random. The extent of chain length reduction depends on the wear and wash history of the respective product [61], [62]. All spinning processes (viscose or Lyocell-type) require cellulosic solutes with a certain average molar mass and molar mass distribution to produce spinnable solution. If the DP of the starting material is too high, it can be adjusted by simple degradation [35]. However, if the DP is too low then a cellulose additive is needed to increase the average chain length and broaden the molar mass distribution. Viscose fibres represent such a challenging substrate because already virgin viscose fibres have a low DP which further reduces during for instance washing [63]. Blending small amounts of BC to viscose fibres can change the rheological properties of the resulting solution to increase the spinnability and, eventually, the properties of the spun fibres. The overall cellulose concentration was kept at 16 weight-%. Starting from a solution consisting of only viscose fibres, the BC content was gradually increased until the solution contained 12%

viscose and 4% BC. Table 7.6 summarizes the spinning trials of the dopes prepared from a mixture of viscose fibres and BC. Their rheological properties were assessed through frequency sweeps like in the case of pure BC solutions (Figure 7.9 & 7.10).
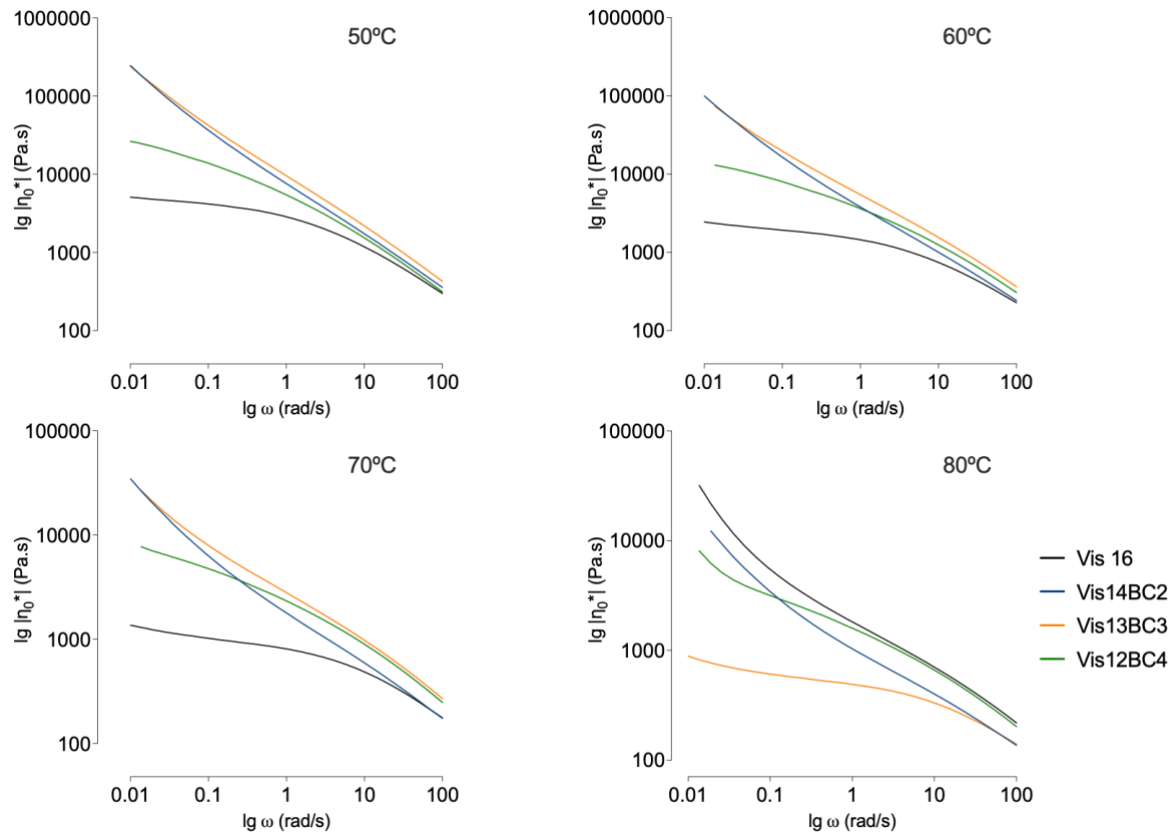
Figure 7.9. Logarithmic of Zero shear viscosity vs logarithmic angular frequency of viscose and viscose/BC in [DBNH][OAc] dopes, from 50-80°C
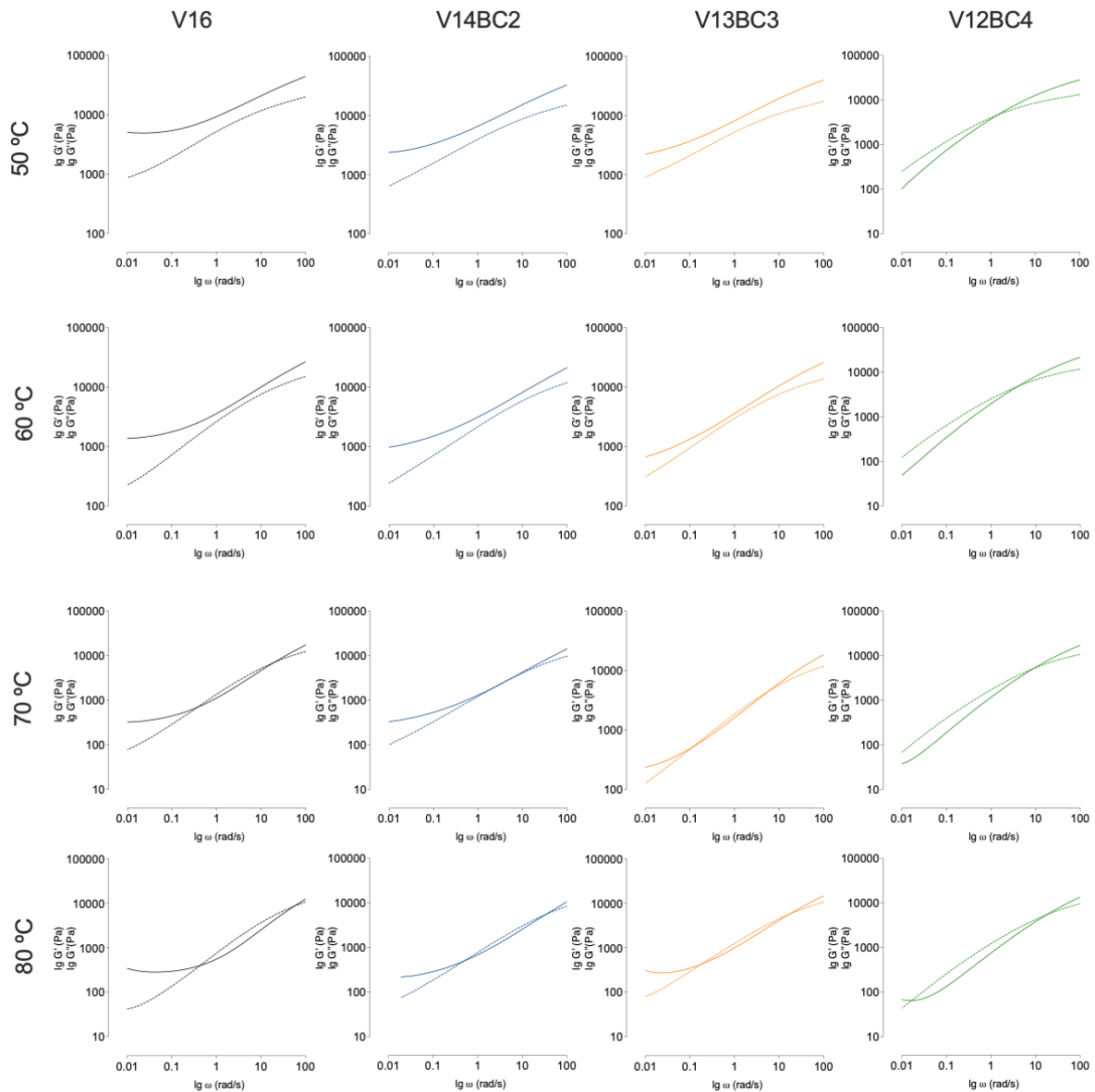
Figure 7.10. Logarithmic of Storage (G') and loss (G'') modulus vs logarithmic angular frequency of viscose and viscose/BC in [DBNH][OAc] dopes, from 50-80°C

The particular behaviour of the complex viscosity did not allow to use the Cross model to calculate the zero-shear viscosity. Overall, the addition of BC to viscose as main cellulosic substrate had little influence on the complex viscosity. However, BC did change the visco-elastic behaviour of the solutions as reflected by the dynamic moduli. The storage and loss moduli represent the elastic and viscous portion of the cellulose solution and are both frequency dependent. At low angular frequency the loss modulus is usually higher. As the frequency is increased the storage and loss moduli intersect at the so-called crossover point (COP) at which the solution behaves predominantly elastically. The COP represents a relaxation time which relates to the molecular weight of the cellulose and is shifted to higher

angular frequencies upon increase of temperature or decrease of cellulose concentration [64]. At 50 °C, the 16% viscose solution did not show a COP which would indicate the transition from dominantly viscose to elastic behaviour. The presence of small amounts of BC (< 4%) did not change this. However, upon the addition of 4% BC such a transition becomes visible at 1.2 s^{-1} (Figure 7.10). At higher temperatures than 50 °C, also the solution of viscose fibres showed a COP at angular frequencies > 10 s^{-1}, which is shifted towards lower frequencies when BC is added. Earlier, a COP at ca. 1 s^{-1} and 5000 Pa was found as indicator for good spinnability [17], [32].

Table 7.6. Dry jet-wet spinning of viscose/BC-[DBNH][OAc] dopes; optimal temperature for spinning, maximum DR achieved; fibre (continuously) at specific DR

Cellulose concentration (%)	Optimal T [°C]	Maximum DR	Spinning	
Viscose 16%	50	8	Non-Continuous	(DR8)
BC 13%	80	18	Continuous	(DR8)
Viscose 14% BC 2%	80	13	Continuous	(DR 8)
Viscose 13% BC 3%	80	13	Continuous	(DR 8)
Viscose 12% BC 4%	78	13	Continuous	(DR 8)

*Fibre collected for more than 4 min;

Spinning of pure viscose fibre solution was challenging, where a maximum DR of 8 was reached but could not be sustained over a longer period of time (Table 7.6). The addition of BC improved the spinnability of the dopes. It allowed for a continuous spinning, and higher maximum DRs of 13 were reached in viscose-based dopes with 2-4 % (m_{BC}/m_{dope}) of BC. The optimal spinning temperature increased (up to 80 °C) with the addition of BC (as compared to the optimal spinning temperature of 50 °C for the pure 16% viscose dope). Table 7.7 summarizes the intrinsic viscosity (and calculated DP values) of the various blends. As

expected, a higher share of BC in the fibres led to an increase in intrinsic viscosity. The presence of longer cellulose chains from BC increased both the viscosity (Figure 7.9) and the viscoelasticity (Figure 7.10), important factors that contribute to the dry-jet wet spinnability of the dope [17], [32]. Michud et al. [32] showed that an increase in the cellulose molar mass had a significant impact on the rheological properties due to improved entanglement of the cellulose chains [65]. This affected directly the spinnability of the resulting solutions.

Table 7.7. Viscosity and the degree of polymerization of the used pulps and produced fibres; data displayed as mean ± standard deviation.

Sample		$[\eta]$ mL g^{-1}	DP$_v$
Pulps	BC pulp	630.4 ± 13.9	1632 ± 11
	Viscose pulp	175.2 ± 5.34	417 ± 3
Fibres	Vis16	162.9 ± 1.58	388 ± 1
	Vis14BC2	199.1 ± 1.26	474 ± 0.5
	Vis13BC3	234.23 ± 6.25	558 ± 4
	Vis12BC4	241.98 ± 4.71	576± 3

Figure 7.11 depicts the mechanical and structural properties of the spun fibres, which showed their typical dependence on the DR. Higher DRs led to a decrease in linear density and elongation, but increase in fibre orientation and tenacity, as was also the case for pure BC fibres and reference fibres spun from PHK pulp (Figures 7.5 & 7.6). The standard viscose fibres used as a substrate had a tenacity of 22-26 cN tex^{-1}, elongation at break of 20-25%, and linear density of 1.7 dtex. The recycled viscose fibres obtained through the Ioncell process exhibited a tenacity of 24.13 cN tex^{-1}, elongation at break of 8.27 % and linear density of 3.13 dtex.

The linear density of the recycled viscose fibres is higher than DR8 fibres spun from pure BC (Figure 7.5) because of the higher polymer concentration. Also, Lyocell-type fibres have a higher molecular orientation than viscose fibres, reflected in the reduction of the elongation [17]. The incorporation of BC improved the mechanical properties notably. Even small amounts of BC increased the tenacity significantly. This is in line with earlier studies by Michud et al. in which the molar mass distribution of the cellulosic solute was varied

systematically [32]. A higher share of long-chain molecules was found to improve the tenacity, which was also observed here upon the gradual increase of BC.
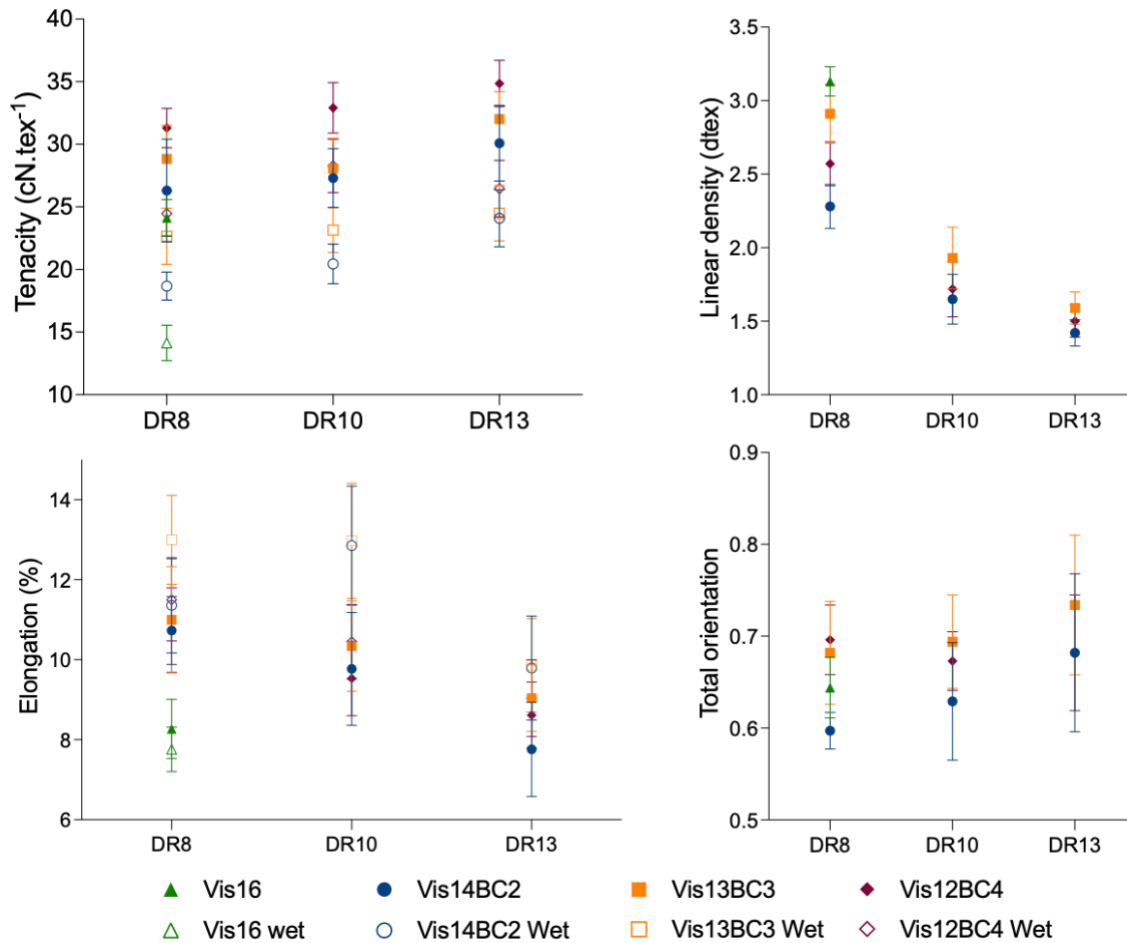
Figure 7.11. Tenacity (cN.tex^{-1}) (conditioned and wet conditions), Elongation at break (%) (conditioned and wet conditions), linear density (dtex) and Total orientation of all collected fibres, from the different dopes produced and at different DR; measurements in wet conditions dashed lines; symbols represent the mean and error bars represent the standard deviation.

The strength properties of MMCFs decrease with increasing moisture content. As mentioned already earlier, water loosens the hydrogen bonds between the cellulose strands, in particular in the more accessible amorphous areas. Therefore, the tenacity of standard viscose fibres can drop up to 50% of its conditioned value upon exposure to water. In addition, the pronounced skin-core structure of viscose fibres causes structural inhomogeneities across the fibre cross section, amplifying the effect of water on the mechanical properties of the

fibre. Due to the higher crystallinity of Lyocell-type fibres the wet-to-dry ratio of the tenacity is much higher (≥0.8). Fibres spun from pure viscose loose strength in the wet state due to the low DP of the cellulose and also the moderate orientation at low DR of 8. However, the wet-to-dry ratio is still significantly above 0.5. The addition of BC and increase in DR also improves the wet strength as seen earlier [17],[32].

7.4.   Conclusions

In this study, bacterial cellulose (BC) was successfully dissolved and dry-jet wet spun into textile fibres using [DBNH][OAc] as the solvent. Despite the high DP and molecular weight of BC, the resulting solutions had visco-elastic properties that allowed for air gap spinning and draw ratios. The resulting fibres revealed remarkable mechanical performance (breaking tenacities between 52 to 57 cN.tex^{-1}; elongation at break ranging from 10% to 12%, and linear density down from 1.5 dtex to 0.83 dtex), with high crystallinity (up 60%) and high total orientation (about 0.7). Fibre spinning trials were successfully scaled and the obtained staple fibres were spun into a yarn and further knitted into a small sample fabric as a proof of concept. To date, only the company *Nanollose* in cooperation with Birla Cellulose produced textile fibres using BC, however in blends with dissolving-grade wood pulp [57]. Scaling the production of BC is still challenging and larger quantities at competitive costs are not yet available. However, small amounts of BC could be a valuable additive for the chemical recycling of cellulosic textile waste with low DP. The gradual incorporation of small amounts of BC can change the molar mass distribution sufficiently to improve the spinnability of waste consisting of for instance viscose staple fibres and to improve the mechanical properties of the resulting fibres.

7.5.   References

[1]   Consulting TFY. The Fiber Year 2023 World Survey on Textiles & Nonwovens [Internet]. 2023 [cited 2023 Aug 17]. Available from: https://thefiberyear.com/

[2]   Woodings, C. (Ed.). (2001). *Regenerated cellulose fibres*. Elsevier.

[3]   Opperskalski, S., Siew, S., Tan, E., & Truscott L. (2019). Preferred Fiber & Materials Market Report 2019.1–87.

[4]   Statista.(2023).   statistic_id263154_global-production-volume-of-textile-fibers-1975-

2021.pdf..

[5]   Textile Exchange (2022). Preferred Fiber & Materials: Market Report 2022. 1–118.

[6]   Felgueiras, C., Azoia, N. G., Gonçalves, C., Gama, M., & Dourado, F. (2021). Trends on the cellulose-based textiles: raw materials and technologies. *Frontiers in Bioengineering and Biotechnology*, *9*, 608826.

[7]   Shen, L., Worrell, E., & Patel, M. K. (2010). Environmental impact assessment of man-made cellulose fibres. *Resources, Conservation and Recycling*, *55*(2), 260-274.

[8]   Shen, X., Ji, Y., Wang, D., & Yang, Q. (2010). Solubility of a high molecular-weight bacterial cellulose in lithium chloride/N, N-dimethylacetamide solution. *Journal of Macromolecular Science, Part B*, *49*(5), 1012-1018.

[9]   Kim, D. B., Pak, J. J., Jo, S. M., & Lee, W. S. (2005). Dry jet-wet spinning of cellulose/N-methylmorpholine N-oxide hydrate solutions and physical properties of lyocell fibers. *Textile research journal*, *75*(4), 331-341.

[10]   Perepelkin, K. E. (2007). Lyocell fibres based on direct dissolution of cellulose in N-methylmorpholine N-oxide: development and prospects. *Fibre Chemistry*, *39*(2), 163-172.

[11]   Elsayed, S., Hummel, M., Sawada, D., Guizani, C., Rissanen, M., & Sixta, H. (2021). Superbase based protic ionic liquids for cellulose filament spinning. *Cellulose*, *28*, 533-547.

[12]   Jiang, X., Bai, Y., Chen, X., & Liu, W. (2020). A review on raw materials, commercial production and properties of lyocell fiber. *Journal of Bioresources and Bioproducts*, *5*(1), 16-25.

[13]   Zhang, S., Chen, C., Duan, C., Hu, H., Li, H., Li, J., ... & Ni, Y. (2018). Regenerated cellulose by the lyocell process, a brief review of the process and properties. *BioResources*, *13*(2), 4577-4592.

[14]   Meksi, N., & Moussa, A. (2017). A review of progress in the ecological application of ionic liquids in textile processes. *Journal of Cleaner Production*, *161*, 105-126.

[15]   Andersson, E. (2018). Dissolution and fibre spinning of cellulose from an ionic liquid.

[16]   Ebner, G., Schiehser, S., Potthast, A., & Rosenau, T. (2008). Side reaction of cellulose with common 1-alkyl-3-methylimidazolium-based ionic liquids. *Tetrahedron Letters*, *49*(51), 7322-7324.

[17]   Sixta, H., Michud, A., Hauru, L., Asaadi, S., Ma, Y., King, A. W., Kilpeläinen, I., & Hummel, M. (2015). Ioncell-F: a high-strength regenerated cellulose fibre. *Nordic pulp & paper research journal*, *30*(1), 43-57.

[18]   Cai, T., Zhang, H., Guo, Q., Shao, H., & Hu, X. (2010). Structure and properties of cellulose fibers from ionic liquids. *Journal of Applied Polymer Science*, *115*(2), 1047-1053.

[19]   Moriam, K., Sawada, D., Nieminen, K., Hummel, M., Ma, Y., Rissanen, M., & Sixta, H. (2021). Towards regenerated cellulose fibers with high toughness. *Cellulose*, 2*8*, 9547-9566.

[20]   Haslinger, S., Hummel, M., Anghelescu-Hakala, A., Määttänen, M., & Sixta, H. (2019). Upcycling of cotton polyester blended textile waste to new man-made cellulose fibers. *Waste Management*, *97*, 88-96.

[21]   Guizani, C., Larkiala, S., Moriam, K., Sawada, D., Elsayed, S., Rantasalo, S., Hummel, M., & Sixta, H. (2021). Air gap spinning of a cellulose solution in [DBNH][OAc] ionic liquid with a novel vertically arranged spinning bath to simulate a closed loop operation in the Ioncell[®] process. *Journal of Applied Polymer Science*, *138*(5), 49787.

[22]   Hestrin, S., & Schramm, M. J. B. J. (1954). Synthesis of cellulose by Acetobacter xylinum. 2. Preparation of freeze-dried cells capable of polymerizing glucose to cellulose. *Biochemical Journal*, *58*(2), 345.

[23]   Soares da Silva, F. A., Fernandes, M., Souto, A. P., Ferreira, E. C., Dourado, F., & Gama, M. (2019). Optimization of bacterial nanocellulose fermentation using recycled paper sludge and development of novel composites. *Applied Microbiology and Biotechnology*, *103*, 9143-9154.

[24]   Jedrzejczak-Krzepkowska, M., Kubiak, K., Ludwicka, K., & Bielecki, S. (2016). Bacterial nanocellulose synthesis, recent findings. In *Bacterial Nanocellulose* (pp. 19-46). Elsevier.

[25]   Jozala, A. F., de Lencastre-Novaes, L. C., Lopes, A. M., de Carvalho Santos-Ebinuma, V., Mazzola, P. G., Pessoa-Jr, A., Grotto, D., & Chaud, M. V. (2016). Bacterial nanocellulose production and application: a 10-year overview. *Applied microbiology and biotechnology*, *100*, 2063-2072.

[26]   Silva, F. A., Dourado, F., Gama, M., & Poças, F. (2020). Nanocellulose bio-based composites for food packaging. *Nanomaterials*, *10*(10), 2041.

[27]   Gama, M., Dourado, F., & Bielecki, S. (Eds.). (2016). *Bacterial nanocellulose: from biotechnology to bio-economy*. Elsevier.

[28]   Kamiński, K., Jarosz, M., Grudzień, J., Pawlik, J., Zastawnik, F., Pandyra, P., & Kołodziejczyk, A. M. (2020). Hydrogel bacterial cellulose: A path to improved materials for new eco-friendly textiles. *Cellulose*, *27*, 5353-5365.

[29] Fernandes, M., Souto, A. P., Gama, M., & Dourado, F. (2019). Bacterial cellulose and emulsified AESO biocomposites as an ecological alternative to leather. *Nanomaterials*, *9*(12), 1710.

[30] Gao, Q., Shen, X., & Lu, X. (2011). Regenerated bacterial cellulose fibers prepared by the NMMO· H2O process. *Carbohydrate polymers*, *83*(3), 1253-1256.

[31] Makarov, I. S., Golova, L. K., Vinogradov, M. I., Levin, I. S., Gromovykh, T. I., Arkharova, N. A., & Kulichikhin, V. G. (2019). Cellulose fibers from solutions of bacterial cellulose in N-methylmorpholine N-oxide. *Fibre Chemistry*, *51*, 175-181.

[32] Michud, A., Hummel, M., & Sixta, H. (2015). Influence of molar mass distribution on the final properties of fibers regenerated from cellulose dissolved in ionic liquid by dry-jet wet spinning. *Polymer*, *75*, 1-9.

[33] Meister, F., & Kosan, B. (2015). A tool box for characterization of pulps and cellulose dopes in Lyocell technology. *Nordic Pulp & Paper Research Journal*, *30*(1), 112-120.

[34] Hummel, M., Michud, A., Tanttu, M., Asaadi, S., Ma, Y., Hauru, L. K., Parviainen, A., King, A. W. T., Kilpeläinen, I., & Sixta, H. (2016). Ionic liquids for the production of man-made cellulosic fibers: opportunities and challenges. *Cellulose chemistry and properties: Fibers, nanocelluloses and advanced materials*, 133-168.

[35] Asaadi, S., Hummel, M., Hellsten, S., Härkäsalmi, T., Ma, Y., Michud, A., & Sixta, H. (2016). Renewable high-performance fibers from the chemical recycling of cotton waste utilizing an ionic liquid. *ChemSusChem*, *9*(22), 3250-3258.

[36] Piribauer, B., & Bartl, A. (2019). Textile recycling processes, state of the art and current developments: A mini review. *Waste Management & Research*, *37*(2), 112-119.

[37] Michud, A., Tanttu, M., Asaadi, S., Ma, Y., Netti, E., Kääriainen, P., Person, A., Berntsson, A., Hummel, H., & Sixta, H. (2016). Ioncell-F: ionic liquid-based cellulosic textile fibers as an alternative to viscose and Lyocell. *Textile Research Journal*, *86*(5), 543-552.

[38] Rissanen, M., Schlapp-Hackl, I., Sawada, D., Raiskio, S., Ojha, K., Smith, E., & Sixta, H. (2023). Chemical recycling of hemp waste textiles via the ionic liquid based dry-jet-wet spinning technology. *Textile Research Journal*, *93*(11-12), 2545-2557.

[39] Pitkänen, L., & Sixta, H. (2020). Size-exclusion chromatography of cellulose: observations on the low-molar-mass fraction. *Cellulose*, *27*(16), 9217-9225.

[40] Roland, C. M. (2013). Chapter 6—Rheological Behavior and Processing of Unvulcanized Rubber. *The Science and Technology of Rubber*, *4*.

[41]   Lenz, J., Schurz, J., & Wrentschur, E. (1994). On the elongation mechanism of regenerated cellulose fibres.

[42]   Hames, B., Ruiz, R., Scarlata, C., Sluiter, A., Sluiter, J., & Templeton, D. (2008). Preparation of samples for compositional analysis. *Laboratory Analytical Procedure (LAP)*, *1617*, 65-71.

[43]   Heydorn, R. L., Lammers, D., Gottschling, M., & Dohnt, K. (2023). Effect of food industry by-products on bacterial cellulose production and its structural properties. *Cellulose*, *30*(7), 4159-4179.

[44]   Einfeldt, L., & Klemm, D. (1997). The Control of Cellulose Biosynthesis by Acetobacter Xylinum in View of Molecular Weight and Molecular Weight Distribution Part I: Change of Molecular Weight of Bacterial Cellulose by Simple Variation of Culture Conditions. *Journal of carbohydrate chemistry*, *16*(4-5), 635-646.

[45]   Hong, J. H., Ku, M. K., Ahn, Y., Kim, H. J., & Kim, H. (2013). Air-gap spinning of cellulose/ionic liquid solution and its characterization. *Fibers and Polymers*, *14*, 2015-2019.

[46]   Kim, T., Kim, D., & Park, Y. (2022). Recent progress in regenerated fibers for "green" textile products. *Journal of Cleaner Production*, 134226.

[47]   Krässig, H. A. (1993). Cellulose: structure, accessibility, and reactivity.

[48]   Asaadi, S., Hummel, M., Ahvenainen, P., Gubitosi, M., Olsson, U., & Sixta, H. (2018). Structural analysis of Ioncell-F fibres from birch wood. *Carbohydrate polymers*, *181*, 893-901.

[49]   Kreze, T., Strnad, S., Stana-Kleinschek, K., & Ribitsch, V. (2001). Influence of aqueous medium on mechanical properties of conventional and new environmentally friendly regenerated cellulose fibers. *Materials Research Innovations*, *4*(2-3), 107-114.

[50]   Sun, L., Chen, J. Y., Jiang, W., & Lynch, V. (2015). Crystalline characteristics of cellulose fiber and film regenerated from ionic liquid solution. *Carbohydrate polymers*, *118*, 150-155.

[51]   Tomé, L. C., Brandao, L., Mendes, A. M., Silvestre, A. J., Neto, C. P., Gandini, A., Freire, C. S. R., & Marrucho, I. M. (2010). Preparation and characterization of bacterial cellulose membranes with tailored surface and barrier properties. *Cellulose*, *17*, 1203-1211.

[52]   Volova, T. G., Prudnikova, S. V., Sukovatyi, A. G., & Shishatskaya, E. I. (2018). Production and properties of bacterial cellulose by the strain Komagataeibacter xylinus B-12068. *Applied microbiology and biotechnology*, *102*, 7417-7428.

[53]   Chaudemanche, C., & Navard, P. (2011). Swelling and dissolution mechanisms of regenerated Lyocell cellulose fibers. *Cellulose*, *18*(1), 1-15.

[54]   Kuzmina, O., Bhardwaj, J., Vincent, S. R., Wanasekara, N. D., Kalossaka, L. M., Griffith, J., Potthast, A., Rahatekar, S., Eichorn, S. J., & Welton, T. (2017). Superbase ionic liquids for effective cellulose processing from dissolution to carbonisation. *Green Chemistry*, *19*(24), 5949-5957.

[55]   Çeven, E. K., & Günaydın, G. K. (2021). Evaluation of some comfort and mechanical properties of knitted fabrics made of different regenerated cellulosic fibres. *Fibers and Polymers*, *22*, 567-577.

[56]   Nanollose. Nullarrbor Fibre [Internet]. [cited 2023 Mar 31]. Available from: https://nanollose.com/products/nullarbor/

[57]   Jinzarli, M. M., Cass, G. A., Moursounidis, J., & Best, W. M. (2023). *U.S. Patent No. 11,597,779*. Washington, DC: U.S. Patent and Trademark Office.

[58]   Parviainen, A., Wahlström, R., Liimatainen, U., Liitiä, T., Rovio, S., Helminen, J. K. J., Hyväkkö, U., King, A. W. T., Suurnäkki, A., & Kilpeläinen, I. (2015). Sustainability of cellulose dissolution and regeneration in 1, 5-diazabicyclo [4.3. 0] non-5-enium acetate: a batch simulation of the IONCELL-F process. *RSC advances*, *5*(85), 69728-69737.

[59]   Rodrigues, A. C., Fontão, A. I., Coelho, A., Leal, M., da Silva, F. A. S., Wan, Y., Dourado, F., & Gama, M. (2019). Response surface statistical optimization of bacterial nanocellulose fermentation in static culture using a low-cost medium. *New Biotechnology*, *49*, 19-27.

[60]   Soares da Silva, F. A., Fernandes, M., Souto, A. P., Ferreira, E. C., Dourado, F., & Gama, M. (2019). Optimization of bacterial nanocellulose fermentation using recycled paper sludge and development of novel composites. *Applied Microbiology and Biotechnology*, *103*, 9143-9154.

[61]   Palme, A., Idström, A., Nordstierna, L., & Brelid, H. (2014). Chemical and ultrastructural changes in cotton cellulose induced by laundering and textile use. *Cellulose*, *21*, 4681-4691.

[62]   Jasińska, I. (2023). Industrial washing conditions as factor that influence the cellulose structure and mechanical strength of bed linens. *Scientific Reports*, *13*(1), 12214.

[63]   Gu, H., He, J., Huang, Y., & Guo, Z. (2012). Water soluble carboxymethylcellulose fibers derived from alkalization-etherification of viscose fibers. *Fibers and Polymers*, *13*, 748-753.

[64]   Schausberger, D., & Möslinger, R. (1999). Rheologie von Celluloselösungen zur Charakterisierung von Cellulose. *Das Papier (Darmstadt)*, *53*(12), 715-721.

[65]   Härdelin, L., Perzon, E., Hagström, B., Walkenström, P., & Gatenholm, P. (2013). Influence of molecular weight and rheological behavior on electrospinning cellulose nanofibers from ionic liquids. *Journal of Applied Polymer Science*, *130*(4), 2303-2310.

CHAPTER 8 – FINAL REMARKS

This chapter contains the principal conclusions drawn from the work described in the previous chapters and proposes recommendations/suggestions for further research.

8.1. General Conclusions

Both food packaging and textile industries face a shared environmental challenge: plastic pollution. Recognizing the urgency of the matter, these industries are actively seeking sustainable and biodegradable alternatives. Nevertheless, finding suitable substitutes for plastics proves to be a challenging task due to the demanding requirements of the envisaged applications. In this work, the potential of bacterial cellulose (BC) as a starting material was assessed. Despite the well-known obstacles associated to BC (such as low yields and high cost, which explain the lack of availability at large scale), its outstanding properties cannot be ignored and were explored with the goal of developing high performing composites for food packaging and textile.

The assessment of food packaging in terms of water vapor permeability, oxygen permeability, and mechanical properties is crucial to determine its suitability for fulfilling packaging requirements. Our primary objective was to develop a layered composite film consisting of BC and PHBV, and evaluate its barrier and mechanical performance. BC, plasticized with glycerol, provided mechanical strength, ensuring that the film could withstand packaging operations and handling during the supply chain. The PHBV coating on BC significantly improved the water vapor barrier of the composite, making it a promising option for the packaging of meat, meat-based products, fruits, vegetables, and fresh salads, as discussed in Chapter 3. This approach offers a straightforward method for producing cellulose-based packaging for certain food items. However, certain limitations were encountered, particularly regarding the oxygen permeability, which showed a significant variability, probably related to the non-uniform fibre network of BC. Another interesting feature of BC is the ability to hold water/solvents, which allows to easily incorporate active substances. On Chapters 4 and 5, BC was functionalized with Zinc oxide nanoparticles (ZnO), to develop an active film for food packaging. A limitation was found in this approach, as the increase in ZnO concentration led to higher particle sizes, which represent a limitation with regards to the obtained antimicrobial activity. Indeed, the developed BC$_{ZnO}$ films showed antimicrobial activity against various bacteria, especially against gram negative pathogen bacteria, yet higher activities would have been desirable. The more vulnerable bacteria were gram negative, which suggests that the main mechanism of action of ZnO relies on the migration of

Zn^{2+} rather than ROS generation – which is more effective towards Gram positive bacteria. The developed composite was particularly effective against *Campylobacter* spp a bacterium of great interest for the poultry sector. The antimicrobial effect against *E. coli* and *Salmonella* may be considered too low, especially taking in account the level of Zn migration found on chicken skin at 4 °C. While developing an active packaging, the migration of an active agent should be also addressed, especially on food models. Migration testing was carried out on chicken skin and it was demonstrated that temperature and pH influenced the migration of Zn^{2+}, surpassing the specific migration limit (SML) at higher temperatures. Although prescribed storage temperatures for meat products are in the range of 4 °C, temperature fluctuations may occur along the food chain supply, triggering higher Zn migration rates. This is a limitation of the developed BC_{ZnO} films. Despite these limitations, the work done so far demonstrated a promising application for BC as active food packaging to meat and meat-based products. This is evident when migration is effectively controlled even upon abusive temperatures.

BC was also used for the development of regenerated cellulose fibres. We explored the spinning of non-depolymerised BC using the lyocell process, challenging the common belief that only celluloses with a DP between 550-650 may be used to manufacture shapeable dopes for dry-wet spinning. In chapter 6, we demonstrate that both non-depolymerized and depolymerized BC could be spun into Lyocell fibres, using NMMO as solvent in the production of the dope. These fibres exhibited promising mechanical performance, especially when non-depolymerized and depolymerized BC were blended prior to dissolution and spinning. Indeed, the blending approach improved the mechanical properties of the regenerated cellulose fibres and highlighted the potential of BC as an additive for other cellulose fibres known to have a very low DP, such as recycled cellulosic waste materials. Given the promising results obtained, BC was explored also using [DBNH][OAc] ionic liquid for the regeneration process, a greener solvent used on the so called Ioncell process (Chapter 7). This is known to provide improved mechanical performance, when compared to lyocell fibres. Using BC, the spun fibres provided great mechanical performance, related to the high crystallinity and orientation observed. The spinning process was successfully upscaled, the resulting staple fibres were easily yarn spun, showcasing competitive mechanical performance (compared to commercial yarns) and knitted into a textile garment (the first ever made using Ioncell process with BC). With the

main goal of approaching the current poor recycling rate of end-of-life fibres, BC was further tested as an additive for viscose fibres. The addition of BC (and its increasing concentration) did hamper the spinnability of viscose fibres, leading to improved mechanical performance (by providing longer cellulose chains from BC) when compared to neat viscose fibres. The European commission is currently addressing strategies for developing sustainable and circular textiles and BC can play a crucial role on upgrading end-of-life fibres such viscose. Our research on BC using both Lyocell and Ioncell processes also provided valuable insights into determining the most suitable process for BC. Despite the better performance of Ioncell process and the resulting fibres, it is important to note that Ioncell process uses [DBNH][OAc] IL, highly sensitive to water. Consequently, to use BC for Ioncell, a drying pre-treatment is strictly necessary. On the other hand, never dried BC can be used in the lyocell process, following the usual approach employed in the lyocell process. This additional pre-treatment required in the case of Ioncell can impact the overall viability of the process as great additional energy is employed to remove the water.

Overall, all the work carried out contributed to better understanding the technological potential of BC, exploiting its properties (mechanical strength, water holding capacity, long cellulose chains) to develop BC-based materials with promising application in active food packaging and textile waste recycling. However, it´s industrial potential can only be exploited if the large-scale production at low cost is successfully achieved. This will certainly require significant breakthroughs, either related to the identification or development of new (more effective) strains, the identification of cheap fermentation substrates, suitable bioreactors able to efficiently process high viscous media generated by the release of BC during fermentation.

8.2.   Future Work

The results obtained are promising, but additional work is yet to be done to further explore the potential of BC on food packaging and textile industries. On a wider perspective, a very important line of research concerns with the evaluation of the large-scale production, attempting to develop a technology capable of delivering BC in large amounts at competitive

cost. Additionally, research concerning the Life Cycle Analysis of BC production is currently in progress. A comparative assessment of BC's sustainability, in relation to other cellulose sources such as cotton and regenerated cellulose from biomass, is crucial as it will aid in understanding how BC could enhance the existing alternatives for these specific applications.

1. **Considering food packaging applications:**

    a. More data should be collected using an oxygen transmission rate (OTR) device with a higher detection limit, to validate the measurements collected so far. This will make possible understanding with higher accuracy, which category of foods can be packed using the composite produced in Chapter 3.

    b. Further reduce the water vapour transmission rate, e.g. by testing other PHA.

    c. To lower the obtained level of Zn migration, a PHBV coating (as carried out in Chapter 3) may be an effective solution. Low adhesion of ZnO in PHBV was already reported elsewhere, which may slow Zn migration from BC. Considering the different levels of grammage applied, the antibacterial efficiency and Zn migration needs to be addressed again, to reach a compromise between antibacterial activity and Zn migration.

    d. Study the combination of two or more active agents, to further improve the antibacterial efficiency and widen the antibacterial activity spectrum. BC_{ZnO} films were especially effective against *campylobacter* species, yet adding other active agents such as silver nanoparticles, can further improve the antimicrobial activity of the overall composite;

2. **Considering textile applications:**

    a. The development of regenerated cellulose fibres, either using Lyocell and Ioncell processes, using BC produced by different strains. Different bacterial strains can produce BC with characteristics, especially with different DP and molar mass distribution.

        i. Correlate the different characteristics of BC (DP and molar mass distribution) with the dope rheology, spinnability and mechanical performance of the resulting fibres.

        ii. The best performing BC could be further chosen to be used as additive for upgrading low DP end-of-life fibres, with the goal of using even

lower amounts than used in Chapter 7. Explore other end-of-life fibres such as cotton or flax fibres; only viscose fibres were tested (chapter 7).

b. The development a composite fibre by combining BC and chitosan through Lyocell technology. By varying the ratios of Chitosan/BC, we can produce a functionalised regenerated BC-Chitosan fibre. Chitosan is renowned for its antimicrobial properties, and the incorporation of BC fibre can potentially improve the fibre's spinnability, as already proven. Therefore, in addition to the characterization conducted in Chapters 6 and 7, it would be interesting to perform antimicrobial tests, as similarly described in Chapter 4 and 5.